NMR Studies of Cobalt Bleomycins and Their Complexes with DNA: A Structural Model for Binding and Cleavage Specificity

by

Wei Wu
B.S., Chemistry, The University of Kansas
(1991)

Submitted to the Department of Chemistry
in Partial Fulfillment of the Requirements
for the Degree of

DOCTOR OF PHILOSOPHY

at the
Massachusetts Institute of Technology

September 1996

Signature of Author _____
Department of Chemistry
August 29, 1996

Certified by _____
Professor JoAnne Stubbe
Thesis Supervisor

Accepted by _____
Dietmar Seyferth
Chairman, Departmental Committee on Graduate Students

This doctoral thesis has been examined by a Committee of the Department of Chemistry as follows:

Professor Stephen J. Lippard_____
Chairperson

Professor JoAnne Stubbe_____
Thesis Supervisor

Professor James R. Williamson_____

To my parents

NMR Studies of Cobalt Bleomycins and Their Complexes with DNA: A Structural Model for Binding and Cleavage Specificity

by

Wei Wu

Submitted to the Department of Chemistry on August 29, 1996
in Partial Fulfillment of the Requirements for the Degree of
Doctor of Philosophy

ABSTRACT

The solution structure of Cobalt Bleomycin (CoBLM) A2 green (the hydroperoxide form of CoBLM) and its complex with oligonucleotide d(CCAGGCCTGG) (cleavage site at C6), has been determined by 2D NMR spectroscopic methods and molecular dynamics calculations. CoBLM A2 green is a stable analog of the activated BLM, the Fe(III)-hydroperoxide. Two screw sense isomers each containing two possible axial ligands (the primary amine of the β-aminoalanine and the carbamoyl nitrogen of the mannose) were considered as viable candidates for the structure of CoBLM A2 green. The favored structure contains the primary amine of β-aminoalanine as the axial ligand with the bithiazole moiety folded back underneath the equatorial plane of the metal binding domain, on the same face as the hydroperoxide ligand. The structure of the complex between CoBLM A2 green and DNA have provided the first structural insight into the mode of binding of the bithiazole tail, the basis for specificity of cleavage at pyrimidines (Py) in d(G-Py) sequences, and the orientation of its terminal oxygen of the hydroperoxide relative to the 4' carbon hydrogen bond being cleaved in the DNA. The bithiazole tail inserts 3' to the C6 cleavage site from the minor groove with the terminal thiazolium ring completely stacked between the bases of G14 and G15 and the penultimate thiazolium ring only partially stacked between the bases of C6 and C7. The metal binding domain and the peptide linker region of CoBLM A2 green bind within the minor groove of the duplex and define the basis for its specificity of DNA cleavage. The 4-amino group and the N3 of the pyrimidine ring of CoBLM A2 green form specific hydrogen bonds with the N3 and the 2-amino group, respectively, of the G5 in the duplex. One of the most remarkable feature of this structure is the observation of the proton associated with the hydroperoxide of CoBLM A2 green and its observed intermolecular NOEs to the minor groove protons of C6 and C7 of the duplex. The molecular modeling reveals that the distal oxygen of the hydroperoxide is 2.5 Å from the 4'-hydrogen of C6.

Thesis Supervisor: Professor JoAnne Stubbe
Title: Ciba-Geigy Professor of Chemistry and Biology

Acknowledgments

I want to be witty and clever, but I am too tired. First, I would like to thank Professor Stubbe for her support and guidance. I will long remember her meticulous approach to science and tireless attending to experimental details.

This thesis could not have been completed in a timely fashion without the contribution of Dana Vanderwall. His expertise in computer modeling was essential to our progress. Not only was his input an integral part of this work, his enthusiasm and dedication to this project has always been inspirational. Our endeavors over the past four years exemplified the ideal kind of collaboration. I want to thank Dr. Chris Turner, with whom I worked closely on many occasions. It was from him I learned the tenet of NMR spectroscopy. I am also grateful to John Battiste, Dr. Jody Puglisi and Prof. Jamie Williamson who showed me the ropes during the initial stage of this project.

Many people in the Stubbe lab, past and present, made graduate student life a bearable one. I want to thank Erik Meyer for his perspectives on life outside the lab. Bike rides to Walden pond and evening skiing trips to Nashoba Valley reminded me the point of weekEND. Wing Hang Tong has always been known for her exceptional taste in food and art. I immensely enjoyed the delicious meals she prepared. I have to thank Squire Booker, Mike Absalon, and Marty Bollinger for their renditions of the classic stories and lines. I want to thank Silvia Hoehn and Dr. Rick Bunt for taking over the Bleo baton. I especially owe Rick a debt of gratitude for carefully proof-reading Chapter 4. I want to thank Kirsten Skogerson for hosting many extraordinary parties in Brookline. Her inborn skill in cookery is a blessing for all of us.

I forever owe gratitude to my parents for their unconditional love and support. They have always been there for me during the most trying times. Finally, I want to thank my girlfriend, Linda Chen, who shared the emotional roller-coaster ride with me over the past five years. Our life together will hopefully begin in the near future.

Table of Contents

Figures

Scheme

1.1: Formation and decomposition of activated FeBLM

Tables

Chapter 1: Bleomycins: A Structural Model for Specificity, Binding and Double Strand Cleavage

The bleomycins (BLMs, Figure 1.1) are a class of glycopeptide antibiotics isolated from *Streptomyces*.[1] They have found clinical use in combination chemotherapy for the treatment of head and neck cancer, certain lymphomas and testicular cancer.[2] The mechanism of cytotoxicity is thought to be related to the ability of BLMs to bind to and degrade duplex DNA in the presence of Fe^{2+}, O_2 and a reductant as required cofactors.[3a] Under *in vitro* conditions, BLM causes both single strand (ss) and double strand (ds) breaks in DNA. The ratio of these two cleavage processes is sequence dependent with ds cleavage being a relatively minor event.[4] *In vivo*, ssDNA cleavage is probably repaired by the human counterparts of prokaryotic DNA repair enzymes.[5] The less frequent dsDNA cleavage, however, is believed to be responsible for the observed cytotoxicity of BLM and its mechanism of repair has not thus far been elucidated.

A unified hypothesis explaining the basis of BLM-DNA recognition and the chemical specificity of cleavage has been an important goal of the field. Beginning with the seminal experiments of Peisach, Horwitz and Burger nearly 20 years ago on the metal and oxygen requirements of BLM,[3, 6] a general consensus has emerged concerning the mechanistic details of the ssDNA cleavage. These studies have been summarized in a number of recent reviews.[7, 8] However, despite the efforts of many groups, the structural basis for the sequence-specific cleavage of DNA by BLM and the mechanistic basis for dsDNA cleavage have remained elusive. This brief review will focus on these two topics. First, the very recent 2D NMR studies of an analog of "activated BLM", a cobalt (III) hydroperoxide (HOO-CoBLM) bound to a specific GpPy binding site in an oligonucleotide will be presented. These studies reveal the basis for sequence selectivity of cleavage and the mode of binding. The relationship of these studies to activated FeBLM's structure and function will be discussed. Second, a chemical and structural model will be presented to explain how a single molecule of BLM can mediate dsDNA cleavage. Taken together this

recent work provides a unifying context for understanding this remarkable class of DNA cleaving agents.

Background. The BLMs bind a variety of metals. In the presence of an oxidant, a number of metallo-BLMs can effect DNA strand scission. Most effort has focused on understanding the iron-BLMs. However, the concentration of free copper in cells and the ability of copper-BLMs to mediate strand scission has generated some interest in these complexes as well.[7, 9, 10] Using a variety of the time-resolved biophysical methods, the Peisach and Horwitz laboratories definitively established the sequence of events (Scheme 1.1) leading to an activated BLM with DNA cleaving capabilities.[6]

Scheme 1.1:

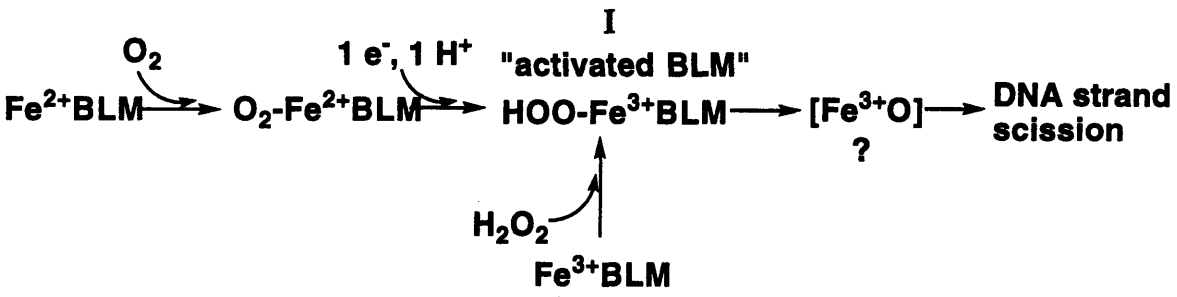

Intermediate I, designated activated BLM, has been identified recently by electrospray mass spectrometry as a ferric hydroperoxide species and is the last detectable intermediate prior to DNA strand scission.[11] Remarkably, this intermediate has a half life of 2 min at 4 °C.[6a] Whether the peroxide itself initiates DNA cleavage or is

Figure 1.1: Structure of Bleomycin A2. Nitrogen ligands coordinating to the metal are underlined.

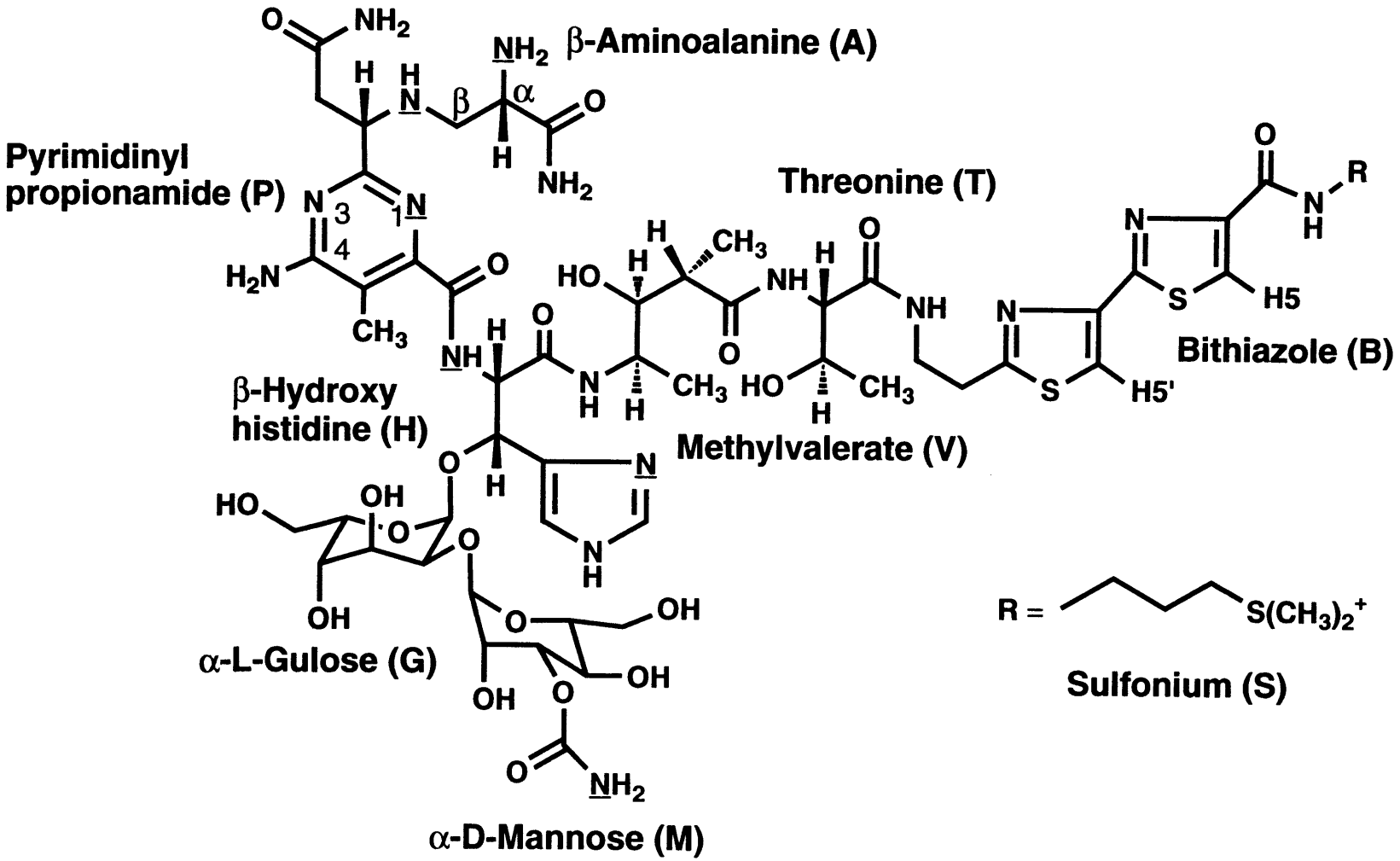
β-Aminoalanine (A)
Pyrimidinyl propionamide (P)
Threonine (T)
Bithiazole (B)
β-Hydroxy histidine (H)
Methylvalerate (V)
α-L-Gulose (G)
α-D-Mannose (M)
R =
S(CH3)2+
Sulfonium (S)

broken down via heterolysis of the O-O bond to an iron oxene equivalent, [$Fe^{3+}O$], which initiates DNA cleavage is the subject of ongoing investigations. Recent circular dichroism, magnetic circular dichroism, and X-ray absorption studies have suggested that a key to the unique chemical reactivity of iron-BLM resides in one of its equatorial ligands, the pyrimidine moiety (P, Figure 1.1).[12a] Strong backbonding from the iron to this ligand reduces the charge transfer between the iron and O_2 and thus decreases the facility of the ternary O_2-Fe^{2+}BLM complex to decompose to $O_2^{\bullet-}$ and Fe^{3+}BLM. A further understanding of the chemistry of the non-heme iron in BLM and its relationship to the well-characterized heme systems thus continues to be an active area of research.[12]

The chemistry of ssDNA cleavage has also been extensively investigated and work from many laboratories is consistent with the mechanism postulated in Figure 1.2.[8, 13, 14] Only 4'-hydrogen abstraction has been observed with duplex DNA and iron BLM[15, 16] resulting in two monomeric products, base and base propenal. Identical kinetic isotope effects are observed on the formation of both products when [4'-^{2}H]dNTPs are incorporated into the DNA. Sequence specific isotope effects can be monitored using polyacrylamide gels and specifically deuterated DNAs.[17] These observations are consistent with the formation of a common intermediate presumably containing a 4'-radical (Figure 1.2). The subsequent partition ratio depends on the concentration of O_2 and the sequence context. The detailed chemistry of these pathways has been reported.[8]

Recent studies from the Giese laboratory have shed additional light on pathway A (Figure 1.2).[18] Using chemical methods to specifically generate a C-4' radical in a single stranded oligonucleotide, detection of the proposed peroxy radical (by ESR spectroscopy) and hydroperoxide (by MALDI-TOF mass spectrometry) intermediates have been reported. Both intermediates presumably result from trapping of a 4'-nucleotide radical with O_2.[18] It is important to note, however, that

Figure 1.2: Proposed Mechanism of FeBLM-mediated DNA Cleavage (ss=single strand and ds=double strand): pathway A requires O_2 over and above that required to form "activated BLM" and pathway B requires no additional O_2 and leads to strand scission only under alkaline conditions.

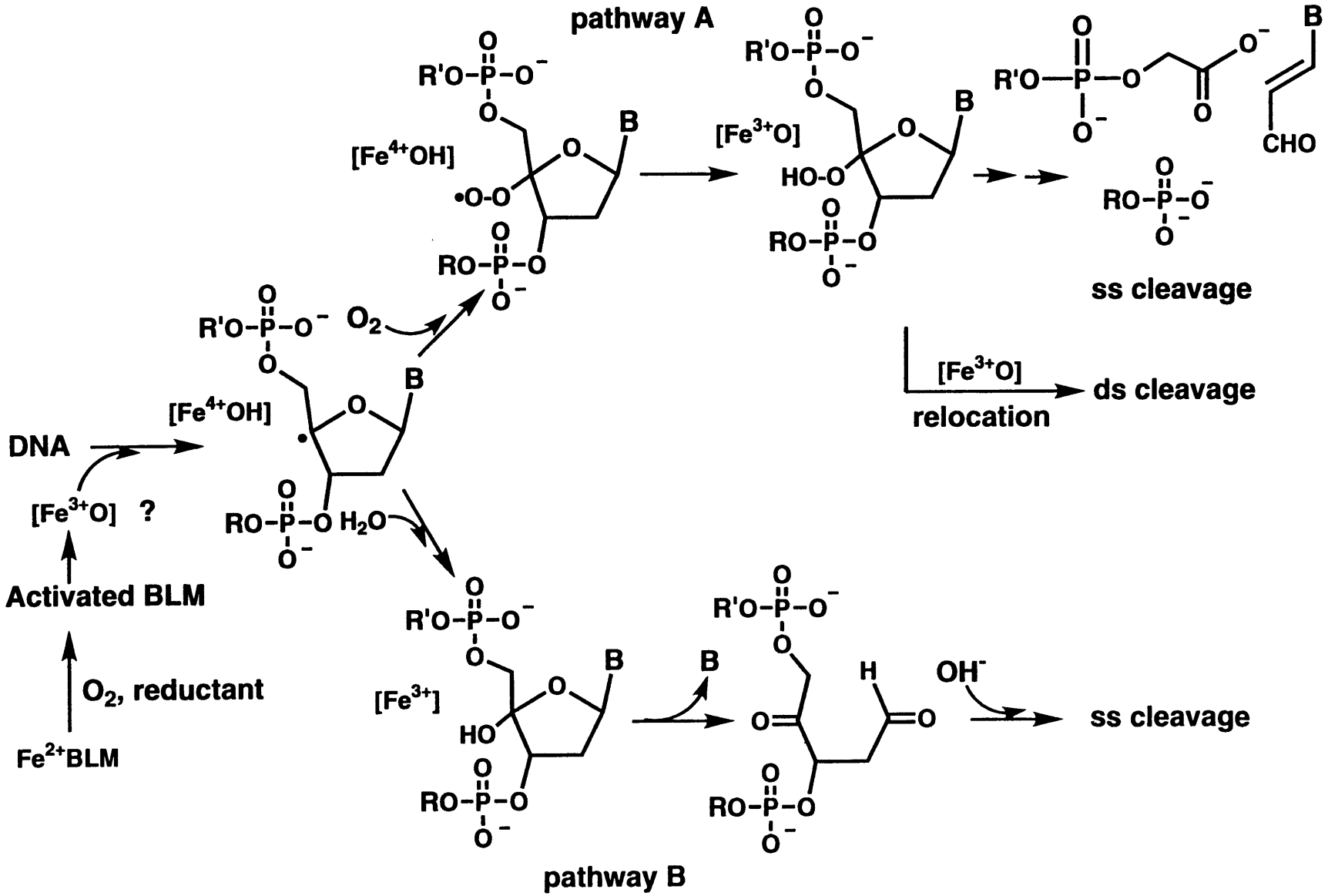
pathway A
[Fe4+OH]
[Fe3+O]
ss cleavage
[Fe3+O]
relocation
ds cleavage
DNA
[Fe3+O] ?
Activated BLM
O2, reductant
Fe2+BLM
O2
H2O
[Fe3+]
OH-
ss cleavage
pathway B

these model systems which give similar and additional products to those observed with BLM and DNA, result from chemistry different from that occurring in BLM-mediated DNA degradation. The products of these model reactions are consistent with rapid formation of a cation radical intermediate (Figure 1.3),[18] initially suggested from pulse radiolysis experiments (under anaerobic conditions) of Schulte-Frohlinde and von Sonntag.[19]

The distinction between the model work of Giese and the observed chemistry of BLM must reflect the relative rates of various reactions and the juxtapostion of a "reducible" iron center adjacent to C4' in the case of the FeBLM system. Thus loss of phosphate, reported by Behrens et al.[19b] to occur with a k_{obs} of ~10^3 s^{-1} and in model nucleotides by Giese et al.[18c] of ~10^5 s^{-1} must be slower than the diffusion controlled rate of reaction of O_2 with the 4'-radical or oxidation of this radical to a carbocation by the putative $Fe^{4+}OH$ species (Figure 1.2). It is difficult however to completely exclude the possibility that this pathway occurs as a minor process that could go undetected with available analytical methods.

This understanding of the mechanism of ssDNA cleavage has been essential for designing experiments to probe the mechanism of dsDNA cleavage. In addition, the demonstration of the importance of the 2-amino group of G in the dGpT(C) sequences experiencing cleavage suggests that the chemistry and specificity of cleavage is dependent on the minor groove environment and has stimulated much speculation on the determinants of this specificity.[20-23] Recent 2D NMR studies summarized below have now provided a framework for explaining these observations.

A structural model for HOO-CoBLM bound to DNA.

As summarized in Scheme 1.1, HOO-Fe^{3+}BLM is the last detectable intermediate before DNA degradation. However, the use of NMR spectroscopy to

Figure 1.3: Proposed mechanism for products generated from a 4'-nucleotide radical intermediate produced by photolysis of 4'-substituted nucleotides.[18a, 19a] The products generated are not consistent with those observed in BLM mediated DNA degradation.

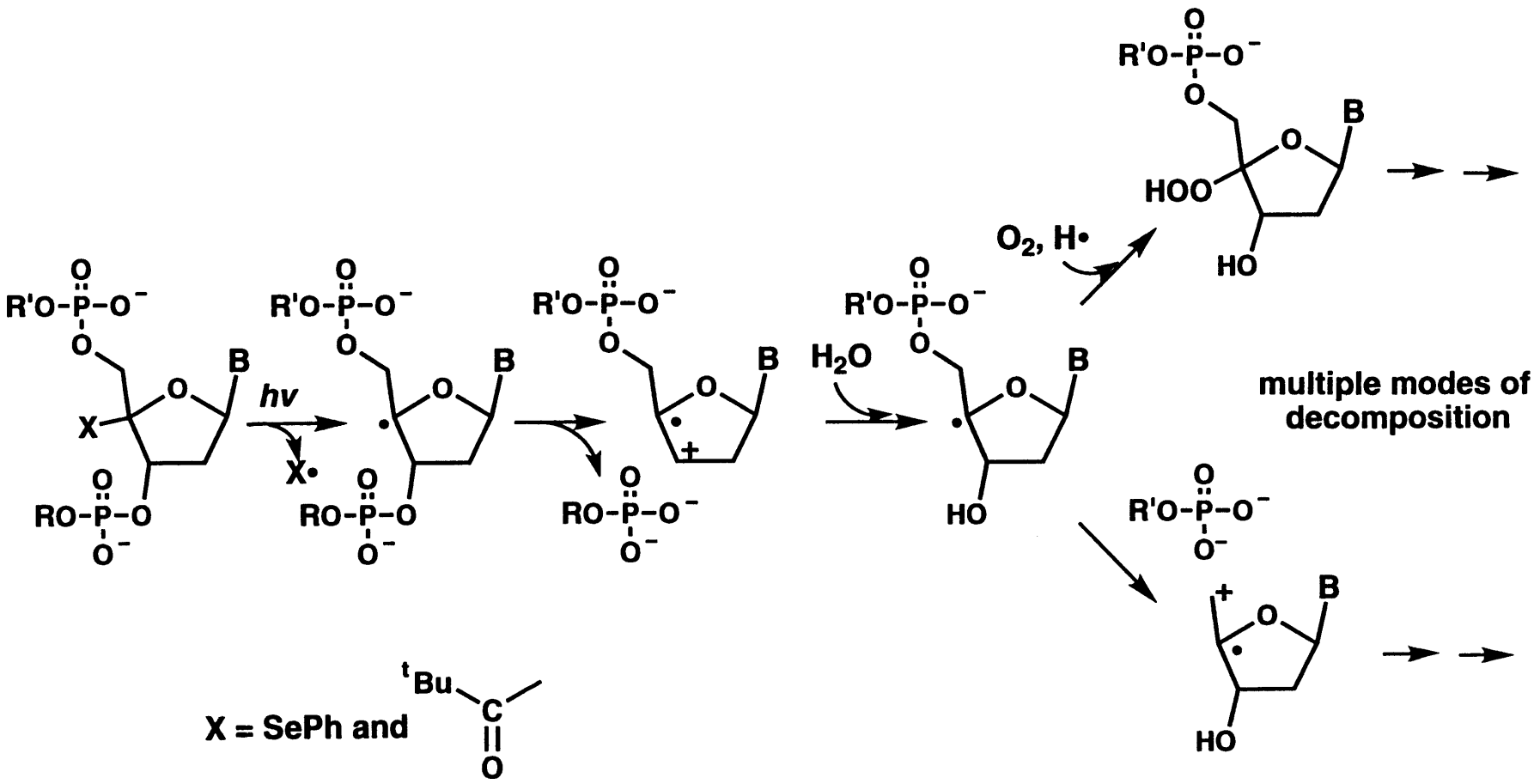
R'O-P-O⁻
O
B
X
RO-P-O
O⁻
hv
X•
H2O
O2, H•
HOO
HO
multiple modes of
decomposition
X = SePh and
tBu
C
O

determine the structure of iron BLM is problematic for several reasons. First, Fe^{3+}BLM is paramagnetic and broadens the protons of greatest interest. Second, Fe^{3+}BLM is not very stable[10] and undergoes substantial decomposition during the time required for data acquisition. Third, binding specificity of Fe^{3+}BLMs to DNA has not been well studied. We and others have therefore sought to use alternative metallo-BLMs for NMR analysis.[24-28] The Oppenheimer and Hecht laboratories performed the first NMR experiments in 1979 on ZnBLM and CO-Fe^{2+}BLM.[29a,b] These complexes have recently been restudied using 2D homonuclear and heteronuclear NMR spectroscopy by Akkerman et al.[30] All of the protons and carbons in these complexes have been assigned as have their structures. In the case of both the Zn and the CO-Fe^{2+}BLM complexes, the amino group of the carbamoyl moiety of mannose has been assigned as an axial ligand. This assignment is based on the proton chemical shift of H3' of the mannose relative to the same proton in metal free BLM, the well defined orientation of the β-hydroxyhistidine relative to the sugars in comparison with metal free BLM, and the coupling constants for the α and β protons of β-aminoalanine. While this data led them to favor the carbamoyl ligation over the primary amine of β-aminoalanine, this later alternative could not be unambiguously ruled out. In addition, the screw sense of the isomers of these and other complexes have not been unambiguously identified. Much research is still being devoted to the characterization of a variety of the metallo-BLMs with the intent of resolving these structural issues.[12b,c, 26a,d, 28a] The possiblility of course needs to be considered that perhaps these features may differ among various metallo-BLMs.[31]

Recently the Petering and Otvos laboratories[26] and our laboratories[28] have focused on the HOO-CoBLM originally described by Chang and Meares.[32a] This compound is appealing for a number of reasons. First, it is an analog of the activated BLM (HOO-FeBLM) and, under conditions of photochemical activation,[32b]

will cleave DNA with the same sequence specificity as activated FeBLM and with exclusive 4'-hydrogen abstraction.[32c, 34, 35] Second, Co^{3+} is diamagnetic, as is the case for the Zn and CO-FeBLMs, and is amenable to NMR spectroscopic analysis. Third, the ligands are exchange inert and sufficiently stable for the extended periods of time, required for data acquisition by NMR methods. Xu et al. in 1994, reported the first structures for a mixture of CoBLMs: A2 green and A2 brown.[26a] The CoBLM A2 green is the hydroperoxide form (II), while the CoBLM A2 brown, III, has a slowly exchangeable H_2O (or OH^-) as an axial ligand. The successful resolution of these two species[28a] has allowed us to obtain additional NOE and dihedral angle constraints for II, not reported by Xu et al.[26a]

Detailed molecular modeling studies using these constraints[28a,] in addition to a variety of chemical and biophysical data summarized by Wu et al.,[28a,b] have allowed us to favor the screw sense isomer reported in Figure 1.4, with the primary amine of the β-aminoalanine moiety (Figure 1.1) as the axial ligand rather than the amino group of the carbamoyl moiety of mannose. Studies of Dabrowiak with a hydrolyzed product of BLM (pseudotetrapeptide A),[33c, 37a] as well as recent crystallographic studies of Tan et al. on CoPMA,[36, 37a] a model of CoBLM, indicate that the axial ligand can be the primary amine of the β-aminoalanine.[37b] In addition, studies of Sugiyama et al. using synthetic models in which the pyrimidine is replaced with substituted pyridine (PYMLs), further demonstrate the importance of the β-aminoalaninamide.[38] Very recently Boger's lab has made BLM A2 without the mannose group and Hecht's group has previously made deglyco and decarbamoyl BLM A2. The DNA cleavage with Fe for all of these BLMs has been found to be almost identical to BLM A2 in sequence selectivity and comparable in efficiency.[29c, 39c,f] These studies suggest that, at a minimum, the carbamoyl group of the mannose is not required as an axial ligand. Finally, the screw sense of the ligand organization has been established by our recent structural studies of II complexed to

several duplex oligonucleotides.[28b] Only the organization of the ligands shown in Figure 1.4 and discussed in detail in Wu et al.[28b] can account for the observed NMR constraints and the cleavage chemistry.

Several remarkable features of the structure of II warrant highlighting. First, the bithiazole tail is folded underneath the metal binding domain on the same face as the hydroperoxide ligand (Figure 1.4, a refined model of one of the two structures originally proposed by Xu et al.[26a]). Second, the valeryl moiety of the peptide linker is in a well defined conformation, which is virtually identical to its conformation when bound to the DNA. Third, modeling suggests that there are H bonding interactions between the penultimate oxygen of the hydroperoxide axial ligand and the hydrogens of the amide moieties of T and V (Figure 1.1). These interactions may account for the unusually high stability of this hydroperoxide.[28a,b]

Titration studies of CoBLMs with generic DNA suggested that the DNA complex of II is in slow exchange with free II and DNA on the NMR time scale.[26c] We were encouraged by this observation and focused on the crucial choice of a defined duplex oligonucleotide with a single binding and cleavage site for II which could serve as the basis for developing a structural model. Our studies resulted in the selection of two oligonucleotides for investigation: d(CCAGGCCTGG) (**1**) and (CCAGTACTGG) (**2**) [the underlined pyrimidine indicates the site of cleavage]. Both possess a single cleavage site and a single binding site, the former determined by gel electrophoresis and the latter quantified by monitoring fluorescence quenching with Scatchard analysis affording Kds of ~10^{-7} M.[28a]

The details of the interaction between **1** and II have recently been described.[28b,c] Approximately 85% of the protons associated with II and 95% associated with **1** have been assigned. This has resulted in the detection of 60 intermolecular NOEs, 61 intramolecular NOEs within II and >200 NOEs within **1**. These constraints have been used in modeling and dynamics calculations, resulting

Figure 1.4: Solution structure of CoBLM A2 green with the primary amine of A moiety as an axial ligand (atoms colored by element, C=green , O=red, N=blue, S=yellow, H=white). The sulfonium moiety and most of the hydrogen atoms have been removed for the sake of clarity. The dotted lines indicates the H bonding interactions between the penultimate oxygen of the hydroperoxide axial ligand and the hydrogens of the amide moieties of T and V (Figure 1.1).

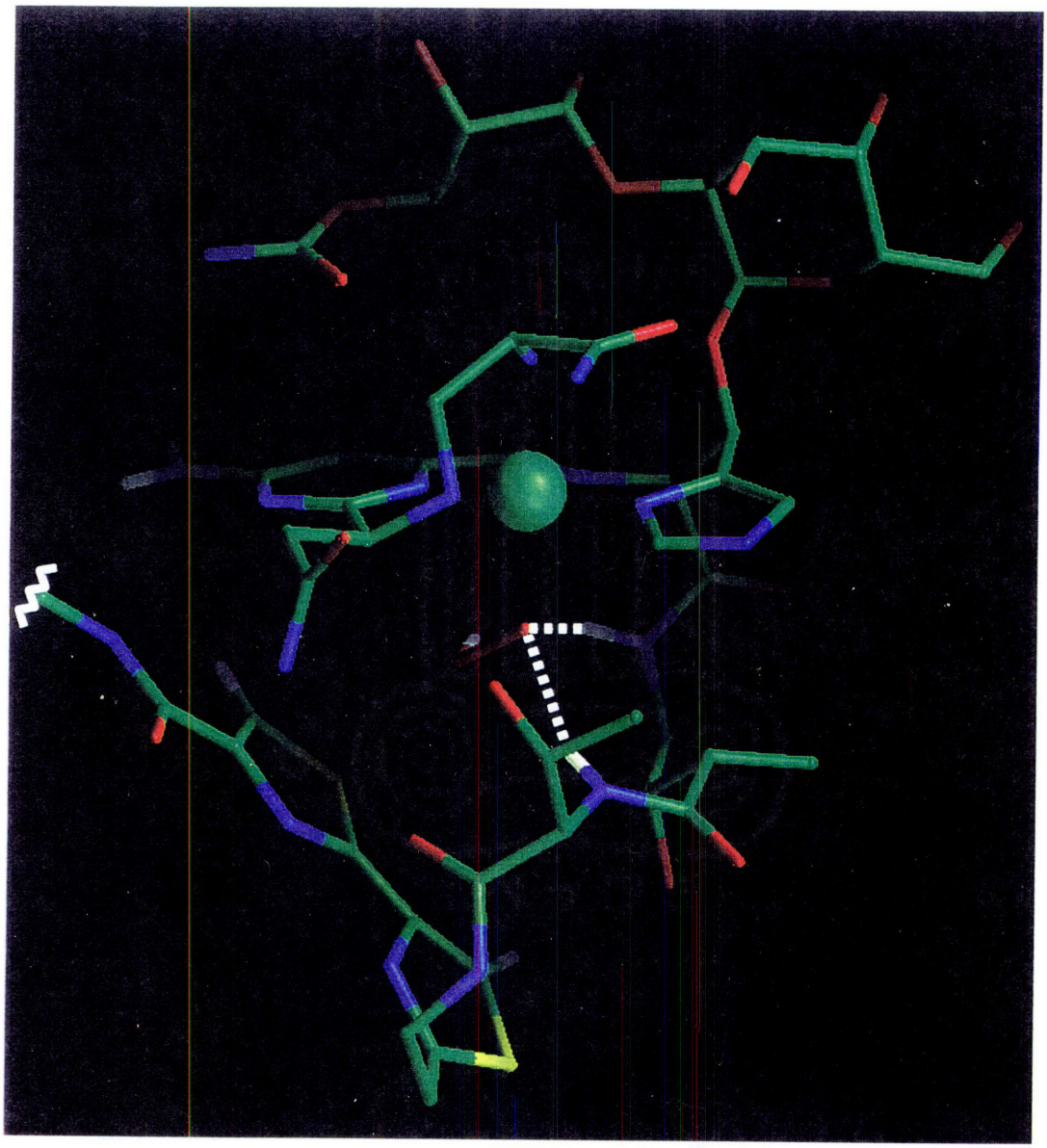

Figure 1.5: The structure of CoBLM A2 green (atoms colored by element, C=green , O=red, N=blue, S=yellow, H=white) bound to DNA (purple, C6-H4′=white). The damaged strand (C1-C2-A3-G4-G5-C6-C7-T8-G9-G10) is in the foreground, running 5′->3′ from the upper right to lower left corner. The dotted lines indicate the H-bond interactions between the P moiety (Figure 1.1) of CoBLM, and the G5 of the DNA. Also indicated is the proximity of the distal oxygen of the hydroperoxide ligand to the C6-H4′ (2.5 Å).

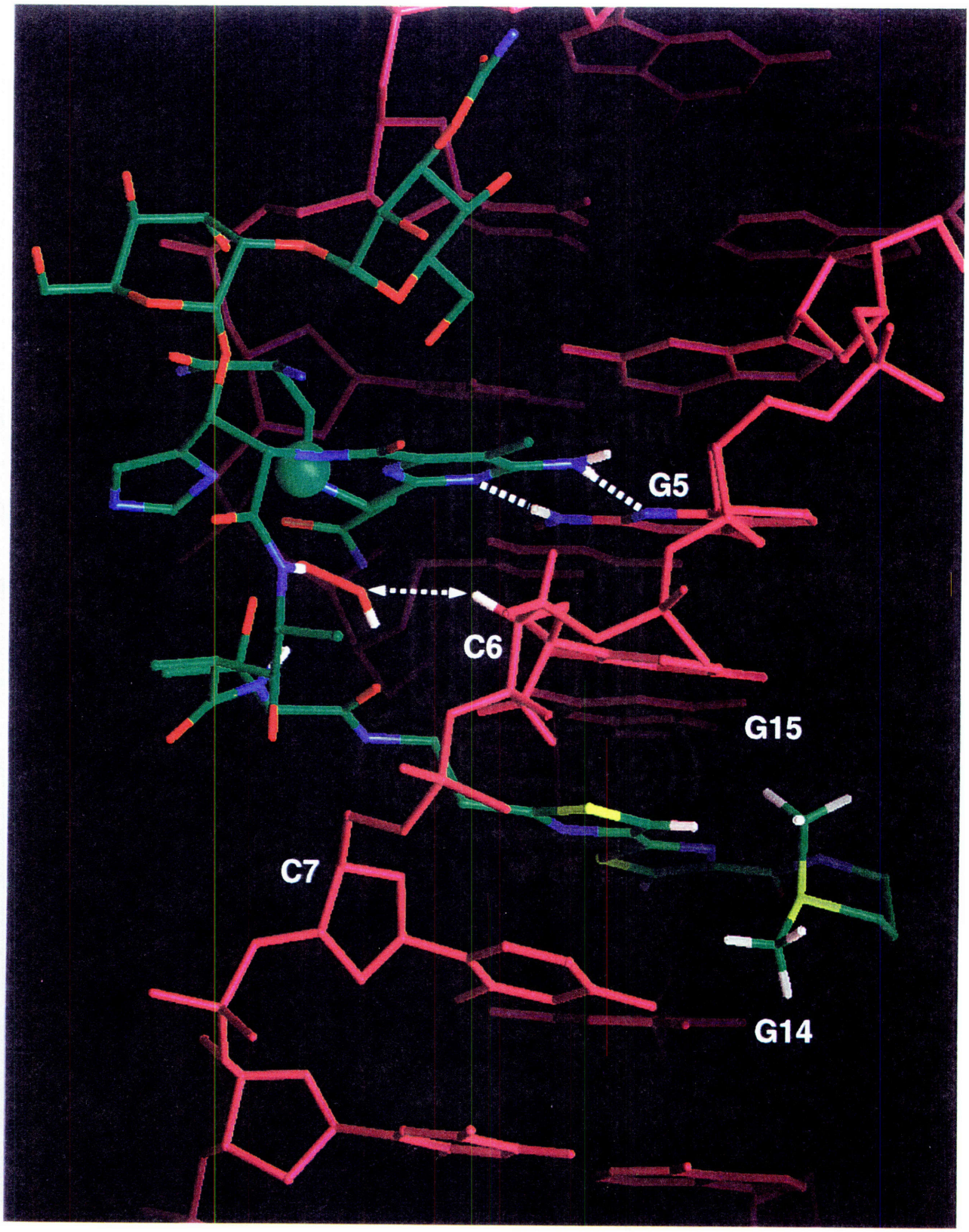
G5
C6
G15
C7
G14

in a model of the structure shown in Figure 1.5. This model provides considerable insight into the three key properties of the interaction of BLMs with DNA: binding, sequence specificity, and cleavage chemistry. The bithiazole tail is a major binding determinant. It is inserted 3' to the cleavage site from the minor groove between C6•G15 and C7•G14, indicative of a partial intercalative mode of binding. The basis for sequence specificity is defined for the first time. The N3 and the amino group of the pyrimidine of CoBLM (Figure 1.1) form H bonding interactions with one of the hydrogens of the 2-amino group of G5 and the N3 amino group of G5, respectively. Finally, the unexpected identification of the hydroperoxide proton in the complex has unambiguously defined the basis of chemical specificity. The terminal oxygen of the hydroperoxide is located 2.5 Å from the C4'H (Figure 1.5), a surprising result given that no constraints involving this interaction were used in the modeling. Each of these three points will be discussed below.

Examination of the binding of the bithiazole tail reveals that the terminal thiazolium ring is completely stacked between G15 and G14, while the penultimate thiazolium ring is only partially stacked between C6 and C7 (Figure 1.6). The H5 and H5' protons of the thiazolium rings (Figure 1.1) are trans to one another. Both these protons are upfield shifted in the NMR spectrum when CoBLM is bound to the oligomer. We have also observed similar upfield shifts of these protons when CoBLM is bound to oligomer **2**. Whether this mode of binding is general remains to be established. However the data is consistent with many of the previous studies on apoBLM (using linear dichroism, NMR, DNA unwinding measurements, fluorescent quenching under conditions of differing ionic strength, etc.) suggesting a partial intercalative mode of binding.[40-44] This binding mode also explains previous studies with phleomycin (PLM), a BLM analog in which the penultimate thiazolium ring is reduced. PLM displays a sequence selectivity and efficiency of cleavage that is similar to the corresponding BLM.[45, 46] This result has suggested to

Figure 1.6: Binding by partial intercalation of the bithiazole tail of CoBLM A2 green to DNA. A view looking down the helical axis showing the terminal thiazolium ring stacked between the bases of G14 and G15 and the penultimate thiazolium ring partially stacked between the bases of C6 and C7.

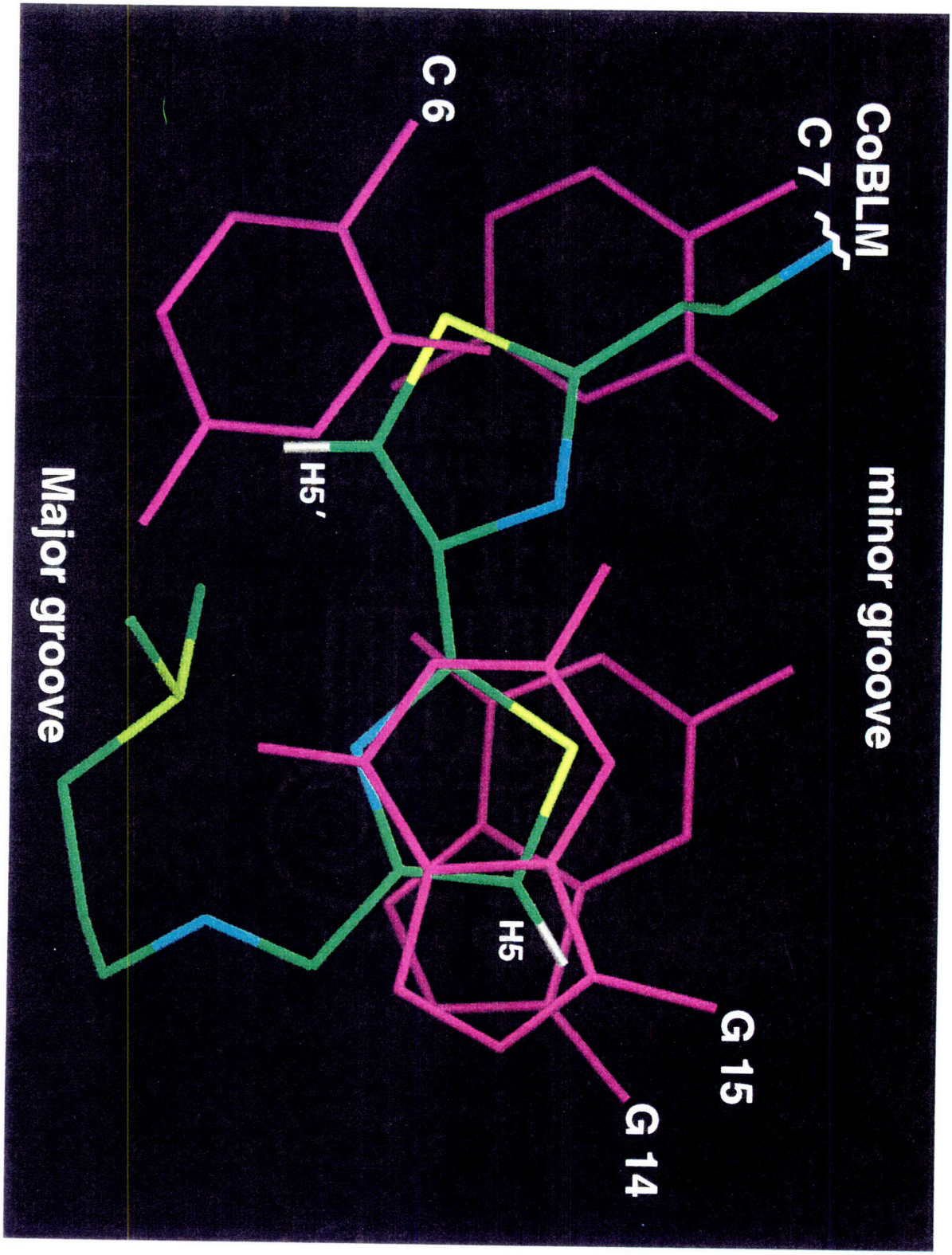
CoBLM
C 7
minor groove
C 6
H5'
H5
G 15
G 14
Major groove

many that intercalation cannot be the mode of binding.[42, 46, 47] However, molecular modeling using the structure in Figure 1.5, shows that PLM can be readily accommodated without significant perturbation of the structure. This type of intercalation is supported by many chemical and biochemical studies suggesting that the bithiazole tail provides no specific interaction with DNA, just the binding energy.[7, 39a, 48, 49a] Finally, intercalation 3' to the cleavage site is also consistent with diethylpyrocarbonate and permanganate cleavage studies with CoBLM[47] and cleavage studies with bulged DNA.[50]

In contrast, recent studies from the Hecht lab using ZnBLM bound to an oligomer (CGCTAGCG) revealed multiple binding modes.[27] The ZnBLM, clearly has a ligand coordination environment different from CO-FeBLM and HOO-CoBLM and thus the observed differences are not surprising.[31] ZnBLM does not effect strand scission and the relevance of the ZnBLM to the active metallo-BLM(s) *in vivo*, thus remains to be established.

The requirement of the 2-amino group of G, 5' to the Py cleavage site, is a feature of the sequence specificity of BLM which is generally agreed upon.[20-24] However, the role of this G, as a specificity determinant, has remained speculative. Our studies reveal an unusual base triple (Figure 1.5) between the P moiety of BLM and G5 of the DNA oligomer. One of the protons of the amino group of the pyrimidine is downfield shifted (from 7.94 or 7.73 ppm in the CoBLM to 10.22 ppm in the complex) and is H bonded to the N3 of the G5. A similar downfield shifted proton is observed in the GTAC sequence (2), suggesting that in this case as well, it is involved as a specificity determinant. The second key feature of the specificity is a H bond between the N3 of the pyrimidine of CoBLM and one of the 2-amino protons of G5. This result explains why replacement of G with an inosine in a GpPy sequence dramatically reduces cleavage by BLM and why cleavage at ApPy sequences is less efficient than at the GpPy sequences.[22, 23, 34b] It is important to note that

neither of these hydrogen bonds were used as constraints in the modeling and dynamics calculations.[28b]

II is postulated to be an analog of "activated FeBLM." Therefore, it was hoped that a model of the structure of activated BLM would provide some insight into the mechanism of 4'-hydrogen atom abstraction (Figure 1.5). The structural determination was facilitated by the unexpected observation of the proton of the hydroperoxide at 8.89 ppm in H_2O. The assignment of the proton was confirmed by the recent determination of the structure of the brown form of CoBLM (III) in which the peroxide is replaced with either a H_2O or OH^- ligand. While the binding of III to **1** is similar to that observed for II,[51] the proton resonance at 8.89 ppm is absent. There are 6 intermolecular NOEs between the hydroperoxide proton of II and the DNA. These constraints in conjunction with molecular dynamics calculations as noted above, have placed the terminal oxygen within 2.5 Å of the 4' hydrogen of C6 that would be abstracted by the activated FeBLM.

Proposals for the mechanism of hydrogen abstraction by activated FeBLM are largely based on heme-iron chemistry, thus favoring a heterolytic cleavage of the oxygen-oxygen bond of the hydroperoxide to generate an iron oxene or its equivalent. By analogy with the well characterized heme peroxidases, this type of cleavage would be facilitated by general acid catalysis, i.e. proton transfer to the terminal oxygen.[52] In the case of II bound to **1**, however, as in the case of II in solution, the H-bonding is to the penultimate oxygen, the one directly bound to the cobalt. The environment of this peroxide is very sequestered with multiple H-bonding interactions, accounting for its detection and stability. The model structure is, therefore, contradistinctive to that "expected" based on the heme-peroxidase chemistry. Unfortunately, the resolution of this model structure is not sufficiently high to warrant further speculation on the chemistry of activation and hydrogen abstraction.

Relationship of CoOOH structure with FeOOH. A brief survey of the extensive FeBLM literature provides a number of observations to support the proposal that II is an excellent analog of activated FeBLM. First, the specificity of cleavage of both species are very similar with the 2-amino group of G playing a key role in this process. It will be interesting to insert 3-deazaguanine in place of guanine in GpPy sequences to further assess similarities (or difference) between these systems, as this substitution would eliminate one of the H bonds defining the specificity. The complementary experiment, addition of a 2-amino group to an adenine (to generate 2,6-diaminopurine, DAP) has recently been reported by Bailly et al.[23] and their results using FeBLM are completely consistent with our model: weak cleavage sites at ApC(T) sequences were transformed into strong cleavage sites at the DAPpC(T) sequences. Second, the mode of binding of II now offers a reasonable explanation for why PLM has similar specificity and cleavage efficiency to FeBLM. Molecular modeling based on the structure in Figure 1.5 suggests that these observations do not require a minor groove binding model as proposed by many investigators.[22, 53] Third, studies of several groups have shown that activated FeBLM, in the absence of DNA, can undergo self-inactivation by modification of the bithiazole tail.[49, 54] Whether this reaction is inter or intra molecular is not known. This data can be explained by a conformation of activated FeBLM similar to that of II in which the tail is folded underneath the metal binding domain and on the same face as the hydroperoxide. Fourth, II is a competitive inhibitor of activated FeBLM, with respect to both its ssDNA and dsDNA cleavage.[32c, 34a, 55b] Fifth, both compounds can abstract the 4'-hydrogen atom from the deoxyribose of a Py and give the same product a 4'-keto-1'-aldehyde with the DNA strand intact.[35, 56] The mechanism of this process with II under photochemical conditions, however, has yet to be defined. Sixth, a recent report of FeBLM-mediated degradation of naked DNA in comparison with the same DNA containing precisely positioned nucleosomes, indicated a

drastic inhibition of cleavage within the nucleosome core region.[57] This large FeBLM-induced perturbation in DNA conformation supports a intercalative mode of binding, as minor groove binding alone normally renders little DNA helical structural changes. Also revealed in their studies is the same extent of inhibition in ssDNA and dsDNA cleavages, an observation consistent with a model in which a single molecule of BLM can effect dsDNA cleavage.[55,58]

Based on these considerations, we believe that II is an excellent model for activated FeBLM. However, the CO-FeBLM has also been proposed to be an analog of the O_2-Fe(II)BLM complex, the direct precursor to HOO-FeBLM and as summarized above, is proposed to have different coordination geometry than the II.[30b] Both can obviously not be excellent models for activated BLM. The user-friendly synthesis of BLM with appropriate ^{15}N-labeled ligands in conjunction with a variety of physical methods is in progress to allow a resolution to this problem.

Summary. The solution structure of CoBLM A2 green complexed with an oligonucleotide has provided the first structural insight into the mode of binding by the bithiazole moiety, the basis for sequence specificity of the cleavage at Py in GPy sequences, and a view of an analog of the reactive intermediate poised to initiate the 4'-hydrogen atom abstraction. Studies are in progress to test the generality of the mode of binding and specificity using various BLM analogs as well as different DNA sequence contexts.

Double-strand cleavage. In addition to catalyzing ssDNA cleavage, BLM can catalyze dsDNA cleavage. The ratio of these processes (ds:ss) has been reported by a number laboratories and varies from 1:6 to 1:20 depending on the assay method.[4] Recent studies of Absalon et al. have observed a ratio of 1:3 in a GTAC sequence, apparently a hot spot for dsDNA cleavage.[55] The paucity of dsDNA cleavage events and the

technical problems associated with investigating them has limited the available information required to understand this process.

The specificity of dsDNA cleavage was examined by Povirk's laboratory using nondenaturing polyacrylamide gel electrophoresis and is shown in Figure 1.7.[58] The examination of 23 dsDNA cleavage sites led to the proposal by Povirk that there is a 1° site which is a good ssDNA cleavage site (G**Py**) and that there is a 2° site of cleavage that is determined by whether a pyrimidine or a purine is located 3' to the Py in the 1° cleavage site. DsDNA cleavage leads to blunt ended or 5'-staggered DNA fragments (Figure 1.7). Absalon et al. have examined another 20 dsDNA cleavage sites using the same methods and observed similar cleavage sites to those reported by Povirk,[55c] in addition to a number that had not been previously observed. Thus, a general rule of sequence specificity for dsDNA cleavage is difficult to infer in light of the relatively small amount of sequence space that has been studied for this phenomenon.

Figure 1.7: Sequence Specificity of ds Cleavage.[58a] Bold and underlined Py denote 1° and 2° cleavage site, respectively.

5'-G-**Py**-Py-Pu-3'	5'-G-**Py**-Pu-Py-3'	5'-G-**Py**-Pu-Pu-3'
3'-C-<u>Pu</u>-Pu-Py-5'	3'-C-Pu-<u>Py</u>-Pu-5'	3'-C-Pu-<u>Py</u>-Py-5'

The most compelling mechanistic model for dsDNA cleavage has been proposed by Povirk and coworkers based on a number of interesting experiments.[58] Many of the features of this model have been recently confirmed by using hairpin oligonucleotides designed to have a single dsDNA cleavage site, which allows quantitation of both ss and ds cleavage events.[55] The basic premise of the Povirk model is that a single molecule of BLM catalyzes both cleavage events without

dissociating from the DNA and that FeBLM must be reactivated for the second cleavage event to occur. The cleavage specificity (Figure 1.7) indicates that this single BLM molecule must move 15-18 Å to participate in C-4' hydrogen atom abstractions on both strands.[55b] The studies of Povirk et al. and of Absalon et al. indicate that the chemistry of cleavage appears to be identical to that previously established for ssDNA cleavage. Isotope effect studies using [4'-^{2}H]-Py in the dsDNA cleavage sites indicate that identical isotope effects are observed on both ssDNA and dsDNA cleavage events suggesting that the mode of binding for both events are identical.[55b] Subsequent to hydrogen atom abstraction, the 4'-radical can lead to two types of products. However, the dsDNA cleavage process can only be observed when the O_2-dependent pathway occurs at the primary site (pathway A, Figure 1.2) leading to the proposal that some intermediate in this pathway is required to reactivate the FeBLM for the second cleavage event.[55b, 58a] Reactivation could involve reduction of the peroxy radical concomitant with $Fe^{4+}OH$ oxidation to $Fe^{5+}{=}O$ (equivalent to [$Fe^{3+}O$]) (Figure 1.2). It should be noted, however, that the events after the formation of HOO-FeBLM (intermediate I in Scheme 1.1) is unknown and there is no chemical precedent for this reactivation. This proposal, therefore, is speculative and serves as our working hypothesis.[55b,c]

The model for dsDNA cleavage predicts that the partitioning ratio between ssDNA and dsDNA cleavage depends ultimately on the relative rates of FeBLM dissociation versus reorganization to the second site where the second cleavage event can occur. Thus, every ssDNA cleavage event could lead, with some probability, to dsDNA cleavage. The structure suggests that during this reorganization, the bithiazole tail is retained within its intercalation site and that the linker peptide (Figure 1.1) serves as a tether to allow for the translocation of the BLM metal binding domain from the first to the second site. The importance of the peptide linker has only recently been recognized in this process with the solution of

the structure and with the studies from Boger's laboratory.[39a,c,g] In the latter case, changes in the peptide linker affect the ratio of ssDNA to dsDNA cleavage (Table 1.1). For example, the replacement of the threonine moiety with a glycine residue reduced the ratio of ss:dsDNA cleavage by ~3 fold (Table 1.1). The detailed structural analysis of these linker mutants complexed to defined DNA sequences is in progress as a complement to the cleavage studies in an effort to understand the role of the linker in the dsDNA cleavage process.

The basis of sequence-specific ssDNA cleavage revealed in the structure (Figure 1.5) has allowed us to begin consideration of the structural basis for the sequence specificity for dsDNA cleavage. Of all the dsDNA sequences that we have examined, only a single hot spot has been detected: 5'-G-**T**-A-C-3'. Furthermore studies of Povirk et al.[58a] have revealed that no dsDNA cleavage has been detected in 5'-G-**C**-3' sites, proposed by a number of investigators to be a likely hot spot for dsDNA cleavage.[4f,59, 60] Both of these observations can easily be rationalized based on the recent structure (Figure 1.5). A good ssDNA cleavage site (G**Py**) is preferred, if not imperative, at the first site of the dsDNA cleavage. Weak binding at the first cleavage site could lead to rapid dissociation precluding BLM's reactivation and reorganization required for dsDNA cleavage. In contrast, tighter binding involving two hydrogen bonds between the guanine in G**Py** and the pyrimidine of BLM will likely exhibit a slower dissociation rate of BLM from DNA and in turn permit sufficient time for the metal binding region to reactivate and relocate to the 2° cleavage site. As for the second cleavage site, although a good ssDNA cleavage site is not obligatory (Figure 1.7) the hot spot for dsDNA cleavage has a G 5′ to the second cleavage site thus potentially offering the same full capacity for sequence recognition and binding observed at the 1° cleavage site. Therefore, the preference of purine over pyrimidine for binding/recognition again represents an important

Table 1.1: Comparison of BLM analogs modified in the linker region: efficiency and ratio of double strand to single strand cleavage.[a]

BLM Analogs	ds:ss	Efficiency
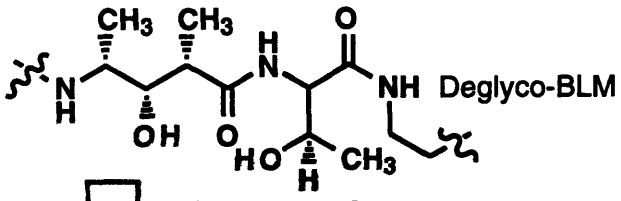 Deglyco-BLM	1:12	1.0
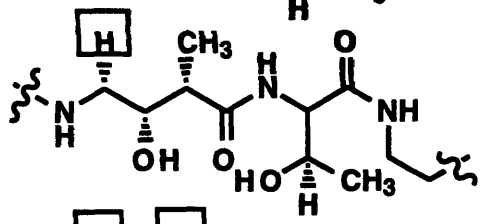	1:15	0.5
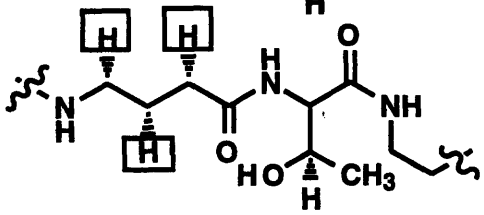	1:13	0.3
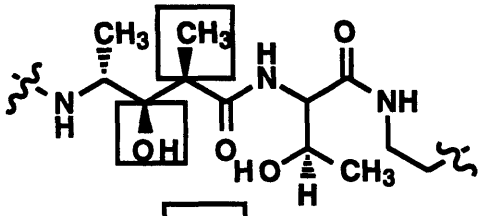	1:13	0.6
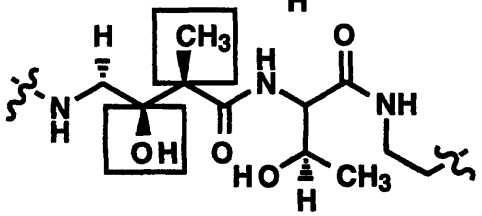	1:15	0.2
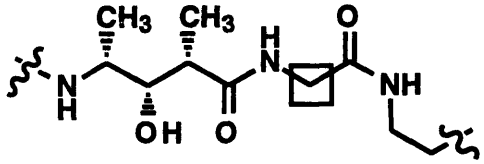	1:29	0.2
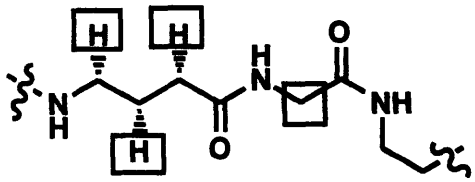	1:33	0.1
Fe^{2+}	1:98	0.04

a. Data taken from Boger et al., 1995;[39g] Boxed area indicates changes in the linker region.

determinant 5' to the second cleavage site. Moreover, because the current model supports the contention that a single BLM can catalyze cleavage on both strands without dissociation, the location of thiazolium rings, 3' to the 1° cleavage site places constraints on where the second cleavage can occur. This constraint makes it sterically impossible for BLM therefore to cleave the second C in the 5'-G-C- sequence.[61] Additional structures need to be examined to determine if the mode of binding described in Figure 1.5 is generic and additional ds-cleavage sites need to be elucidated quantitatively to determine if any general rules will evolve. These types of studies, in conjunction with peptide linker mutant BLMs ought to allow, in the near future, a model for the structural basis for dsDNA cleavage to be proposed.

Summary. The new experimental information about BLM's interactions with DNA summarized above has focused on structure/function studies carried out in *vitro*. A question can be legitimately posed as to how these observations relate to the observed cytotoxicity *in vivo*.[10] While it has been demonstrated that BLM can get into the nucleus of the cell at low concentrations, when and where the metal cofactor is acquired, when and where the activation process occurs and whether a DNA cleavage event(s) or more recently proposed RNA cleavage events[62, 63] are responsible for cell kill remain to be elucidated. Designing experiments to address these questions has been difficult due to our lack of understanding of metal homeostasis, of the interplay between iron and copper metabolism and of the DNA repair. Recent studies in yeast provide an excellent model system to design experiments to address both the role of the metal[64] and the importance of ssDNA and dsDNA repair processes in BLM's cytotoxicity.[65]

The recent user-friendly total synthesis from Boger's Lab,[39] coupled to the structural studies[28] and quantitative double-stranded cleavage assays[55] should open a new vista for examining the structure and function of the BLMs and to test the

proposed model that a single molecule of BLM effects dsDNA cleavage by reorganization involving its peptidal linker and/or the penultimate thiazolium ring. The basic principles learned from these studies could lead to design of more effective dsDNA cleavers.

References:

(1) Umezawa, H.; Maeda, K.; Takeuchi, T.; Okami, Y. *J. Antibiot.* **1966**, *19*, 200-209.

(2) (a) Sikic, B. I.; Rozencweig, M.; Carter, S. K. Ed., In *Bleomycin Chemotherapy*, Academic Press: Orlando, Florida, 1985. (b) Umezawa, H. in *Anticancer agents based on natural product models*; Cassady, J. M. Douros, J. Ed.; Academic Press, Inc., New York, 1980; Vol. pp 147-166. (c) Hecht, S. M. Ed., In *Bleomycin: Chemical, Biochemical, and Biological Aspects*; Springer-Verlag: New York, 1979.

(3) (a) Sausville, E. A.; Peisach, J.; Horwitz, S. B. *Biochem. Biophys. Res. Commun.* **1976**, *73*, 814-822. (b) Sausville, E. A.; Peisach, J.; Horwitz, S. B. *Biochemistry* **1978**, *17*, 2740-2746.

(4) (a) Povirk, L. F.; Wübker, W.; Köhnlein, W.; Hutchinson, F. *Nuleic. Acids Res.* **1977**, *4*, 3573-3580. (b) Mirabelli, C. K.; Huang, C.-H.; Crooke, S. T. *Cancer Res.* **1980**, *40*, 4173-4177. (c) Mirabelli, C. K.; Huang, C.-H.; Fenwick, R. G.; Crooke, S. T. *Antimicrob. Agents Chemother.* **1985**, *27*, 460-467. (d) Povirk, L. F.; Houlgrave, C. W. *Biochemistry* **1988**, *27*, 3850-3857. (e) Lloyd, R. S.; Haidle, C. W.; Hewitt, R. R. *Cancer Res.* **1978**, *38*, 3191-3196. (f) Lloyd, R. S.; Haidle, C. W.; Robberson, D. L. *Biochemistry* **1978**, *17*, 1890-1896. (g) Bradley, M. O.; Kohn, K. W. *Nucleic Acids Res.* **1979**, *7*, 793-804.

(5) (a) Demple, B.; Harrison, L. *Annu. Rev. Biochem.* **1994**, *63*, 915-948. (b) Brazilay, G.; Hickson, I. D. *BioEssays* **1995**, *17*, 713-719. (c) Bennett, R. A.; Swerdlow, P. S.; Povirk, L. F. *Biochemistry* **1993**, *32*, 3188-3195. (d) Tainer, J. A.; Thayer, M. M.; Cunningham, R. P. *Curr. Opin. in Struct. Biol.* **1995**, *5*, 20-26. (e) Lindahl, T.

Mutation Research **1990**, *238*, 305-311. (f) Hilbert, T. P.; Boorstein, R. J.; Kung, H. C.; Bolton, P. H.; Xing, D.; Cuningham, R. P.; Teebor, G. *Biochemistry* **1996**, *35*, 2505-2511.

(6) (a) Burger, R. M.; Peisach, J.; Horwitz, S. B. *J. Biol. Chem.* **1981**, *256*, 11636-11644. (b) Burger, R. M.; Kent, T. A.; Horwitz, S. B.; Münck, E.; Peisach, J. *J. Biol. Chem.* **1983**, *258*, 1559-1564.

(7) Kane, S. A.; Hecht, S. M. in *Progress in Nucleic Acid Research and Molecular Biology*; Cohn, W. E. Moldave, K. Ed.; Academic Press, San Diego, 1994; Vol. 49, pp 313-352.

(8) Stubbe, J.; Kozarich, J. W. *Chem. Rev.* **1987**, *87*, 1107-1136 and references therein.

(9) Umezawa, H.; Takita, T. in *Structure and Bonding*; Dunitz, J. D.; Hemmerich, P.; Jørgensen, C. K.; Reiner, D.; Goodenough, J. B.; Ibers, J. A.; Neilands, J. B. Williams, R. J. P. Ed.; Springer-Verlag, New York, 1980; Vol. 40, pp 73-99.

(10) Petering, D. H.; Byrnes, R. W.; Antholine, W. E. *Chem.-Biol. Interactions* **1990**, *73*, 133-182.

(11) Sam, J. W.; Tang, X.-J.; Peisach, J. *J. Am. Chem. Soc.* **1994**, *116*, 5250-5256.

(12) (a) Loeb, K. E.; Zaleski, J. M.; Westre, T. E.; Guajardo, R. J.; Mascharak, P. K.; Hedman, B.; Hodgson, K. O.; Solomon, E. I. *J. Am. Chem. Soc.* **1995**, *117*, 4545-4561. (b) Westre, T. E.; Loeb, K. E.; Zaleski, J. M.; Hedman, B.; Hodgson, K. O.; Solomon, E. I. *J. Am. Chem. Soc.* **1995**, *117*, 1309-1313. (c) Veselov, A.; Sun, H.; Sienkiewicz, A.; Taylor, H.; Burger, R. M.; Scholes, C. P. *J. Am. Chem. Soc.* **1995**, *117*, 7508-7512. (d) Burger, R. M.; Tian, G.; Drlica, K. *J. Am. Chem. Soc.* **1995**, *117*, 1167-1168. (e) Sam, J. W.; Tang, X.-J.; Magliozzo, R. S.; Peisach, J. *J. Am. Chem. Soc.* **1995**, *117*, 1012-1018.

(13) (a) McGall, G. H.; Rabow, L. E.; Ashley, G. W.; Wu, S. H.; Kozarich, J. W.; Stubbe, J. *J. Am. Chem. Soc.* **1992**, *114*, 4958-4967. (b) Rabow, L. E.; Stubbe, J.;

Kozarich, J. W. *J. Am. Chem. Soc.* **1990**, *112*, 3196-3203. (c) Rabow, L. E.; McGall, G. H.; Stubbe, J.; Kozarich, J. W. *J. Am. Chem. Soc.* **1990**, *112*, 3203-3208.

(14) Burger, R. M.; Drlica, K.; Birdsall, B. *J. Biol. Chem.* **1994**, *269*, 25978-25985.

(15) Wu, J. C.; Kozarich, J. W.; Stubbe, J. *J. Biol. Chem.* **1983**, *258*, 4694-4697.

(16) Worth, L. Jr.; Frank, B. L.; Christner, D. F.; Absalon, M. J.; Stubbe, J.; Kozarich, J. W. *Biochemistry* **1993**, *32*, 2601-2609.

(17) Kozarich, J. W.; Worth, L. Jr.; Frank, B. L.; Christner, D. F.; Vanderwall, D. E.; Stubbe, J. *Science* **1989**, *245*, 1396-1399.

(18) (a) Giese, B.; Beyrich-Graf, X.; Erdmann, P.; Petretta, M.; Schwitter, U. *Chem. & Biol.* **1995**, *2*, 367-375. (b) Giese, B.; Beyrich-Graf, X.; Erdmann, P.; Giraud, L.; Imwinkelried, P.; Muller, S. N.; Schwitter, U. *J. Am. Chem. Soc.* **1995**, *117*, 6146-6147. (c) Giese, B.; Erdmann, P.; Giraud, L.; Göbel, T.; Petretta, M.; Schäfer, T. *Tetahedron Lett.* **1994**, *35*, 2683-2686.

(19) (a) von Sonntag, C.; Hagen, U.; Schön-Bopp, A.; Schulte-Frohlinde, D. *Adv. Radiat. Biol* **1981**, *9*, 109. (b) Behrens, G.; Koltzenburg, G.; Ritter, A.; Schulte-Frohlinde, D. *Int. J. Radiat. Biol. Relat. Stud. Phys. Chem. Med.* **1978**, *33*, 163.

(20) D'Andrea, A. D.; Haseltine, W. A. *Proc. Natl. Acad. Sci. USA* **1978**, *75*, 3608-3612.

(21) Takeshita, M.; Grollman, A. P.; Ohtsubo, E.; Ohtsubo, H. *Proc. Natl. Acad. Sci. USA* **1978**, *75*, 5983-5987.

(22) Kuwahara, J.; Sugiura, Y. *Proc. Natl. Acad. Sci. U.S.A.* **1988**, *85*, 2459-2463.

(23) (a) Bailly, C.; Waring, M. J. *J. Am. Chem. Soc.* **1995**, *117*, 7311-7316. (b) Bailly, C.; Kénani, A.; Waring, M. J. *FEBS lett.* **1995**, *372*, 144-147.

(24) Gamcsik, M. P.; Glickson, J. D.; Zon, G. *J. Biomol. Struct. Dyn.* **1990**, *7*, 1117-1133.

(25) Hiroaki, H.; Nakayama, T.; Ikehara, M.; Uesugi, S. *Chem. Pharm. Bull.* **1991**, *39*, 2780-2786.

(26) (a) Xu, R. X.; Nettesheim, D.; Otvos, J. D.; Petering, D. H. *Biochemistry* **1994**, *33*, 907-916. (b) Xu, R. X.; Antholine, W. E.; Petering, D. H. *J. Biol. Chem.* **1992**, *267*, 944-949. (c) Xu, R. X.; Antholine, W. E.; Petering, D. H. *J. Biol. Chem.* **1992**, *267*, 950-955. (d) Otvos, J. D.; Antholine, W. E.; Wehrli, S.; Petering, D. H. *Biochemistry* **1996**, *35*, 1458-1465. (e) Mao, Q.; Fulmer, P.; Li, W.; DeRose, E. F.; Petering, D. H. *J. Biol. Chem.* **1996**, *271*, 6185-6191.

(27) (a) Manderville, R. A.; Ellena, J. F.; Hecht, S. M. *J. Am. Chem. Soc.* **1995**, *117*, 7891-7903. (b) Manderville, R. A.; Ellena, J. F.; Hecht, S. M. *J. Am. Chem. Soc.* **1994**, *116*, 10851-10852.

(28) (a) Wu, W.; Vanderwall, D. E.; Lui, S. M.; Tang, X.-J.; Turner, C. J.; Kozarich, J. W.; Stubbe, J. *J. Am. Chem. Soc.* **1996**, *118*, 1268-1280. (b) Wu, W.; Vanderwall, D. E.; Turner, C. J.; Kozarich, J. W.; Stubbe, J. *J. Am. Chem. Soc.* **1996**, *118*, 1281-1294. (c) Wu, W.; Vanderwall, D. E.; Stubbe, J.; Kozarich, J. W.; Turner, C. J. *J. Am. Chem. Soc.* **1994**, *116*, 10843-10844.

(29) (a) Oppenheimer, N. J.; Rodriguez, L. O.; Hecht, S. M. *Proc. Natl. Acad. Sci. USA* **1979**, *76*, 5616-5620. (b) Oppenheimer, N. J.; Rodrigues, L. O.; Hecht, S. M. *Biochemsitry* **1979**, *18*, 3439-3445. (c) Sugiyama, H.; Kilkuskie, R. E.; Chang, L.-H.; Ma, L.-T.; Hecht, S. M.; van der Marel, G.; van Boom, J. H. *J. Am. Chem. Soc.* **1986**, *108*, 3852-3854.

(30) (a) Akkerman, M. A. J.; Haasnoot, C. A. G.; Hilbers, C. W. *Eur. J. Biochem.* **1988**, *173*, 211-225. (b) Akkerman, M. A. J.; Neijman, E. W. J. F.; Wijmenga, S. S.; Hilbers, C. W.; Bermel, W. *J. Am. Chem. Soc.* **1990**, *112*, 7462-7474.

(31) Recent studies by Otvos et al.[26d] using ^{113}Cd NMR, ^{113}Cd-^{13}C coupling constants, and ^{13}C line width analysis reveal that CdBLM undergoes ligand reorganization between 5-54 °C. Temperature dependence of ^{13}C line widths are also observed with ZnBLM. In light of this work and recent crystallographic evidence of a trigonal-bipyramidal structure of a ZnBLM model compound

(Kurosaki, H.; Hayashi, K.; Ishikawa, Y.; Goto, M. *Chem. Lett.* **1995**, *8*, 691-692.), the ligand coordination and exchange behavior in ZnBLM needs to be reinvestigated.

(32) (a) Chang, C.-H.; Dallas, J. L.; Meares, C. F. *Biochem. Biophys. Res. Commn.* **1983**, *110*, 959-966. (b) Chang, C.-H.; Meares, C. F. *Biochemistry* **1982**, *21*, 6332-6334. (c) Chang, C.-H.; Meares, C. F. *Biochemistry* **1984**, *23*, 2268-2274.

(33) (a) Dabrowiak, J. C. *J. Inorg. Chem.* **1980**, *13*, 312-337. (b) Dabrowiak, J. C. in *Adv. Inorganic Biochemistry*; Eichhorn, G. L. Marzilli, L. G. Ed.; Elsevier Biomedical, New York, 1982; Vol. 4, pp 69-113. (c) Dabrowiak, J. C.; Tsukayama, M. *J. Am. Chem. Soc.* **1981**, *103*, 7543-7550.

(34) (a) McLean, M. J.; Dar, A.; Waring, M. J. *J. Mol. Recognit.* **1989**, *1*, 184-192. (b) Nightingale, K. P.; Fox, K. R. *Eur. J. Biochem.* **1994**, *220*, 173-181.

(35) Saito, I.; Morii, T.; Sugiyama, H.; Matsura, T.; Meares, C. F.; Hecht, S. M. *J. Am. Chem. Soc.* **1989**, *111*, 2307-2308.

(36) Tan, J. D.; Hudson, S. E.; Brown, S. J.; Olmstead, M. M.; Mascharak, P. K. *J. Am. Chem. Soc.* **1992**, *114*, 3841-3853.

(37) (a) Pseudotetrapeptide A includes A, P, H, V, moieties of BLM in Figure 1.1; PMA is 2-((N-(aminoethyl)amino)methyl)-4-(N-(2-(4-imidazolyl)-ethyl)carbamoyl)-5-bromopyrimidine. (b) Although neither of these compounds possesses a carbamoyl ligand, these studies substantiate the feasibility of the primary amine as an axial ligand to the cobalt. In addition, to our knowledge, no crystallograpic examples have been reported in which a carbamoyl group serves as an axial ligand to cobalt.

(38) Sugiyama, T.; Ohno, M.; Shibasaki, M.; Otsuka, M.; Sugiura, Y.; Kobayashi, S.; Maeda, K. *Heterocycles* **1994**, *37*, 275-282.

(39) (a) Boger, D. L.; Colletti, S. L.; Honda, T.; Menezes, R. F. *J. Am. Chem. Soc.* **1994**, *116*, 5607-5618. (b) Boger, D. L.; Honda, T.; Dand, Q. *J. Am. Chem. Soc.* **1994**, *116*, 5619-5630. (c) Boger, D. L.; Honda, T.; Menezes, R. F.; Colletti, S. L. *J. Am. Chem.*

Soc. **1994**, *116*, 5631-5646. (d) Boger, D. L.; Honda, T. *J. Am. Chem. Soc.* **1994**, *116*, 5647-5656. (e) Boger, D. L.; Teramoto, S.; Honda, T.; Zhou, J. *J. Am. Chem. Soc.* **1995**, *117*, 7338-7343. (f) Boger, D. L.; Teramoto, S.; Zhou, J. *J. Am. Chem. Soc.* **1995**, *117*, 7344-7356. (g) Boger, D. L.; Colletti, S. L.; Teramoto, S.; Ramsey, T. M.; Zhou, J. *Bioorg. Med. Chem.* **1995**, 3, 1281-1295.

(40) Booth, T. E.; Sakai, T. T.; Glickson, J. D. *Biochemistry* **1983**, *22*, 4211-4217.

(41) Fisher, L. M.; Kuroda, R.; Sakai, T. T. *Biochemistry* **1985**, *24*, 3199-3207.

(42) Povirk, L. F.; Hogan, M.; Dattagupta, N. *Biochemistry* **1979**, *18*, 96-101.

(43) Huang, C.; Galvan, L.; Crooke, S. T. *Biochemistry* **1980**, *19*, 1761-1767.

(44) Chen, D. M.; Sakai, T. T.; Glickson, J. D.; Patel, D. J. *Biochem. Biophys. Res. Commun.* **1980**, *89*, 534-541.

(45) Takeshita, M.; Kappen, L. S.; Grollman, A. P.; Eisenberg, M.; Goldberg, I. H. *Biochemistry* **1982**, *20*, 7599-7606.

(46) (a) Kross, J.; Henner, D.; Hecht, S. M.; Haseltine, W. A. *Biochemistry* **1982**, *21*, 4310-4318. (b) Kane, S. A.; Hecht, S. M.; Sun, J.-S.; Garestier, T.; Héléne, C. *Biochemistry* **1995**, *34*, 16715-16724.

(47) (a) Fox, K. R.; Grigg, G. W. *Nucleic Acids Res.* **1988**, *16*, 2063-2075. (b) Nightingale, K. P.; Fox, K. R. *Biochem. J.* **1992**, *284*, 929-934.

(48) Hamamichi, N.; Natrajan, A.; Hecht, S. M. *J. Am. Chem. Soc.* **1992**, *114*, 6278-6291.

(49) (a) Morii, T.; Matsuura, T.; Saito, I.; Kuwahara, J.; Sugiura, Y. *J. Am. Chem. Soc.* **1986**, *108*, 7089-7094. (b) Morii, T.; Matsuura, T.; Kuwahara, J.; Sugiura, Y. *J. Am. Chem. Soc.* **1987**, *109*, 938-939

(50) Williams, L. D.; Goldberg, I. H. *Biochemistry* **1988**, *27*, 3004-3011.

(51) Our unpublished results indicate that III binds to d(CCAGGCCTGG) by intercalation of the bithiazole tail 3' to the cleavage site (C). Recent studies of Mao et al. have reported the studies with II and III and d(GGAAGCTTCC).[26e] Their

preliminary NMR studies reveal a binding mode for II similar to what we have reported,[28b] although their assignment of the exchangeable proton at 10.22 ppm to a proton of the amino group of G5 is perhaps incorrect.[28b] However their studies with III contrast with our results indicate that III is in rapid exchange on the NMR time scale with no detectable intermolecular NOEs between the bithiazole tail and the oligonucleotide.[26e] The reasons for the differences with III remain to be explained.

(52) English, A. M.; Tsaprailis, G. *Adv. Inorg. Chem.* **1995**, 43, 79.

(53) Dickerson, R. E. in *Mechanism of DNA Damage and Repair: Implications for Carcinogenesis and Risk Assessment Basic Life Sciences*; Smi, M. G. Grossman, L. Ed.; Plenum, New York, 1986; Vol. 38, pp 245-255.

(54) Nakamura, M.; Peisach, J. *J. Antibiot.* **1988**, *41*, 638-647.

(55) (a) Absalon, M. J.; Stubbe, J.; Kozarich, J. W. *Biochemistry* **1995**, *34*, 2065-2075. (b) Absalon, M. J.; Wu, W.; Stubbe, J.; Kozarich, J. W. *Biochemistry* **1995**, *34*, 2076-2086. (c) Absalon, M. J., Ph.D. Thesis, Massachusetts Institute of Technology, 1994.

(56) Sugiyama, H.; Kawabata, H.; Fujiwara, D., Y.; Saito, I. *J. Am. Chem. Soc.* **1990**, *112*, 5252-5257.

(57) Smith, B. L.; Bauer, G. B.; Povirk, L. F. *J. Biol. Chem.* **1994**, *269*, 30587-30594.

(58) (a) Povirk, L. F.; Han, Y.-H.; Steighner, R. J. *Biochemistry* **1989**, *28*, 5808-5814. (b) Steighner, R. J.; Povirk, L. F. *Proc. Natl. Acad. Sci. USA* **1990**, *87*, 8350-8354.

(59) Keller, T. J.; Oppenheimer, N. J. *J. Biol. Chem.* **1987**, *262*, 15144-15150.

(60) Mirabelli, C. K.; Ting, A.; Huang, C.-H.; Mong, S.; Crooke, S. T. *Cancer Res.* **1982**, *42*, 2779-2785.

(61) Povirk has reported dsDNA cleavage at 5'-GPyNPuC-3' site. With the binding mode shown in Figure 1.5, a single molecule of BLM could not catalyze this cleavage.

(62) Magliozzo, R. S.; Peisach, J.; Ciriolo, M. R. *Mol. Pharmacol.* **1989**, *35*, 428-432.

(63) (a) Hecht, S. M. *Bioconjugate Chem.* **1994**, *5*, 513-526. (b) Keck, M. V.; Hecht, S. M. *Biochemisry* **1995**, *34*, 12029-12037.

(64) Klausner, R. D.; Dancis, A. *FEBS Lett.* **1994**, *335*, 109-133.

(65) Hays, S. L.; Firmenich, A. A.; Berg, P. *Proc. Natl. Acad. Sci. USA* **1995**, *92*, 6925-6929.

Chapter 2: Studies of Co•Bleomycin A2 green: Its Detailed Structural Characterization by NMR and Molecular Modeling, and its Sequence-Specific Interaction with DNA Oligonucleotides

Introduction

Since the discovery of bleomycins (BLMs) by Umezawa and coworkers and their recognition as antitumor agents,[1] much effort has been focused on understanding the basis for their therapeutic efficacy and their side effects.[2] Seminal experiments by Peisach and Horwitz and their coworkers[3] revealed that two cofactors, a metal and O_2, are required for the BLMs to degrade double stranded (ds)-DNA, the presumed therapeutic target. Recent studies have also shown that unusual tertiary structures of RNA as well as RNA/DNA hybrids are susceptible to degradation by metallo-BLMs.[4] While the mechanisms of degradation of DNA by the BLMs are understood at a moderately detailed molecular level,[5, 6] the structural basis for the molecular recognition responsible for the observed sequence specificity of this cleavage has yet to achieve a comparable level of resolution.

The observation that BLM cleaves DNA by specific 4'-hydrogen atom abstraction supports the hypothesis that the metal binding domain (Figure 2.1) interacts specifically within the minor groove.[7] This model is further corroborated by the observations that reagents known to specifically block, covalently or noncovalently, the minor groove, such as anthramycin and distamycin, inhibit BLM mediated DNA degradation.[8, 9] Furthermore, studies of Kuwahara and Sugiura using homopolymers of poly dG•poly dC and poly dI•poly dC show significantly reduced binding in the latter case, supporting the importance of the 2-amino group of guanine in the minor groove in a position 5' to the cleavage site.[9] Recent cleavage studies using sequence specific incorporation of deoxyinosine into defined fragments of DNA also substantiate these earlier studies on homopolymers.[10]

On the other hand, major groove modifiers aflatoxin B (a guanine N-7 binder), 5-methylcytidines, and 5-(glucosyloxy)methyl groups, all seem to have

little effect on the ability of BLM to mediate DNA degradation.[11, 12, 13] However, the methylation of the N-6 moiety of adenosine, also in the major groove does perturb DNA cleavage.[13] The reasons for this are at present not known and the results contradict other studies with major groove binders.

Over the past decade, a variety of biophysical methods have been used to define the role of the bithiazole moiety of BLM in binding to DNA. Early studies of Porvirk et al.[14] monitoring the unwinding and lengthening of DNA upon binding of BLM provided the first experimental evidence for intercalation of the bithiazole rings (Figure 2.1). Results of other methods including NMR studies with poly (dA-dT), viscometric studies, and fluorescence quenching studies as a function of ionic strength have been interpreted to support multiple modes of binding including one involving partial intercalation of the bithiazole rings.[15] Very recent studies of Wu et al. on CoBLM A2 green binding to a d(CCAGGCCTGG), where C is the site of cleavage, have established unambiguously that the mode of binding is specific and involves partial intercalation.[16] Alternatively, recent studies of Manderville et al.[17] with ZnBLM and a defined oligomer have indicated multiple modes of binding including one involving binding of the bithiazole tail within the minor groove as originally proposed by Dickerson.[18] Thus, there is no consensus regarding the binding mode(s), although the bithiazole moiety clearly provides binding energy. That different metallo-BLMs in different sequence contexts have alternative binding modes cannot be excluded.

Recent studies from the Hecht laboratory using synthetic BLM congeners suggest that the sequence selectivity of cleavage is governed almost completely by the metal binding domain of BLM.[5] This hypothesis is supported by their studies using a series of demethylated and deglyclo BLM A2 analogs in which the bithiazole C-terminus was separated from the metal binding domain by

Figure 2.1: Structure of Bleomycin A2

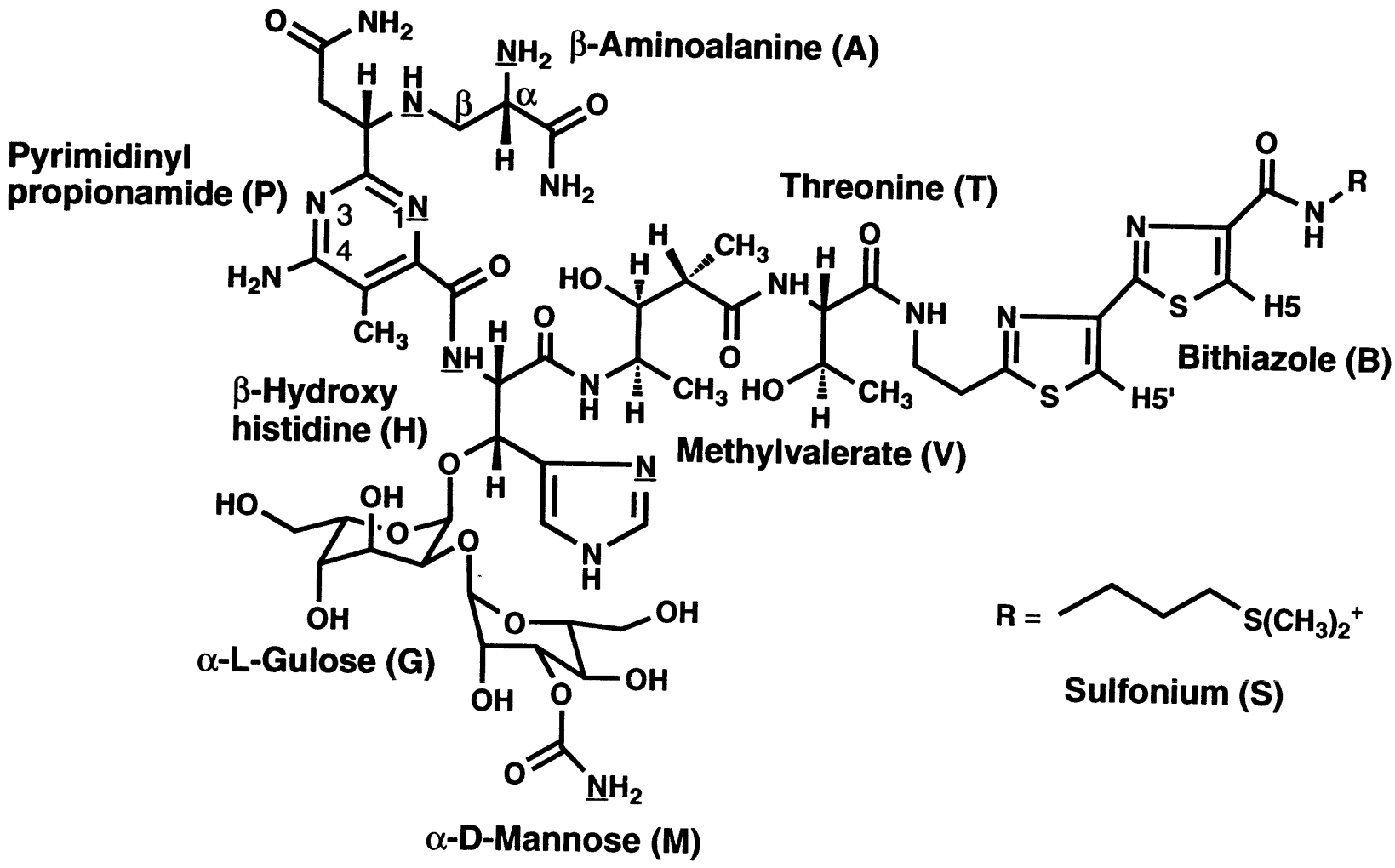
β-Aminoalanine (A)
Pyrimidinyl propionamide (P)
Threonine (T)
Bithiazole (B)
β-Hydroxy histidine (H)
Methylvalerate (V)
α-L-Gulose (G)
α-D-Mannose (M)
R = S(CH3)2+
Sulfonium (S)

replacing the threonine moiety (Figure 2.1) with oligomeric glycine spacers of different lengths (n=0, 1, 2, 4).[19] The specificity of the cleavage pattern with these analogs (n=1, 2 or 4) was very similar to the corresponding demethylated, deglyco BLM A2 itself, thus supporting the hypothesis that specificity is governed by the metal binding domain. This proposal is further supported by studies with phleomycin (PLE), a BLM analog in which the bithiazole moiety is replaced by a thiazolinylthiazole, that is, the penultimate thiazolium ring is reduced and non-planar (Figure 2.1). The sequence specificity of PLE, despite this altered structure, is almost identical to the that of BLM.[20] This observation has dampened the enthusiasm for the partial intercalative mode of binding of the bithiazole tail, and has been interpreted as strong support for the importance of the metal binding domain in specificity.

Perhaps the most dramatic evidence defining the importance of the metal binding domain in specificity is the remarkable claim of Mascharak and coworkers that a synthetic BLM analog (Fe^{2+}(PMA)Cl•MeOH) lacking the sugars, peptidyl linker, and bithiazole tail, also exhibits the same sequence selectivity as BLM, although cleavage requires much higher concentrations.[21] Studies of the Boger laboratory,[22] however, in which the metal binding domain (without the sugars) of BLM was assayed for cleavage specificity, revealed no cleavage. In addition, their studies with the metal binding domain containing the two sugars gave non-specific cleavage.[22] Furthermore, studies by Hecht and coworkers replacing each thiazolium ring with a methylthiol-like amino acid also showed non-specific cleavage.[23]

It is clear from the above summary that the basis for molecular recognition is in strong need of structural information provided by either X-ray crystallographic or NMR spectroscopic methods. We have determined, using NMR methods, the structure of CoBLM A2 green and its binding to the self-

complementary oligonucleotides d(CCAGGCCTGG) (1) and d(CCAGTACTGG) (2). This metallo-BLM was chosen as studies of Chang and Meares,[24] Saito et al.,[25] and McLean et al.,[26] and our own studies[27] have revealed a similar sequence selectivity for cleavage as that observed with FeBLM. Three additional considerations led us to the choice of CoBLM A2 green: the ligands are exchange inert, the complex itself is diamagnetic, and the stable Co-hydroperoxide (CoOOH) is an excellent model of activated BLM (FeOOH). Furthermore, cleavage mediated by CoBLM A2 green occurs only in the presence of light and its binding affinity for generic DNA has been reported to be ten times higher than the FeBLM.[24]

The utility of CoBLM A2 green as a model for activated BLM was also apparent to the Petering and Otvos laboratories.[28] In 1994, they reported chemical shift assignments of the mixture of CoBLM A2s (green and brown forms) using 2D NMR spectroscopic methods. Using their observed NOE constraints and molecular modeling, they described several structures of both the green (hydroperoxide as the sixth ligand) and brown (H_2O as the sixth ligand) forms of the CoBLMs which were consistent with their results. In both of the structures with CoBLM A2 green, their most interesting observation was that the bithiazole tail folded back, underneath and across the metal binding domain. In one structure the tail was on the same face as the putative hydroperoxide axial ligand (this is structure A in their nomenclature and will be defined as structure I subsequently). In the second structure, the tail was in a less energetically favorable conformation, on the opposite face from the hydroperoxide ligand (this is structure B in their nomenclature and will be defined here as structure III). At the time of their report, we had also completed a detailed 2D NMR study of CoBLM A2 green. In contrast to their report, in our hands the green form is stable for several months at room temperature and at neutral pH and is easily

isolable in excellent yields. We have, therefore, focused our efforts specifically on CoBLM A2 green.

This chapter and chapter 3 report the details of 2D NMR studies which have been used to obtain a structural model providing, for the first time, the definition of the role of the bithiazole tail in binding to DNA and the basis for specificity of cleavage at d(G-Py). In this chapter we report the detailed NMR studies of CoBLM A2 green which have allowed us to define unambiguously the screw sense of the ligand binding to the cobalt and the nature of the axial ligands.

The NMR assignment of the protons and carbons of CoBLM A2 green and the resulting structure by molecular modeling are just the first steps toward solving the structure of CoBLM A2 green with DNA. We also, therefore, report the studies of this CoBLM with two decameric self-complementary oligonucleotides: d(CCAGGCCTGG) and d(CCAGTACTGG), and show that cleavage occurs at a single pyrimidine (underlined) in each case. Fluorescent binding studies of the CoBLM A2 green to the decamers have allowed us to determine the K_ds for a single binding site in each oligomer. Finally, preliminary NMR titration studies with d(CCAGTACTGG) are presented, which suggest that the mode of binding of CoBLM A2 green to this oligomer is similar to that reported for d(CCAGGCCTGG) in detail in chapter 3.

Materials and Methods

Preparation of CoBLM A2 green. Blenoxane (15 units) provided by Bristol-Myers Company was dissolved in H_2O and the pH adjusted to 7 with dilute NaOH. $CoCl_2$ (1.1 equiv.) was then added to a rapidly stirred solution to ensure oxygenation, and the reaction was allowed to proceed for 2 h at room temperature. The mixture of products was separated using a semi-preparative

reverse phase Alltech Econosil C-18 column (10 μm) and the elution system of 0.1 M ammonium acetate (pH 6.8) as solvent A and acetonitrile as solvent B. The products were eluted at a flow rate of 3 mL/min using a linear gradient from 12 to 15 % A over 60 min. (Compound, Retention time in min): CoBLM A2 brown, 13; CoBLM A2 green, 19; CoBLM B2 brown, 27; CoBLM B2 green, 40. The lyophilized samples were redissolved in 50 mM sodium phosphate, pH 6.8, and stored at -80 °C.

Extinction Coefficient of CoBLM A2 green. The cobalt in the CoBLM A2 green was measured using a Varian AA-1475 Atomic Absorption Spectrophotometer with a Varian GTA-95 graphite tube atomizer using a lamp current of 7 mA and a λ of 240.7 nm. CoBLM A2 green (50 μL of a 10 μM solution) was diluted with 1 % (w/v) HNO_3 in a 5 mL volumetric flask and incubated for 12 h. A standard curve was prepared using a cobalt atomic absorption standard solution obtained from Aldrich which was diluted with 1 % HNO_3 to 0.03 to 0.17 μM in cobalt. In the case of both the standards and the CoBLM A2 green, the protocol involves ashing at 900°C for 40 s followed by atomization at 2300°C for 4 s. The procedure was a modification of one previously reported for the quantitation of vitamin B_{12}.[29] The extinction coefficient was redetermined for vitamin B_{12} as a control. The extinction coefficient was $2.1 \pm 0.2 \times 10^4$ $M^{-1}cm^{-1}$ at 290 nm for CoBLM A2 green.

Characterization of CoBLM A2 green by Electrospray Mass Spectrometry. All mass spectra were obtained using an PE-SCIEX API III triple quadruple mass spectrometer (SCIEX, Thornhill, ON, Canada) equipped with an ionspray (pneumatically assisted electrospray) interface. A Macintosh computer was used for instrument control, data acquisition and data processing. The CoBLM A2

green samples in deionized H_2O were introduced directly into the mass spectrometer at a flow rate of 2 μL/min using a syringe pump. Typically, mass scans were performed with a step size of 0.05 to 0.1 Da and a dwell time per step of 0.5 to 1 ms. Ten scans were usually accumulated to yield a mass spectrum. A mass spectrum with unit mass resolution (peak width of 1 Da) was first acquired for each sample to give a representative profile, then the resolution of the spectrometer was tuned to give a peak width of 0.3 to 0.5 Da (full width at half maximum) across the mass range of interest, so that the doubly charged and triply charged species could be identified unambiguously.

Purification of d(CCAGGCCTGG) (1) and d(CCAGTACTGG) (2).

Oligonucleotides **1** and **2** were synthesized on a 10 μmol scale at the MIT Biopolymer Laboratory. These oligomers with 5'-dimethoxytrityl (DMT) group retained were purified on a semipreparative reverse-phase C-18 HPLC column using a linear triethylammonium acetate (pH 7.0)/acetonitrile gradient (10% MeCN to 40% MeCN in 60 min). Under these conditions, the oligomers eluted at 50 min. The oligomer was then detritylated with 80% acetic acid for 1 h followed by extractions with ether. After lyophilization to dryness, each oligomer was exchanged into sodium phosphate buffer (pH 6.8) in a microdialysis chamber (Bethesda Research Laboratories) equipped with a Spectra/Por® 6 (SPECTRUM®) membrane (1,000 mw cutoff). For the NMR experiments described subsequently, each oligonucleotide was lyophilized three times from 99.9% D_2O and finally dissolved in 99.996% D_2O. For experiments in H_2O, the lyophilized material was dissolved in 90% H_2O/10% D_2O. A typical DNA NMR sample contained 2 mM of duplex in 50 mM sodium phosphate buffer (pH 6.8). Similar lyophilization procedures were carried out on CoBLM A2 green and the

final lyophilized product was redissolved in 99.996% D_2O at a final concentration of 2 to 5 mM.

Cleavage of 1 and 2 by CoBLM A2 green. Oligomers **1** and **2** with the protecting groups removed were obtained from the MIT Biopolymer Laboratory. ^{32}P labeling of **1** and **2** on their 5'-ends was accomplished using T4 polynucleotide kinase and [γ-^{32}P] ATP purchased from New England Nuclear/Dupont. Labeled oligomer was separated from the unincorporated ^{32}P using a NENSORB-20 column (Dupont New England Nuclear).

Cleavage reactions were carried out in 80 μL containing 50 μM (in duplex) of unlabeled oligomer **1** (or **2**), and ~5 μM of ^{32}P-**1** (or **2**), 500 μM of sodium phosphate buffer pH 7.0 and 50 to 200 μM CoBLM A2 green. Two control reactions (without UV light irradiation or without CoBLM) were also carried out. Each reaction mixture was transferred to a 6 mm x 50 mm Kimble borosilicate glass culture tube, which was suspended from a copper wire in the center of a Rayonet photochemical reactor and irradiated at 350 nm for 10 min in a 4 °C cold room (The temperature in the center of the reactor was 20 °C). After the completion of irradiation, the DNA was isolated by making the solution 0.3 M in NaOAc and the adding of 4 volumes of ethanol. The mixture was placed on dry ice for 20 min and the precipitated DNA isolated. The DNA pellets were then suspended in 100 μL of 10 % piperidine at 90 °C for 10 min. The solution was cooled and subjected to a second ethanol precipitation. The recovered DNA pellets were suspended in the gel loading buffer (0.1 % w/v bromophenol blue and 0.1 % xylene cyanol) and loaded onto a 20% denaturing polyacrylamide sequencing gel (19:1 crosslink, 43 cm x 38 cm x 0.4 mm). The gel was run for 2 h at 90 w (constant power). The radioactivity was visualized using a Molecular Dynamics Phosphorimager with Image-Quant software (version 3).

Titration of CoBLM A2 green with 1 and 2. The CoBLM A2 green concentration was determined optically ($\varepsilon = 2.1 \times 10^4\ M^{-1}cm^{-1}$) as described above. Absorbances of the duplexes **1** and **2** were measured at 260 nm and their concentrations were determined from their calculated extinction coefficients $\varepsilon = 1.0 \times 10^5\ M^{-1}cm^{-1}$ and $\varepsilon = 1.2 \times 10^5\ M^{-1}cm^{-1}$, respectively.[30] Various aliquots of CoBLM A2 green (0-1 equiv.) were added to the solution of duplex in D_2O and the complex formation was followed by monitoring the changes in the 1D ^1H NMR spectrum.

Determination of the Number of Binding Sites and K_ds of CoBLM A2 green to 1 and 2 Monitoring the Fluorescence Changes. The binding parameters were obtained from the fluorescence measurements by methods analogous to those previously described by Chien et al.[31] and Chang and Meares.[24] Fluorescence intensities were measured at 353 nm on a Perkin-Elmer Fluorometer (LS 50) at 20°C with excitation at 300 nm. Conditions were chosen so that each set of experiments covered as wide a range of percent-bound CoBLM as practical. A minimum of 1 μM CoBLM A2 green was needed for an adequate fluorescence intensity measurement. The K_ds are subject to some uncertainty since they were determined using μM solutions of CoBLM and are on the order of 10^{-7} M.

NMR Experiments. All 1D NMR spectra were recorded on a Varian VXR 500 MHz instrument, or a home-built 500 MHz instrument in Francis Bitter Magnet Laboratory, and data were transferred to a Silicon Graphics XS24 workstation, and processed using Felix software (version 2.3, Biosym Technologies, Inc.). ^1H and ^{13}C chemical shifts are referenced to an internal standard, sodium 3-(trimethylsilyl)-1-propanesulfonate (TSP) at 0.00 ppm.

2D NOESY (100, 200, 400 ms mixing times), P.E. COSY, and TOCSY (MLEV-17 spin lock pulse with 35 and 70 ms mixing times) experiments on CoBLM A2 green in D_2O or 90 % H_2O/10 % D_2O were recorded at 5 °C. During the relaxation delay period the HDO solvent signal was selectively irradiated for 1.5 s. 2D NOESY experiments with a Jump and Return pulse sequence[32] were also collected at 100 and 200 ms mixing times. Data sets with 4096 complex points in t_2 and 512 complex points in t_1 were acquired with 5500 Hz sweep widths in both dimensions and 32 scans per t_1 increment. The t_1 dimension was zero-filled to 4096 data points. Spectra were processed with a combination of exponential and gaussian weighting functions. Ridges in t_1 were reduced by multiplying the first point in t_1 by one half prior to the Fourier transform. Baselines were corrected with a polynomial or an automatic baseline correction routine in t_2 when necessary.

HMQC[33] (J_{C-H} set at 135, 165 or 195 Hz) and HMBC[34] (τ=60 or 80 ms) experiments on CoBLM A2 green were recorded at 5 °C. During the relaxation delay period, the HDO solvent signal was selectively irradiated for 1.0 s. For the HMQC experiment, data sets with 2048 x 256 complex points were acquired with 6000 Hz sweep width in the proton dimension and 25000 Hz in the carbon dimension. 128 scans were collected per t_1 increment. For the HMBC experiments, data sets with 4096 x 256 complex points were acquired with the same sweep widths as in the HMQC experiments. 64 scans were collected per t_1 increment. HMQC and HMBC spectra were processed with exponential weighting functions.

Molecular Modeling of CoBLM A2 green. All calculations were carried out with Quanta 4.0/CHARMm 22 (Molecular Simulations Inc.; Waltham, MA) on a Silicon Graphics 4D/35 or Indigo. Non-bonded van der Waals interaction was

cut-off at 11.5 Å, using a cubic switching function between 9.5 and 10.5 Å. The distance-dependent dielectric constant algorithm in the CHARMm package was used. Non-bonded term was updated every 20 steps. The terms for electrostatic interactions and hydrogen bonds were not included in any calculations. The SHAKE algorithm[35] was used to fix all bond lengths to hydrogen atoms. Molecular dynamics calculations used the Verlet algorithm, with a .001 ps time step, and scaling every 100 steps. During molecular dynamics calculations, all force constants for bond distance and angles were set at 1000 kcal mol^{-1} $Å^{-2}$ and 500 kcal mol^{-1} rad^{-2}, respectively. All energy minimizations used the standard CHARMm potential.[36] Distance constraints were applied using a square well potential and dihedral constraints were applied using a simple harmonic function.

Bleomycin A2 was constructed in Chemnote. Bond lengths between nitrogen and cobalt were set at 1.956 Å for the primary amine (axial ligand), 1.996 Å for the secondary amine, 1.851 Å for the N1 of pyrimidine, 1.910 Å for the histidine amide nitrogen, and 1.923 Å for the $N\delta$ of the imidazole, based on the crystal structure of CoPMA-Cl.[37] The bond length for Co-O was set at 2.038 Å.[38] N-Co-N bond angles were set to 90°, and the axial N-Co-O (hydroperoxide) angle was set at 180°. Force constants of 288 kcal mol^{-1} $Å^{-2}$ for Co-N bond lengths, and 72 kcal mol^{-1} rad^{-2} for N-Co-N bond angles were derived from parameters used in the MM2 force field calculations on similar cobalt-N compounds.[39] A new CHARMm atom type was also created for a sulfonium sulfur atom. The parameters for bond lengths, bond angles, dihedral, and improper angles for the sulfur were determined by *ab initio* calculations using dimethylpropyl sufonium cation as a model for the BLM sulfonium tail. Geometry optimization was carried out using the 3-21G* basis set and the Moller-Plesset correction (MP2)

using Spartan (Wavefunction Inc., Irvine, CA). The charges for the CoBLM A2 green were determined using the template method of Quanta assuming a total charge of + 2.0 and smoothing over all atoms. Color figures were made using Setor.[40]

Sizes of NOEs were classified as strong, medium, or weak based on visual inspection of the NOESY spectra collected at 200 ms mixing time in D_2O and H_2O. NOE derived distance constraints with a force of 60 kcal mol^{-1} $Å^{-1}$ were set at 1.8-3.0 Å, 1.8-4.0 Å, and 1.8-5.0 Å for strong, medium, and weak NOEs, respectively. An additional 1 Å was added to the upper limit of the constraints on methyl or methylene hydrogen pseudoatoms. Coupling constants were measured in the 1D or 2D P.E. COSY spectra collected in D_2O and H_2O. A Karplus equation that considers the electronegativity of substituents[41] was used to derive dihedral angle constraints for the coupling constants not associated with the amide protons. Coupling constants involving amide protons were evaluated using the standard Karplus equation and the parameters of Hoch et al.[42] Because there is no evidence for any interaction between the sulfonium moiety of CoBLM A2 green and any other moiety within this molecule, dihedral constraints were used to maintain an extended conformation of this moiety.

Four models (vide infra), structure I, II, III, and IV of CoBLM A2 green (Figure 2.7), were used as starting structures for molecular dynamics simulated annealing calculations. The structures were first minimized with no constraints by the steepest descent method, followed by conjugate gradient minimization to a rms gradient < 0.1. The distance and dihedral constraints were then applied at 60 kcal mol^{-1} $Å^{-2}$, and 50 kcal mol^{-1} rad^{-2}, and the minimization steps were repeated. These structures were used in the molecular dynamics simulated annealing calculations. For each structure five calculations were run starting

with a different seed for the initial velocities. The structure was heated and equilibrated over 6 ps, from 5-1000 K in 10 K increments, with velocities assigned every 0.1 ps from a Gaussian approximation to the Maxwell-Boltzman distribution. No distance or dihedral angle constraints were used in this first step in order to randomize the structure prior to the application of the constraints. Molecular dynamics was then run for 4 ps with the distance constraints applied with a force constant of .06 kcal mol^{-1} $Å^{-2}$. Next, the force constants for the distance constraints were scaled to 120 kcal mol^{-1} $Å^{-2}$ over 7.6 ps, in a series of 0.4 ps molecular dynamics runs. The system was allowed to evolve for 6 ps, then cooled to 300 K over 7 ps. At 300 K the force constants of the distance constraints were reduced to the final value of 60 kcal mol^{-1} $Å^{-2}$. The dihedral constraints were then introduced with a force constant of 50 kcal mol^{-1} rad^{-2}, and the system was allowed to equilibrate for 4 ps, followed by the final 15 ps molecular dynamics run. The coordinates of the final 5 ps of the 15 ps molecular dynamics were averaged, and minimized by 1000 steps of conjugate gradient with distance and dihedral angle constraints.

Results and Discussion

Preparation and Characterization of CoBLM A2 green. CoBLM A2 green has been prepared by a modification of the procedure of Chang et al.[43] from $CoCl_2$ and blenoxane. The reaction is complete within two hours and the resulting products, hydroperoxide and aquo derivatives, are separated using reverse phase HPLC. CoBLM A2 green, the most efficient CoBLM mediator of DNA cleavage and a putative analog of activated BLM, was selected for examination in more detail. Given the time required for the acquisition of NMR

data, the stability of this congener was examined by both HPLC and 1D NMR spectroscopy (data not shown). Both studies revealed that over a period of several months, at 20°C and pH 7.0, that no change in the compound was detectable. These studies contrast with those reported by Xu et al.[44] for reasons that are at present not clear.

Recent studies of Sam et al. investigating the structure of activated BLM (FeOOH), suggested that an excellent way to characterize a peroxide ligand, the putative sixth ligand in CoBLM A2 green, is by use of electrospray mass spectrometry.[45] This method is sufficiently mild that the OOH ligand is not lost during the analysis. An electrospray mass spectrum of CoBLM A2 green is shown in Figure 2.2. It gives a m/z of 752.8 (calculated MW=1505.4, m/z=752.7) which indicates that the charge of this form of CoBLM is +2. This result suggests, given the assumption that the charge of CoBLM in solution is similar to that observed by mass spectrometry, that the histidine amide must be deprotonated and is consistent with the sixth ligand being $^{-}$OOH. However, the spectrum shows that the isotopic distribution differs from that calculated[46] (see inset in Figure 2.2). Why this species has a mass at 753.4, significantly larger than the expected 72% contribution calculated from isotopic distributions, is at present not clear. Despite this anomaly, these studies provide strong support for the proposal of Chang and Meares[43] that CoBLM A2 green contains a hydroperoxide ligand. The stability studies in conjunction with the mass spectrometric characterization thus suggest that CoBLM A2 green is an appropriate choice for characterization by NMR spectroscopic methods.

Choice of Oligonucleotides and Their Interactions with CoBLM A2 green. Several considerations led to the choice of oligomers to be used in NMR structural investigations. Self-complementary decameric oligonucleotides were

Figure 2.2: Electrospray mass spectrum of CoBLM A2 green. The inset shows the isotope distribution of the peak at m/z of 752.8.

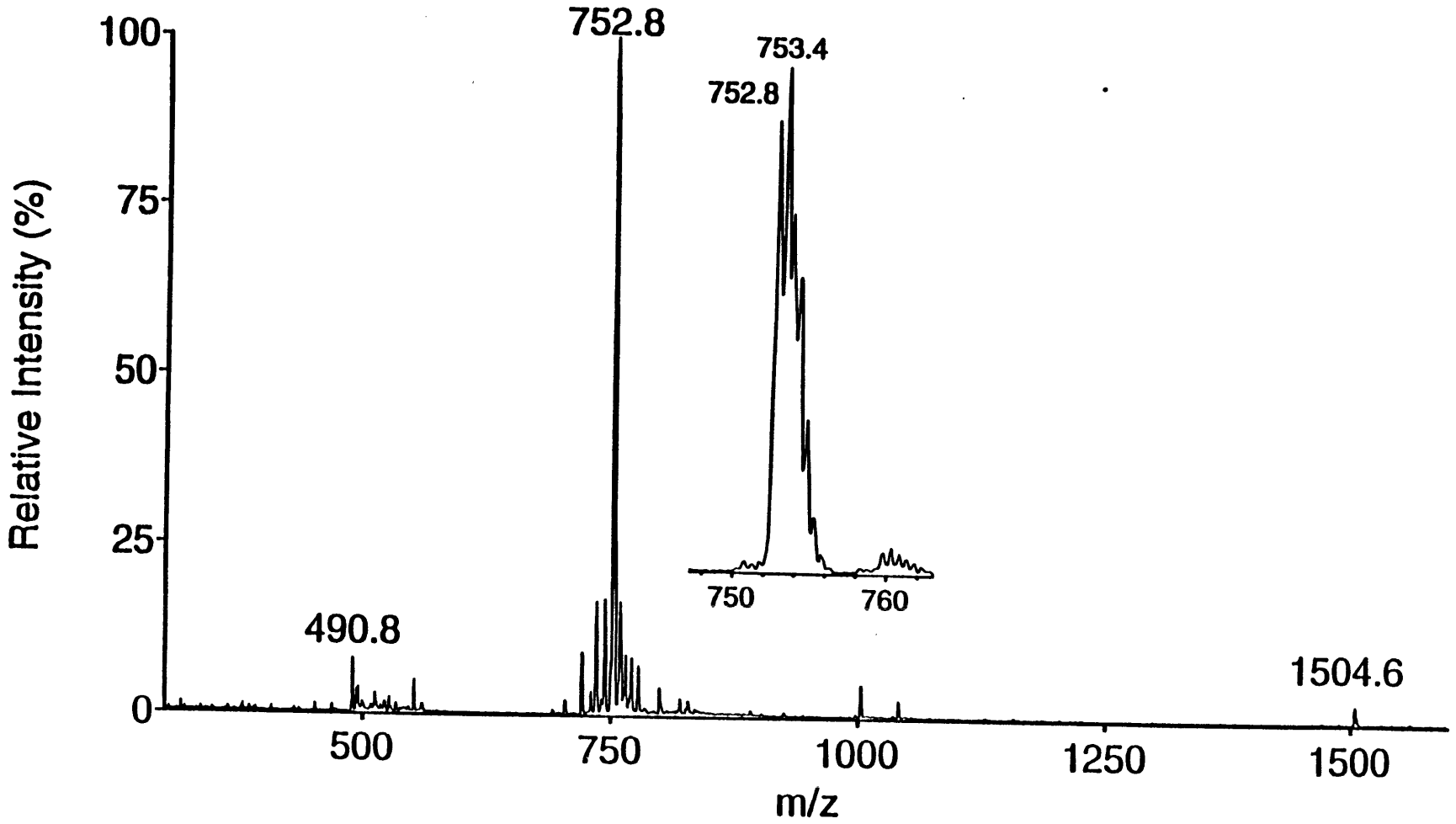
752.8
753.4
752.8
100
75
50
25
0
Relative Intensity (%)
490.8
750
760
1504.6
500
750
1000
1250
1500
m/z

chosen as the resulting duplexes were sufficiently stable to allow data acquisition at 20 °C. The sequences were also chosen to contain a single CoBLM binding site and a single cleavage site. In addition, the self-complementarity facilitates the assignments of the proton chemical shifts and the determination of whether a single CoBLM binding site was present during a titration with CoBLM monitored by 1D NMR spectroscopy.

Two oligomers, d(CCAGGCCTGG) (**1**) and d(CCAGTACTGG) (**2**) fulfilled these requirements. In both cases, when 5'-^{32}P-end labeled oligomer was incubated with CoBLM A2 green and subjected to light-mediated cleavage, a single major cleavage product subsequent to the piperidine treatment[27] was observed (Figure 2.3, cleavage shown for d(CCAGGCCTGG)). This major product persists even when the ratio of drug to oligomer is 4:1. These results and the fact that structural information was available on the duplex DNA alone,[47] solidified our choice of d(CCAGGCCTGG) for further investigation as described in chapter 3.[48]

In an effort to determine whether a single cleavage site is correlated with a single binding site, each oligomer was titrated with CoBLM A2 green and changes in fluorescence were monitored. Previous studies revealed that binding of FeBLM and CoBLM to generic DNA resulted in fluorescence quenching.[24, 31] A Scatchard analysis of the data (not shown) confirmed that both **1** and **2** appear to have a single CoBLM binding site with apparent K_ds on the order of 1.7×10^{-7} M and 1.5×10^{-7} M for d(CCAGGCCTGG) and d(CCAGTACTGG), respectively. These values are similar to one previously reported by Chang and Meares of ~ 10^{-7} M for generic calf thymus DNA at pH 8.0.[24]

Titration of CoBLM A2 green with d(CCAGTACTGG) (2): Recent studies of Absalon et al. have revealed that GTAC is a "hot spot" for double-stranded

Figure 2.3: Autoradiography of a 20% denaturing polyacrylamide gel showing single site cleavage by CoBLM A2 green on the 5′-^{32}P labeled-d(CCAGGCCTGG) (**1**). Lane 1-4 are controls. Lane 1: DNA without CoBLM but with UV light and with piperidine treatment. Lane 2: DNA with CoBLM but with no light and with piperidine treatment. Lane 3: same as Lane 1 but with no piperidine treatment. Lane 4: same as Lane 2 but with no piperidine treatment. Lane 5-7 are reactions with different ratios of CoBLM A2 green to DNA with UV light and piperidine treatment. Lane 5: 1:1 (CoBLM A2 green:DNA). Lane 6: 2:1 (CoBLM A2 green:DNA). Lane 7: 4:1 (CoBLM A2 green:DNA).

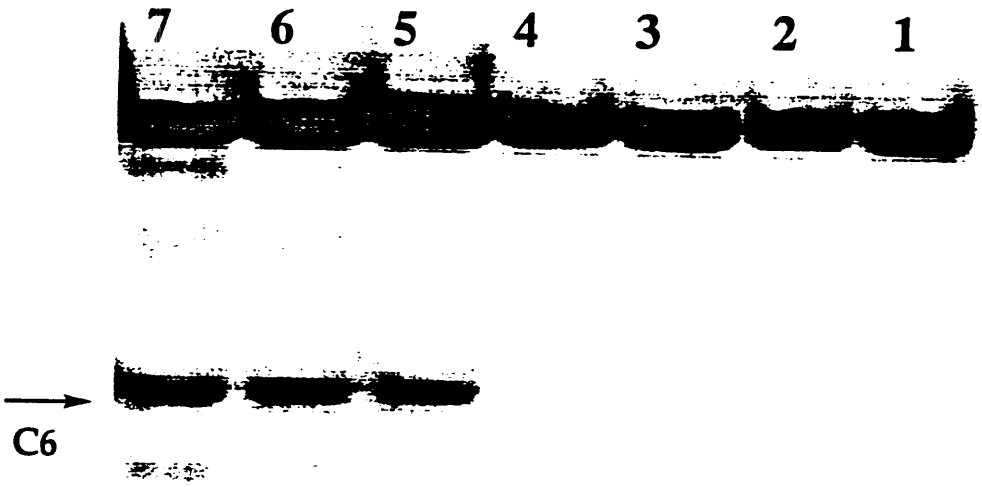
7
6
5
4
3
2
1
C6

Table 2.1: Comparison of Proton Chemical Shifts (ppm) of Apo and Metallo-BLMs Protons

		Apo [a] 297K pH 7	Zn [a] 277K pH 7	Fe [a] 277K pH 7	Co [b] 268K pH7.4	Co [c] 278 K pH 6.8	Protons		Apo [a] 297K pH 7	Zn [a] 277K pH 7	Fe [a] 277K pH 7	Co [b] 268K pH7.4	Co [c] 278K pH6.8
P	CαH	2.62	2.87	2.86	3.34	3.20	B	CαH'			3.12	3.26	3.25
	CαH'	2.69	3.24	3.08	3.52	3.51		CβH	3.60	3.51	3.35	3.45	3.44
	CβH	3.96	4.50	4.34	5.43	5.10		CβH'			3.51	3.86	3.83
	CH_3	2.01	2.38	2.24	2.47	2.46		C5H	8.20	8.21	8.11	8.14	8.17
	4-NH_2		7.02	6.91		7.73/7.94		C5'H	8.00	8.04	7.85	7.81	7.82
H	CαH	5.05	4.85	4.93	5.00	4.98		NH		8.36	8.33	8.62	8.57
	CβH	5.26	5.20	5.19	5.52	5.53	S	$C\alpha H_2$	3.38	3.36	3.31	3.42	3.36
	C2H	7.79	8.04	7.86	8.73	8.72		$C\beta H_2$	2.16	2.13	2.09	2.18	2.13
	C4H	7.26	7.31	7.23	7.59	7.60		CγH	3.60	3.57	3.53	3.62	3.51
A	CαH	3.84	3.72	3.76	3.38	3.41		CγH'	3.60	3.57	3.53	3.62	3.63
	CβH	2.83	2.46	2.42	2.72	2.74		$(CH_3)_2$	2.91	2.88	2.83	2.99	2.94
	CβH'	2.88	3.36	2.88	3.23	3.22		NH		8.94	8.90	9.04	8.66
	NH		4.32	5.38	6.01	6.01	G	C1H	5.25	5.30	5.26	5.38	5.35
V	αCH_3	1.10	0.98	1.03	0.62	0.62		C2H	4.01	4.06	4.03	4.13	4.11
	γCH_3	1.12	0.93	0.96	1.02	0.98		C3H	4.09	4.03	4.02	4.12	4.10
	CαH	2.45	1.95	2.36	0.95	0.94		C4H	3.84	3.71	3.72	3.83	3.80
	CβH	3.70	3.42	3.64	3.37	3.33		C5H	3.99	3.85	3.73	3.83	3.84
	CγH	3.86	3.62	3.58	3.51	3.50		C6H	3.40	3.61	3.60	3.76	3.70
	NH		7.55	7.75	8.92	8.89		C6H'	3.53	3.69	3.72		3.84
T	CH_3	1.08	1.02	0.99	1.22	1.19	M	C1H	4.99	4.89	4.89	4.94	4.93
	CαH	4.21	4.10	4.03	4.41	4.39		C2H	4.04	4.08	4.06	4.02	4.00
	CβH	4.08	4.00	3.93	4.27	4.25		C3H	4.68	4.03	4.14	4.00	4.05
	NH		7.96	8.20	8.97	8.92		C4H	3.78	3.67	3.61	3.88	3.78
B	CαH	3.24	3.16	3.08	3.07	3.06		C5H	3.78	3.70	3.73	3.89	3.73
								C6H	3.78	3.79	3.74	3.71	3.84
								C6H'	3.92	3.97	3.93		3.98

[a] Akkerman et al.[51] [b] Xu et al.[28] in phosphate buffer. [c] This study, 50 mM phosphate buffer; underlines indicate the chemical shifts difference greater than 0.05 ppm between b and c.

cleavage (at T) with the ratio of ss:ds cleavage being 3:1.[49] In order to determine whether the mode of binding at GT steps is the same as GC steps and to establish whether binding of CoBLM A2 green can be detected at both the primary and the secondary cleavage sites involved in ds cleavage, preliminary studies with **2** were carried out. A typical titration of CoBLM A2 green with **2**, analyzed by 1D NMR spectroscopy, is shown in Figure 2.4 (6.5 to 9.5 ppm). Several features suggest that the predominant species is a ~ 1:1 complex between CoBLM A2 green and **2**. The major complex is in slow exchange on the NMR time scale. In the free DNA (Figure 2.4a), two resonances at 8.24 and 8.26 ppm have been assigned to the H8 protons of A3 and A6, respectively. Upon addition of 0.5 equivalent of CoBLM A2 green (Figure 2.4b), these resonances diminish in intensity and four new resonances appear. Upon addition of 1 equivalent of CoBLM A2 green, the A-H8 protons of the free DNA have disappeared and the same four resonances have increased in intensity. Similarly in the upfield region of the NMR spectrum, between 0 and 3.5 ppm (data not shown), the CH_3 groups of T5 (1.38 ppm) and T8 (1.59 ppm) in free DNA decrease in magnitude upon addition of CoBLM, and four new methyl resonances at 1.57ppm (T8), 1.19 ppm (T15), 1.55 ppm (T18) and 1.45 ppm (T5) appear. In addition, the CH_3 group of the pyrimidine moiety in CoBLM (Figure 2.1) shifts downfield from 2.48 to 2.67 ppm. Finally, heteronuclear ^1H-^{13}C NMR experiments, discussed subsequently, reveal upfield shifts of the bithiazole H5 and H5' protons from 8.21 to 6.87 ppm and 7.87 to 7.04 ppm, respectively when CoBLM binds to the duplex (Figure 2.4). These observations are reminiscent of our previous studies with d(CCAGGCCTGG)[16] and suggest that the drug binds via partial intercalation of its bithiazole tail. In addition, a minor complex (Figure 2.4, resonances with *), accounting for 20 % of the total DNA, is also apparent.

Figure 2.4: Titration of d(CCAGTACTGG) (**2**) with CoBLM A2 green at 20°C. Downfield region of the ^{1}H NMR: CoBLM in 50 mM sodium phosphate (pH 6.8) and decameric duplex DNA (2.0 mM) in 50 mM sodium phosphate (pH 6.8) with 0, 0.5, and 1 equivalent of CoBLM added. Asterisks indicate the presence of a minor complex.

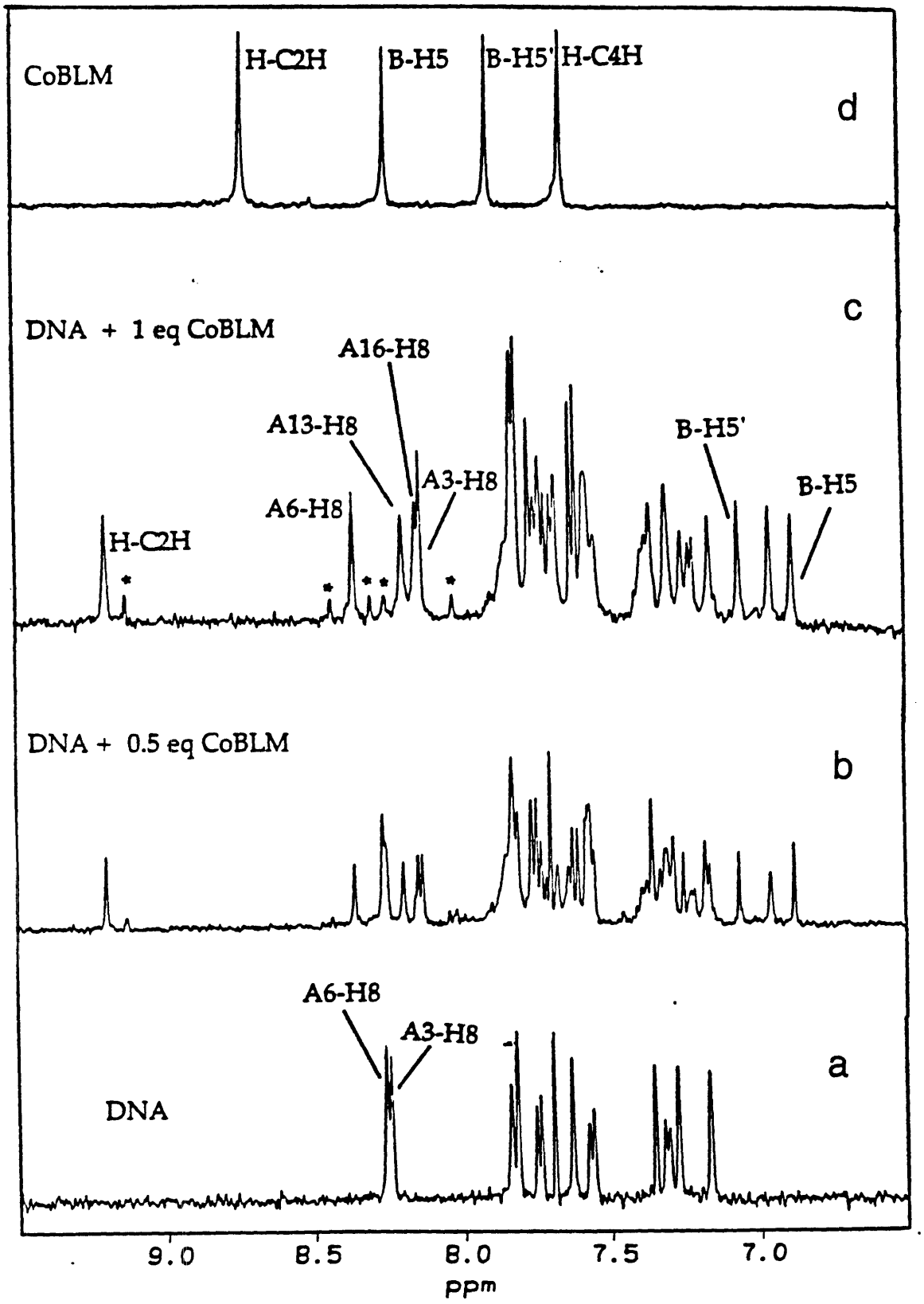
CoBLM
H-C2H
B-H5
B-H5'
H-C4H
d
DNA + 1 eq CoBLM
c
A16-H8
A13-H8
A3-H8
A6-H8
H-C2H
B-H5'
B-H5
DNA + 0.5 eq CoBLM
b
A6-H8
A3-H8
a
DNA
9.0
8.5
8.0
7.5
7.0
ppm

^{1}H and ^{13}C Assignments of CoBLM A2 green. The assignments of the ^{13}C chemical shifts of the bithiazole moiety of CoBLM A2 green and of the ^{1}H and ^{13}C chemical shifts of its sugars have played a key role in distinguishing between various models for the structure of CoBLM A2 green and its structure bound to DNA of defined sequence.[48] The strategy for proton assignments in CoBLM A2 green is similar to that previously reported by Akkerman et al. for the assignments of ZnBLM and FeBLM-CO.[50, 51] Furthermore, the proton assignments of a mixture of CoBLMs A2 (green and brown forms) were recently reported by Xu et al.[28] Our assignments of the proton chemical shifts of CoBLM A2 green at 5 °C, pH 6.8, are in most cases within ±0.05 ppm of those reported by Xu et al. at -5 °C, pH 7.4 (Table 2.1, differences are underlined). The availability of homogeneous CoBLM A2 green however, has allowed the assignment of all sugar proton resonances of gulose and mannose and all carbon resonances of CoBLM. This unique information has allowed us to define the chirality of the cobalt as well as the nature of the axial ligands of CoBLM A2 green.

Assignment of the Proton Chemical Shifts of Gulose and Mannose. Heteronuclear ^{1}H-^{13}C NMR methods, HMQC and HMBC, played an essential role in the completion of the sugar assignments. The HMQC spectrum allowed identification of the gulose and mannose anomeric C/H cross peaks, as the characteristic anomeric carbon chemical shifts between 80 ppm and 100 ppm are well separated from the rest of the sugar carbon resonances. The G-C1H can be distinguished from the M-C1H in the HMBC spectrum as two unique cross peaks are observed between the H-CβH and the G-C1, and between the H-Cβ and the G-C1H. With the chemical shifts of G-C1H and M-C1H established, the assignments of the G-C2H, M-C2H, M-C3H and the M-C4H are straightforward from the P. E. COSY spectrum (for M-C2H, M-C3H and M-C4H, see A and C,

Figure 2.5). The assignment of the M-C3H has proven to be an important piece of information for distinguishing between the structures of several alternative CoBLM A2 green isomers. Acquisition of the HMQC spectrum provided sufficient dispersion in the carbon dimension to spread out all the sugar C/H cross peaks for identification of the chemical shifts of the remaining protons. The H6 and H6' sugar protons are distinctive, as each C6 carbon exhibits cross peak patterns to two protons (see E, E' and F, F', Figure 2.6). Corroboratively, large COSY cross peaks are observed between these geminal methylene protons (see D and E, Figure 2.5). The M-C6 carbon can be distinguished from the G-C6 carbon by a cross peak in the HMBC spectrum between the carbon resonance at 63.5 ppm (M-C6) and the proton resonance at 3.78 ppm (M-C4H). The assignment of the M-C4H allowed the chemical shift assignment of M-C5H. The M-C4H in the HMBC spectrum shows a cross peak to the M-C5 at 77.0 ppm allowing the assignment of the M-C5H by the HMQC method. Thus, the assignments of the mannose carbon and proton chemical shifts are complete.

The assignments of the carbon and proton chemical shifts of C-3, 4, and 5 of gulose have been more problematic. The G-C/H3 chemical shifts were initially assigned from the HMQC spectrum (B , Figure 2.6, Table 2.2). The chemical shift of G-C3H (4.10 ppm) and its similarity to that of G-C2H (4.11 ppm) provides an explanation for the inability to detect connectivity in the P.E. COSY spectrum; it is too close to the diagonal (Figure 2.5). Further support for the assignment of G-C3 comes from its cross peak to G-C1H in the HMBC spectrum and from this assignment the G-C4H can be readily identified from the P.E. COSY spectrum (B, Figure 2.5). Identification of the G-C4H allowed the assignment of G-C4. Finally the only remaining unassigned carbon in the HMQC spectrum is G-C5, which then allowed the identification of the G-C5H. The G-C5H shows a cross peak

Figure 2.5: Expanded P.E. COSY spectrum of the sugar region in D_2O at 5 °C pH 6.8. Peak assignments are: A. M-C2H (4.00 ppm) to M-C3H (4.05 ppm); B. G-C3H (4.10 ppm) to G-C4H (3.80 ppm); C. M-C3H (4.05 ppm) to M-C4H (3.78 ppm); D. M-C6H (3.85 ppm) to M-C6H′ (3.98 ppm); E. G-C6H (3.71 ppm) to G-C6H′ (3.84 ppm).

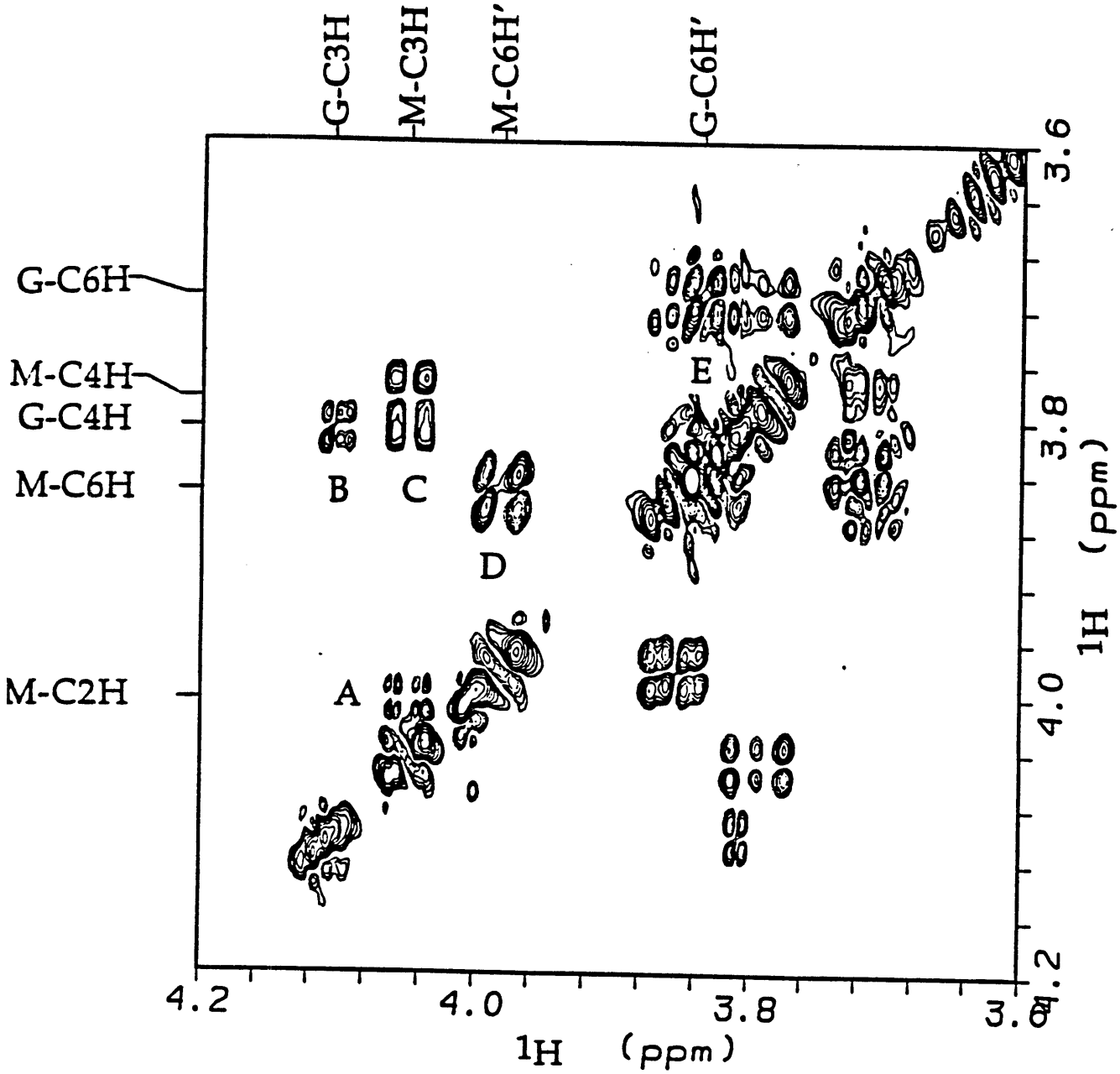
G-C3H
M-C3H
M-C6H'
G-C6H'
G-C6H
M-C4H
G-C4H
M-C6H
M-C2H
A
B
C
D
E
4.2
4.0
3.8
3.6
1H (ppm)

Figure 2.6: Expanded HMQC spectrum of the sugar region in D_2O at 5 °C pH 6.8. Peak assignments (proton chemical shift in ppm, carbon chemical shift in ppm) are: A. G-2 (4.11, 69.9); B. G-3 (4.10, 68.4); C. M-3 (4.05, 77.6); D. M-2 (4.00, 70.3); E and E'. M-6 (3.85/3.98, 63.5); F and F'. G-6 (3.71/3.84, 63.9); G. M-4 (3.78, 66.7); H. G-5 (3.84, 70.8); I. G-4 (3.80, 71.8); J. M-5 (3.84, 70.8).

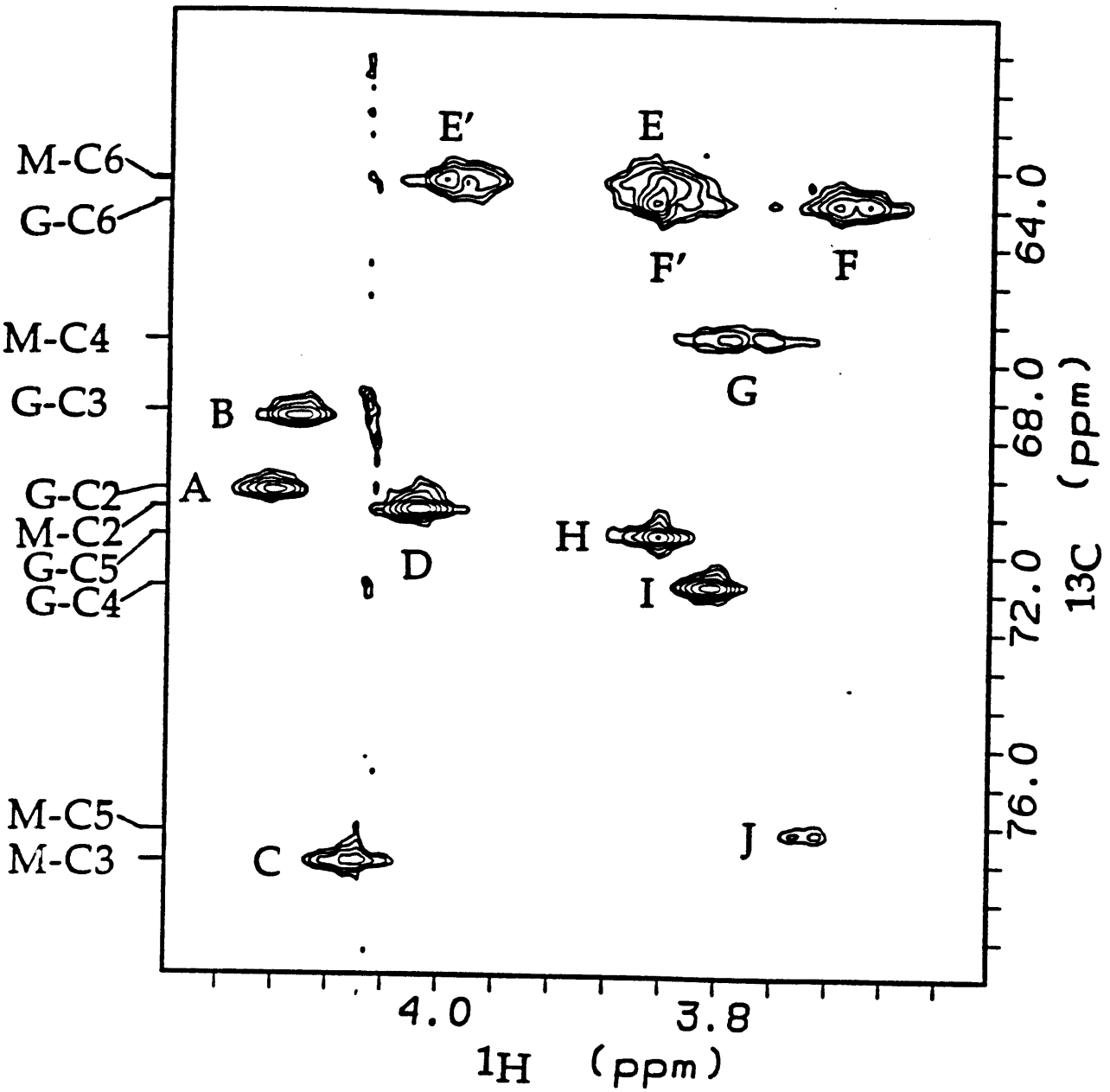
M-C6
G-C6
M-C4
G-C3
G-C2
M-C2
G-C5
G-C4
M-C5
M-C3
E′
E
F′
F
G
B
A
D
H
I
C
J
64.0
68.0
72.0
76.0
13C (ppm)
4.0
3.8
1H (ppm)

Table 2.2: Comparison of Carbon Chemical Shifts (ppm) of Apo and Metallo-BLMs.

Carbons		Apo [a] 297K pH 7	Zn [a] 277K pH 7	Fe [a] 277K pH 7	Co [b] 278K pH 6.8
P	Cα	40.6	33.9	34.1	35.5
	Cβ	60.1	56.1	64.0	65.1
	CH_3	11.2	11.1	10.0	12.0
	C2	165.7	161.6	167.5	171.5
	C4	165.0	168.0	166.4	169.4
	C5	112.6	114.2	117.2	119.9
	C6	152.5	148.4	153.1	152.9
	HNC=O	168.0	169.3	173.1	176.7
	H_2NC=O	176.5	176.6	175.4	177.3
H	Cα	57.3	61.1	55.6	60.1
	Cβ	73.4	70.6	69.2	71.7
	C2	137.3	137.8	142.2	144.8
	C4	118.0	118.2	119.8	122.2
	C5	135.2	135.5	135.9	136.0
	C=O	169.4	172.0	170.0	173.6
A	Cα	53.0	52.5	55.9	59.3
	Cβ	47.8	45.0	49.4	51.8
	C=O	172.3	173.8	173.4	173.6
V	αCH_3	12.3	12.1	13.2	9.81
	γCH_3	15.1	15.0	14.3	20.4
	Cα	43.0	43.0	43.4	42.9
	Cβ	74.7	74.7	74.4	77.7
	Cγ	47.9	47.3	47.8	49.6
	C=O	177.8	177.6	177.8	179.9
T	CH_3	19.3	19.3	19.3	22.4
	Cα	59.5	59.7	59.7	60.0

Carbons		Apo [a] 297K pH 7	Zn [a] 277K pH 7	Fe [a] 277K pH 7	Co [b] 278K pH 6.8
T	Cβ	67.4	67.4	67.3	72.4
	C=O	172.4	172.2	172.4	174.7
B	Cα	32.4	32.4	32.5	35.5
	Cβ	39.4	39.6	39.5	41.9
	C5	125.5	125.5	126.0	127.5
	C5'	119.4	119.5	119.6	121.3
	C4	149.1	149.1	149.4	151.2
	C4′	147.3	147.3	147.3	149.9
	C2	163.0	163.1	163.6	165.3
	C2′	170.9	171.0	171.5	173.8
	C=O	163.7	163.7	164.0	165.8
S	Cα	41.3	41.3	41.3	43.4
	Cβ	24.0	24.0	24.1	26.6
	Cγ	38.0	38.0	38.1	40.3
	$(CH_3)_2$	25.1	25.1	25.1	27.3
G	C1	97.8	95.6	94.9	97.4
	C2	70.6	68.3	68.1	69.9
	C3	68.2	66.6	66.6	68.4
	C4	69.5	70.1	69.7	71.8
	C5	67.4	67.7	68.1	70.8
	C6	60.6	61.6	61.6	63.9
M	C1	98.5	97.2	96.7	98.5
	C2	68.7	68.3	68.1	70.3
	C3	74.7	75.5	75.3	77.6
	C4	65.1	64.5	64.7	66.7
	C5	73.9	74.7	74.6	77.0
	C6	61.3	61.3	61.4	63.5
	C=O	158.3	157.7	157.8	160.2

with G-C6 in the HMBC spectrum, confirming this assignment. The results of these assignments are summarized in Table 2.1 and Table 2.2.

Assignment of the Carbon Chemical Shifts in CoBLM A2 green.

Using the complementary HMQC and HMBC methods, all of the ^{13}C assignments were successfully completed.[52] Essential to understanding the mode of binding of the bithiazole moiety in the drug-DNA complex is distinguishing between the B-C5′ and B-C5. These assignments allowed the unambiguous identification of the B-C5'H and B-C5H resonances. The HMBC method can assign the bithiazole quaternary carbons as B-C2′ shows cross peaks to the B-CαH, B-CβH as well as to B-C5′H, while B-C2 has cross peaks to B-C5′H and B-C5H. B-C4′ and B-C4 are assigned based on their single cross peak to the B-C5′H and B-C5H, respectively. Thus the B-C5H and B-C5'H can be assigned to 8.17 and 7.82 ppm in CoBLM A2 green and their upfield shifts when bound to duplex DNA have been monitored using the HMQC method.

Assignment of the Exchangeable Protons of CoBLM A2 green. The assignment of exchangeable protons of metallo-BLMs by NOESY experiments carried out in H_2O has previously provided important information about the ligands coordinated to ZnBLM and FeBLM-CO[50, 51] and thus we have undertaken to make these assignments for CoBLM A2 green. The secondary amine proton of β-aminoalanine (A-NH) and all but one of the secondary amide protons were readily assigned by standard methods (Table 2.1). As in the case of previous metallo-BLMs, the secondary amide hydrogen of the β-hydroxyhistidine moiety was not detected. This is consistent with previously published data[50, 51] that strongly suggest that this amide is deprotonated and is a ligand to the cobalt. In

the case of the ZnBLM and FeBLM-CO, four additional sets of exchangeable, paired protons have been reported. Two have been assigned to the primary amides of the β-aminoalanine (A) and the pyrimidinylpropionamide (P) moieties. A third has been assigned to the primary amine of A due to an NOE with A-CαH and the fourth to the carbamoyl group of mannose based on their rapid exchange with H_2O. In the case of CoBLM A2 green, only two of the four sets of protons have been detected in the NOESY spectra in H_2O. Studies in which the pH is lowered to minimize the exchange rate are not possible with CoBLM as it is chemically unstable under acidic conditions. The pairs of exchangeable proton resonances observed with CoBLM A2 green have chemical shifts at 8.08/7.32 ppm and 6.76/6.18 ppm and exhibit strong NOEs to each other, but not to any other protons, therefore assignment of these protons was not possible. Furthermore, no protons assignable to the primary amine of β-aminoalanine have been detected. Finally, a pair of exchangeable proton resonances at 7.73 and 7.94 ppm have been assigned to the 4-amino protons of the pyrimidine by virtue of their NOEs to each other and to the P-CH_3. This assignment is important as one of these protons plays a key role in binding of CoBLM A2 green to DNA, as described in chapter 3.[48]

NOE and Dihedral Angle Constraints. An essential step in defining the screw sense and the ligation state of CoBLM A2 green, and ultimately its structure, is to obtain distance and dihedral angle constraints from the NMR data . The assignments of all the ^1H and ^{13}C chemical shifts have allowed us to determine 55 non-trivial NOEs for use as distance constraints, as shown in Table 2.3. These data can be compared with the NOE constraints previously reported by Xu et al. and with those of Akkerman et al. for the FeBLM-CO and ZnBLM complexes[50, 51] (Table 2.3).

Table 2.3: Comparison of NOEs in Metallo-BLMs.

CoBLM A2 green[a] Mixing time (200 ms)	size	CoBLM[b] (300 ms)	FeBLM-CO[c] (400 ms)	ZnBLM[d] (400 ms)	CoBLM A2 green[a] (200 ms)	size	CoBLM[b] (300 ms)	FeBLM-CO[c] (400 ms)	ZnBLM[d] (400 ms)
H-C2H---A-CβH′	m	y	y		G-C1H---M-C5H	m		y	y
H-C2H---A-CβH	w		y		G-C1H---G-C6H	w			
A-CβH---P-CαH′	m		y	y	G-C1H---G-C4H	w			
P-CβH---A-CβH	w		y	y	G-C1H---M-C2H	w			
H-C2H---A-NH	m	y	y	y	H-CαH---G-C6H	w			
H-C2H---P-CβH	w		y		H-CαH---M-C5H	m			y
H-C2H---T-CH_3	s	y			H-CαH---M-C3H	w			
H-C2H---T-CβH	w				M-C1H---G-C2H	s			y
H-C2H---T-CαH	w				M-C1H---G-C3H	s			y
H-C2H---T-NH	w				M-C1H---G-C4H	w			
H-C2H---V-CαH	m	y			T-CαH---T-CH_3	m	y	y	
H-C2H---V-αCH_3	w	y			V-αCH_3---V-CγH	s	y		
H-C4H---V-CαH	w	y			V-γCH_3---V-CβH	s	y		
H-C4H---V-αCH_3	m	y		y	V-αCH_3---V-CβH	m	y	y	
P-CβH---T-CβH	w				B-NH---T-CαH	m	y	y	
H-C4H---H-CβH	s	y	y		B-NH---T-CβH	w	y	y	y
B-C5′ H---V-CβH	m	y			B-NH---B-CαH	w			
B-C5′ H---V-γCH_3	m	y			B-NH---B-CαH′	w			
B-C5H---P-CH_3	m	y			T-NH---V-αCH_3	w	y	y	y
G-C1H---H-CβH	s	y			V-NH---V-CβH	s	y	y	y
H-CαH---G-C1H	s		y	y	T-NH---V-CβH	m	y	y	y
M-C1H---G-C1H	w				T-NH---T-CH_3	w	y	y	
H-C4H---G-C5H	w		y	y	B-NH---T-CH_3	w	y	y	y
H-C4H---G-C6/6′H	w/w		y	y	V-NH---V-CαH	m		y	y
H-CβH---G-C6H	w				V-NH---V-γCH_3	m	y	y	y
H-CβH---G-C4H	w				T-NH---V-CαH	m	y	y	y
H-CβH---G-C2H	w	y			T-NH---V-γCH_3	m			y

Table 2.4: Comparison of Coupling Constants (Hz) in Metallo-BLMs.

Protons	CoBLM A2 green [a]	FeBLM-CO [b]	ZnBLM [b]	Apo BLM [b]
H-CαH to H-CβH	2.7 ± 0.3	3.1 ± 0.2	3.1 ± 0.2	5.8 ± 0.2
G-C1H to G-C2H	3.9 ± 0.3		4.9	
P-CβH to P-CαH (3.20 ppm)	8.3 ± 0.3			
P-CβH to P-CαH′ (3.51 ppm)	4.6 ± 0.3			
T-CαH to T-CβH	2.9 ± 0.3			
M-C1H to M-C2H	1.2 ± 0.3		1.8	
T-NH to T-CαH	8.7 ± 0.3			
V-NH to V-CγH	7.9 ± 0.3			
A-NH to P-CβH	<3			
A-NH to A-CβH′ (3.22 ppm)	5 ± 2			
A-NH to A-CβH (2.74 ppm)	5 ± 2			
V-CαH to V-CβH	1.8 ± 1.2			
V-CβH to V-CγH	9.5 ± 1.2			
A-CβH′ (3.22 ppm) to A-CαH	3.0 ± 0.5	4.2 ± 0.2	2.0 ± 0.2	5.2 ± 0.2
A-CβH (2.74 ppm) to A-CαH	4.0 ± 1.2	7.2 ± 0.2	3.8 ± 0.2	7.2 ± 0.2

[a] This study, 50 mM phosphate, pH 6.8 at 5 °C. [b] Akkerman et al.[51]

Analysis of the coupling constants for the H, A, P, T, and V moieties (Table 2.4) allowed for the incorporation of 8 dihedral angle constraints for use in molecular modeling. Additionally, the coupling constants for H1 and H2 of the sugars G and M (Table 2.4) and the previous calculations of these coupling constants by Akkerman et al.[50] for the two chair conformations have allowed us to assume the chair conformations shown in Figure 2.1. Only limited information on the coupling constants of the other metallo-BLMs has previously been reported in the literature. The additional structural definition provided by the dihedral angle constraints played an important role in identification of the axial ligands and the refinement of our model.

Previous Model Building Studies. Xu et al.[28] have recently reported the first 2D NMR studies on CoBLMs and proposed, based on their NOE constraints and molecular modeling, two models for A2 green: A and B (our versions of their structures are shown in Figure 2.7a and 2.7c). They made several assumptions to arrive at these models. They assumed that the secondary amine of A, the N1 of P, the deprotonated amide of H, and the Nδ of H (Figure 2.1, Ns), are equatorial ligands to cobalt and that one of the axial ligands is a hydroperoxide. These assumptions are consistent with biophysical studies by many investigators.[53] They also assumed that the second axial ligand is provided by the primary amino group of A. In the case of both ZnBLM and FeBLM-CO, however, previous workers have interpreted their 2D NMR studies to indicate that an axial ligand is provided by the carbamoyl nitrogen of mannose.[50, 51] This ligation state was not considered as an option in the models proposed by Xu et al. Finally, Xu et al. favored the A form (Figure 2.7a) over the B form (Figure 2.7c) based on their relative energetics, although they were unable to distinguish between these structures with their NMR data.[28]

Figure 2.7: Four isomers of CoBLM A2 green: same screw sense isomers (a) structure I with primary amine of A, or (b) structure II with carbamoyl nitrogen of M as an axial ligand; and the opposite screw sense isomers (c) structure III with the primary amine of A, or (d) structure IV with carbamoyl nitrogen of M as an axial ligand. The sulfonium tail has been excluded from the figure for clarity.

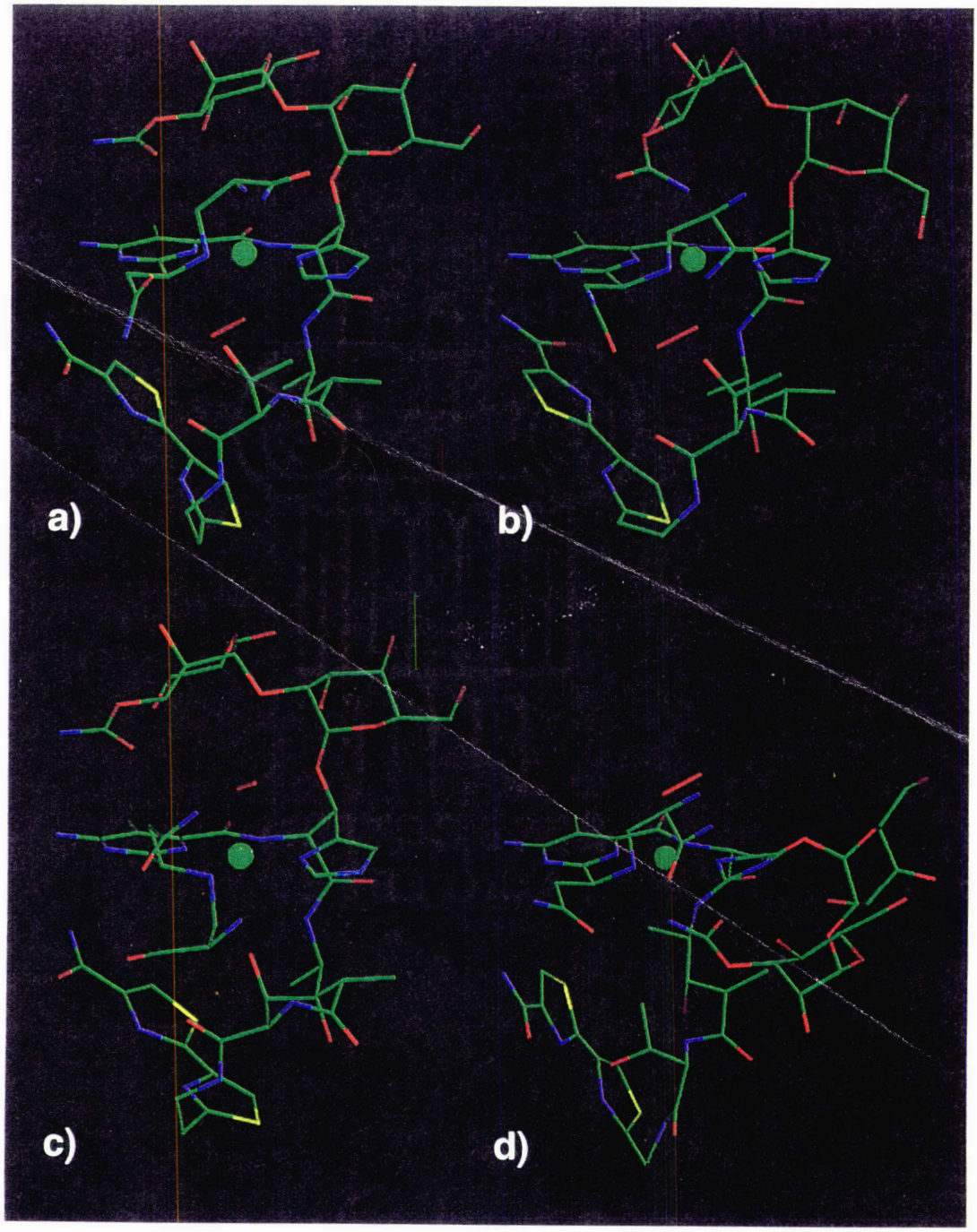
a)
b)
c)
d)

Solution Structure of CoBLM A2 green. On the basis of previous studies on chelation to cobalt[53] and the ambiguity in the axial ligation state, we have initially considered four theoretically possible structures, I, II, III, and IV in Figure 2.7a, 7b, 7c, and 7d, respectively. These four structures reflect the two alternative screw senses which define the stereochemistry of ligand arrangement around the metal and the two possible axial ligands, either primary amine of A or carbamoyl nitrogen of M, for each of the screw sense isomers. Structures I and II have the same screw sense, while structures III and IV have the opposite screw sense. Structures I and III contain the primary amine of A as the axial ligand, while structures II and IV have the carbamoyl nitrogen of M at that position. In the discussion that follows, arguments will be made based on our NMR data, that only structure I, which contains a primary amine of A as the axial ligand meets all of the constraints. In addition, our data will be compared and contrasted with previous 2D NMR information on the ZnBLM and FeBLM-CO complexes.

Using the dihedral angle and NOE constraints, we have built models of the four isomers discussed above. The easiest models to eliminate are structures III and IV. Structure IV with a carbamoyl axial ligand (Figure 2.7d) can be eliminated as a significant number of NOE constraints are violated. These specifically include the NOEs between the H and V residues, and those between the H-CαH and sugar protons.[54] Furthermore this structure requires a trans configuration between the H-CαH and the H-CβH which is inconsistent with the small coupling constant observed (2.7 Hz, Table 2.4). These problems and the extremely high CHARMm potential energy in comparison with structures I and II (Table 2.5) allow us to eliminate this model.

Table 2.5: Structure and Energy Statistics from Molecular Dynamics Calculations.

	Structure I		Structure II	
	all structures	final avg. structure[a]	all structures	final avg. structure
rmsd from distance restraints (Å)	0.0100 ± 0.0026	0.0093	0.0147 ± .0045	0.0480
potential energy terms[a]				
total	98.2 ± 3.5	95.9	128.0 ± 3.4	124.0
NOE constraint	0.176± 0.093	0.144	0.420 ± 0.084	0.437
dihedral constraint	1.04 ± 0.07	1.14	1.52 ± 0.36	1.50
van der Waals	-70.1 ± 2.1	-72.9	-62.8 ± 1.9	-63.7
bond	5.93 ± 0.13	5.80	8.71 ± 0.36	8.63
angle	93.7 ± 1.4	94.4	108.0 ± 0.8	107.0
dihedral angle	64.3 ± 1.7	64.7	68.8 ± 1.0	66.1
improper angle	3.19 ± 0.11	2.61	3.25 ± .06	3.70
atomic rmsd for all atoms[c] (Å)	0.7680	0.7709[d]	0.7542	0.9854

	Structure III		Structure IV	
	all structures	final avg. structure	all structures	final avg. structure
rmsd from distance restraints (Å)	0.0859 ± 0.0440	0.0641	0.2003 ± 0.0034	0.2064
potential energy terms				
total	118.0 ± 0.9	120.0	467.0 ± 1.4	473.0
NOE constraint	4.33 ± 0.69	4.80	66.6 ± 1.8	70.4
dihedral constraint	2.47 ± 0.62	2.04	20.9 ± 0.5	22.0
van der Waals	-61.3 ± 1.1	-61.3	11.7 ± 1.9	14.4
bond	6.55 ± 0.12	6.03	24.7 ± 0.4	19.5
angle	97.7 ± 0.5	97.8	220.0 ± 4.5	221.0
dihedral angle	67.4 ± 0.6	67.5	111.0 ± 1.0	112.0
improper angle	2.77 ± 0.29	2.86	12.5 ± 1.6	13.8
atomic rmsd for all atoms (Å)	0.5216	0.6828	0.5672	0.72[illegible]

[a] The coordinates of the final structures of the individual molecular dynamics calculations, averaged, and minmized. [b] Energy terms in kcals mol^{-1}. [c] Because of the expected disorder and lack of NOEs to the sulfonium tail, and the possibility of either a cis or trans orientation of the the thiazolium rings of the bithiazole, these moieties were not included in the rms calculation. [d] All structures vs. the final average structure.

Structure III with the primary amine of A as a ligand is the B conformation proposed by Xu et al. for CoBLM A2 green. Our molecular dynamics calculations also suggest that this model is of higher energy than that of structure I (Table 2.5), and in general, does not satisfy the experimentally derived constraints. Additionally, if all of the NOEs and the dihedral angle constraints are satisfied, the model predicts that the V, T, and B moieties of CoBLM A2 green must be located on the same side and in close contact to the primary amine ligand (Figure 2.7c). This location requires the existence of a number of NOEs between the A spin system and the V and T spin systems that would be easily detected, such as A-CαH to V-CβH (strong), A-CαH to V-CαH (medium), A-CβH to T-CβH (medium), and A-CαH to V-CβH (medium). None of these NOEs are observed, thereby eliminating this isomer, a variant of structure B of Xu et al.,[28] from further consideration. Finally, as described in chapter 3, neither of these isomers (structures III and IV) can bind to DNA and successfully satisfy the wealth of NMR information available on the DNA-drug complex.

Energy minimized models for the other screw sense isomers, structures I and II with the primary amine of A and the carbamoyl of M as the axial ligand respectively, are shown in Figure 2.7a and Figure 2.7b, and in more detail in Figure 2.8a and 8b. In contrast to the screw sense isomers discussed above, in the structures I and II the peptide linker region and the bithiazole moiety are located on the bottom face of the metal plane, sharing the same face with the hydroperoxide ligand. The possible axial ligands, both reside on the top face of the metal plane, which makes differences between the two structures rather subtle. In fact, both the primary amine and carbamoyl group can be interchanged as axial ligands with relatively minor structural reorganization of CoBLM A2 green.

Figure 2.8: Two isomers of CoBLM A2 green (same screw sense): (a) structure I with the primary amine of A, or (b) structure II with carbamoyl nitrogen of M as an axial ligand. The two structures are shown in slightly different orientations to provide the optimal view of the axial nitrogen ligand in each case, and the bithiazole and sulfonium moieties have both been excluded (~~).

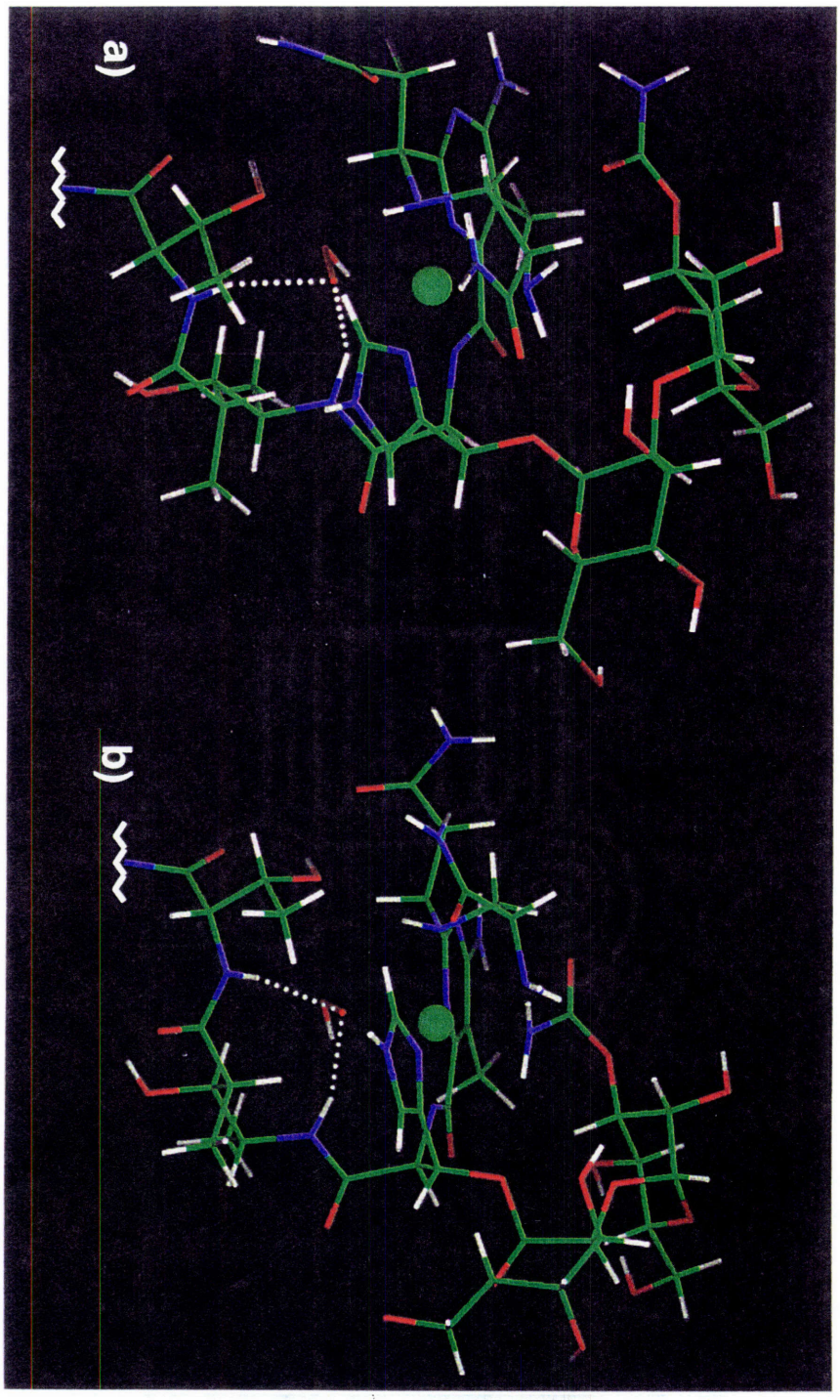
(a)
(b)

A number of considerations outlined subsequently have allowed us to favor the structure I with the primary amine of A as a ligand. One difference between the two, illustrated in Figure 2.8a and Figure 2.8b, involves the M-C3H. Specifically, in the carbamoyl isomer, the M-C3H to H-CβH and to H-CαH are predicted to be strong and medium NOEs, receptively (Figure 2.8b). The alanine isomer predicts a weak and no NOE respectively, which is the observed result (Figure 2.8a, Table 2.3). Thus, in the carbamoyl isomer the M-C3H is closer to the H moiety, primarily due to the mannose group being restricted to the ligation sphere of cobalt.

Examination of the coupling constants between the α and β protons of A, has provided additional support for the structure shown in Figure 2.8a. These coupling constants have been previously used by Akkerman et al. studying ZnBLM and FeBLM-CO as predictors of whether the primary amine of A is actually an axial ligand in these complexes.[50, 51] In apo BLM, the coupling constants between the α and β protons of A (7.2 and 5.2 Hz, Table 2.4) are indicative of rapidly interconverting conformations. Similar sizes of these coupling constants (7.2 Hz and 4.2 Hz) have been reported for the FeBLM-CO and have been interpreted to indicate that the primary amine is not an axial ligand in this complex. In ZnBLM however, the coupling constants (3.8 Hz and 2.0 Hz) are substantially different from those observed with apo BLM. These values have been interpreted to suggest that in this complex, the primary amine is a ligand and that it is constrained to a gauche-gauche conformation of the Cα-Cβ bond. The values of couplings constants in the A moiety of CoBLM A2 green (3.0 and 4.0 Hz) and the calculated rotamer population of the Cα-Cβ bond are also indicative of a gauche-gauche conformation (>80 %) and support the hypothesis that the primary amine is an axial ligand in this complex as well.

Finally, the linewidths of the the A-CαH and A-CβH are slightly larger than the rest of the protons of the CoBLM A2 green suggestive of a local movement of the Cα-Cβ bond within this ligation state.

NOE patterns observed for the H-C2H to the A-CαH and A-CβHs are also consistent with the primary amine as the axial ligand of CoBLM A2 green, although the conclusions must be drawn cautiously. With the carbamoyl group as a ligand, medium and weak to medium NOEs are predicted between H-C2H to A-CαH and to A-CβHs, respectively. With the primary amine as an axial ligand, weak to medium NOEs are also predicted from H-C2H to A-CβHs. However, the NOE between H-C2H to A-CαH is predicted to be very weak. Weak to medium NOEs between the H-C2H to A-CβHs are observed in 200 ms mixing time NOESY spectrum. Only at 400 ms is an additional weak NOE observed between H-C2H and A-CαH consistent with the primary amine of A being an axial ligand.

A number of additional pieces of information support the primary amine ligation state (Figure 2.8a). The first is that studies with deglycoBLM and more recently with demannosylBLM, reveal that despite the absence of the carbamoyl group, that cleavage of DNA occurs with similar sequence selectivity and efficiency (approximately 30 to 50 %) as the corresponding intact FeBLM.[22] These studies suggest that the carbamoyl group is not a ligand. Second, ample chemical precedent suggests that if cobalt has a choice between a primary amine and a carbamoyl nitrogen ligand, and there are no unusual geometrical constraints involved in the comparison of these options, that the former is a more nucleophilic ligand and hence would be favored. Third, previous studies of Dabrowiak et al.[53] using cobalt-containing pseudotetrapeptide A of BLM, a hydrolysis product of CoBLM A2 green indicate that the primary amine can be a

ligand to cobalt. Fourth, recent crystallographic studies of Tan et al. on CoPMAs, a series of CoBLM model compounds, also show that a primary amine group can be an axial ligand to cobalt.[37] Finally, the energy calculation using all available experimental distance and dihedral constraints reveals that structure I with primary amine of A as the axial ligand is energetically more favorable in all aspects of potential energy terms, when compared with structure II with the carbamoyl nitrogen of M as the axial ligand (Table 2.5). This information, in addition to the model studies and the analysis of NOEs and coupling constants presented above, allow us to favor structure I with the amino group of A as the axial ligand as the structure of CoBLM A2 green.

A Comparison of CoBLM A2 green with Other Metallo-BLMs. The structures of ZnBLM and FeBLM-CO, based on 2D NMR analysis have previously been reported by Akkerman et al.[50, 51] In the case of FeBLM-CO the axial ligand has been proposed to be the carbamoyl group and in the case of ZnBLM the axial ligands have been proposed to be the carbamoyl of M and the primary amine of A.[50, 51] The equatorial ligands in all metallo-BLMs are non-controversial. The idea of screw sense isomer has not been previously considered with these complexes.

The most conspicuous differences between the CoBLM A2 green and its Zn and Fe counterparts, result from the observation of unique long range NOEs between the B-H5 and the P-CH_3 and the B-H5' and the V moiety in the case of CoBLM A2 green (Table 2.3, D, E, F in Figure 2.9). These NOEs are identical to those previously reported by Xu et al.[28] and, as described above, allowed them to propose a compact model for CoBLM A2 green in which the bithiazole tail is folded back underneath the equatorial plane of the metal binding domain[28] (Figure 2.7a). These NOEs have not previously been detected in the case of the

Figure 2.9: Expanded NOESY spectrum (200 ms mixing time, 500 MHz) of CoBLM A2 green in D_2O at 5 °C (50 mM sodium phosphate, pH 6.8). NOE assignments are: A. H-C2H to V-CαH; B. H-C2H to T-CH_3; C. H-C2H to A-CβH'; D. B-C5H to P-CH_3; E. B-C5'H to V-γCH_3; F. B-C5'H to V-CβH; G. H-C4H to V-αCH_3; H. H-C4H to V-CαH.

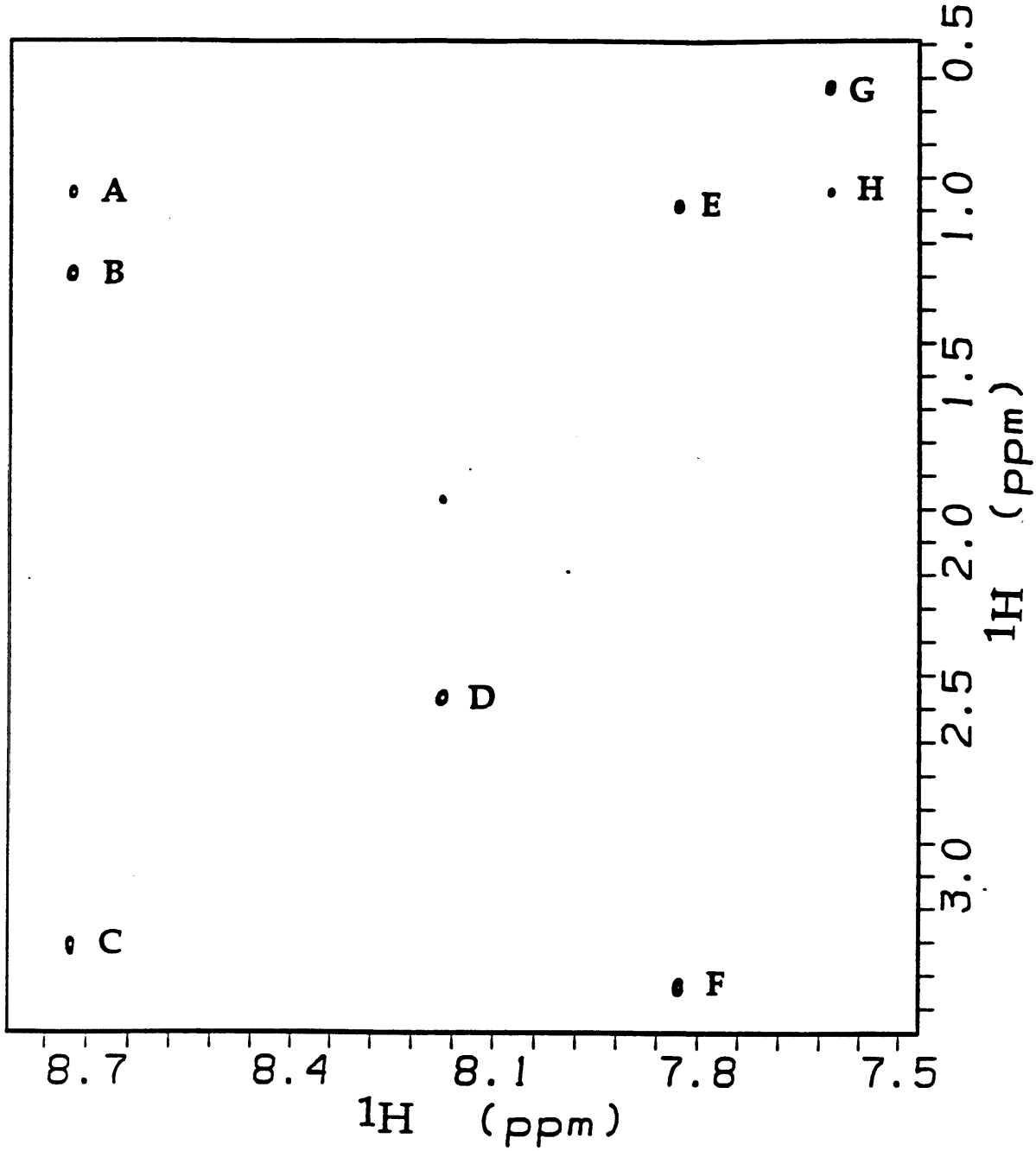
A
B
C
D
E
F
G
H
8.7
8.4
8.1
7.8
7.5
1H (ppm)
0.5
1.0
1.5
2.0
2.5
3.0
1H (ppm)

FeBLM-CO and ZnBLM and, as a consequence, the bithiazole tail has been ignored in the molecular modeling of these structures. The resulting proximity of the pyrimidine to the penultimate thiazolium ring in CoBLM A2 green (Figure 2.7a and 2.8a) is presumably responsible for the inequivalence of the chemical shifts of the two P-NH_2 protons (Figure 2.1, Table 2.1). These two protons are degenerate in both ZnBLM and FeBLM-CO complexes.

A second major difference between the CoBLM A2 green and the other metallo-BLMs is that the conformation of V and T linker region is well defined. The coupling constants in the V and T moieties of CoBLM A2 green placed constraints on four out of the six backbone dihedral angles (Table 2.4). As a result, the dihedral angles[55] in the final structure give rise to a turn that maintains the peptide linker region underneath the metal coordination plane (Figure 2.8a). This conformation provides an explanation for a number of initially puzzling observations made by NMR concerning this linker region. The chemical shifts of the V-αCH_3 and V-CαH are dramatically upfield shifted in CoBLM A2 green in comparison with the apo BLM, the ZnBLM and FeBLM-CO complexes. Specifically, a comparison between the apo BLM and CoBLM reveals a shift from 1.10 to 0.62 ppm for V-αCH_3 and 2.45 to 0.94 ppm for V-CαH. The structure reveals that both the V-αCH_3 and the V-CαH are positioned directly underneath the imidazole ring of H whose ring current causes shielding and hence large upfield shifts. Examination of the NOESY spectrum of CoBLM A2 green reveals that both V-αCH_3 and V-CαH show NOEs to H-C2H and H-C4H of the imidazole ring (Figure 2.8a, Table 2.3), consistent with this constrained structure. A similar trend in the chemical shifts is also observed with ZnBLM, but with much smaller upfield changes (Table 2.1). Examination of the NOE patterns for ZnBLM reveals that unlike the CoBLM A2 green, only an NOE from

H-C4H to V-αCH_3 is reported. In complete contrast, the FeBLM-CO complex shows no unusual chemical shifts of the V-CαH and V-αCH_3, and no NOEs from imidazole protons to the valeryl protons are reported.

These structural differences raise an interesting question as to why the CoBLM A2 green adopts this well-defined compact structure in the peptide linker region. In structure I with the primary amine of A as a ligand (Figure 2.8a), the amide protons of the V and T moieties are well positioned to form hydrogen bonds with the proximal oxygen of the hydroperoxide ligand,[56] which could stabilize the observed conformation. This hypothesis is supported by the large downfield chemical shift changes (~ 1ppm) of the V-NH and T-NH relative to those observed in ZnBLM and FeBLM-CO (Table 2.1).

How good a model is CoBLM A2 green for activated BLM? Unfortunately, the only direct comparison that can be made is to FeBLM-CO in which the metal is in the +2 oxidation state and possesses a CO ligand in place of a hydroperoxide anion ligand. In the FeBLM-CO complex of Akkerman et al., the second axial ligand is proposed to be provided by the carbamoyl group.[51] The evidence in support of this assignment is based on the 0.54 ppm upfield chemical shift of the M-C3H relative to its chemical shift in apo BLM. However, with CoBLM A2 green we see an even larger upfield chemical shift change for this proton (0.63 ppm) and we have now established that the carbamoyl group is not a ligand in CoBLM A2 green. Thus, the chemical shift argument does not provide strong support for their conclusion concerning axial ligation. Their second argument in favor of the carbamoyl ligand was that the two protons of this ligand were nonequivalent and distinguishable, thus suggesting ligation to iron. However, the assignment of these protons is based solely on the argument that they are the protons most rapidly exchanging with H_2O. This tentative assignment, the fact that amines are better ligands than carbamoyl

groups when all other factors are equivalent, leads us to suggest that the primary amine of A could be an axial ligand in FeBLM-CO as in the CoBLM A2 green case. To account for the large coupling constants between the A-CαH and A-CβHs in the FeBLM-CO complex, one, then, could propose that the ligand can undergo exchange on the NMR time scale.[57] Regardless of the structure of the FeBLM-CO complex, it is not unreasonable to assume in the $Fe^{3+}OOH$ complex that the primary amine of A is a ligand. Further analysis of this problem using ^{15}N labeled β-aminoalanine is warranted and should be readily accessible given the recent user friendly synthesis of BLM by Boger's group.[58] Based on these arguments, we believe that the isomer with the primary amine of A as an axial ligand is an excellent model for activated BLM.

Choice of Oligonucleotide Sequence for Examination of the Structure of CoBLM A2 green Bound to DNA. The final prerequisite for defining the basis of molecular recognition between CoBLM A2 green and DNA is the choice of an appropriate oligonucleotide. Our recently reported preliminary studies have shown that CoBLM A2 green forms a 1:1 complex with d(CCAGGCCTGG)[16] and has led to a solution structure of the complex described in chapter 3.[48] We have shown herein that there is a single cleavage site (C6) in this duplex as predicted (Figure 2.3) and, furthermore, studies monitoring the fluorescence quenching have allowed the determination of a single binding site with an apparent K_d of 10^{-7} M. As indicated in our preliminary studies and defined in detail in chapter 3, CoBLM A2 green binds by partial intercalation 3' to C6 and inserts through the minor groove.[16, 48]

To determine if this mode of binding is unique to this oligomer or to dGpC steps, we have investigated a second self-complementary oligonucleotide d(CCAGTACTGG). This oligomer was chosen as our recent studies revealed that

the T of GTAC is a hot spot for ds-cleavage by a single molecule of FeBLM, with the ratio of ds:ss cleavage of 1:3.[49] Thus, this oligomer offered an opportunity to examine a GpT step and had the possibility of allowing us to examine how a metallo-BLM might interact with two different cleavage sites without dissociation from the duplex. The preliminary studies are intriguing and informative. First, a major complex of 0.8:1 is formed in slow exchange on the NMR time scale. The bithiazole protons are upfield shifted indicative of partial intercalation as observed with **1**. Second, a minor complex, 0.2:1, is also readily apparent. This complex has not yet been examined in any detail, but could be indicative of the secondary cleavage site of this hot spot for ds-cleavage. These studies thus reveal that CoBLM can bind to both GpT and GpC sequences in a similar fashion giving some hope that the structure reported in detail in chapter 3 may be a generic one.

References:

(1) Umezawa, H.; Maeda, K.; Takeuchi, T.; Okami, Y. *J. Antibiot.* **1966**, *19*, 200-209.

(2) (a) Sikic, B. I.; Rozencweig, M.; Carter, S. K. Ed., In *Bleomycin Chemotherapy*, Academic Press: Orlando, Florida, 1985. (b) Umezawa, H. in *Anticancer agents based on natural product models*; Cassady, J. M., Douros, J., Ed.; Academic Press, Inc., New York, 1980; Vol. pp 147-166. (c) Hecht, S. M. Ed., In *Bleomycin: Chemical, Biochemical, and Biological Aspects*; Springer-Verlag: New York, 1979.

(3) (a) Sausville, E. A.; Peisach, J.; Horwitz, S. B. *Biochem. Biophys. Res. Commun.* **1976**, *73*, 814-822. (b) Sausville, E. A.; Peisach, J.; Horwitz, S. B. *Biochemistry* **1978**, *17*, 2740-2746.

(4) (a) Hecht, S. M. *Bioconjugate Chem.* **1994**, *5*, 513-526. (b) Absalon, M. J.; Krishnamoorthy, C. R.; McGall, G.; Kozarich, J. W.; Stubbe, J. *Nucleic Acids Res.* **1992**, *20*, 4179-4185. (c) Krishnamoorthy, C. R.; Vanderwall, D. E.; Kozarich, J.; Stubbe, J. *J. Am. Chem. Soc.* **1988**, *110*, 2008-2009. (d) Morgan, M.; Hecht, S. M. *Biochemistry* **1994**, *33*, 10286-10293. (e) Holmes, C. E.; Carter, B. J.; Hecht, S. M. *Biochemistry* **1993**, *32*, 4293-4307.

(5) Kane, S. A.; Hecht, S. M. in *Progress in Nucleic Acid Research and Molecular Biology*; Cohn, W. E. Moldave, K. Ed.; Academic Press, San Diego, 1994; Vol. 49, pp 313-352.

(6) Stubbe, J.; Kozarich, J. W. *Chem. Rev.* **1987**, *87*, 1107-1136.

(7) Wu, J. C.; Stubbe, J.; Kozarich, J. W. *Biochemistry* **1985**, *24*, 7569-7573.

(8) Sugiura, Y.; Suzuki, T. *J. Biol. Chem.* **1982**, *257*, 10544-10546.

(9) Kuwahara, J.; Sugiura, Y. *Proc. Natl. Acad. Sci. U.S.A.* **1988**, *85*, 2459-2463.

(10) Zhang, G., Ph.D. Thesis, University of Maryland, 1993.

(11) Suzuki, T.; Kuwahara, J.; Sugiura, Y. *Biochem. Biophys. Res. Commun.* **1983**, *117*, 916-922.

(12) Long, E. C.; Hecht, S. M.; van der Marel, G. A.; van Boom, J. H. *J. Am. Chem. Soc.* **1990**, *112*, 5272-5276.

(13) Hertzberg, R. P.; Caranfa, M. J.; Hecht, S. M. *Biochemistry* **1988**, *27*, 3164-3174.

(14) Povirk, L. F.; Hogan, M.; Dattagupta, N. *Biochemistry* **1979**, *18*, 96-101.

(15) (a) Huang, C.; Galvan, L.; Crooke, S. T. *Biochemistry* **1980**, *19*, 1761-1767. (b) Chen, D. M.; Sakai, T. T.; Glickson, J. D.; Patel, D. J. *Biochem. Biophys. Res. Commun.* **1980**, *89*, 534-541.

(16) Wu, W.; Vanderwall, D. E.; Stubbe, J.; Kozarich, J. W.; Turner, C. J. *J. Am. Chem. Soc.* **1994**, *116*, 10843-10844.

(17) (a) Manderville, R. A.; Ellena, J. F.; Hecht, S. M. *J. Am. Chem. Soc.* **1994,** *116,* 10851-10852. (b) Manderville, R. A.; Ellena, J. F.; Hecht, S. M. *J. Am. Chem. Soc.* **1995,** *117,* 7891-7903.

(18) Dickerson, R. E. in *Mechanism of DNA Damage and Repair: Implications for Carcinogenesis and Risk Assessment Basic Life Sciences;* Smi, M. G. Grossman, L. Ed.; Plenum, New York, 1986; Vol. 38, pp 245-255.

(19) (a) Carter, B. J.; Murty, V. S.; Reddy, K. S.; Wang, S.-N.; Hecht, S. M. *J. Biol. Chem.* **1990,** *265,* 4193-4196. (b) Carter, B. J.; Reddy, K. S.; Hecht, S. M. *Tetrahedron* **1991,** *47,* 2463-2474.

(20) Kross, J.; Henner, W. D.; Hecht, S. M.; Haseltine, W. A. *Biochemistry* **1982,** *21,* 4310-4318.

(21) Guajardo, R. J.; Hudson, S. E.; Brown, S. J.; Mascharak, P. K. *J. Am . Chem. Soc.* **1993,** *115,* 7971-7977.

(22) (a) Boger, D. L.; Teramoto, S.; Honda, T.; Zhou, J. *J. Am. Chem. Soc.* **1995,** *117,* 7338-7343. (b) Boger, D. L.; Teramoto, S.; Zhou, J. *J. Am. Chem. Soc.* **1995,** *117,* 7344-7356.

(23) Hamamichi, N.; Natrajan, A.; Hecht, S. M. *J. Am. Chem. Soc.* **1992,** *114,* 6278-6291.

(24) Chang, C.-H.; Meares, C. F. *Biochemistry* **1984,** *23,* 2268-2274.

(25) Saito, I.; Morii, T.; Sugiyama, H.; Matsura, T.; Meares, C. F.; Hecht, S. M. *J. Am. Chem. Soc.* **1989,** *111,* 2307-2308.

(26) McLean, M. J.; Dar, A.; Waring, M. J. *J. Mol. Recognit.* **1989,** *1,* 184-192.

(27) Worth, L., Jr.; Frank, B. L.; Christner, D. F.; Absalon, M. J.; Stubbe, J.; Kozarich, J. W. *Biochemistry* **1993,** *32,* 2601-2609.

(28) Xu, R. X.; Nettesheim, D.; Otvos, J. D.; Petering, D. H. *Biochemistry* **1994,** *33,* 907-916.

(29) Peck, E. *Anal. Lett.* **1978,** *B11,* 103-117.

(30) (a) Cantor, C. R.; Warsaw, M. M. *Biopolymers* **1970**, *9*, 1059. (b) Puglisi, J. D.; Tinoco, I. J. *Methods Enzymol.* **1989**, *22*, 304-325.

(31) Chien, M.; Grollman, A. P.; Horwitz, S. B. *Biochemistry* **1977**, *16*, 3641-3647.

(32) Guéron, M.; Plateau, P.; Decorps, M. *Prog. Nucl. Magn. Reson. Spectrosc.* **1991**, *23*, 161.

(33) Bax, A.; Subramanian, S. *J. Magn. Reson.* **1986**, *67*, 565-569.

(34) Bax, A.; Summers, M. F. *J. Am. Chem. Soc.* **1986**, *108*, 2093-2094.

(35) van Gunsteren, W. F.; Berendsen, H. J. C. *Mol. Phys.* **1977**, *34*, 1311-1327.

(36) Brooks, B. R.; Bruccoleri, R. E.; Olafson, B. D.; States, D. J.; Swaminathan, S.; Karplus, M. *J. Comp. Chem.* **1983**, *4*, 187-217.

(37) Tan, J. D.; Hudson, S. E.; Brown, S. J.; Olmstead, M. M.; Mascharak, P. K. *J. Am. Chem. Soc.* **1992**, *114*, 3841-3853.

(38) Busch, D. H.; Jackson, P. J.; Kojima, M.; Chmielewski, P.; Matsumoto, N.; Stevens, J. C.; Wu, W.; Nosco, D.; Herron, N.; Ye, N.; Warburton, P. R.; Masarwa, M.; Stephenson, N. A.; Christoph, G.; Alcock, N. W. *Inorg. Chem.* **1994**, *33*, 910-923.

(39) (a) Hancock, R. D. *Prog. Inorg. Chem.* **1989**, *37*, 187-291. (b) Charles, R.; Ganly-Cunningham; Warren, R.; Zimmer, M. *J. of Mol. Struct.* **1992**, *265*, 385-395.

(40) Evans, S. V. *J. Mol. Graphics* **1993**, *11*, 134-138.

(41) Haasnoot, C. A. G.; De Leeuw, F. A. A. M.; Altona, C. *Tetrahedron* **1980**, *36*, 2783-2792.

(42) Hoch, J. C.; Dobson, C. M.; Karplus, M. *Biochemistry* **1985**, *24*, 3831-3841.

(43) Chang, C.-H.; Dallas, J. L.; Meares, C. F. *Biochem. Biophys. Res. Commn.* **1983**, *110*, 959-966.

(44) Xu, R. X.; Antholine, W. E.; Petering, D. H. *J. Biol. Chem.* **1992**, *267*, 944-949.

(45) Sam, J. W.; Tang, X.-J.; Peisach, J. *J. Am. Chem. Soc.* **1994**, *116*, 5250-5256.

(46) Theoretical isotopic distribution for CoBLM A2 green is: 752.7, 100%; 753.2, 72%; 753.7, 44%; 754.2, 19%.

(47) Heinemann, U.; Alings, C. *J. Mol.Biol.* **1989**, *210*, 369-381.

(48) Wu, W.; Vanderwall, D. E.; Turner, C. J.; Kozarich, J. W.; Stubbe, J. *J. Am. Chem. Soc.* Second paper in this issue.

(49) Absalon, M. J.; Stubbe, J.; Kozarich, J. W. *Biochemistry* **1995**, *34*, 2065-2075.

(b) Absalon, M. J.; Wu, W.; Stubbe, J.; Kozarich, J. W. *Biochemistry* **1995**, *34*, 2076-2086.

(50) Akkerman, M. A. J.; Haasnoot, C. A. G.; Hilbers, C. W. *Eur. J. Biochem.* **1988**, *173*, 211-225.

(51) Akkerman, M. A. J.; Neijman, E. W. J. F.; Wijmenga, S. S.; Hilbers, C. W.; Bermel, W. *J. Am. Chem. Soc.* **1990**, *112*, 7462-7474.

(52) There are two exceptions. A distinction could not be made between the amide carbonyl carbons of the P and H moieties as both of them have cross peaks to the H-CαH proton and neither show cross peaks to the H-CβH proton. Previous studies of Akkerman et al. permitted assignment of these two resonances in the FeBLM-CO based on an observed cross peak to the H–CβH.[51] Assignments reported in Table 2.2 for these two carbonyls are based on the relative chemical shifts and previous assignments and should be considered tentative.

(53) (a) Dabrowiak, J. C.; Tsukayama, M. *J. Am. Chem. Soc.* **1981**, *103*, 7543-7550. (b) Dabrowiak, J. C. in *Adv.anced Inorganic Biochemistry*; Eichhorn, G. L. Marzilli, L. G. Ed.; Elsevier Biomedical, New York, 1982; Vol. 4, pp 69-113.

(54) Most noticeably, NOEs between the H-C4H and the V-αCH_3; H-CαH and G-C1H; H-CαH and G-C6/6'H; and H-CαH and M-C5H are all violated by more than 0.6 Å.

(55) Backbone angles are H-CO, V-N ,V-Cγ, V-Cβ =118°; V-N, V-Cγ, V-Cβ, V-Cα =-59°; V-Cγ, V-Cβ, V-Cα, V-CO =178°; V-Cβ, V-Cα. V-CO, T-N =-68°; V-CO, T-N, T-Cα, T-CO=-122°; T-N, T-Cα, T-CO, B-N =120°.

(56) V-NH to O: distance=2.1 Å, N—H---O angle=126°; T-NH to O: distance=2.3 Å, N—H---O angle=161°. Note that no hydrogen bond or electrostatic terms were included in any structure calculations.

(57) Lippard, S. J.; Berg, J. M. *Principles of Bioinorganic Chemistry*; University Science Books: Mill Valley, California, 1994, pp 28-29. (b) Basolo, F.; Pearson, R. G. *Mechanisms of Inorganic Reactions*; John Wiley & Sons, Inc.: New York, 1967, pp 124-246.

(58) (a) Boger, D. L.; Colletti, S. L.; Honda, T.; Menezes, R. F. *J. Am. Chem. Soc.* **1994**, *116*, 5607-5618. (b) Boger, D. L.; Honda, T.; Dand, Q. *J. Am. Chem. Soc.* **1994**, *116*, 5619-5630. (c) Boger, D. L.; Honda, T.; Menezes, R. F.; Colletti, S. L. *J. Am. Chem. Soc.* **1994**, *116*, 5631-5646. (d) Boger, D. L.; Honda, T. *J. Am. Chem. Soc.* **1994**, *116*, 5647-5656.

Chapter 3: Solution Structure of Co•Bleomycin A2 green Complexed with d(CCAGGCCTGG)

Introduction

The bleomycins (BLMs) are a family of glycopeptide antibiotics used clinically in the treatment of head and neck and testicular cancers.[1] Their mode of cytotoxicity has been proposed to be related to their ability to bind to and cleave DNA.[2, 3] Despite the intensive investigation of the BLMs in the last two decades, however, the basis for the specificity of BLM for cleavage at pyrimidines in d(G-Py) sequences and the mode of its binding to DNA have remained controversial and elusive. While most investigators agree that the positively charged bithiazole tail of BLM (Figure 3.1) provides the binding affinity of the drug for DNA,[2, 3] it is less clear whether that is its sole role or whether it is important, as is the metal binding domain,[2, 3] for defining the sequence selectivity.

Given these ambiguities, we decided to investigate the structural details of the interaction of BLM with DNA using 2D NMR and X-ray crystallographic methods. Other investigators have used a similar approach as evidenced by the recent and past literature on the determination of the structure of a variety of metallo-BLMs including: ZnBLM,[4] FeBLM-CO,[5] and CoBLMs.[6, 7] In addition several investigators have also reported efforts to look at metallo-BLMs with oligonucleotide duplexes.[8, 9, 10] All of these studies have been unsuccessful in elucidation of the two predominant structural questions: (1) What is the mode(s) of binding of the bithiazole tail? and (2) What defines the specificity of the cleavage event?

We have chosen to examine the interaction of CoBLM A2 green with decameric oligonucleotides. Moreover, the CoBLM A2 green, as delineated in chapter 2, was chosen for a number of reasons. First, the specificity of CoBLM A2 green mediated DNA degradation is very similar to that of the FeBLM.[11] The CoBLM A2 green is diamagnetic and the cleavage of DNA requires light[12]

and is not affected by the presence of O_2.[11] Thus, the problems associated with paramagnetism of FeBLM and its O_2-mediated cleavage are avoided with the cobalt congener. Second, as described in the preceding chapter, we have been able to purify and structurally characterize the hydroperoxide form of the CoBLM A2 (designated CoBLM A2 green or CoOOH). It is remarkably stable at neutral pH and the ligands are exchange inert. Third, this CoOOH is an excellent analog of the FeOOH, that is, the activated BLM.[13] Fourth, CoBLMs were demonstrated by Chang and Meares to bind to generic DNA (K_d~10^{-7} M) ten fold more tightly than the FeBLM.[11] As reported previously, we have shown that CoBLM A2 green can bind to the self-complementary d(CCAGGCCTGG) (**1**) with an apparent K_d of 1.6×10^{-7} M and that, in the presence of light, this duplex is cleaved selectively at C6.[7] Fifth, early studies of Xu et al.[14] alluded to the possibility that CoBLMs bound to DNA would be in slow exchange on the NMR time scale, which has been shown to be the case with **1**.[15]

We now report the details of our efforts using 2D NMR methods and molecular modeling to successfully determine the solution structure of CoBLM A2 green-DNA complex, and elucidate the mode of binding of the bithiazole tail of CoBLM A2 green and the basis for its sequence specificity. These results also shed insight on how a single molecule of BLM can effect double-stranded, blunt-ended, cleavage in duplex DNA and make a number of predictions that can be tested experimentally given the recent modular synthesis of BLM analogs.[16]

Materials and Methods:

Sample Preparation. The decamer d(CCAGGCCTGG) was synthesized on a 10 μmol scale at the MIT biopolymer lab and characterized as described in the preceding chapter. The purified DNA was desalted in a dialysis chamber against 50 mM sodium phosphate, pH 6.8. CoBLM A2 green was prepared using a modified published procedure.[7, 17]

NMR Experiments. All NMR experiments were performed on 750 MHz or 500 MHz Varian NMR spectrometers or on 600 MHz or 500 MHz home-built instruments at the Francis Bitter Magnet Laboratory. Data were then transferred to a Silicon Graphics work station and processed using Felix software (version 2.3, Biosym Technologies, Inc.). ^{1}H and ^{13}C chemical shifts are referenced to an internal standard, sodium 3-(trimethylsilyl)-1-propanesulfonate at 0.00 ppm. ^{31}P chemical shifts are referenced to an external sample of trimethyl phosphate, which is 3.53 ppm downfield of 85 % H_3PO_4.

A typical NMR sample contained ~3 mM complex and 50 mM sodium phosphate at pH 6.8 and was prepared by adding sequential amounts of CoBLM A2 green to the DNA sample until a 1:1 complex was apparent by NMR spectroscopy. For experiments in D_2O, the complex sample was lyophilized three times from 99.9% D_2O and then dissolved in 99.996% D_2O; for the experiments in H_2O, the complex was dissolved in 90% H_2O/10% D_2O.

DQF-COSY, TOCSY (MLEV-17 spin lock pulse with 35 ms, 70 ms, and 100 ms mixing times) and NOESY (50 ms, 200 ms, and 400 ms mixing times) experiments were recorded at 20 °C in D_2O or H_2O. Selected experiments were also recorded at 10 °C and 30 °C. Data sets with 4096 x 512 complex points were acquired with sweep widths of 5500 Hz (500 MHz instrument) or 8000 Hz (750 MHz instrument) in both dimensions and 32 scans per t_1 increment. During the relaxation delay period, a 2.0

s presaturation pulse was used for solvent suppression. For the NOESY experiments in H_2O, a Jump and Return pulse sequence[18] was used, and data sets with 4096 x 512 complex points were acquired with sweep widths of 12000 Hz in both dimensions. The t_1 dimension was zero-filled to 4096 data points and spectra were processed with a combination of exponential and gaussian weighting functions or a phase-shifted sine-bell weighting function. In all cases, ridges in t_1 were reduced by multiplying the first point in t_1 by one half prior to the Fourier transform. Baselines are corrected with a polynomial or an automatic baseline correction routine in t_2 when necessary.

HMQC[19] spectra were recorded at 20°C in D_2O with a J_{C-H} coupling constant of 135 Hz, 165 Hz, or 195 Hz. Data sets with 2048 x 256 complex points were acquired with 6000 Hz (^1H) and 25000 Hz (^{13}C) sweep widths on a 500 MHz instrument. 128 scans were collected for every t_1 increment. During the relaxation delay period, a 1.5 s presaturation pulse was used for solvent suppression. The t_1 dimension was zero-filled to 2048 data points. Spectra were then process with an exponential weighting function.

A 2D indirect detection ^{31}P-^1H COSY experiment[20] in D_2O was recorded at 20 °C and 30 °C on a 600 MHz instrument. Data sets with 4096 x 128 complex points were acquired with 7000 Hz in the ^1H dimension and 2000 Hz in the ^{31}P dimension. Data processing was carried out as described before.

Molecular Modeling. All calculations were carried out with Quanta 4.0/CHARMm 22 (Molecular simulations, Inc.; Waltham, MA) on a Silicon Graphics 4D/35 or Indigo. Non-bonded van der Waals and electrostatic interactions were cut-off at 11.5 Å, using a cubic switching function between 9.5 and 10.5 Å. The distance-dependent dielectric constant algorithm in the CHARMm package was used. Hydrogen bonds were cut off at 5.0 Å, and

switched between 3.5 and 4.5 Å. Hydrogen bonds were also cut off at 90° and switched between 50° and 70°. Non-bonded and hydrogen bond terms were updated every 20 steps. The SHAKE algorithm[21] was used to fix all bond lengths to hydrogen atoms. Molecular Dynamics calculations used the Verlet algorithm, with a .001 ps time step, and scaling every 100 steps. During molecular dynamics all force constants for bond distances and angles were set at 1000 kcal mol^{-1} $Å^{-2}$ and 500 kcal mol^{-1} rad^{-2} respectively. All energy minimizations used the standard CHARMm potential.[22] Distance constraints were applied using a square well potential and dihedral constraints were applied using a simple harmonic function.

Bleomycin A2 was constructed in Chemnote as described in detail in the preceding chapter. The DNA was constructed in Quanta assuming a B-form conformation. Since no counter-ions or solvent molecules were used in these studies, the charges on the non-bridging oxygens of the phosphate groups were reduced to lower the overall charge on phosphate to -0.32.[23] Color figures were made using Setor.[24] DNA conformational parameters were measured using NEWHELIX93 (Protein Data Bank).

Experimental Constraints. Intramolecular NOEs within DNA or within CoBLM A2 green, and intermolecular NOEs between the DNA and CoBLM A2 green were classified as strong, medium, or weak based on visual inspection of the cross peak intensities in the 200 ms NOESY spectra. CoBLM-DNA intermolecular and CoBLM A2 green intramolecular NOE derived distance constraints were set at 1.9-3.0 Å, 1.9-4.0 Å, and 3.0-5.0 Å for strong, medium, and weak NOEs respectively. An additional 1 Å was added to the upper limit of constraints on methyl or methylene hydrogen pseudoatoms.

DNA intramolecular constraints were set at 1.9-3.0 Å, 2.5-4.0 Å, and 3.5-5.0 Å for strong, medium, and weak NOEs respectively.

For CoBLM A2 green itself, the generalized Karplus equation that considers the electronegativity of substituents was used to derive the dihedral angle constraints.[25] In the 1D or 2D spectra of the CoBLM A2 green complexed with DNA, spectral broadening (line width > 5 Hz) and overlap have placed constraints on accurate assessment of the coupling constants. The analysis of the coupling constants in CoBLM A2 green is thus based on visual inspection of the cross peak sizes in the DQF-COSY spectrum. A large coupling constant (> 10Hz) has been used to define a trans orientation of the protons involved, while a small coupling constant (< 5 Hz) has been used to define a gauche conformation.

For DNA, the backbone angles, α, β, γ, ε, and ζ, were constrained to B-form values,[26] with force constants applied as described in the molecular dynamics section. The δ and χ angles were not constrained. Dihedral angle constraints with a force constant of 30 kcal mol^{-1} $Å^{-2}$ rad^{-2} were used throughout the molecular dynamics simulations on the DNA base pairs to prevent excessive propeller twist and buckling. These constraints were not applied at the intercalation site (C6•G15 and C7•G14).

Initial Structure. The initial structure was constructed by manually docking the bithiazole moiety between C6•G15 and C7•G14. Only one orientation of the bithiazole with respect to the DNA, and of each of the thiazolium rings with respect to one another was consistent with the observed NOEs. This was confirmed in the preliminary modeling in which the bithiazole moiety alone was placed >7 Å from DNA, and the molecular dynamics with the intermolecular NOE constraints consistently resulted in

the same orientation of the bithiazole moiety between C6•G15 and C7•G14. The bithiazole, threonine and valeryl (B, T, V, Figure 3.1) backbone dihedral angles were manipulated to relieve bad contacts between the metal binding region and the minor groove. After this crude positioning, the structure was minimized by 200 steps of the steepest descent method, followed by conjugate gradient minimization to a rms gradient < 0.1. The structure was then further minimized by the conjugate gradient method using the dihedral and distance constraints, to a rms gradient < 0.1.

Molecular Dynamics. To begin the restrained molecular dynamics simulated annealing, the distance constraints on the initial structures used a force constant of 0.6 kcal mol^{-1} $Å^{-2}$. The structure was heated and equilibrated over 4 ps, from 5-1000 K in 10 K increments, with velocities assigned every 0.1 ps from a Gaussian approximation to the Maxwell-Boltzman distribution. The force constants for the distance constraints were then scaled to 120 kcal mol^{-1} $Å^{-2}$ over 6.5 ps. The system was allowed to evolve for 10 ps, then cooled to 300 K over 7 ps. At 300 K the force constants of the distance constraints were reduced to the final value of 60 kcal mol^{-1} $Å^{-2}$. The dihedral constraints were then introduced with a force constant of 5 kcal mol^{-1} rad^{-2}, and increased to 50 kcal mol^{-1} rad^{-2} in 4 stages over 10 ps. The dihedral angle constraints on the DNA backbone angles β, γ, and ε at the intercalation site and the adjacent base pairs were applied with force constants of 5 and 10 kcal mol^{-1} rad^{-2} respectively. The electrostatic and hydrogen bond energy terms were introduced and the system was allowed to equilibrate for 4 ps, followed by a final 30 ps molecular dynamics run. The system was coupled to a heat bath at 300 K with a time factor of 0.1 ps during the final 30 ps.

The structures from the final 5 ps of the 30 ps molecular dynamics simulations were averaged and minimized. A 1000 steps of conjugate gradient minimization with the distance constraints and CoBLM dihedral angle constraints were used. The DNA backbone constraints were not used in the minimization. This process was repeated from a starting structure using eight different seeds for initial velocity assignments.

Results and Discussion

In preliminary experiments we reported that titration of d(CCAGGCCTGG) (**1**) with CoBLM A2 green resulted in the formation of a 1:1 complex that is in slow exchange on the NMR time scale.[15] The 1D ^{1}H NMR spectrum of the titration in the range of 0.5 to 3.0 ppm is shown in Figure 3.2. The free oligonucleotide **1** is self-complementary and hence gives rise to one set of resonances for symmetry-related protons (e.g., T-CH_3 at 1.68 ppm). Titration with CoBLM A2 green resulted in new sets of resonances corresponding to the CoBLM-DNA complex in which the symmetry has been disrupted (T8-CH_3, 1.64 ppm and T18-CH_3, 1.72 ppm, Figure 3.2).

In addition, upon binding of CoBLM A2 green to the oligonucleotide, the chemical shift of the methyl group of the pyrimidine moiety of the drug in the metal binding region (Figure 3.1) has changed from 2.48 ppm to 2.61 ppm and the two equivalent terminal methyl groups (2.94 ppm) of the sulfonium moiety (Figure 3.1) have become nonequivalent (2.97 ppm and 3.00 ppm) (Figure 3.2). In contrast, the peak intensities and chemical shifts of the α and γ methyl groups of the methylvaleryl moiety (V) and the methyl group of the threonine moiety (T), both in the peptide linker region of CoBLM A2 green, are almost identical to those in the free

Figure 3.1: Structure of Bleomycin A2

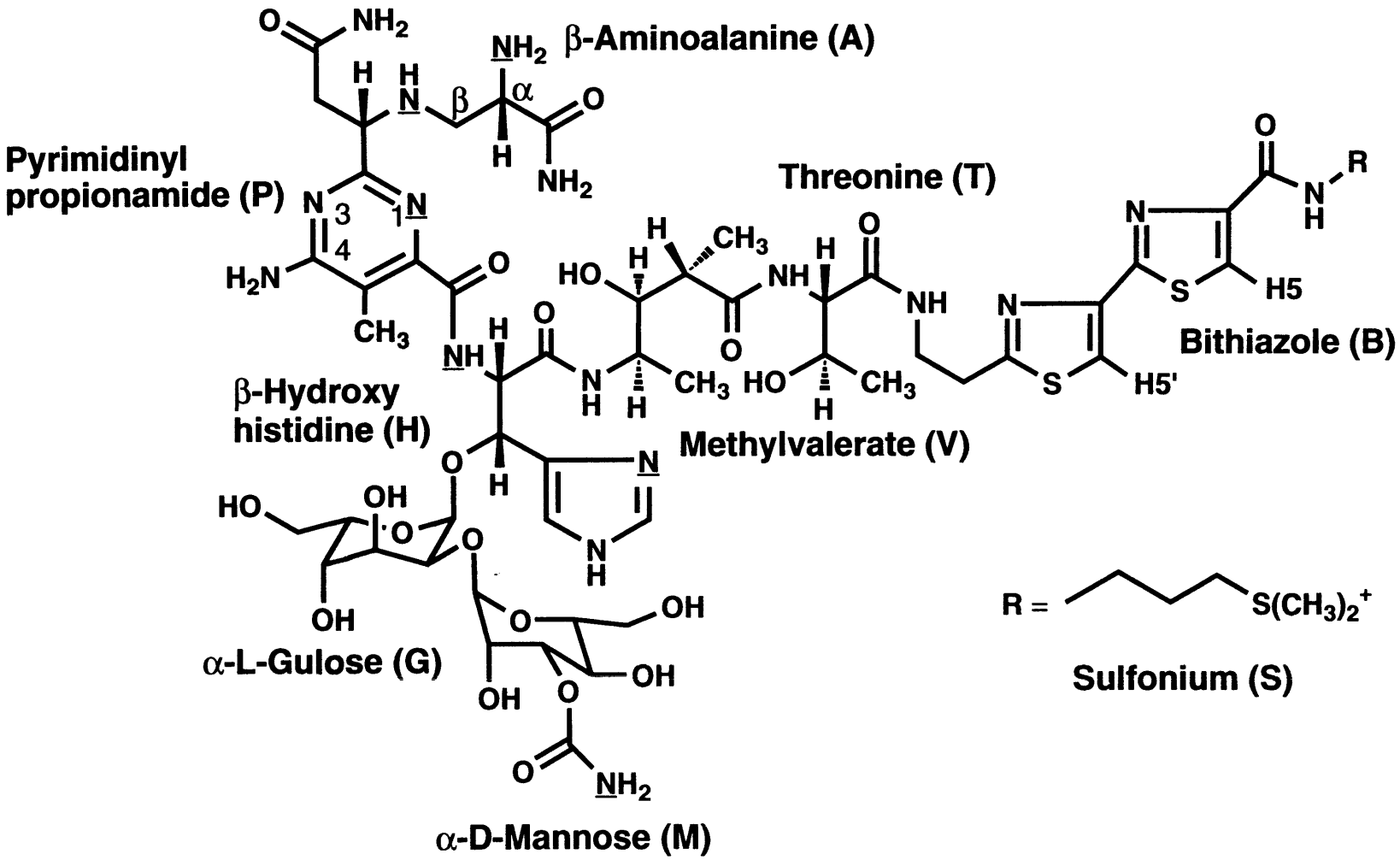
β-Aminoalanine (A)
Pyrimidinyl propionamide (P)
Threonine (T)
Bithiazole (B)
β-Hydroxy histidine (H)
Methylvalerate (V)
α-L-Gulose (G)
α-D-Mannose (M)
Sulfonium (S)
R = S(CH3)2+

Figure 3.2: Titration of d(CCAGGCCTGG) with CoBLM A2 green at 20°C. Upfield region of the ^{1}H NMR (500 MHz): CoBLM A2 green in 50 mM sodium phosphate (pH 6.8) and decameric duplex DNA (2.0 mM) in 50 mM sodium phosphate (pH 6.8) with 0, 0.5, and 1 equivalent of CoBLM A2 green added.

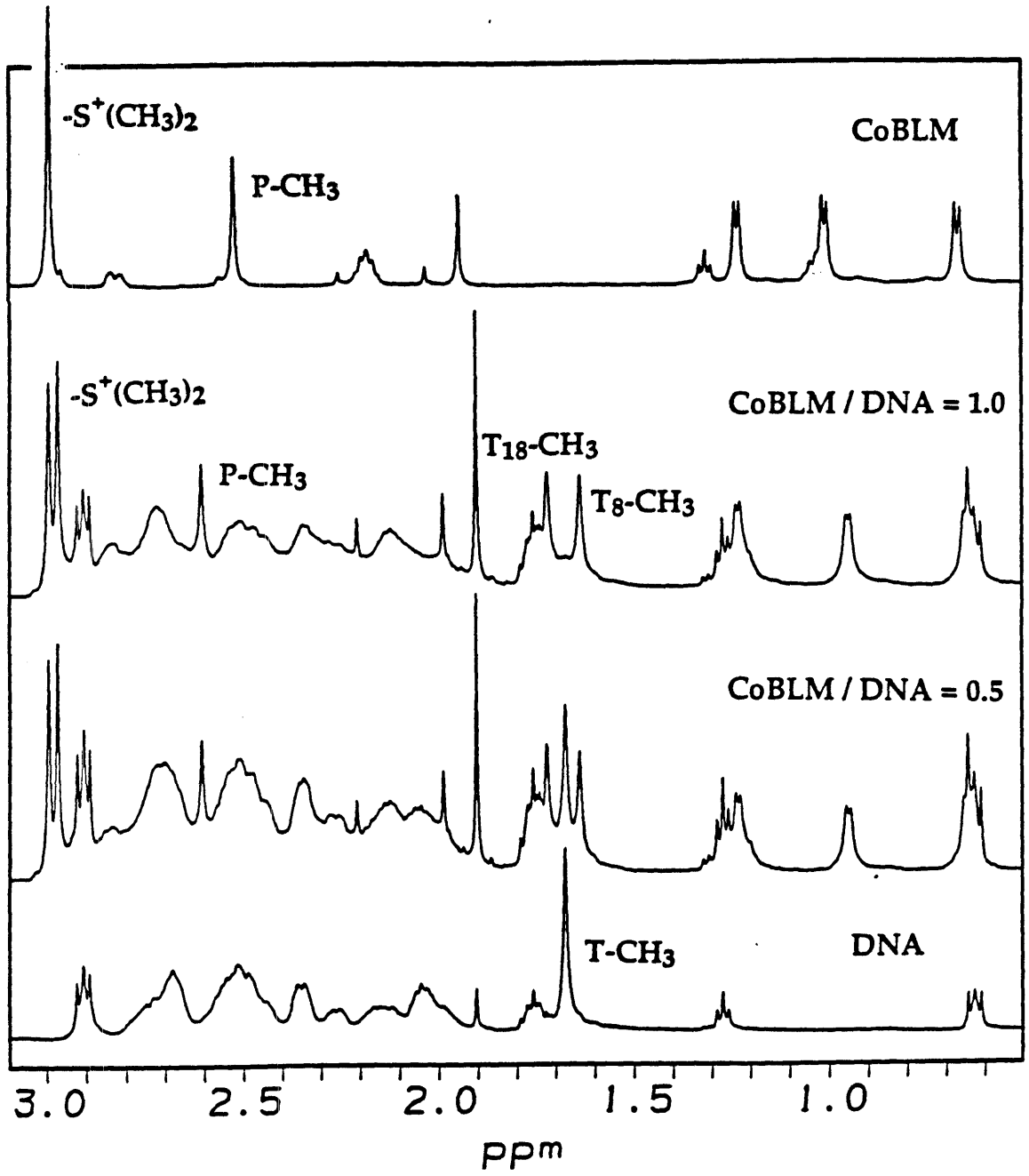
-S+(CH3)2
CoBLM
P-CH3
-S+(CH3)2
CoBLM / DNA = 1.0
T18-CH3
P-CH3
T8-CH3
CoBLM / DNA = 0.5
T-CH3
DNA
3.0
2.5
2.0
1.5
1.0
ppm

CoBLM (Table 3.1, Figure 3.2). These resonances thus conveniently provided the starting points for the assignments of V and T spin systems.

Proton and carbon assignments of the CoBLM A2 green in the complex. For the V spin system, proton assignments were established through the expected connectivity patterns in the DQF-COSY and TOCSY spectra in H_2O and D_2O. The cross peak between V-CαH and V-CβH, however, is absent in the COSY and TOCSY spectra, indicating a small coupling constant between these two protons. This observation along with the unusual upfield chemical shift of the V-αCH_3 (0.65 ppm) are also apparent in the free CoBLM A2 green (Table 3.1). Nevertheless, a strong NOE between the V-CαH and the V-CβH as well as NOEs to other protons within the spin system confirm the assignments. Additional confirmation comes from the carbon chemical shifts for this spin system, which have been assigned using the HMQC method. The carbon chemical shifts of the V-αCH_3, V-γCH_3, V-αC, V-βC, and V-γC are very similar to those in the free CoBLM (Table 3.1). When a COSY spectrum was run in H_2O, an exchangeable proton at 6.79 ppm was observed which showed a cross peak to the V-CβH proton. This proton also showed TOCSY cross peaks to V-CβH and V-CγH and NOEs to all the methylvalerate protons (Table 3.3). This resonance was thus assigned to the proton of the β-OH group of V, suggesting that it must be H-bonded in the complex with DNA. This proton, as expected, is not detected in the free CoBLM A2 green.

The proton chemical shift assignments for the T, the β-hydroxyhistidine (H) and the pyrimidinylpropionamide (P) spin systems (Figure 3.1) were obtained by inspection of the COSY and TOCSY spectra in both H_2O and D_2O (Table 3.1). The identification of the T-CH_3 resonance (1.23 ppm) facilitated the assignment of T-CαH and T-CβH. The T-NH is shifted 0.44 ppm downfield

Table 3.1: Proton and Carbon Chemical Shifts (ppm) of Free CoBLM A2 green and CoBLM A2 green Complexed with DNA.

		free pH 6.8 5 °C	complex pH 6.8 20 °C	free pH 6.8 5 °C	complex pH 6.8 20 °C
		Carbons		Protons	
P	CαH	35.5		3.20	2.78
	CαH'	35.5		3.51	3.69
	CβH	65.1	65.7	5.10	5.16
	CH_3	12.0	12.3	2.46	2.61
	4-NH_2			7.73,7.94	7.14,10.36
H	CαH	60.1	62.0	4.98	5.01
	CβH	71.7	73.3	5.53	5.48
	C2H	144.8	146.5	8.72	9.10
	C4H	122.2	122.0	7.60	7.60
A	CαH	59.3	60.0	3.41	3.37
	CβH	51.8	50.3	2.74	2.46
	CβH'	51.8	50.3	3.22	3.24
	NH			6.01	5.69
V	αCH_3	9.81	9.60	0.62	0.65
	γCH_3	20.4	20.4	0.98	0.96
	CαH	42.9	42.8	0.94	1.21
	CβH	77.7	76.1	3.33	3.73
	CγH	49.6	50.4	3.50	3.51
	NH			8.89	8.78
	OH				6.79
T	CH_3	22.4	21.6	1.19	1.23
	CαH	60.0	59.6	4.39	4.53
	CβH	71.7		4.25	4.51
	NH			8.92	9.36
B	CαH	35.5	34.7	3.06	2.83

		free pH 6.8 5 °C	complex pH 6.8 20 °C	free pH 6.8 5 °C	complex pH 6.8 20 °C
		Carbons		Protons	
B	CαH'	35.5	34.7	3.25	2.76
	CβH	41.9		3.44	2.93
	CβH'	41.9		3.83	3.76
	C5H	127.5	126.8	8.17	7.26
	C5'H	121.3	117.5	7.82	7.21
	NH			8.57	8.62
S	C$αH_2$	43.4	43.4	3.36	3.56,3.46
	C$βH_2$	26.6	25.7	2.13	2.07,2.16
	CγH	40.3	40.0	3.51	3.43
	CγH'	40.3	40.0	3.63	3.43
	$(CH_3)_2$	27.3	27.4	2.94	2.97,3.00
	NH			8.66	7.81
G	C1H	97.4	99.9	5.35	5.40
	C2H	69.9		4.11	4.04
	C3H	68.4		4.10	4.13
	C4H	71.8		3.80	3.73
	C5H	70.8		3.84	
	C6H	63.9		3.70	
	C6H'	63.9		3.84	
M	C1H	98.5	103.3	4.93	4.95
	C2H	70.3		4.00	3.96
	C3H	77.6		4.05	
	C4H	66.7		3.78	
	C5H	77.0		3.73	
	C6H	63.5		3.84	
	C6H'	63.5		3.98	
CoOOH					8.89

Table 3.2: Proton and Phosphorus Chemical Shifts (ppm) of DNA in the Complex at 20 °C.

	H6/H8	H5/H2	Methyl	H1'	H2'	H2"	H3'	H4'	H5',5"	^{31}P
C1	7.77	5.96		5.95	2.12	2.53	4.69	4.12	3.77	-0.66
C2	7.58	5.70		5.49	2.14	2.49	4.88	4.13		-0.44
A3	8.35	7.50		5.96	2.85	2.85	5.07	4.41	4.15,4.06	-0.78
G4	7.56			5.87	2.40	2.82	5.03	4.42	4.14	-0.96
G5	7.81			5.41	2.68	2.36	4.97	4.45	4.21	0.91
C6	7.43	5.59		5.98	1.76	2.36	4.81	3.25	3.81,4.00	-0.84
C7	7.63	5.97		5.91	2.21	2.25	4.77	3.98	3.74,3.32	-0.82
T8	7.34		1.64	5.53	2.09	2.26	4.82	4.14	4.05,3.95	-0.30
G9	7.85			5.69	2.73	2.73	4.99	4.36	3.98,4.08	-0.44
G10	7.84			6.12	2.56	2.33	4.67	4.19	4.19,4.11	
C11	7.74	5.94		5.94	1.99	2.45	4.65	4.11	3.73	-0.61
C12	7.58	5.70		5.13	2.12	2.29	4.79	4.05		-0.28
A13	8.00	7.89		5.99	2.53	2.72	5.01	4.33	4.07,3.91	-0.82
G14	7.38			5.23	2.42	2.72	5.02	4.31	4.10	1.71
G15	7.60			5.73	2.52	2.71	4.79	4.44	4.29,4.00	-1.18
C16	7.36	5.25		5.52	2.30	2.30	4.77	4.26	4.13	-0.44
C17	7.59	5.53		5.98	1.94	2.64	4.79	3.60	3.95	-0.83
T18	7.14		1.72	5.44	1.70	2.02	4.71	3.73	3.93,3.89	-0.52
G19	7.81			5.71	2.68	2.72	4.98	4.37	4.06,3.94	-0.55
G20	7.77			6.11	2.51	2.33	4.64	4.19		

	Imino	C amino
C1•G20		
C2•G19	12.91	8.65, 6.95
A3•T18	14.62	
G4•C17	13.24	8.96, 6.81
G5•C16	12.91	8.55, 6.35
C6•G15	12.54	7.79, 6.59
C7•G14	11.84	8.23, 7.18
T8•A13	14.24	
G9•C12	13.15	8.56, 6.96
C10•C11		

Table 3.3: Nontrivial Intramolecular NOEs within CoBLM A2 green in the Complex at 20 °C.[a]

H-C2H---A-CβH	w	G-C1H---H-CαH	m	B-NH---B-CαH′	m
H-C2H---A-CβH′	w	A-CβH---P-CαH′	m	V-NH---V-CαH	s
H-C2H---A-NH	m	A-CβH′---P-CαH′	w	S-CαH---S-CH_3 (1)	w
H-C2H---P-CβH	w	A-CβH---P-CβH	w	S-CαH′---S-CH_3 (1) and (2)	w
H-C2H---T-CH_3	m	A-CβH′---P-CβH	w	V-OH---V-CαH	w
H-C2H---T-CβH	w	A-CβH′---P-CαH	m	V-OH---V-αCH_3	w
H-C2H---T-CαH	w	A-CαH---P-CαH	w	V-OH---V-γCH_3	s
H-C2H---T-NH	w	A-CβH---P-CαH	m	V-OH---V-CβH	s
H-C2H---V-CαH	m	V-γCH_3---P-CH_3	w	P-NH_2 (1)---P-CH_3	m
H-C2H---V-αCH_3	w	V-αCH_3---V-CγH	s	P-NH_2 (2)---P-CH_3	m
H-C2H---V-CβH	w	V-γCH_3---V-CβH	s	CoOOH---V-NH	w
H-C4H---V-CαH	w	V-αCH_3---V-CβH	m	CoOOH---T-NH	m
H-C4H---V-αCH_3	m	V-αCH_3---V-γCH_3	m	CoOOH---V-αCH_3	w
H-C4H---H-CαH	w	V-γCH_3---V-CαH	m	CoOOH---V-γCH_3	w
A-NH---T-CH_3	w	T-NH---V-CαH	m	CoOOH---V-CγH	w
P-CβH---B-CβH	w	T-NH---V-NH	m	CoOOH---V-CαH	m
G-C1H---H-CβH	s	V-NH---V-γCH_3	s	CoOOH---P-CβH	m
G-C1H---M-C1H	m	V-NH---V-αCH_3	s	CoOOH---V-OH	w
V-CγH---H-CβH	w	B-NH---T-CαH	m	CoOOH---A-NH	w
V-αCH_3---H-CβH	w	B-NH---T-CH_3	m	CoOOH---H-C2H	w
M-C1H---H-CβH	w	B-NH---B-CαH	m		

[a] w, m, s: weak, medium, strong NOE at 200 ms mixing time. P-NH_2 (1), 10.36 ppm; P-NH_2 (2), 7.14 ppm. S-CH_3 (1), 3.00 ppm; S-CH_3 (2), 2.98 ppm.

relative to its chemical shift in the free CoBLM A2 green and showed a TOCSY cross peak to the T-CαH in H_2O. Similarly, through-bond connectivities are observed from H-CαH to H-CβH, H-C2H to H-C4H (weak four-bond coupling), and from P-CαHs to P-CβH. Intramolecular NOEs between protons in these spin systems are all consistent with these assignments. In none of the experiments recorded in H_2O was the amide proton of the β-hydroxyhistidine (H-NH) observed. This result is consistent with previous studies on other metallo-BLMs in which there is general agreement that this amide is deprotonated and is one of the ligands to cobalt.[4, 5]

The assignment of the protons associated with the bithiazole moiety (Figure 3.1) of CoBLM A2 green is essential to defining its mode of binding to the DNA duplex. As previously reported by Akkerman et al., the H5 proton of the terminal thiazolium ring and the H5' of the penultimate thiazolium ring can be assigned using HMQC and HMBC methods.[5] We have used these methods to unambiguously assign B-C/H5 (127.5 ppm, 8.17 ppm) and B-C/H 5' (121.3 ppm and 7.82 ppm) in the free CoBLM A2 green. The HMBC method applied to the complex has been unsuccessful because of the signal-to-noise and overlap problems. However, we have previously reported use of the HMQC method to assign the two bithiazole protons to resonances at 7.21 ppm and 7.26 ppm. By making the assumption that the ^{13}C chemical shift of the carbon attached to each of these protons in the complex has not dramatically shifted relative to those in the free CoBLM A2 green, the resonance at 7.21 ppm has been assigned to the B-H5' (B-C5' at 117.5 ppm) and the one at 7.26 ppm to B-H5 (B-C5 at 126.8 ppm).

The identification of the methylene protons associated with the bithiazole moiety of CoBLM A2 green has proven more difficult due to the spectral overlap with the H2' and H2'' protons of DNA in the region of 2 to 3

ppm. Initially, the B-CαHs and B-CβHs were located using a TOCSY experiment in H_2O in which cross peaks have been detected between the B-NH proton and these two sets of protons. Subsequent re-examination of the COSY and TOCSY spectra collected in D_2O confirm the assignments via the through-bond couplings between B-CαHs and B-CβHs. Further confirmation of these assignments is provided by the observation of strong intramolecular NOEs between B-NH proton and the T protons and trivial NOEs within the B spin system itself.

For the assignments of the proton chemical shifts in the dimethyl sulfonium (S) spin system (Figure 3.1), the methylene protons of CαH, CβH, and CγH show strong COSY cross peaks to each other and to their adjacent protons. In the TOCSY spectrum collected in H_2O, the amide proton (S-NH) is easily identified through its cross peak to S-CγH at a short mixing time (35 ms) and to both S-CγH and S-CβH at a longer mixing time (70 ms). The assignments of S spin system and bithiazole ring protons are corroborated by a weak NOE between B-C5H and S-CγH in the NOESY spectrum at 400 ms mixing time (absent at 200 ms mixing time). The carbon chemical shifts of the sulfonium group, assigned using the HMQC method, exhibit little variation with respect to the free CoBLM A2 green (Table 3.1).

The most difficult chemical shift assignments have been associated with the β-aminoalanine moiety (A), the axial ligand of CoBLM A2 green. In the TOCSY or the COSY spectra in H_2O, the secondary amine (A-NH) has not been located. Furthermore, in the DQF-COSY and TOCSY experiments collected in D_2O, no ABX spin system could be assigned to the A-CαH proton and the A-CβH protons. The chemical shift assignments of this spin system have been achieved as outlined subsequently. Protons with chemical shifts at 2.46 and 3.24 ppm are strongly coupled to each other in the DQF-COSY

spectrum and both show weak NOEs to the P-CβH proton (Table 3.3). These protons were initially assigned to the A-CβHs. A resonance at 3.37 ppm was assigned to the CαH, based on its strong NOEs to both A-CβHs and a weak NOE to the P-CαH. As further confirmation of these tentative assignments, the carbon chemical shifts of the A-αC and A-βC in the free CoBLM A2 green at 59.3 and 51.8 ppm respectively, were compared with the ^{13}C chemical shifts associated with the putative A-Cα and A-Cβ in the complex: 60.0 and 50.3 ppm. These similarities support the above assignments. Finally, re-examination of the NOESY spectrum in H_2O allowed us to assign the A-NH proton (5.69 ppm), which shows trivial NOEs to A-CβHs as well as several additional, structurally informative, intramolecular NOEs (Table 3.3).

The absence of the COSY cross peaks between the A-CαH and A-CβHs is attributed to the small coupling constants between these protons, which is reminiscent of the small values (3 Hz and 4 Hz) observed between the same set of protons in the free CoBLM A2 green. Based on the arguments presented in the preceding chapter,[7] the small coupling constants between the A-CαH and A-CβHs in the complex are consistent with the model in which the primary amine of A serves as an axial ligand to cobalt. Thus, the identity of this axial ligand in CoBLM A2 green is similar to that in its complex with DNA.

The final assignments in CoBLM A2 green to be made are the protons associated with the gulose (G) and mannose (M) residues. Unfortunately, these protons reside in a region of the spectrum (~4 ppm) which has extensive overlap with the 4' and 5' protons of the deoxyribose of the DNA. Despite this spectral crowding, DQF-COSY and TOCSY spectra have allowed assignments of G-H1' through G-H4' for the gulose and M-H1' and M-H2' for the mannose (Table 3.1).

Assignment of the Exchangeable Protons of the DNA in the Complex. A 1D ^1H NMR spectrum of the complex in H_2O at 20 °C displays eight imino resonances, whereas in the free DNA, only four imino protons are observed. At 5 °C, all five imino protons of the free DNA are observed with the terminal G•C imino hydrogen, as expected, being very broad. These results, described previously by Wu et al.,[15] indicate that the formation of a 1:1 complex of the DNA with CoBLM A2 green results in the disruption of the DNA symmetry.

The assignments of the imino protons have been made using standard NOESY experiments. The two most downfield resonances are at 14.62 ppm and 14.24 ppm and have been assigned to the two thymine imino protons of T18 and T8, respectively based on their strong NOEs to their base-pairing adenine H2. The assignments of the adenine H2, in D_2O, are confirmed by the observed weak NOEs (400 ms mixing time) to their own H1', the 3'-neighboring H1' and the 5'-neighboring H1' on the opposite strand.

Sequential imino-imino NOEs from the two A•T imino protons have allowed assignment of all the remaining imino protons with the exception of terminal G•C base pairs and those associated with C6•G15 and C7•G14. As outlined below the connectivity between the base pairs associated with C6 and C7 is disrupted due to the intercalation between them of the bithiazole ring tail of CoBLM A2 green (Figure 3.3). The imino protons of the terminal G•C pairs are not observed at 20 °C, presumably due to exchange broadening. The guanine imino protons also show strong NOEs to the protons of the 4-amino groups and weak NOEs to the H5 protons of their base-paired cytosine partners. Each cytosine amino proton also exhibits strong NOEs to its own H5 proton.

Figure 3.3: Imino to imino region of the NOESY spectrum (200 ms mixing time, 500 MHz) of a 1:1 complex of CoBLM and **1** in H_2O. CoBLM A2 green and **1** (5.0 mM) in 90% H_2O/10% D_2O in 50 mM sodium phosphate (pH 6.8) at 20°C. The sequential imino to imino cross peaks are traced by connecting lines. The missing NOE between the imino proton of G14 to that of G15 is indicated by a box. Intermolecular NOEs are (A) P-NH_2 (10.36 ppm) to the imino proton of G4•C17, (B) P-NH_2 (10.36 ppm) to the imino proton of G5•C16.

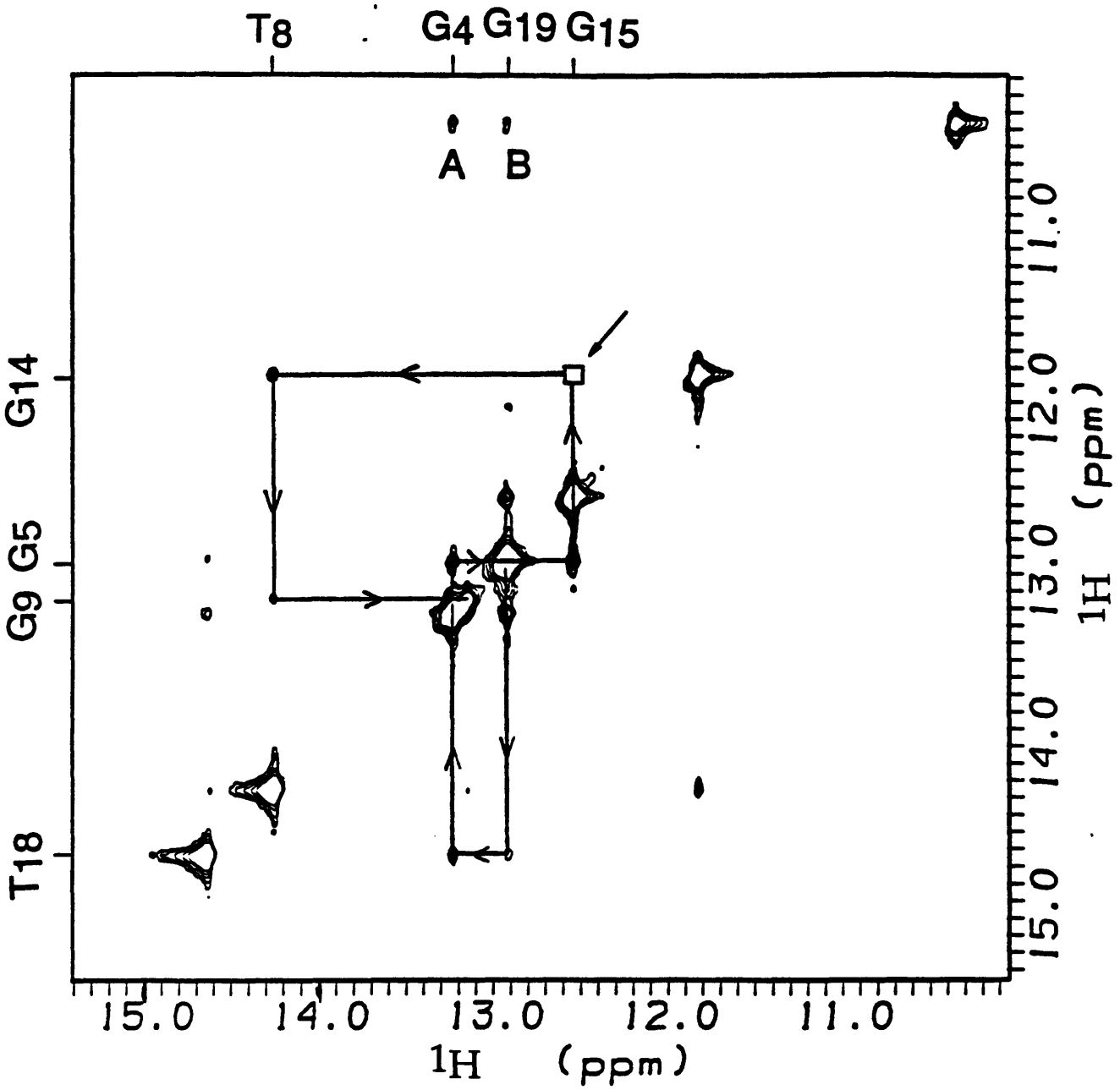
T8
G4 G19 G15
A B
G14
G9 G5
T18
15.0
14.0
13.0
12.0
11.0
1H (ppm)
11.0
12.0
13.0
14.0
15.0
1H (ppm)

Two exchangeable protons with unusual chemical shifts have also been detected whose assignments have provided much structural insight. The proton at 8.89 ppm is proposed to be associated CoBLM A2 green and the other proton at 10.36 ppm, tentatively assigned to the G5 amino proton of the DNA[15] is, as outlined below, also shown to be associated with CoBLM A2 green. It is one of the protons of the 4-amino group attached to the pyrimidine ring (Figure 3.1). The reassignment of the proton at 10.36 ppm is based on its strong NOE to another exchangeable proton at 7.14 ppm, the second proton of the amino group of the pyrimidine ring, and the fact that both 4-amino protons show medium NOEs to the P-CH_3 (Figure 3.1). Additional NOEs to the DNA (for example to G5-H4', Table 3.4) and molecular modeling described subsequently, support this assignment. The interaction of a G5 amino proton with its G5-H4' would have required a drastic distortion of the generic B-form DNA as the distance between these protons is greater than 7 Å in B-form DNA. No evidence for this type of distortion exists from a detailed analysis of the sugar puckers of the deoxyribose rings outlined below. Second, there is no detectable NOE between the amino proton at 7.14 ppm and the G5•C16 imino proton as would be expected if this proton were associated with the amino of G5. Thus the unusual downfield shifted amino proton of P from 7.94 or 7.73 ppm in the free CoBLM A2 green to 10.36 ppm in the complex and its NOEs to DNA have important structural implications.

The second exchangeable proton of interest at 8.89 ppm has been assigned to the proton associated with the axial hydroperoxide ligand of CoBLM A2 green. This resonance shows six NOEs to the C6 and C7 sugar protons of DNA (Table 3.4), and ten NOEs to the protons associated with the metal binding region and the V and T moieties in the peptide linker of

Table 3.4: Intermolecular NOEs between CoBLM A2 green and DNA at 20 °C.

5′ end	Strand 1	BLM residues	3′ end	Strand 2	BLM residues
A3			T18	H4'	P-CαH /w
				H4′	A-CαH /m
				H5′*[b]	A-CαH /s
G4	NH	P-NH_2(1)[a] /w	C17	H1′	A-CαH /w
				H4′	A-CβH′ /w
					A-CβH /w
					A-CαH /s
					P-CαH /w
G5	H4′	P-CH_3 /m	C16		
		P-NH_2(1) /w			
		P-NH_2(2) /w			
	H1′	P-CH_3 /w			
		P-NH_2(1) /m			
		P-NH_2(2) /m			
	NH	P-NH_2(1) /w			
C6	H5″	P-CH_3 /s	G15	H1′	B-C5H /w
		V-γCH_3 /m		H4′	B-C5H /w
	H5′	P-CH_3 /s		H5′	B-C5H /m
		V-γCH_3 /m		NH	B-C5H′ /m
	H4′	CoOOH /m			B-CβH′ /w
		P-CH_3 /m			B-CβH /w
		V-NH /w		H8	B-C5H /m
		V-γCH_3 /m			
	H2″	CoOOH /w			
	H2′	CoOOH /w			
	H1′	CoOOH /m			
		P-CH_3 /w			
		P-CβH /m			
	NH2h	B-C5H′ /m			
	NH2e	B-C5H′ /m			
C7	H5″	T-CαH /m	G14	H1′	B-C5H /s
	H5′	CoOOH /w		H2″	B-C5H /s
		V-OH /w		H2′	B-C5H /m
		T-CαH /m		H3′	B-C5H /w
	H4′	CoOOH /w		H4′	B-C5H /w
		T-CH3 /w		NH	B-C5H′ /w
		T-CαH /m		H8	B-C5H /m
		B-NH /m			S-CβH′ /w
	H1′	B-CαH′ /w			S-CβH /w
		B-CαH /w			S-CγH /m
		B-NH /m			
T8			A13	H8	S-CH_3 /w
3′ end	Strand 1		5′ end	Strand 2	

[a] P-NH_2 (1) and P-NH_2 (2) are the hydrogens at 10.36 ppm and 7.14 ppm, respectively. [b] Used the H5' pseudoatom.

CoBLM A2 green (Table 3.3). A number of additional facts allow us to favor this unusual assignment. No scalar connections from this proton to other protons can be observed in either the TOCSY or the COSY spectra. No NOEs are detected between this proton and any of the imino or amino protons associated with the DNA, thus making it unlikely that it is a proton associated with the decamer itself. Finally, the possibility that this proton is associated with one of the unassigned exchangeable protons of CoBLM A2 green, such as the primary amine of the A or terminal amino protons of the primary amides, can be ruled out because NOE patterns expected from these amino protons are incompatible with the NOE patterns associated with this resonance.[27] As outlined below, molecular modeling provides very strong support for this unusual and structurally significant assignment.

Assignment of the Nonexchangeable Protons of DNA in the Complex. Protons associated with DNA bases and sugars have been assigned by analyzing the NOESY, TOCSY , DQF-COSY and ^{31}P-^{1}H COSY spectra using standard sequential strategies.[28] The assignments are summarized in Table 3.2 and the sequential connectivities for strands 1 and 2 of the decamer are summarized in Figure 3.4 and Figure 3.5.

For strand **1** (C1 to G10), the sequential base to base and base to H1′ NOEs can be readily traced from the H8 of G10 to the H6 of C7. There are no NOEs observed, however, from the H6 of C7 to the H6 of C6, or from the H6 of C7 to the H1′ of C6 (Figure 3.4). The disruption of this connectivity revealed in the final structural model, is a function of the penultimate thiazolium ring being stacked between C6 and C7. Starting with C6 , one can easily follow the sequential connectivity from C6 to the C1 (Figure 3.4). For strand **2** (C11 to G20, Figure 3.5), the sequential NOEs can be followed from

Figure 3.4. Expanded NOESY spectrum (400 ms mixing time, 500 MHz) of the base to sugar H1′ region of strand 1 (C1~C2~A3~G4~G5~C6~C7~T8~G9~G10) in the complex. The sequential connectivities are indicated by the connecting lines, and the break in the sequential connectivities at the C6~C7 step is shown by an arrow with a box.

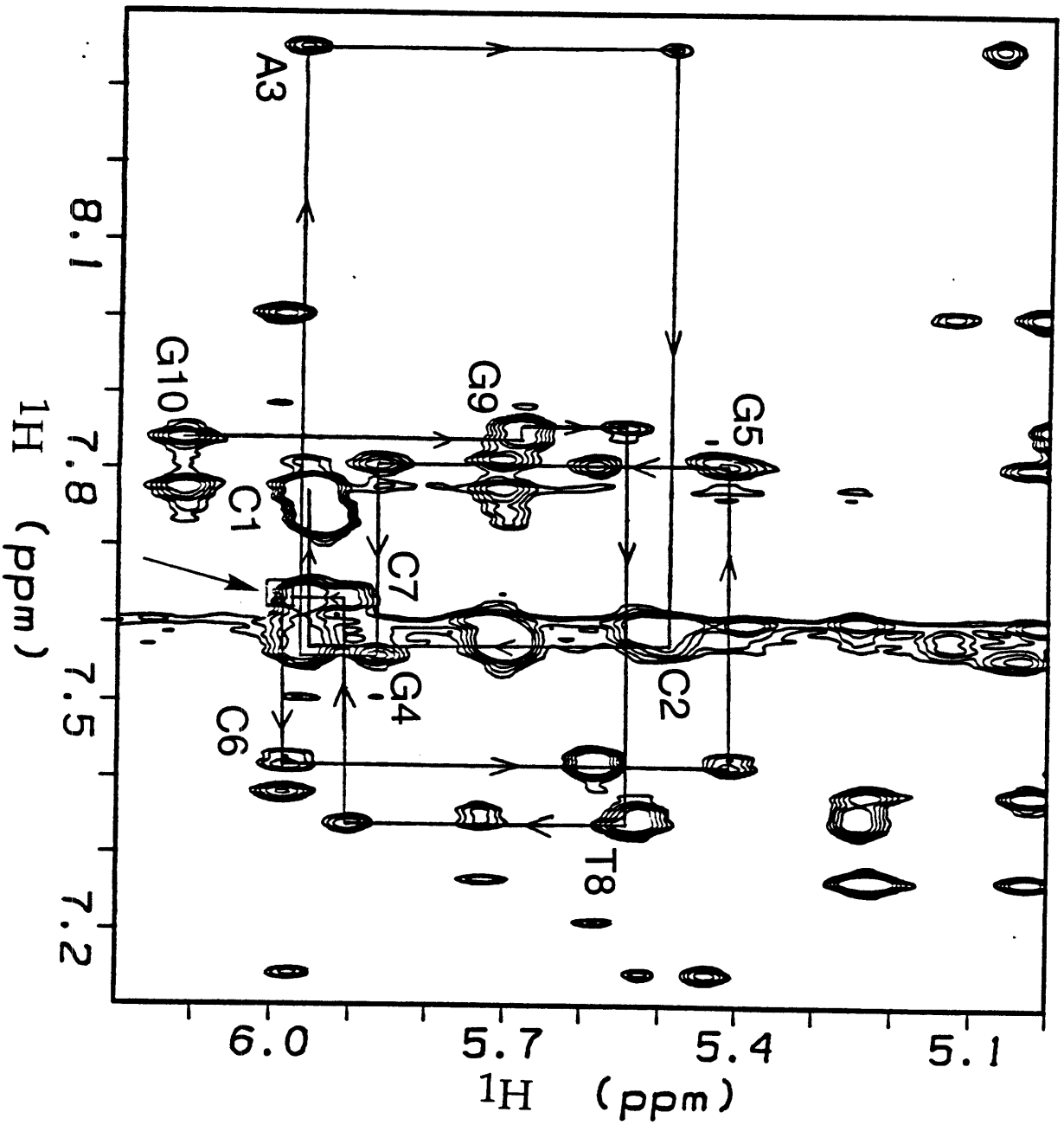
A3
G10
G9
G5
C1
C7
G4
C2
C6
T8
8.1
7.8
7.5
7.2
1H (ppm)
6.0
5.7
5.4
5.1
1H (ppm)

Figure 3.5: Expanded NOESY spectrum (400 ms mixing time, 500 MHz) of the base to sugar H1′ region of strand 2 (C11~C12~A13~G14~G15~C16~C17~T18~G19~G20) in the complex. The sequential connectivities are indicated by the connecting lines, and the break (shown by the arrow with a box) in the sequential connectivities at the G14~G15 step is obscured by other overlapping peaks in the same region.

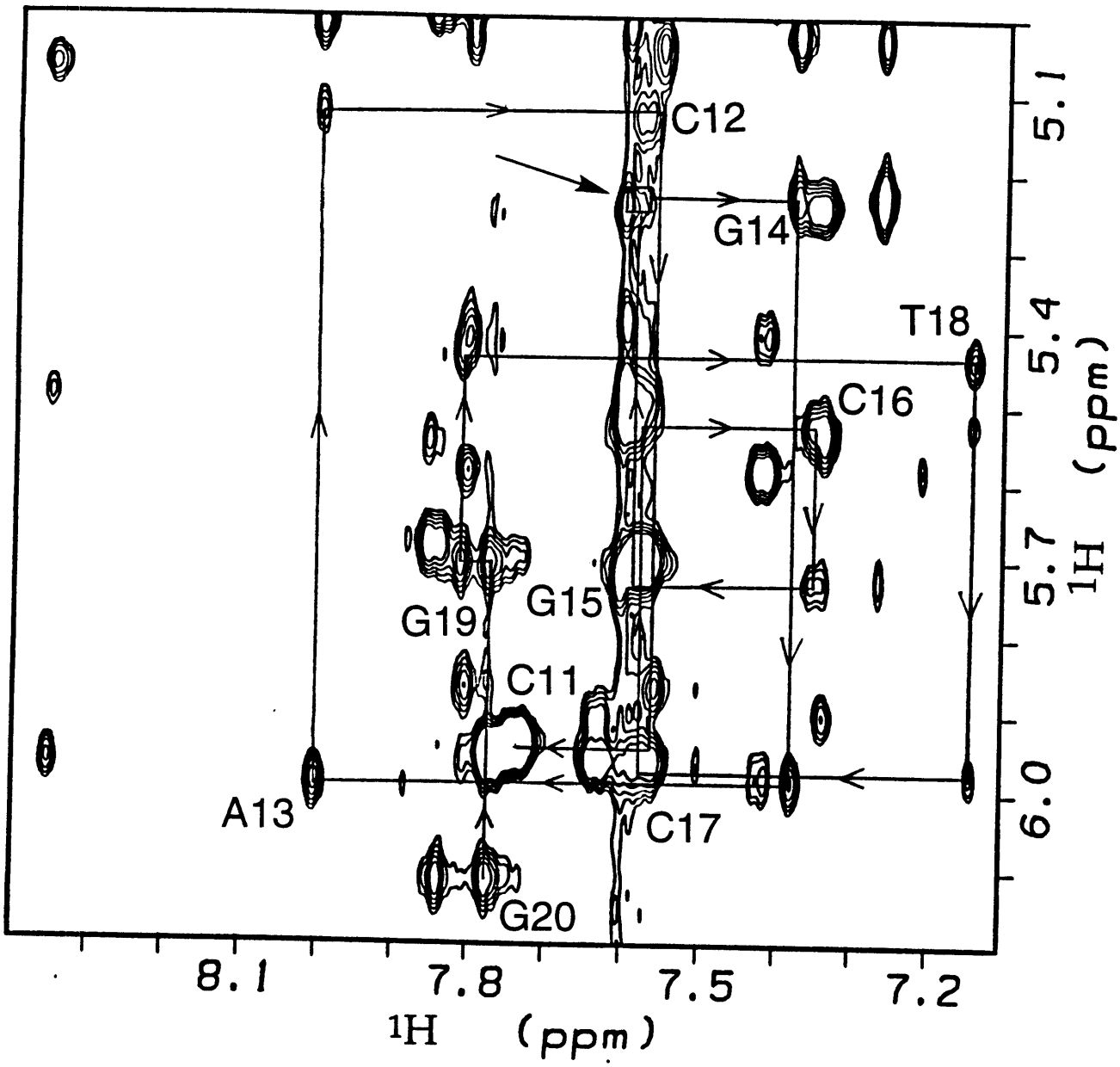
C12
G14
T18
C16
G15
G19
C11
A13
C17
G20
8.1
7.8
7.5
7.2
1H (ppm)
5.1
5.4
5.7
6.0
1H (ppm)

G20 to G15. No connectivity is observed between the H8 of the G15 and the H8 of the G14 due to the intercalation of the terminal thiazolium ring between these two bases. However, in the region of 7.6 and 5.9 ppm, there is extensive spectral crowding and therefore, it is not possible to assess if the connectivity from the G15-H8 to G14-H1' has been interrupted as would be predicted from the final model. The sequential NOEs from G14 to C11 are readily observed (Figure 3.5).

The sugar protons (H2', H2", H3', and H4') of each nucleotide have been assigned by their connectivities with their own H1' protons using TOCSY experiments carried out at various mixing times (30 ms for H2' and H2"; 70 ms and 100 ms for H3' and H4'). The H2' protons have been distinguished from the H2" protons using the NOESY spectrum collected at 50 ms mixing time, where regardless of the sugar pucker, the NOE between the H1' and the H2", should be larger than that between the H1' to the H2'.[29] In the DQF-COSY spectrum, all H1' to H2' cross peaks, except for C6, are indicative of sugars having C2'-endo like puckers. For C6 (the site of CoBLM A2 green light mediated cleavage), the H1' to H2" and H3' to H4' cross peaks are readily detected, while the H1' to H2' is absent. These observations are consistent with a C3'-endo like sugar pucker.[29] The implications of the altered sugar pucker of C6 will be discussed subsequently.

The assignments for H2' and H2" have been confirmed using a NOESY experiment (200 ms) by tracing the NOEs between the base to its own 2' and 2" protons and the sequential NOEs between the base and its 5'- neighboring H2' and H2". No NOEs are observed between the H6 of the C7 to H2' and H2" of C6. The NOEs between the H8 of G15 to the H2' and H2" of the G14 are obscured due to spectral crowding. The H3' proton assignments can also be confirmed using the 200 ms NOESY experiment by following the

sequential NOEs between the base to its own and to its 5'-neighboring H3' protons.

The assignments for the H5' and H5" of the DNA are more problematic due to spectral crowding. TOCSY experiments using long mixing times (100 ms to 200 ms) have not allowed the assignments of H5' and H5" from H1'. Attempts to use the DQF-COSY method to identify cross peaks between H4' to H5' and H5" were also unsuccessful because of spectral crowding between 4 and 4.5 ppm (Table 3.2). Thus assignments of the H5' and H5" protons were made in the ^{31}P-^{1}H spectrum (vide infra), as well as in the NOESY spectrum by assuming a standard B-form DNA structure, where weak NOEs from the base proton to its own H5' and H5" would be expected to be observed. As noted in Table 3.2, some of these assignments were still not possible.

Assignments of the Carbons of DNA in the Complex. The HMQC spectrum has been useful since the carbon chemical shifts associated with the bases and the deoxyribose residues are predictable: that is, they are not altered substantially between the free and the complexed DNA. Thus association of a carbon with a proton having an unusual chemical shift would provide further confirmatory evidence for the proton assignment. Two examples of the usefulness of the data from an HMQC spectrum follow. First, the chemical shift of the H4' of C6 has been assigned to 3.24 ppm, dramatically upfield shifted in comparison with the other H4' protons (Table 3.2). The HMQC spectrum reveals a carbon chemical shift of 83.8 ppm associated with this proton. This chemical shift is typical of C4' carbons[30] and thus this method provides additional confidence in the proton assignment. A second interesting example is provided by C7-H5" which has been upfield shifted

dramatically relative to other H5'/H5" protons, to 3.32 ppm. The carbon chemical shift associated with this proton is 66.7 ppm, typical of a C5' of a deoxyribose moiety[30]. These protons with unusual chemical shifts have been highlighted as they possess interesting intermolecular NOEs to CoBLM A2 green (Table 3.4). The correct assignments of these shifted protons have been essential in the structure elucidation.

^{31}P Assignments of DNA in the Complex. In the free DNA, nine DNA phosphorus resonances are present, which become doubled in the presence of CoBLM A2 green. Two of the phosphorus signals are downfield shifted from the normal envelope of the ^{31}P resonances and have been assigned to the phosphates connecting G5~C6 and G14~G15 using a ^{31}P-^{1}H COSY spectrum (Figure 3.6). This type of downfield movement is indicative of an intercalative mode of binding for CoBLM A2 green.[31]

Finally, the ^{31}P-^{1}H COSY experiment also provides an independent verification of the assignments of the H3' and some of the H4' and H5'/H5" protons of the deoxyribose residues. Eighteen phosphorus to H3' cross peaks are discernible and assigned by the correlation between the ^{31}P and its 5'-coupled H3'. Additionally, ^{31}P is coupled to its 3'-neighboring H4' and H5'/H5". Although the complete sequential assignments from the phosphorus to the H4', H5'/H5" protons have not been attainable because of overlap, the assignments of sugar protons near the intercalation site are confirmed (Figure 3.6).

Figure 3.6: ^{31}P-^{1}H COSY spectrum of the complex at 30 °C.

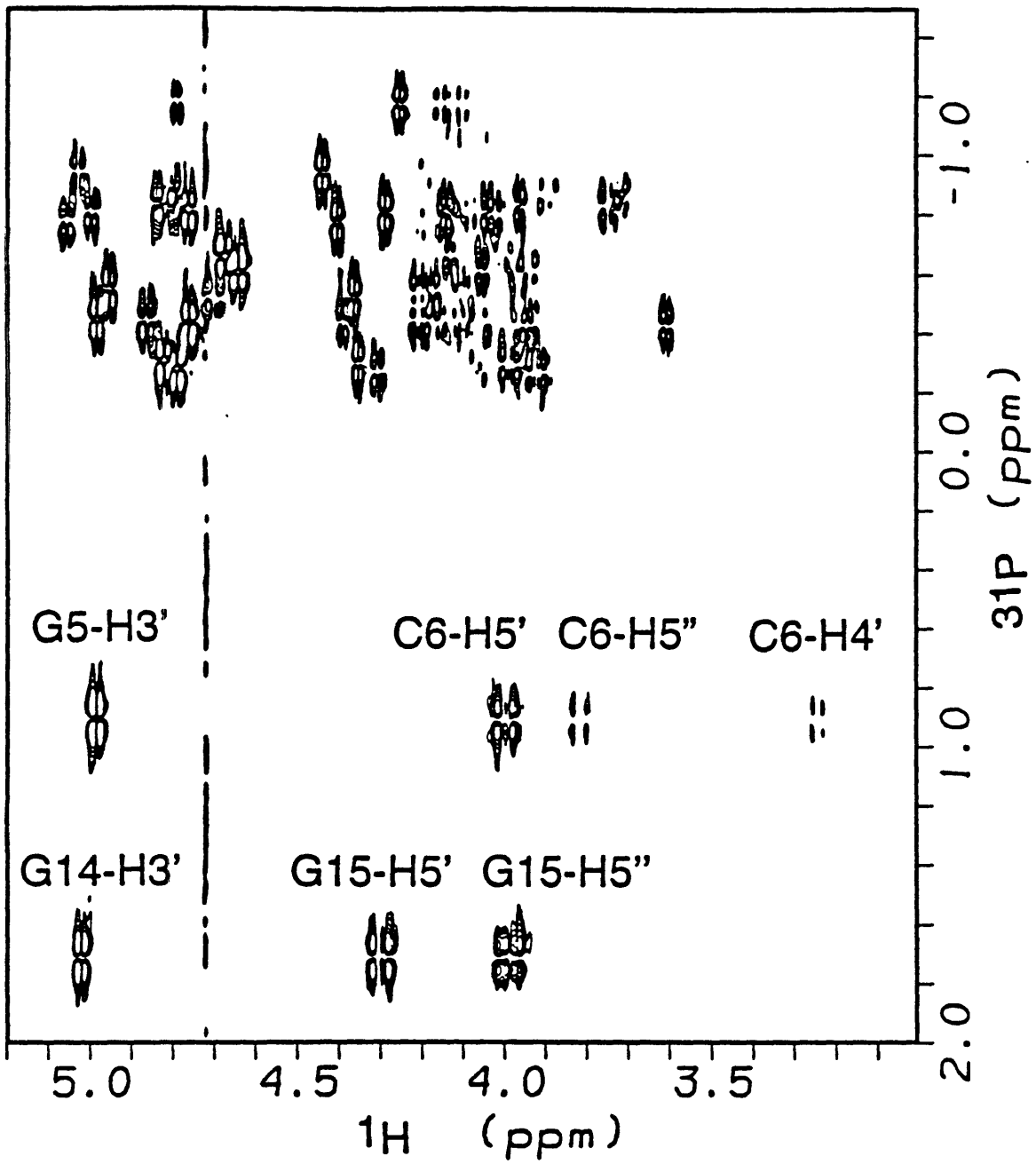
G5-H3'
C6-H5'
C6-H5"
C6-H4'
G14-H3'
G15-H5'
G15-H5"
5.0
4.5
4.0
3.5
1H (ppm)
-1.0
0.0
1.0
2.0
31P (ppm)

Molecular Modeling

Distance Constraints. Intramolecular NOEs within DNA or within CoBLM A2 green, and intermolecular NOEs between DNA and CoBLM A2 green were classified based on visual inspection of the cross peak intensities in the 200 ms NOESY spectra collected in H_2O and D_2O. There are total of 60 intermolecular NOEs (Table 3.4), 61 intramolecular CoBLM NOEs (Table 3.3), 206 intramolecular DNA NOEs and 28 Watson-Crick hydrogen bond constraints.

Dihedral Constraints. Ten dihedral angle constraints of CoBLM A2 green were derived as described in Materials and Methods. DNA backbone β, γ and ε angles have been constrained using standard B-form DNA parameters.[26] Lower force constants were used on the base pairs of the intercalation site, and those directly adjacent to it, to allow for potential distortion of the DNA as a result of the intercalation of the bithiazole moiety. The use of generic DNA constraints was based on a qualitative analysis of the NMR data, which suggested, with the exception of the structural variations described below, that the DNA backbone was not significantly distorted. It was found that, in the preliminary structural calculations, these constraints significantly improved the fit of the structure to the NOE data. Additionally, no notable NOE violations were observed in the region of DNA in contact with CoBLM A2 green, thus the reduced force constants of the dihedral angle constraints in this region allowed sufficient flexibility to satisfy the experimental data. The constraints for the backbone α and ζ angles were qualitatively derived from the ^{31}P chemical shift information (Table 3.2) in the complex[32] as discussed subsequently. In duplex B-form DNA, the gauche(-), gauche(-) (g^-,g^-; ζ,α)

geometry about the P-O bonds in the backbone is energetically favored, and this geometry is associated with a more shielded ^{31}P resonance. The other significantly populated conformation, the trans, gauche(-) (t,g^-; ζ,α) geometry, results in a more downfield shifted ^{31}P resonance.[32] Accordingly, the two downfield shifted phosphates (Figure 3.6) in our complex, one between G5 and C6, and the other between G14 and G15, were constrained to the trans and gauche(-) conformation for the ζ and α angles respectively, while the remaining phosphates have been constrained to the gauche(-) and gauche(-) geometry for these angles, respectively.

The range of pseudorotation angles for each sugar pucker has been estimated from the analysis of the consecutive intranucleotide sugar proton coupling constants in the DQF-COSY spectrum in D_2O.[29] In particular, the size of the coupling constants of H1'-H2', H2"-H3' and H3'-H4' are informative because of their sensitivity to the sugar conformation. In a generic C2'-endo sugar pucker, a large coupling constant between H1'-H2' is expected, while both the coupling constants between H2"-H3' and H3'-H4' are small. For a generic C3'-endo sugar pucker, a small coupling constant is expected between H1'-H2', while large coupling constants are expected between H2"-H3' and H3'-H4'. In the eight calculated structures, the pseudorotation angles were found to be consistent with experimentally determined ranges. In particular, the pseudorotation angle of the cleavage site C6 was 70° ± 5°, consistent with a C3'-endo like sugar pucker as previously mentioned.

The glycosidic torsion angles, χs, were determined from the intensity of the intranucleotide H8/H6-H1' NOEs.[33] Nucleotides with a *syn* glycosidic conformation have a characteristic short distance of ~2 Å that will be

observed in NOESY spectrum at a short mixing time. In the complex of CoBLM A2 green with DNA, no intranucleotide H8/H6-H1' NOEs were observed above the background in the NOESY spectrum at 50 ms mixing time. Thus, all the nucleotides in the complex were expected to be in *anti* conformations with χ angles between -72° to -180°, and all the structures were found to lie within this range.

Molecular Dynamics Studies. A structure for the complex of CoBLM A2 green with DNA was obtained using NOE distance constraints derived from NMR experiments and molecular modeling methods as outlined subsequently. The initial starting structure was constructed by positioning the bithiazole moiety of the previously determined solution structure of CoBLM A2 green (structure I, Figure 2.7a, preceding chapter[7]) between the C6•G15 and C7•G14 base pairs. The initial orientation was based on the NOE data described above showing specific interactions of B-H5 and B-H5' with residues of G14, G15, and C6 (Table 3.4). This initial structure was then submitted to minimizations and molecular dynamics simulated annealing calculations described in Materials and Methods. An overlay of the structures from the eight separate calculations are shown in Figure 3.7. A summary of results from the structural calculations is presented in Table 3.5. The final distances are in very good agreement with rms deviations from the distance constraints of 0.034 ± 0.002, and no constraint errors are over 0.2 Å. A final structure was obtained by averaging eight separately determined structures, followed by the minimization of the averaged coordinates. This structure is the basis for the remaining discussion.

Figure 3.7: An overlay of the eight molecular dynamics structures. These structures are in excellent agreement with the experimental constraints, and one another. The total pairwise rmsd for all atoms in the complex is 1.248 Å. If only the inner six base pairs (AGGCCT), and the bound CoBLM A2 green without the sugars (G and M), or the sulfonium tail (S) are considered the rmsd is significantly lowered to 0.651 Å. The total rms deviation from the distance constraints was 0.0344 ± 0.0015 Å.

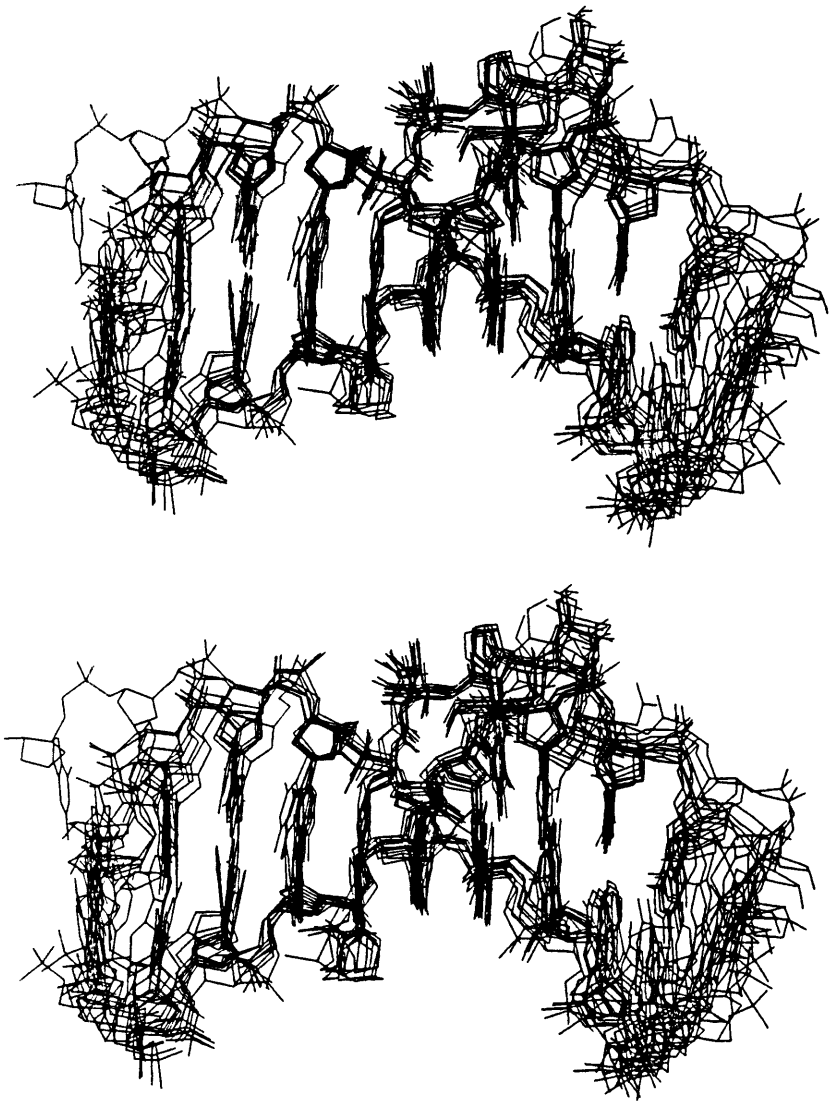

Overall Structure. The minimized structure is shown in Figure 3.8. The model reveals as indicated by preliminary studies of Wu et al.,[15] that the bithiazole tail binds via partial intercalation between base-pairs C6•G15 and C7•G14 with the sulfonium tail extending into the major groove. This intercalation site is 3' to the cleavage site at C6. The metal binding region is positioned within the minor groove with a number of contacts between the drug molecule and the DNA (Table 3.4). Specific contacts between G5 and the pyrimidine moiety of the drug suggest a basis for sequence specificity. This structure also positions the distal oxygen of the metal bound peroxide, approximately 2.5 Å from the 4'-hydrogen of C6, the site of C-H bond cleavage. The model as presented provides insight into the mode of binding of CoBLM A2 green to DNA, the molecular basis for the observed specificity and mechanism of cleavage of DNA. In the following sections each of these unique features of the structure in Figure 3.8 will be presented and discussed.

Binding. Multiple modes of binding for metallo-BLMs have been suggested since its discovery.[2, 3] Some investigators have focused on potential minor groove binding properties of the B moiety based on its similarity in structure relative to other known minor groove binders such as distamycin and netropsin.[34] The sequence specificity has been suggested to be related to the 2-amino group of guanine 5' to the cleavage site, which provides a hydrogen bond to the nitrogen(s) of the thiazolium rings of the B moiety.[35] Recent NMR studies by Hecht and coworkers with ZnBLM have been interpreted to indicate that one mode of binding to a defined oligonucleotide is within the minor groove.[10] Their studies are complicated however, by the observation of multiple binding motifs and minimal NOEs.[10] In addition, the

Figure 3.8: The structure of Co•BLM A2 green (atoms colored by element, C=green, O=red, N=blue, S=yellow) bound to DNA (purple, C6-H4′=white). The damaged strand is in the foreground, running 5′->3′ from the upper right to lower left corner. The dotted lines indicate the H-bond interactions between the P moiety of CoBLM, and the G5 of the DNA. Also indicated is the proximity of the distal oxygen of the hydroperoxide ligand to the C6-H4′ (2.5 Å).

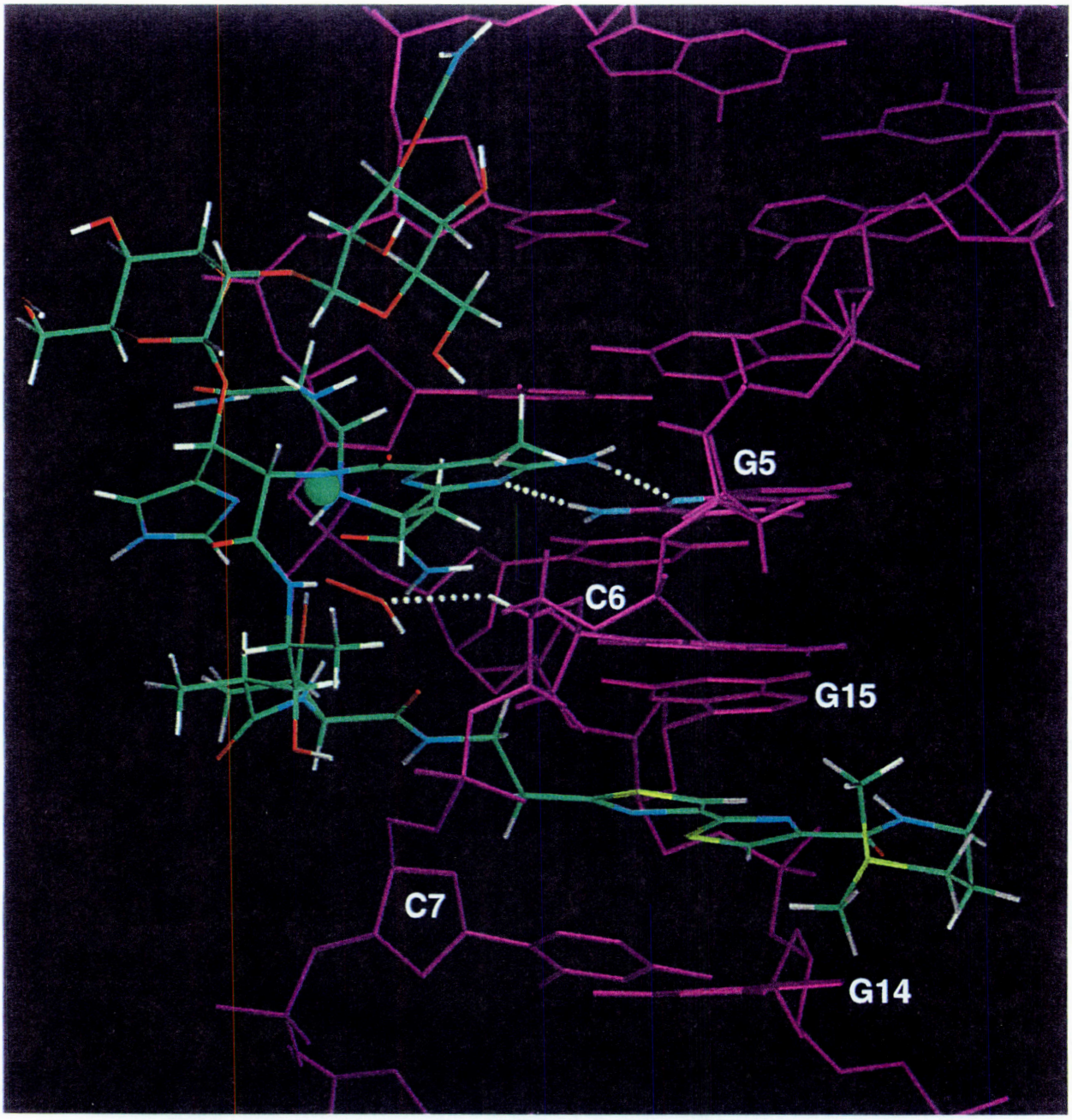
G5
C6
G15
C7
G14

relationship between ZnBLM and the Fe or CoBLMs is not clear, because ZnBLM is structurally unique[36] among metallo-BLMs and is chemically unreactive.

Other investigators have interpreted their physical and biochemical studies to support a mode of binding that involves partial intercalation of the B moiety of the drug.[8, 37] Studies of Williams and Goldberg using a series of bulged oligonucleotides have suggested the BLM's mode of binding involving bithiazole intercalation, would require its insertion 3′ to the cleavage site.[38] Recent 2D NMR studies from our laboratory[15] have provided the first direct evidence for this intercalative model and are elaborated herein.

The key to defining the mode of binding of B has been identification of the B-H5 and B-H5' protons using heteronuclear NMR methods presented in the preceding chapter.[7] These protons are upfield shifted 0.91 and 0.61 ppm, respectively from the chemical shifts observed with the free CoBLM A2 green, a hallmark of intercalation.[39a] Complete assignments of the protons of CoBLM A2 green in the complex (>85 %) and of the DNA protons (>95 %) has allowed us to identify the interactions of these B protons with the DNA (Tables 3.3 and 3.4). These NOEs define the position of the B within the base-pairing structure and also define the orientation of the side chain extending out from the intercalation site. In addition the NOEs between the B-CαH and B-NH and the DNA (H1' of C7 for example in Table 3.4) suggest unambiguously that intercalation occurs from the minor groove 3′ to the cleavage site.

The present solution structure provides us with a model for the B moiety in the complex (Figure 3.9). The terminal thiazolium ring is in the trans configuration[39b] and is completely stacked between the bases of G14 and G15. The plane of the terminal thiazolium ring essentially assumes the

Figure 3.9: Binding by partial intercalation of the bithiazole tail of CoBLM A2 green to DNA. A view looking down the helical axis showing the terminal thiazolium ring stacked between the bases of G14 and G15 and the penultimate thiazolium ring partially stacked between the bases of C6 and C7. Also shown is the kinked sulfonium tail close to the major groove as evidenced by the NOE between one of the sulfonium methyls and A13-H8.

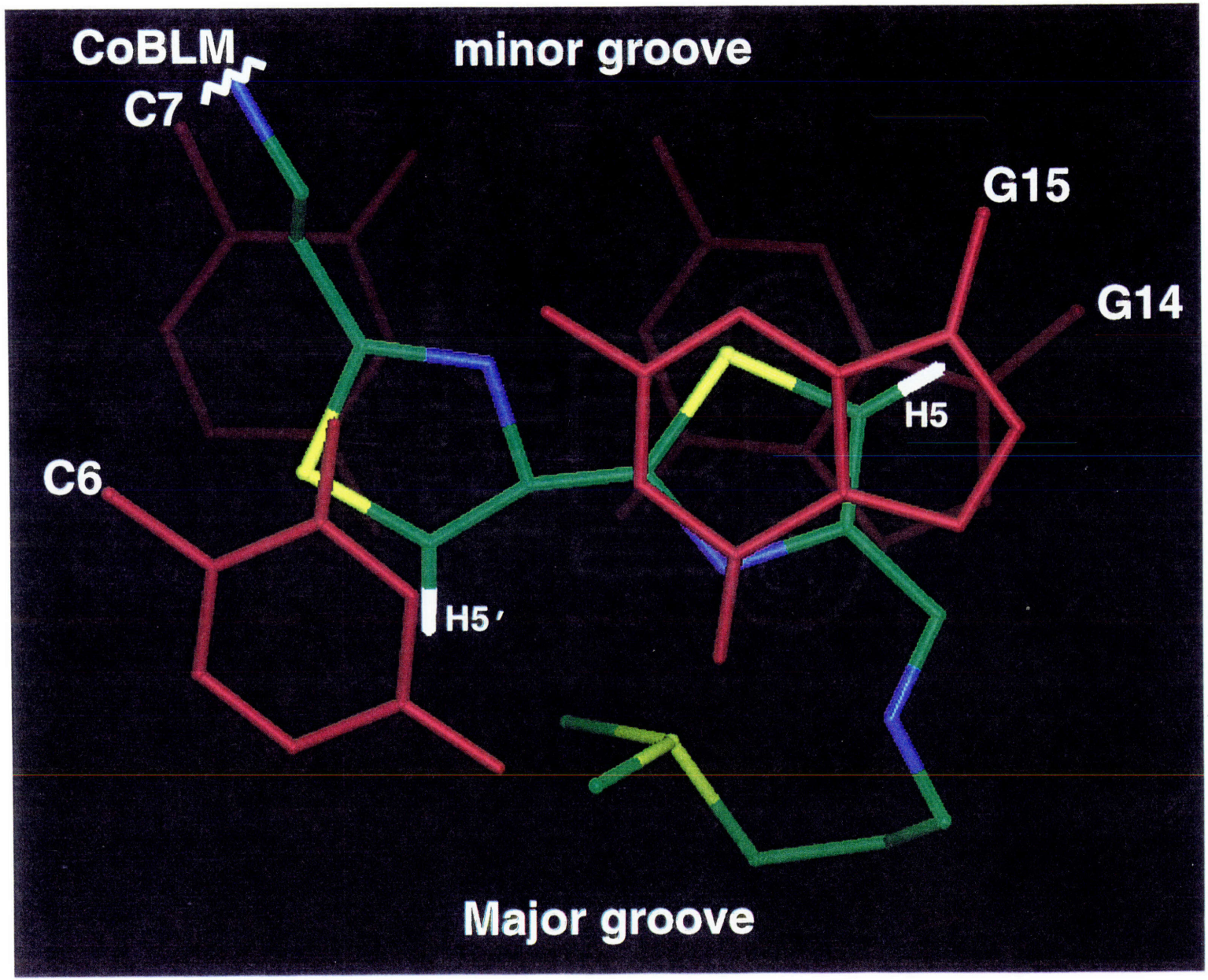
CoBLM
C7
minor groove
G15
G14
H5
C6
H5'
Major groove

position of another base, approximately 3.4 Å from the planes of G14 and G15 bases. This model is supported by the ^{31}P NMR experiments which indicate that the phosphorus between G14 and G15 is shifted downfield by ~ 2 ppm. The penultimate thiazolium ring is only partially stacked between the bases of C7 and C6. This model is in agreement with previous studies of many investigators on FeBLMs (summarized in a review by Stubbe and Kozarich[2]) where the data supported a partial, rather than a complete mode of intercalation. For example, DNA unwinding studies reveal an unwinding of 12° by FeBLM rather than 23° for a classic parallel intercalator such as ethidium bromide.[40]

In the present structure, the DNA is distorted in a manner more consistent with a "perpendicular" rather than "parallel" intercalator.[41] The DNA is unwound a total of ~13° over the three steps, (G5•C16)~(C6•G15)~(C7•G14)~(T8•A13). The intercalation site is only unwound ~6°, whereas the base step after it is unwound by ~8.5°, and the step before the intercalation site slightly overwound by ~1.5°. The base pairs before and after the intercalation site are also buckled by -7.8° and 25.2° respectively, a conformational feature also found in the X-ray crystal structures of daunomycin and nogalamycin.[42] This buckling has been proposed to increase favorable van der Waals contact between the drug and DNA.

The question can be raised as to whether the mode of binding for d(GpC) steps in the present studies are similar to d(GpT) steps. Results reported in the preceding chapter with an oligonucleotide containing a d(GTAC) ds-cleavage site, suggests a partial intercalative mode of binding at this site as well.[7] In fact many of the features reported with **1** are also apparent with this second oligomer **2**.

The model in Figure 3.9 also suggests a role for the sulfonium ion in the intercalation phenomenon. The nonequivalence of the sulfonium ion methyl groups (Figure 3.2) and a key observed NOE between one methyl group of S and A13-H8 reflects the limited range of motion of the sulfonium ion tail within the major groove. This observation requires that the intercalation of the B moiety extends into the major groove. The positioning of the sulfonium ion suggests a role for this group in anchoring the intercalated bithiazole, through an electrostatic interaction between the positively charged sulfonium group and the negatively charged region of the major groove. This would suggest that caution must be exercised in interpretation of mechanistic studies with synthetic BLM analogs lacking this group.[43, 44]

The absence of any observable sequence specific interactions between the bithiazole moiety and the DNA suggests that this binding mode is not specifically inherent to any sequence motif. This is in accord with many previous studies, but provides the first structural evidence in support of this hypothesis.

Specificity. The most significant prediction of our model is its clear demonstration that the basis for sequence specificity resides predominately in the metal binding domain. Many previous biochemical studies have demonstrated the importance of the 2-amino group of G in d(G-Py) sequences, for the specificity of BLM-mediated cleavage.[35, 45] Our studies now provide the first molecular basis for understanding the role of the 2-amino group in specificity. In addition, these studies reveal for the first time the importance of the N3 of guanine (or any purine) in the recognition of the metallo-BLM.

The key interactions are shown in Figure 3.10. This structure reveals two critical H bonds between the pyrimidine of the metal binding domain of CoBLM A2 green and the G5 of the DNA sequence. The N3 of the pyrimidine on CoBLM A2 green is H-bonded to the non base-pairing hydrogen of the 2-amino of G5 of DNA at a distance[46] of 2.3 Å and an angle[46] of 176°. Second, one of the hydrogens of the 4-amino group of the pyrimidine on CoBLM A2 green is H-bonded to the N3 of G5 of DNA at a distance of 1.9 Å and an angle of 155°. The H-bonding between one of the hydrogens of the P-NH_2 group and the N3 of G5 is dramatically demonstrated in the NMR spectrum by its position at 10.36 ppm relative to that observed in CoBLM A2 green itself at 7.34 or 7.91 ppm. It is important to emphasize that this H bonding network (Figure 3.10) was not used as a constraint in the molecular dynamics calculations. In fact this H-bonding network was a result of the many intermolecular NOEs observed between the P and A moieties of the CoBLM A2 green with the DNA (Table 3.4). These two hydrogen bonds represent a unique base triple like interaction between the G5•C16 and the pyrimidine of the drug in the minor groove.

Finally, three other potential hydrogen bonds are observed in the final structure of the complex that are more speculative in nature. One is between the other the 4-amino proton of the pyrimidine on CoBLM A2 green and the O4' of the deoxyribose ring of G5 at a distance of 2.2 Å and an angle of 143°. However, the O4' oxygen resides in a less than ideal orientation to participate as a hydrogen bond acceptor and thus far there is no indication of a sugar pucker of G5 different from that expected for a generic B-form DNA that is more favorable for this H bonding interaction. The other potential hydrogen bond observed in the model is between the primary amide proton of the propionamide on CoBLM A2 green and the O2 of the C16 base (paired with

Figure 3.10: The basis for specificity of BLM cleavage at d(G-Py) sequences. The P moiety of CoBLM A2 green forms a minor groove base triple like interaction with the G5•C16 base pair. The dotted lines indicate H-bonds between the P moiety of CoBLM and G5, as well as the Watson-Crick H-bonds.

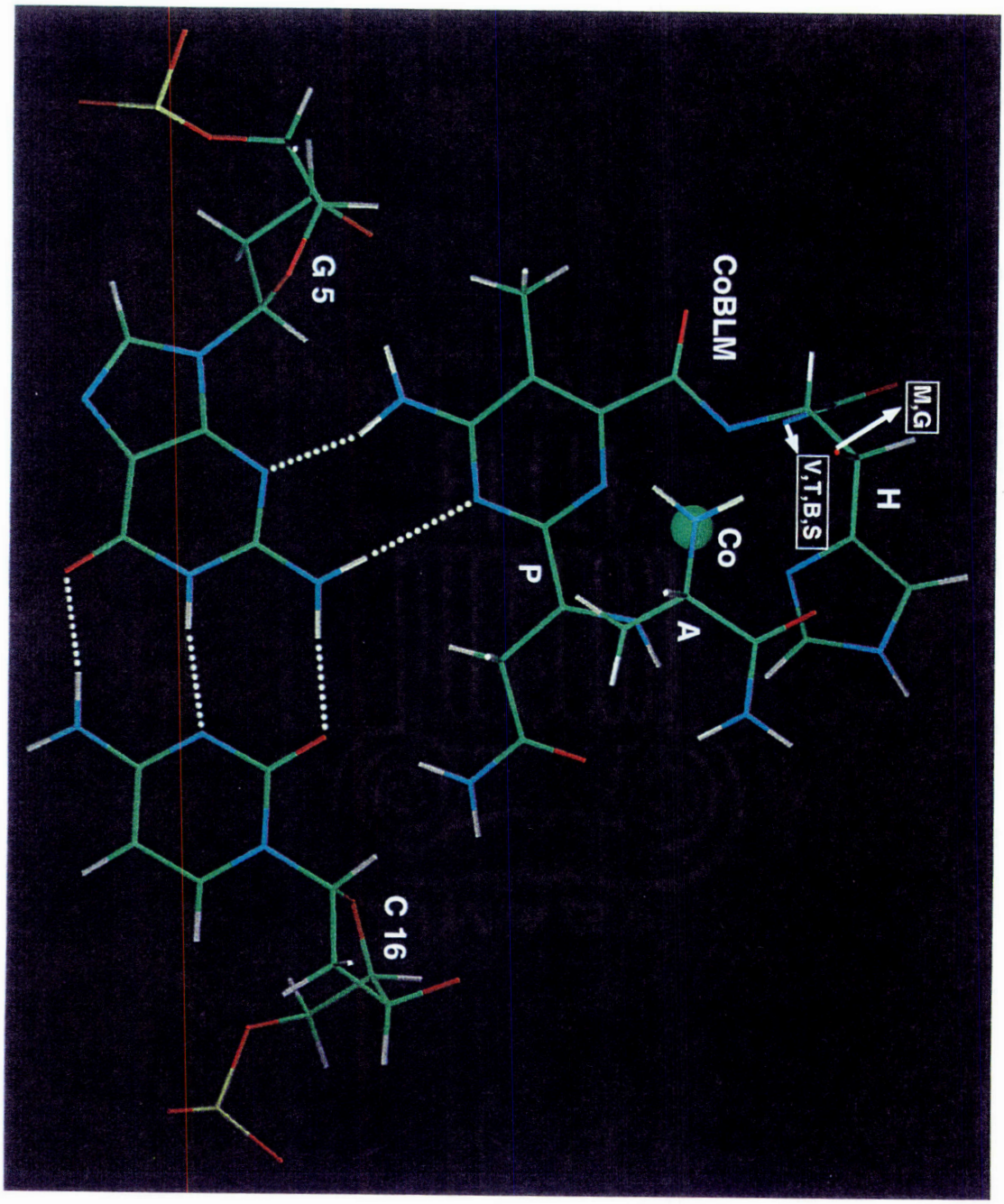
M,G
V,T,B,S
H
CoBLM
Co
A
P
G 5
C 16

G5) at a distance of 1.8 Å and an angle of 162° (Figure 3.10). Finally, a third putative interaction involves the carbonyl oxygen of the amide of P which is within H-bonding distance of the hydroxyl proton of the T in the linker (distance=1.7 Å; angle=147°). As will be discussed subsequently, the T moiety appears to participate in a number of additional putative H bonding interactions perhaps playing a key role in the alignment of the activated oxygen species for 4' hydrogen atom abstraction.

The interaction with N3 of the purine has not been previously suggested and may provide an explanation of the decreased cleavage of pyrimidines adjacent to dAs. Although there is a loss of binding energy by the absence of the 2-amino group, one could propose that the H-bond between the NH_2 group of P and the adenine is still in place to define a weak specificity for d(A-Py). This minimal interaction would be missing at pyrimidine-pyrimidine steps.

Mascharak et al. have recently reported the synthesis of the metal binding domain of BLM missing the 4-amino group of the pyrimidine, a key H-bonding partner in our model. These analogs are reported to cleave DNA with identical sequence selectivity to that observed with metallo-BLMs.[47] In contrast, recent studies from the Hecht and Boger laboratories using a metal binding domain identical to BLM, revealed no such cleavage.[3, 48] Thus the basis of specificity with Mascharak's analogs is mystifying. The Hecht and Boger results clearly suggest an important interplay between the binding of the B moiety (intercalation) and the metal binding domain (selectivity) in the overall cleavage process.[3, 48] In summary, our observations provide the first proposal for sequence selectivity that accounts for the specificity of G and accounts for the general observations that pyrimidines adjacent to dGs are cleaved more efficiently than pyrimidines adjacent to dAs.

Chemistry. Our structure (Figure 3.8) provides, to our knowledge, the first opportunity to assess a model of the reactive activated BLM (FeOOH). Furthermore, the model allows the first direct insight into the relationship between the metal and the 4' hydrogen of the pyrimidine being cleaved. As shown in Figure 3.11, the calculated structure places the distal oxygen of the hydroperoxide to within 2.5 Å of the H4' of C6, the closest DNA proton to the hydroperoxide. This interaction was not used as a constraint for calculation of the model. Instead this interaction was the result of the following set of observations. Initially the model was derived using NOE constraints from non-exchangeable protons of the metal binding domain of CoBLM A2 green with the DNA (Table 3.4). A key observation was that of an initially unassignable, exchangeable proton at 8.89 ppm. Subsequent to the molecular modeling, the only proton which could give rise to this exchangeable proton is that of the hydroperoxide. This result is particularly intriguing and insightful as this proton exhibits six intermolecular NOEs to C6 and C7 (Table 3.3), the region of DNA cleavage. While all of the exchangeable hydrogens of CoBLM A2 green and DNA have yet to be assigned, this is the only hydrogen in this region of the complex that could give rise to these NOEs. Thus these NOE distance constraints were added to our other constraints, and molecular dynamics calculations gave rise to the structure reported in Figure 3.11. Support for the proximity of the metal to C6-H4' is also derived from the NMR analysis in which this hydrogen is dramatically upfield shifted from the free DNA (4.22 ppm to 3.25 ppm).

The observation of the proton of the hydroperoxide of CoBLM A2 green is a fortuitous piece of information which allows the verification of the location of a putative reactive oxygen intermediate of the metallo-BLM

Figure 3.11: The position of the hydroperoxide oxygens of CoBLM A2 green relative to the 4' hydrogen of C6, the site of cleavage. A complete hydrogen bonding network involving the hydroperoxide ligand in CoBLM A2 green complexed with DNA is apparent. H-bonds are indicated from the NH protons of V and T to the proximal hydroperoxide oxygen, the T carbonyl oxygen to the hydroperoxide hydrogen, and the V-OH to the phosphate between C6 and C7.

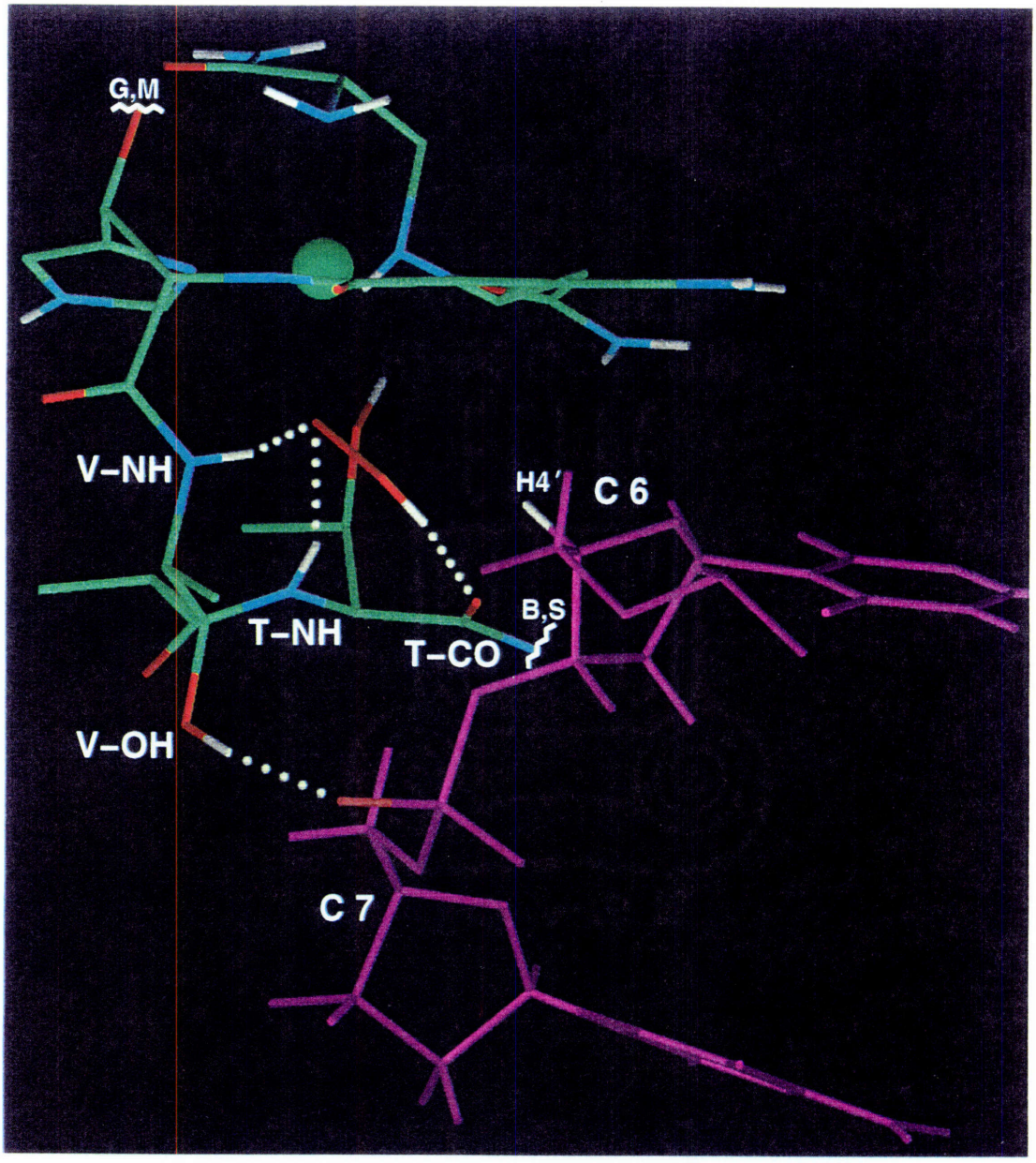
G,M
V–NH
H4′
C 6
B,S
T–NH
T–CO
V–OH
C 7

relative to its site of hydrogen atom abstraction (C6-H4'). This model provides a structural basis for our previous studies which showed that metallo-BLMs cannot mediate hydrogen atom abstraction from the H1' position of a Py. The steric and NOE constraints inherent in the model would prevent access of the hydroperoxide to this hydrogen. This model also suggests that H5' chemistry would be difficult to effect. The distance between the distal hydroperoxide oxygen and any H5/H5" protons is 4.2 Å or greater. Thus, for chemistry to occur at H5'/H5" position, the movement of the metal binding region as the result of positioning the hydroperoxide ligand within a reasonable distance of the H5'/H5" would result in the disruption of the hydrogen bonding network between the pyrimidine and the G5 of DNA.

The observation of an excellent analog of an intermediate along a reaction pathway may give a rare opportunity to speculate on the chemistry involved in hydrogen atom abstraction of H4′ from C6. The chemistry of reactive intermediates in mononuclear non-heme systems is at present speculative based on analogy with the better characterized heme systems.[49] The question arises as to whether the hydroperoxide or an undetected additional intermediate resulting from the heterolytic or homolytic oxygen-oxygen bond cleavage of this hydroperoxide actually results in removal of the 4′ hydrogen atom. In the case of heme peroxidase systems, it is clear that appropriate acid and base catalysts are precisely positioned to assist in heterolytic oxygen-oxygen bond scission. It is speculated that heme monooxygenases involve similar reactive intermediates to heme peroxidases.

The structure in Figure 3.8 was therefore carefully scrutinized to identify similar groups that might assist in catalysis. No such groups are apparent. Instead the hydrogens of amide moieties of both T and V in the linker region make excellent H-bonds (1.9 Å and 1.8 Å), respectively with the

penultimate oxygen, not the terminal oxygen as required for a heterolytic cleavage mechanism. A third additional H bonding interaction is also apparent between the proton of the hydroperoxide and carbonyl of the T (distance=1.9 Å; angle=163°). Finally, as discussed above, the hydroxyl proton of T appears to be H-bonded to the carbonyl oxygen of terminal amide of the propionamide. This H-bonding network suggests a very sequestered, and ordered environment for the hydroperoxide moiety and may provide an explanation for Boger's cleavage studies using synthetic analogs modified in the linker region. They showed that the replacement of T with a glycine resulted in a FeBLM analog that cleaves DNA with 5 % of the efficiency of the wild type FeBLM. Glycine is conformationally more flexible than T, and thus the position of its carbonyl relative to the hydroperoxide could be substantially altered. Unfortunately, these observations about the hydroperoxide environment have provided no insight into the chemistry of oxygen-oxygen bond cleavage as the H-bonding network is interacting with the wrong oxygen. Instead, the H-bonding network to the penultimate oxygen may contribute to the unusual stability of the cobalt hydrogenperoxide complex (CoBLM A2 green). Given the low resolution of this structure, however, speculation about the chemistry of the hydrogen atom abstraction is thus premature.

Comparison of Free and Bound CoBLM A2 green. The NOE patterns and the coupling constants observed for the metal binding domain and the valeryl moiety in the linker region of CoBLM A2 green in the DNA complex are similar to those observed in the free CoBLM A2 green. In particular, intramolecular NOEs from the H-C2H to the V protons are nearly identical to those reported in the preceding chapter, positioning the valeryl moiety

underneath the metal coordination plane as observed in the free CoBLM A2 green. The absence of any observable coupling between the V-CαH and V-CβH, and a large coupling constant between the V-CβH and the V-CγH essentially define the the same conformation for the V reported for free CoBLM A2 green (Figure 3.12).[7] The V-NH as well as T-NH are again well position to participate in hydrogen bonding network to the proximal oxygen of the hydroperoxide ligand (V-NH to O: distance=1.8 Å; angle=155°; T-NH to O: distance=1.8 Å, angle=152°).[46] An additional hydrogen bond is noted between the V-OH and one of the non-bridging oxygens of the phosphate between C6 and C7 (Figure 3.11), which accounts for the NMR observation of this exchangeable proton. The remainder of the T moiety and B moiety however undergo a significant conformational reorganization as a consequence of insertion of the bithiazole rings between the base pairs (Figure 3.12). This is most obvious in the change of T-Cα-T-CO dihedral angle from 120° in the free CoBLM A2 green to -180° in the complex with DNA (Figure 3.12). This change in conformation reorients the threonine carbonyl oxygen to be in good position to act as an hydrogen bond acceptor for the hydroperoxide hydrogen (distance=1.9 Å and angle=163°). The existence of such a hydrogen bond is corroborated by the observation of the exchangeable proton on the hydroperoxide.

One of the intriguing questions that can be raised is what makes the CoBLM A2 green's octahedral environment different from the octahedral environments of the previously characterized ZnBLM and FeBLM-CO. The ZnBLM as pointed out earlier, has a dramatically altered coordination environment in that both the primary amine of A and the carbamoyl nitrogen of M are proposed to be ligands in contrast with other metallo-BLMs. This altered coordination, and hence altered structure[36] and the lack of

Figure 3.12: An overlay of CoBLM A2 green in the free (red) and the bound (white) forms, showing the high degree of similarity in the metal binding region, the V moiety and portions of the T moiety. For clarity, only the first thiazolium ring of the B moiety is shown, and the sugars are excluded.

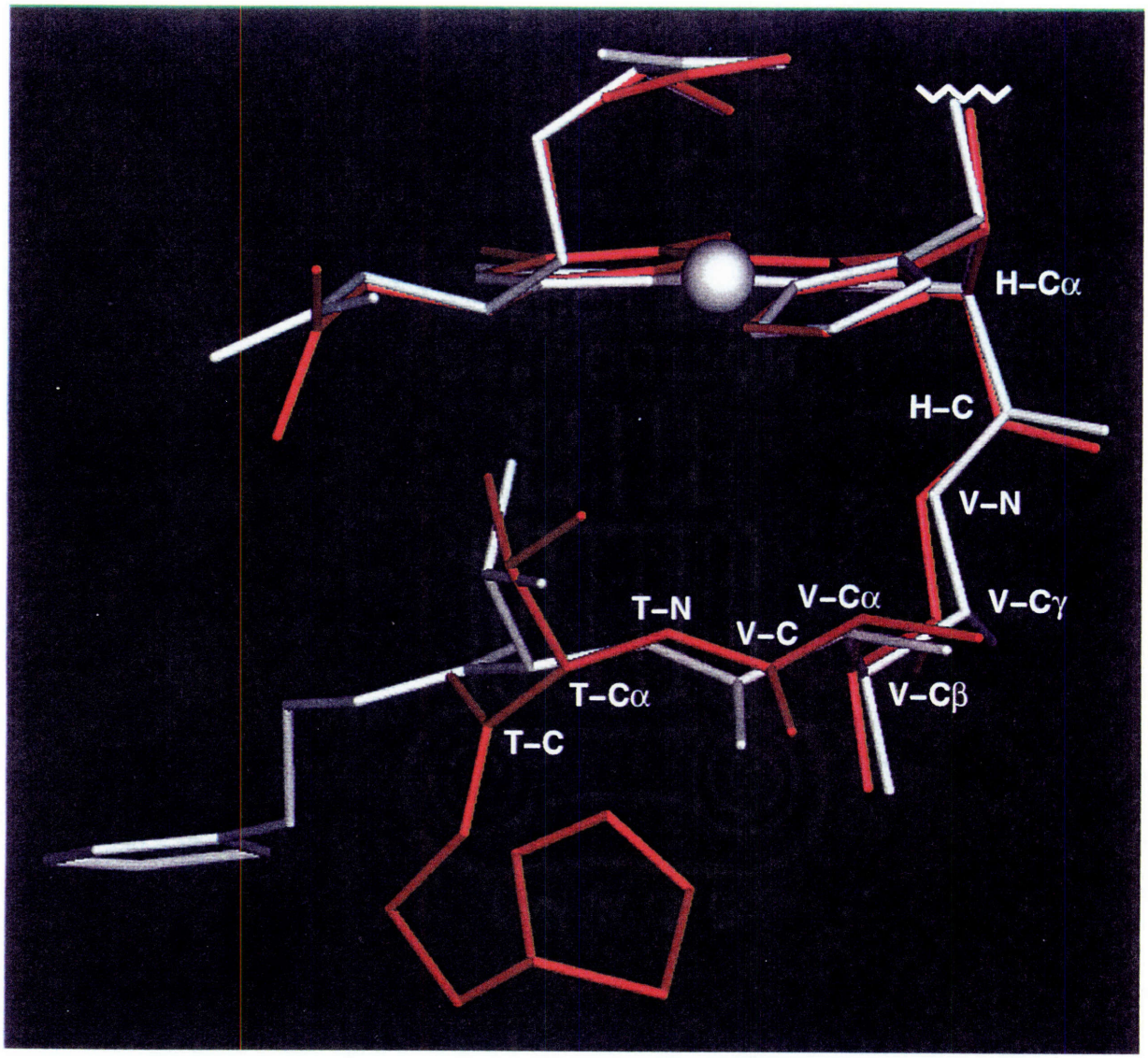
H–Cα
H–C
V–N
V–Cγ
V–Cα
T–N
V–C
V–Cβ
T–Cα
T–C

chemical reactivity of ZnBLM, suggests it is not a good model for metallo-BLM mediated DNA degradation. The FeBLM-CO complex may likewise not be a good model for activated BLM, as discussed in the preceding chapter.[7] The oxidation state of iron in this complex, the absence of an appropriate "oxygen ligand" and the ability of ligands to undergo chemical exchange with other ligands, all suggest that activated BLM might be structurally different from the FeBLM-CO.

New Insights and Predictions from the Structure of CoBLM A2 green Complexed with DNA. The modular total synthesis of BLM[16] and the ability to make DNA using nucleotide analogs warrants speculative predictions from the structure reported herein. These analogs can then be examined quantitatively with regard to the binding and cleavage of defined DNA sequences, and the structure determined by NMR.

The peptide linker region is of great interest in that recent studies from Boger's laboratory with mutations in this region[48] and from our own laboratories on the ds-cleavage process[50] suggest that it plays a key role in subtly coordinating binding and cleavage. Our structure suggests that one could now synthesize conformationally restrained valeryl analogs. These analogs would be predicted to accelerate rates of cleavage for FeBLM in that now all of the binding energy could be used in catalysis. The location of the V moiety in the structure provides a great deal of flexibility in synthetic design. The structure in the linker region also predicts that the T and V NHs are H-bonded to the peroxide. The importance of these H bonds to both structure and catalysis can be assessed by the synthesis of the appropriate ester analog.

Boger's recent studies have indicated the importance of the T moiety in cleavage.[48] In these studies however glycine replaced T. Our structure would

suggest that the side chain may play a key role in defining the correct conformation of the carbonyl of the T. This model can also be tested experimentally using constrained T analogs. Quantitative differences can be assessed by examining the binding and cleavage and comparison with the structural information. The model for ds-cleavage we have recently put forth, suggests as originally proposed by Povirk,[51] that a single molecule of BLM can effect cleavage on both strands of DNA without dissociation from the DNA. This model requires flexibility in the linker region, which could be readily tested quantitatively with linkers of constrained conformations and our assay for ds-cleavage.[50]

The proposed basis for specificity is more difficult to test experimentally, as it is clear that the pyrimidine moiety plays a key role not only in coordination of the metal,[52] but also in the observed chemistry. However, the observation of a base triple-like interaction from the minor groove is unusual and should allow modification of both the 5'-nucleotide and the pyrimidine of the CoBLM to effect a similar recognition pattern. Once again, quantitative structural studies can be carried out to test this prediction.

Summary. The studies reported herein delineate for the first time the role of both the 2-amino and N-3 of the guanine, 5' to the pyrimidine cleavage site, in forming the basis for specificity involving the 4-amino group and N3 of the pyrimidine of the CoBLM A2 green. The linker plays a key role in appropriately positioning the bithiazole tail for binding by intercalation from the minor groove and thus providing the affinity for DNA. The use of CoBLM A2 green, a hydroperoxide analog of activated BLM, gives an unprecedented glimpse of the orientation of this group relative to the

position on the DNA where chemistry occurs. Studies are in progress to test the generality of the observation with regard to both binding and specificity. We propose that CoBLM A2 green is an excellent model for activated BLM.

References:

(1) (a) Sikic, B. I.; Rozencweig, M.; Carter, S. K. Ed., In *Bleomycin Chemotherapy*, Academic Press: Orlando, Florida, 1985. (b) Umezawa, H. in *Anticancer agents based on natural product models*; Cassady, J. M. Douros, J. Ed.; Academic Press, Inc., New York, 1980; Vol. pp 147-166. (c) Hecht, S. M. Ed., In *Bleomycin: Chemical, Biochemical, and Biological Aspects*; Springer-Verlag: New York, 1979.

(2) Stubbe, J.; Kozarich, J. W. *Chem. Rev.* **1987**, *87*, 1107-1136.

(3) Kane, S. A.; Hecht, S. M. in *Progress in Nucleic Acid Research and Molecular Biology*; Cohn, W. E. Moldave, K. Ed.; Academic Press, San Diego, 1994; Vol. 49, pp 313-352.

(4) Akkerman, M. A. J.; Haasnoot, C. A. G.; Hilbers, C. W. *Eur. J. Biochem.* **1988**, *173*, 211-225.

(5) Akkerman, M. A. J.; Neijman, E. W. J. F.; Wijmenga, S. S.; Hilbers, C. W.; Bermel, W. *J. Am. Chem. Soc.* **1990**, *112*, 7462-7474.

(6) Xu, R. X.; Nettesheim, D.; Otvos, J. D.; Petering, D. H. *Biochemistry* **1994**, *33*, 907-916.

(7) Wu, W.; Vanderwall, D. E.; Lui, S. M.; Tang, X.-J.; Turner, C. J.; Kozarich, J. W.; Stubbe, J. *J. Am. Chem. Soc.* First paper in this issue.

(8) Gamcsik, M. P.; Glickson, J. D.; Zon, G. *J. Biomol. Struct. Dyn.* **1990**, *7*, 1117-1133.

(9) Hiroaki, H.; Nakayama, T.; Ikehara, M.; Uesugi, S. *Chem. Pharm. Bull.* **1991**, *39*, 2780-2786.

(10) (a) Manderville, R. A.; Ellena, J. F.; Hecht, S. M. *J. Am. Chem. Soc.* **1994**, *116*, 10851-10852. (b) Manderville, R. A.; Ellena, J. F.; Hecht, S. M. *J. Am. Chem. Soc.* **1995**, *117*, 7891-7903.

(11) Chang, C.-H.; Meares, C. F. *Biochemistry* **1984**, *23*, 2268-2274.

(12) Chang, C.-H.; Meares, C. F. *Biochemistry* **1982**, *21*, 6332-6334.

(13) Burger, R. M.; Peisach, J.; Horwitz, S. B. *J. Biol. Chem.* **1981**, *256*, 11636-11644.

(14) Xu, R. X.; Antholine, W. E.; Petering, D. H. *J. Biol. Chem.* **1992**, *267*, 950-955.

(15) Wu, W.; Vanderwall, D. E.; Stubbe, J.; Kozarich, J. W.; Turner, C. J. *J. Am. Chem. Soc.* **1994**, *116*, 10843-10844.

(16) (a) Boger, D. L.; Colletti, S. L.; Honda, T.; Menezes, R. F. *J. Am. Chem. Soc.* **1994**, *116*, 5607-5618. (b) Boger, D. L.; Honda, T.; Dand, Q. *J. Am. Chem. Soc.* **1994**, *116*, 5619-5630. (c) Boger, D. L.; Honda, T.; Menezes, R. F.; Colletti, S. L. *J. Am. Chem. Soc.* **1994**, *116*, 5631-5646. (d) Boger, D. L.; Honda, T. *J. Am. Chem. Soc.* **1994**, *116*, 5647-5656.

(17) Chang, C.-H.; Dallas, J. L.; Meares, C. F. *Biochem. Biophys. Res. Commn.* **1983**, *110*, 959-966.

(18) Guéron, M.; Plateau, P.; Decorps, M. *Prog. Nucl. Magn. Reson. Spectrosc.* **1991**, *23*, 161.

(19) Bax, A.; Subramanian, S. *J. Magn. Reson.* **1986**, *67*, 565-569.

(20) Maudsley, A. A.; Ernst, R. R. *Chem. Phys. Lett.* **1977**, *50*, 368-372.

(21) van Gunsteren, W. F.; Berendsen, H. J. C. *Mol. Phys.* **1977**, *34*, 1311-1327.

(22) Kross, J.; Henner, W. D.; Hecht, S. M.; Haseltine, W. A. *Biochemistry* **1982**, *21*, 4310-4318.

(23) Manning, G., S. *Q. Rev. Biophys.* **1978**, *II*, 179-246.

(24) Evans, S. V. *J. Mol. Graphics* **1993**, *11*, 134-138.

(25) Haasnoot, C. A. G.; De Leeuw, F. A. A. M.; Altona, C. *Tetrahedron* **1980**, *36*, 2783-2792.

(26) Dickerson, R. E. *Methods Enzymol.* **1992**, *211*, 67-111.

(27) Recent studies with CoBLM A2 brown (in which an H_2O ligand has replaced the hydroperoxide ligand) demonstrate that it binds **1** in an analogous fashion to CoBLM A2 green. The exchangeable proton, however, at 8.89 ppm is absent.

(28) Wüthrich, K. *NMR of Proteins and Nucleic Acids;* John Wiley & Sons, Inc: New York, 1986.

(29) (a) Majumdar, A.; Hosur, R. V. *Prog. NMR Spectrosc.* **1992**, *24*, 109. (b) Hosur, R. V.; Ravikumar, M.; Chary, K. V. R.; Sheth, A.; Govil, G.; Zu-Kum, T.; Miles, H. T. *FEBS* **1986**, *205*, 71-76. (c) van Wijk, J.; Huckriede, B. D.; Ippel, J. H.; Altona, C. *Methods enzymol.* **1992**, *211*, 286-306.

(30) Leupin, W.; Wagner, G.; Denny, W. A.; Wüthrich, K. *Nucleic Acids Res.* **1987**, *15*, 267-275.

(31) (a) Gao, X.; Patel, D. J. *Biochemistry* **1988**, *27*, 1744-1751. (b) Addess, K. J.; Gilbert, D. E.; Olsen, R. K.; Feigon, J. *Biochemistry* **1992**, *31*, 339-350.

(32) Gorenstein, D. G. *Methods Enzymol.* **1992**, *211*, 254-286.

(33) Kim, S.; Lin, L.; Reid, B. R. *Biochemistry* **1992**, *31*, 3564-3574.

(34) (a) Dickerson, R. E. in *Mechanism of DNA Damage and Repair: Implications for Carcinogenesis and Risk Assessment Basic Life Sciences;* Smi, M. G. Grossman, L. Ed.; Plenum, New York, 1986; Vol. 38, pp 245-255. (b) Klevit, R. E.; Wemmer, D. E.; Reid, B. R. *Biochemistry* **1986**, *25*, 3296.

(35) Kuwahara, J.; Sugiura, Y. *Proc. Natl. Acad. Sci. U.S.A.* **1988**, *85*, 2459-2463.

(36) Based on the arguments presented in the preceding paper[7] and as shown in the studies of Akkerman et al. on ZnBLM,[4] for the Zn to accommodate both the primary amine of A and the carbamoyl nitrogen of M as axial ligands, it must adopt a structure similar to III in the preceding chapter (Figure 3.7c).

(37) Povirk, L. F.; Hogan, M.; Dattagupta, N. *Biochemistry* **1979**, *18*, 96-101.

(38) Williams, L. D.; Goldberg, I. H. *Biochemistry* **1988**, *27*, 3004-3011.

(39) (a). Although the penultimate thiazolium ring as a whole is partially stacked between the bases of C6 and C7, the B-H5' proton is positioned almost directly below the base of C6, which causes the upfield chemical shift change (0.61 ppm) due to the ring current effect. The B-H5 proton is completely stacked between G14 and G15 (Figure 3.9) and thus experiences even larger upfield chemical shift change (0.91 ppm). (b). The bithiazole tail is sufficiently flexible in the free CoBLM A2 green such that the orientation of the thiazolium rings relative to one another is not discernible.

(40) (a) Tsai, C.; Jain, S. C.; Sobell, H. M. *J. Mol. Biol.* **1977**, *114*, 301-305. (b) Tsai, C.; Jain, S. C.; Sobell, H. M. *J. Mol. Biol.* **1977**, *114*, 317-331.

(41) Williams, L. D.; Egli, M.; Gao, Q.; Rich, A. *DNA Intercalation: Helix Unwinding and Neighbor-Exclusion*; Adenine Press: Schenectady, NY, 1992.

(42) (a) Frederick, C. A.; Williams, L. D.; Ughetto, G.; van der Marel, G. A.; van Boom, J. H.; Rich, A.; Wang, A. H. *Biochemistry* **1990**, *29*, 2538-2549. (b) Gao, Y.; Liaw, Y.; Robinson, H.; Wang, A. H. *Biochemistry* **1990**, *29*, 10307-10316.

(43) (a) Carter, B. J.; Murty, V. S.; Reddy, K. S.; Wang, S.-N.; Hecht, S. M. *J. Biol. Chem.* **1990**, *265*, 4193-4196. (b) Carter, B. J.; Reddy, K. S.; Hecht, S. M. *Tetrahedron* **1991**, *47*, 2463-2474.

(44) Levy, M. J.; Hecht, S. M. *Biochemistry* **1988**, *27*, 2647-2650.

(45) Zhang, G., Ph.D. Thesis, University of Maryland, 1993.

(46) The H bond distance is between the proton and the H bond acceptor atom in all cases. The H bond angle is determined by the donor atom, the hydrogen and the acceptor atom.

(47) Guajardo, R. J.; Hudson, S. E.; Brown, S. J.; Mascharak, P. K. *J. Am . Chem. Soc.* **1993**, *115*, 7971-7977.

(48) (a) Boger, D. L.; Teramoto, S.; Honda, T.; Zhou, J. *J. Am. Chem. Soc.* **1995**, *117*, 7338-7343. (b) Boger, D. L.; Teramoto, S.; Zhou, J. *J. Am. Chem. Soc.* **1995**, *117*, 7344-7356. (c) Boger, D. L.; Colletti, S. L.; Teramoto, S.; Ramsey, T. M.; Zhou, J. *Bioorg. Med. Chem.* **1995**, 3, 1281-1295.

(49) English, A. M.; Tsaprailis, G. *Adv. Inorg. Chem.* **1995**, in press.

(50) (a) Absalon, M. J.; Stubbe, J.; Kozarich, J. W. *Biochemistry* **1995**, *34*, 2065-2075. (b) Absalon, M. J.; Wu, W.; Stubbe, J.; Kozarich, J. W. *Biochemistry* **1995**, *34*, 2076-2086.

(51) Povirk, L. F. in *Molecular Aspects of Anti-Cancer Drug Action*; Neidle Waring Ed.; 1983; Vol. pp 157-181.

(52) Loeb, K. E.; Zaleski, J. M.; Westre, T. E.; Guajardo, R. J.; Mascharak, P. K.; Hedman, B.; Hodgson, K. O.; Solomon, E. I. *J. Am. Chem. Soc.* **1995**, *117*, 4545-4561.

Chapter 4: NMR Studies of Co-deglycoBLM A2 green and Solution Structure of Co-deglycoBLM A2 green complexed with oligonucleotide d(CCAGGCCTGG): Implications in DNA Cleavage Efficiency and Specificity by deglycoBLM

Introduction:

The bleomycins (BLMs) belong to a family of glycopeptide derived antibiotics that are clinically used in the treatment of squamous cell carcinomas, lymphomas and testicular cancer.[1-3] The cytotoxicity of the BLMs is generally believed to be associated with their abilities to inflict both single strand (ss) and double strand (ds) breaks in chromosomal DNA with the latter thought to be more cytotoxic due to the difficulties associated with ds-break repair.[4,5] Recent studies, however, have also demonstrated that RNAs (t, m and r) are susceptible to degradation by BLM, albeit at low frequency, requiring that these targets must also be considered as contributing to the observed cytotoxic effects.[6] DNA cleavage mediated by BLM requires the presence of a metal and O_2 as cofactors and has been found to be both sequence specific with cleavages at pyrimidines in d(G<u>Py</u>) sequences and site specific with cleavage being initiated at the 4' position of the deoxyribose of the <u>Py</u>.[7,8] Only recently has progress been made in defining the structural basis for these observations.[9-17]

Two dimensional NMR studies of the hydroperoxide form of cobalt BLM A2 (HOO-CoBLM) bound sequence specifically to several oligonucleotides have been reported.[9,11,15-17] The HOO-CoBLM was chosen as it is a stable analog of the iron BLM hydroperoxide (HOO-FeBLM), the last detectable reactive species in the DNA degradative process. The basis for the assumption of the congruence between the HOO-FeBLM (activated BLM) and the HOO-CoBLM has been previously described and is assumed throughout.[9-11] These studies have revealed that the metalloBLMs are finely tuned machines, in which the whole is much more sophisticated than the sum of its parts. In the present chapter, a model of the structure of the hydroperoxide form of cobalt deglycoBLM A2 (HOO-Co-deglycoBLM) bound to

d(CCAGGCCTGG) (**1**) is described based on the constraints derived from NMR studies. This model in comparison with that previously reported for HOO-CoBLM[10,11] allows further definition of the role of the sugars in this finely tuned machine and the suitability of deglycoBLM analogs, synthetically more accessible than the corresponding BLMs, as probes of the ds cleavage process mediated by BLM.

DeglycoBLMs have been the focus of attention since the report of their preparation by acid catalyzed degradation of BLMs.[18] The sugar domain of BLM consists of α-L gulose and 3'-carbamoyl α-D mannose connected via a β linkage to the hydroxy group of the β-hydroxyhistidine moiety (Figure 4.1). Extensive synthetic efforts coupled to *in vitro* DNA cleavage experiments and *in vivo* cytotoxicity experiments have suggested multiple roles for these sugars.[19-27] Of particular importance to our studies is the proposal that the carbamoyl moiety of the mannose functions as an axial ligand to the metal, and hence would play a major role in the cleavage process.[28-30] In addition, the proposal has been made by several groups that the sugars function to protect the chemically reactive hydroperoxide ligand.[31-35] However, our recent structure of HOO-CoBLM, if applicable to HOO-Co-deglycoBLM, indicates that neither of these proposal is correct.[10,11] In the HOO-CoBLM structure, the axial ligand is the primary amine of the β-aminoalanine moiety, and the sugars are on the same face as the β-aminoalanine in this octahedral complex and are not adjacent to the axial hydroperoxide ligand on the opposite face. This study will address the similarities and the differences between the HOO-Co-deglycoBLM and its glycosylated parent and hence will provide insight into the function of the sugar domain.

Extensive biochemical investigations have established that deglycoBLM exhibits the same general cleavage specificity, cleavages at Py in

d(GPy) sequences, as the corresponding BLM.[19-24] However, a number of recent studies also point out a number of subtlties in sequence preference.[22-24,36] In addition, the DNA cleavage efficiency by deglycoBLM is about half of that of the intact BLM.[19-24] The structural basis for the above observations remains to be elucidated.

In an effort to understand how a single BLM molecule can effect ds-DNA cleavage, a model for the importance of the linker region in this process has been put forth.[9,37,38] BLM analogs have been prepared to further refine the role of the linker and to facilitate their synthesis, these analogs have been made without the sugars attatched.[39] Therefore, as a starting point to use deglyco analogs to investigate the mechanism of ds cleavage, the ability of deglycoBLM to mediate ds cleavage has been investigated using a hairpin oligonucleotide method recently developed by Absalon et al.[37,38] Second, a model of the structure of the HOO-Co-deglycoBLM has been established by 2D NMR methods and molecular modeling, and a comparison with the corresponding BLM is reported herein. These studies established that deglycoBLM analogs should be good models to investigate the ds-cleavage mechanism both mechanistically and structurally and provide additional insight into the function of the sugars in the natural product.

Figure 4.1: Structure of BLM A2. Nitrogen ligands coordinating to the metal are underlined.

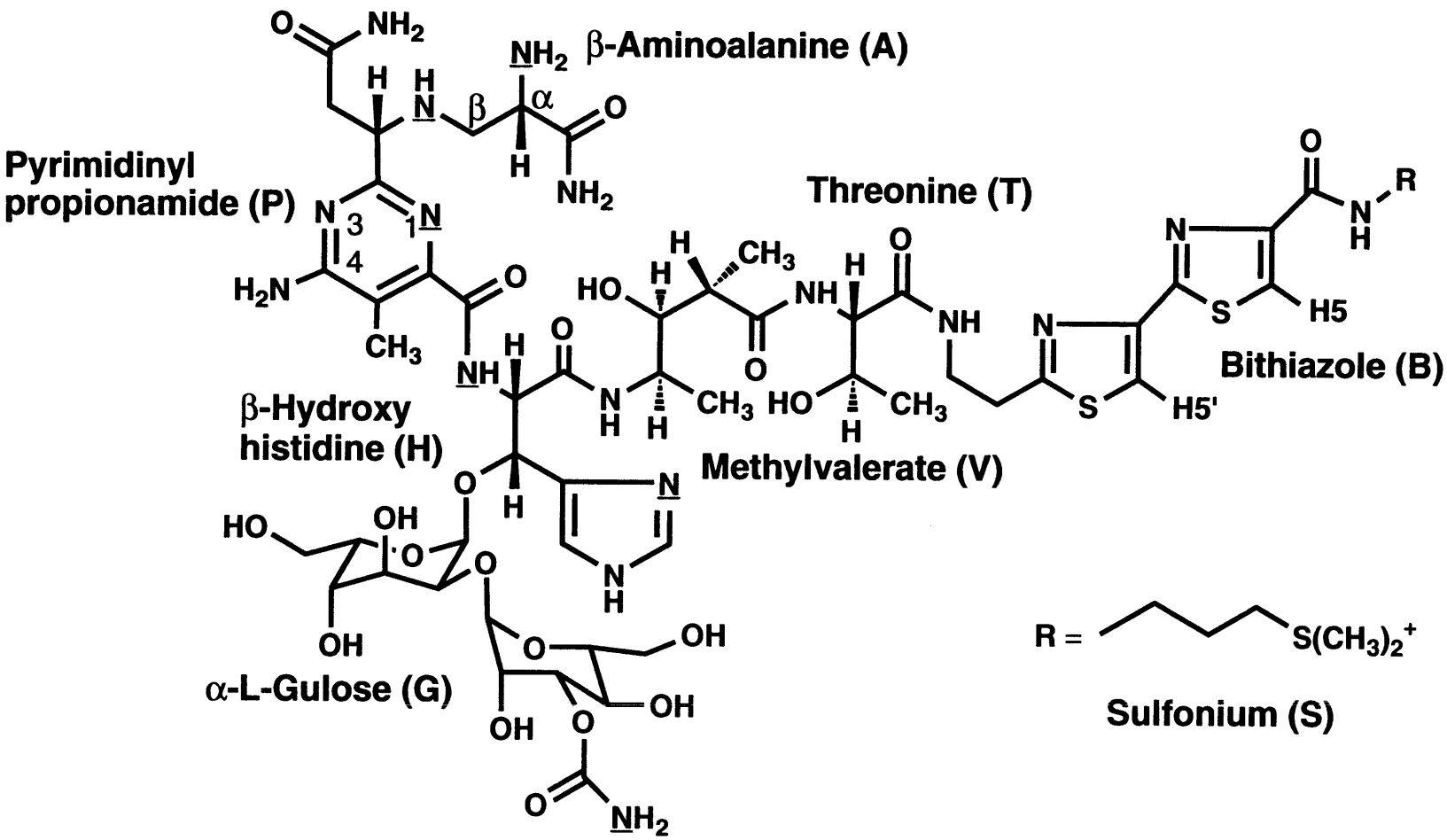
β-Aminoalanine (A)
Pyrimidinyl propionamide (P)
Threonine (T)
Bithiazole (B)
β-Hydroxy histidine (H)
Methylvalerate (V)
α-L-Gulose (G)
α-D-Mannose (M)
R =
S(CH3)2+
Sulfonium (S)

Materials and Methods

Preparation of HOO-Co-deglycoBLM. Apo deglycoBLM (4.7 mg) was dissolved in 100 mM sodium phosphate buffer (3 mL, pH 6.8). $CoCl_2$ (1.1 equiv.) was then added to a rapidly stirred solution to ensure oxygenation. The reaction was allowed to proceed for 12 h at room temperature. The mixture of products was separated using a semi-preparative reverse phase Alltech Econosil C-18 column (10 mm) and the elution system of 0.1 M ammonium acetate (pH 6.8) as solvent A and acetonitrile as solvent B. The products were eluted at a flow rate of 3 mL/min using a linear gradient from 12 to 16 % A over 60 min (compound, retention time in min, yield in mg): Co-deglycoBLM A2 brown (H_2O-Co-deglycoBLM), 18, 1.6; HOO-Co-deglycoBLM, 22, 1.4. The lyophilized samples were redissolved in 50 mM sodium phosphate (pH 6.8) and stored at -80 °C.

Characterization of HOO-Co-deglycoBLM. The extinction coefficient of HOO-Co-deglycoBLM was measured using Inductively Coupled Plasma (ICP) methods for cobalt quantitation as previously described[10] and was determined to be $2.05 \pm 0.2 \times 10^4$ M^{-1} cm^{-1} at 290 nm. The electrospray mass spectrum of HOO-Co-deglycoBLM was obtained as described previously.[10]

Titration and binding studies of HOO-Co-deglycoBLM with 1. Oligonucleotide **1** was prepared and quantitated as previously described.[10] Aliquots of HOO-Co-deglycoBLM (0-1 equiv.) were added to the solution of duplex DNA in D_2O and the complex formation was followed by monitoring the changes in the ^1H NMR spectrum. The K_d of HOO-Co-deglycoBLM to **1**

were measured by monitoring fluorescence quenching followed by Scatchard analysis.[10]

Ss- and Ds- Cleavages of a hairpin Oligonucleotide.

Methods are identical to those previously described by Absalon et al. except that deglycoBLM (5 μM to 20 μM at 4 °C) replaced BLM.[37,38]

NMR Experiments. All NMR experiments were performed on 750 MHz or 500 MHz Varian NMR spectrometers or on 600 MHz or 500 MHz home-built instruments at the Francis Bitter Magnet Laboratory. Data were then transferred to a Silicon Graphics work station and processed using Felix software (version 2.3, Biosym Technologies, Inc.). ^{1}H and ^{13}C chemical shifts are referenced to an internal standard, sodium 3-(trimethylsilyl)-1-propanesulfonate at 0.00 ppm.

DQF-COSY, TOCSY (MLEV-17 spin lock pulse with 70 ms mixing times) and NOESY (50 ms, 200 ms, and 400 ms mixing times) experiments were recorded at 20 °C in D_2O or H_2O on the DNA/HOO-Co-deglycoBLM complex. Data sets with 4096 x 512 complex points were acquired with sweep widths of 5000 Hz (500 MHz instrument) or 8000 Hz (750 MHz instrument) in both dimensions and 32 scans per t_1 increment. During the relaxation delay period, a 2.0 s presaturation pulse was used for solvent suppression. For the NOESY experiments in H_2O, a WATERGATE gradient pulse sequence was used, and data sets with 4096 x 512 complex points were acquired with sweep widths of 12000 Hz (500 MHz instrument) or 15000 Hz (750 MHz instrument) in both dimensions. The spectra were processed as previously reported.[11]

The HMQC[40]spectrum was recorded at 20°C in D_2O with a J_{C-H} coupling constant of 190 Hz on the DNA/HOO-Co-deglycoBLM complex. Data sets with 2048 x 256 complex points were acquired with 6000 Hz (^{1}H) and

25000 Hz (^{13}C) sweep widths on a 500 MHz instrument. 256 scans were collected for every t_1 increment. During the relaxation delay period, a 1.5 s presaturation pulse was used for solvent suppression. The spectrum was processed as described previously.[11]

2D NOESY (100, 200, 400 ms mixing times) and DQF-COSY experiments at 20 °C on HOO-Co-deglycoBLM in D_2O or 90 % H_2O/10 % D_2O were similarly recorded and processed.[10] The ROESY experiment[41] at 20 °C was acquired in D_2O with 3.1 kHz rf field strength on a 500 MHz instrument.

Molecular Modeling. All calculations were carried out with Quanta 4.0/CHARMm 22 (Molecular Simulations Inc.; Waltham, MA) on a Silicon Graphics Indigo2, or a Cray Y-MP or J-90. The methodology used has been described previously.[10,11] Only notable changes are described here in detail. The calculation of non-bonded van der Waals and electrostatic interactions were truncated at 13.0 Å using the force switching function between 8.0 and 12.0 Å and a distance-dependent dielectric constant. The list of non-bonded terms was updated every 20 steps, except in the final molecular dynamics run, where the list was updated if an atom moved < 0.5 Å. The terms for electrostatic interactions and hydrogen bonds were only included in the final 15 ps step of the calculations for the DNA/HOO-Co-deglycoBLM complex. Hydrogen bonds were cut off at 5.0 Å and switched between 3.5 and 4.5 Å. Hydrogen bonds were also cut off at 90° and switched between 130° and 110°. Following heating, the temperature was maintained by scaling the velocities of the atoms to keep the temperature at 300 ± 10 K. In the final 15ps molecular dynamics phase, scaling was only required 2-3 times.

All force constants for bond distance, angles, distance constraints and dihedral constraints were set analogously to those previously described.[10,11]

Molecular Dynamics (MD) Simulated Annealing. Eleven calculations of restrained molecular dynamics simulated annealing were run, following the same protocol described previously.[11] The MD was initiated with the distance constraints applied using a force constant of 0.6 kcal mol^{-1} $Å^{-2}$. The structure was heated and equilibrated over 4 ps, the force constants for the distance constraints were then scaled to 120 kcal mol^{-1} $Å^{-2}$ over 6.5 ps, and the system was allowed to evolve for 10 ps before being cooled to 300 K over 7 ps. The dihedral constraints were applied gradually, starting with a force constant of 5 kcal mol^{-1} rad^{-2}, and increasing to 50 kcal mol^{-1} rad^{-2} in 4 stages over 10 ps. The dihedral angle constraints on the DNA backbone angles β, γ, and ε at the intercalation site and the adjacent base pairs were applied with force constants of 5 and 10 kcal mol^{-1} rad^{-2} respectively. The electrostatic and hydrogen bond energy terms were introduced and the system was allowed to equilibrate for 4 ps, followed by the final 15 ps MD run. The final structure for each iteration was generated by averaging the coordinates of the final 5 ps of the 15 ps molecular dynamics simulation, followed by 1000 steps of conjugate gradient minimization with the distance constraints and dihedral angle constraints were used. The DNA backbone constraints were not used in the minimization.

Results and Discussion:

Preparation and Characterization of HOO-Co-deglycoBLM.

HOO-Co-deglycoBLM was prepared by a modification of the previously published procedure for HOO-CoBLM.[10,42] In the present case, the pH was maintained by running the reaction in phosphate buffer (pH 6.8, 100 mM) and the number of side products was minimized by extending the reaction to 12 hrs.

The products (a mixture of desired hydroperoxide and aquo or hydroxide forms) were readily separated by HPLC (see methods) and the UV/Vis spectrum of the hydroperoxide analog and its extinction coefficient (ε_{290}= 2.0 x 10^4 M^{-1} cm^{-1}) are almost identical to HOO-CoBLM (ε_{290}= 2.1 x10^4 M^{-1} cm^{-1}). The ^{1}H NMR spectrum exhibits four singlets H-C2H, H-C4H, B-C5H and B-C5'H, indicative of a compound of > 95 % homogeneity. Examination of the NMR spectrum (20 °C, pH 6.8) over a period of several months reveals no decomposition, a requirement for the acquisition of 2D NMR data.

To establish that the axial ligand is in fact the hydroperoxide, electrospray mass spectrometry was used. This method has previously been employed to characterize both activated BLM (HOO-FeBLM) and HOO-CoBLM.[10,43] The electrospray mass spectrum is shown in Figure 4.2 and exhibits a m/z of 569.0 (shown in the inset) with the calculated isotopic distribution (calculate MW of 1138.32). A total charge of +2 in the HOO-Co-deglycoBLM is consistent with a deprotonated β-hydroxyhistidine amide (-1), a hydroperoxide ligand (-1), Co(+3) and a positively charged sulfonium tail (+1).

Figure 4.2: Electrospray mass spectrum of HOO-Co-deglycoBLM. The inset shows the isotope distribution of the peak at m/z of 569.0.

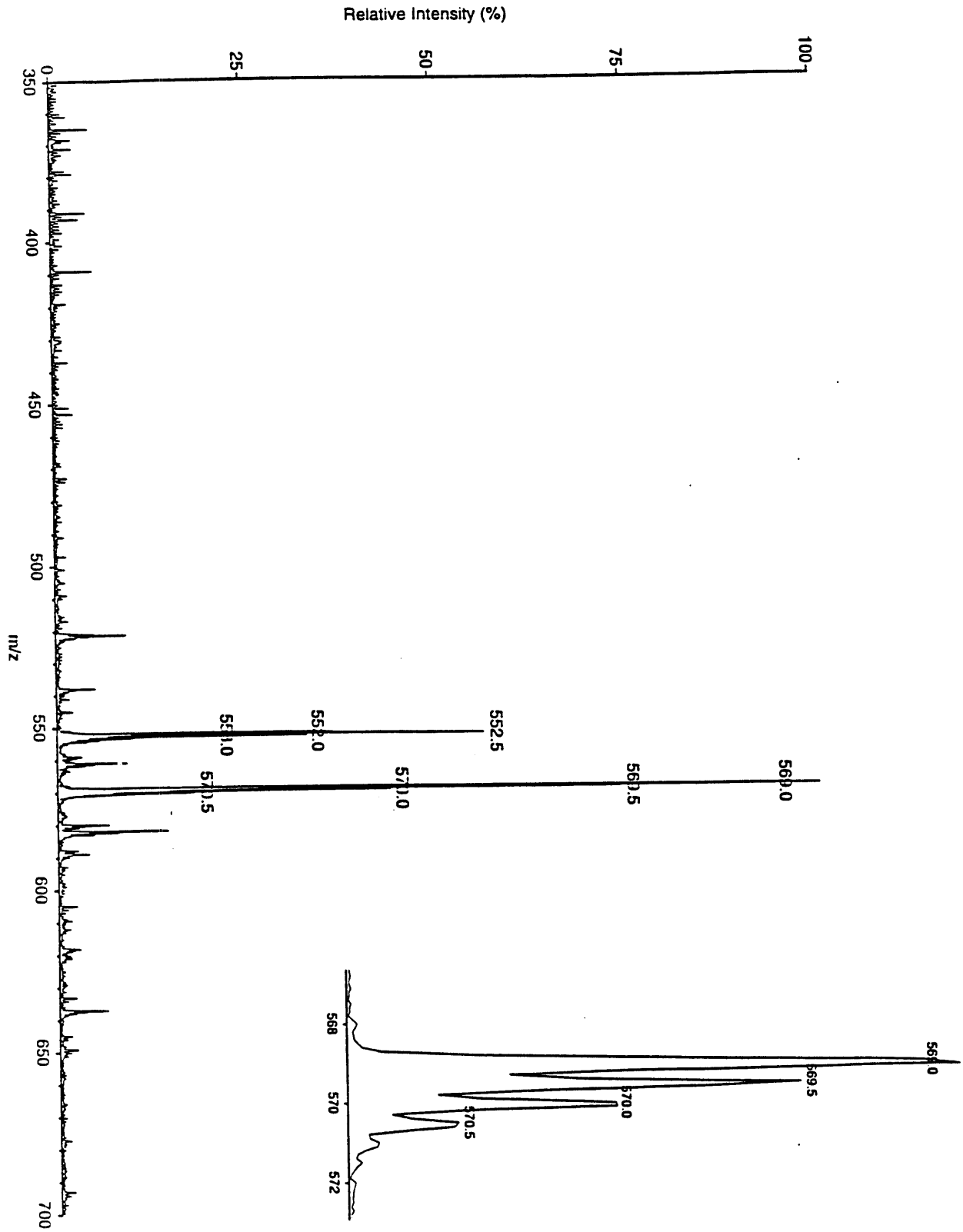
Relative Intensity (%)
0
25
50
75
100
350
400
450
500
550
600
650
700
m/z
552.5
560.0
560.5
570.0
568
570
572
569.5
570.0
570.5

Proton Chemical Shifts and Coupling Constants of HOO-Co-deglycoBLM: A Comparison with HOO-CoBLM.

In order to examine the structure of HOO-Co-deglycoBLM bound to an oligonucleotide, the free HOO-Co-deglycoBLM needs to be characterized first. The chemical shifts of both the exchangeable and nonexchangeable protons were assigned through COSY connectivities using strategies previously established for CO-FeBLM, ZnBLM, and HOO-CoBLM[10,29,30] and are reported in Table 4.1. The uncoupled B-C5H and B-C5'H protons were assigned based on their chemical shift similarity to the corresponding values in HOO-CoBLM (Table 4.1). In an effort to obtain information about through-space interactions, NOESY experiments at various mixing times (100, 200, and 400 ms) were carried out. However, they were unsuccessful, presumably due to the molecular weight of HOO-Co-deglycoBLM (MW 1138) falling into the range of correlation time where the NOEs approach zero.[44] The unavailability of concentrated solutions of HOO-deglycoBLM hampered attempts to use ROESY methods. No quantifiable interresidue ROEs were observed, although small cross-peaks between spatially close intraresidue protons were identified. The lack of NOE and ROE information has precluded the determination of the structure of the free HOO-Co-deglycoBLM.

The successful structure determination of the parent HOO-CoBLM,[10] however, has given us insight into the corresponding HOO-Co-deglycoBLM structure by direct comparison of the NMR data. The chemical shifts of most of the protons (pH 6.8 and 20 °C) are within 0.1 ppm of the parent compound (pH 6.8 and 5 °C) (Table 4.1). Of notable exception are the protons associated

Table 4.1: Comparison of Proton Chemical Shifts (ppm) of ApoBLM, Metallo-BLMs, and HOO-Co-deglycoBLM.

Protons		Deglyco[a] 293 K pH 6.8	Apo[b] 297K pH6.7	Co[c] 278 K pH 6.8	Zn[d] 277K pH 7	Fe[d] 277K pH 7	Protons		Deglyco[a] 293K pH 6.8	Apo[b] 297K pH6.7	Co[c] 278K pH6.8	Zn[d] 277K pH 7	Fe[d] 277K pH 7	
P	CαH	3.22	2.62	3.20	2.87	2.86	NH		9.12		8.89	7.55	7.75	
	CαH'	3.58	2.69	3.51	3.24	3.08	T	CH_3		1.19	1.08	1.19	1.02	0.99
	CβH	5.23	3.96	5.10	4.50	4.34		CαH		4.34	4.21	4.39	4.10	4.03
	CH_3	2.56	2.01	2.46	2.38	2.24		CβH		4.20	4.08	4.25	4.00	3.93
	4-NH_2			7.73/7.94	7.02	6.91		NH		8.89		8.92	7.96	8.20
H	CαH	4.85	5.05	4.98	4.85	4.93	B	CαH		3.14	3.24	3.06	3.16	3.08
	CβH	5.44	5.26	5.53	5.20	5.19		CαH'		3.29	3.24	3.12	3.26	
	C2H	8.71	7.79	8.72	8.04	7.86		CβH		3.49	3.60	3.44	3.51	3.35
	C4H	7.62	7.26	7.60	7.31	7.23		CβH'		3.84	3.60	3.51	3.86	
A	CαH	3.24	3.84	3.41	3.72	3.76		C5H		8.21	8.20	8.17	8.21	8.11
	CβH	2.85	2.83	2.74	2.46	2.42		C5'H		7.93	8.00	7.82	8.04	7.85
	CβH'	3.16	2.88	3.22	3.36	2.88		NH		8.67		8.57	8.36	8.33
	NH	6.27		6.01	4.32	5.38	S	$C\alpha H_2$		3.40	3.38	3.36	3.36	3.31
V	αCH_3	0.65	1.10	0.62	0.98	1.03		$C\beta H_2$		2.16	2.16	2.13	2.13	2.09
	γCH_3	1.00	1.12	0.98	0.93	0.96		CγH		3.57	3.60	3.51	3.57	3.53
	CαH	0.98	2.45	0.94	1.95	2.36		CγH'		3.63	3.60	3.63	3.57	3.53
	CβH	3.38	3.70	3.33	3.42	3.64		$(CH_3)2$		2.95	2.91	2.94	2.88	2.83
	CγH	3.52	3.86	3.50	3.62	3.58		NH		8.82		8.66	8.94	8.90

[a] HOO-Co-deglycoBLM, 50 mM phosphate buffer. [b] Akkerman et al. [c] HOO-CoBLM, 50 mM phosphate buffer [d] Akkerman et al.

with the β-aminoalanine moiety, A-CαH and A-NH, which are downfield shifted by 0.17 and 0.26 ppm, respectively relative to the parent HOO-CoBLM.

A comparison of the coupling constants of these two molecules (Table 4.2) are also virtually identical with the exception, once again, being associated with β-aminoalanine protons of A-CαH and A-CβHs (13.1 and 3.2 Hz in HOO-Co-deglycoBLM vs 4.0 and 3.0 in HOO-CoBLM). These observed differences reflect a significant change in the rotamer population around the Cα-Cβ bond of the β-aminoalanine moiety.

The similarities in the chemical shifts, coupling constants and the physical properties suggest that HOO-Co-deglycoBLM is very similar to its parent, with the exception of the configuration of the putative axial ligand, the primary amine of the β-aminoalanine moiety. This point will be returned to subsequently.

Screw Sense and the Linker Conformation.

The solution structure of HOO-CoBLM determined using extensive NOE and dihedral angle constraints derived from NMR studies in conjunction with molecular modeling revealed that its linker peptide adopts a well defined conformation, and its bithiazole tail folds underneath the equatorial coordination plane on the same face as the hydroperoxide.[10] This information is compatible with a single screw sense isomer that is shown in Figure 4.4a. This model, important with respect to defining the role of the sugars, places the sugars on the same face as the β-aminoalanine moiety whose primary amine functions as an axial ligand. The question then arises as to whether, despite the lack of NOE information, an argument can be made that HOO-Co-deglycoBLM has the same ligands and screw sense as its parent. Two lines of argument allow us to answer this question in the affirmative.

Table 4.2: Comparison of Coupling Constants (Hz) in Metallo-BLMs and Metallo-deglycoBLMs.

Protons	HOO-Co BLM[a]	HOO-Codeglyco BLM[b]	CO-FeBLM[c]	CO-Fe deglycoBLM[d]	ZnBLM [c]	Apo BLM [c]
G-C1H to G-C2H	3.9 ± 0.3				4.9	
M-C1H to M-C2H	1.2 ± 0.3				1.8	
H-CαH to H-CβH	2.7 ± 0.3	3.3 ± 0.3	3.1 ± 0.2	3.4	3.1 ± 0.2	5.8 ± 0.2
P-CβH to P-CαH	8.3 ± 0.3	9.2 ± 0.3		8.2		
P-CβH to P-CαH′	4.6 ± 0.3	4.3 ± 0.3		6		
T-CαH to T-CβH	2.9 ± 0.3	3.4 ± 0.3				
T-NH to T-CαH	8.7 ± 0.3	7.6 ± 0.3				
V-NH to V-CγH	7.9 ± 0.3	8.0 ± 0.3				
V-CαH to V-CβH	1.8 ± 1.2	1.5 ± 0.3				
V-CβH to V-CγH	9.5 ± 1.2	9 ± 1.2				
A-NH to P-CβH	<3	<3				
A-NH to A-CβH′	5 ± 2	<3				
A-NH to A-CβH	5 ± 2	4 ± 2				
A-CβH′ to A-CαH	3.0 ± 0.5	3.2 ± 0.3	4.2 ± 0.2	3.7	2.0 ± 0.2	5.2 ± 0.2
A-CβH to A-CαH	4.0 ± 1.2	13.1 ± 0.3	7.2 ± 0.2	13.0	3.8 ± 0.2	7.2 ± 0.2

[a] 50 mM phosphate, pH 6.8 at 5 °C. [b] This study, 50 mM phosphate, pH 6.8 at 20 °C. [c] Akkerman et al. [d] Oppenheimer et al.

The first involves the similarities in the conformation of the linker region apparent from comparison of chemical shifts and coupling constants of V and T moieties. The second, and arguably the most convincing, is the structure of HOO-Co-deglycoBLM bound to **1** described below. The constrained conformation of V is apparent from the observed coupling constants (1.8 Hz) between V-CαH and V-CβH, indicative of a gauche conformation between these two protons and the 9.5 Hz coupling constants between V-CβH and V-CγH, indicative a trans conformation between these protons (Table 4.2). In addition, the chemical shifts of V-CαH at 0.94 ppm and V-αCH$_3$ at 0.62 ppm are dramatically upfield shifted relative to apoBLM (Table 4.1), while, the V-NH and T-NH of the linker region are downfield shifted by average 0.9 ppm relative to other metallo-BLMs. The dramatic downfield shifts are due to shielding by the imidazole ring. The dramatic downfield shifts appear to be associated with H bonding of these amide hydrogens to the penultimate oxygen of the hydroperoxide in the parent compound and by inference in the deglycosylated congener.

The similarities in both the coupling constants and unusual chemical shifts of the parent within the V and T moieties between HOO-Co-deglycoBLM and its glycosylated parent provide strong support for assignment of a similar screw sense arrangement of the ligands in the HOO-Co-deglycoBLM to that observed in the parent.

Figure 4.3: Structure of HOO-CoBLM with the primary amine of A moiety as an axial ligand.

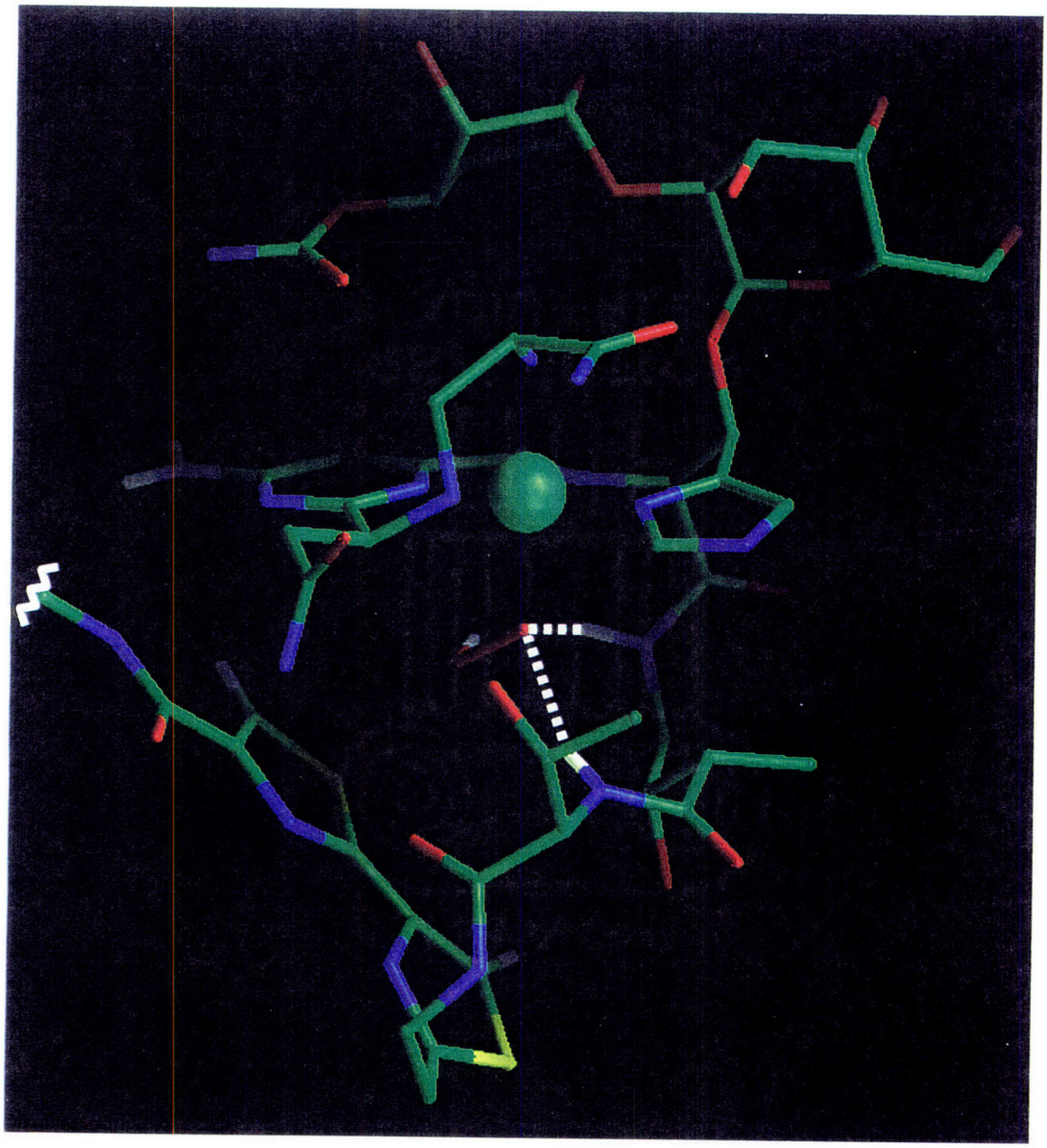

Figure 4.4: Two screw sense isomers of HOO-CoBLM.

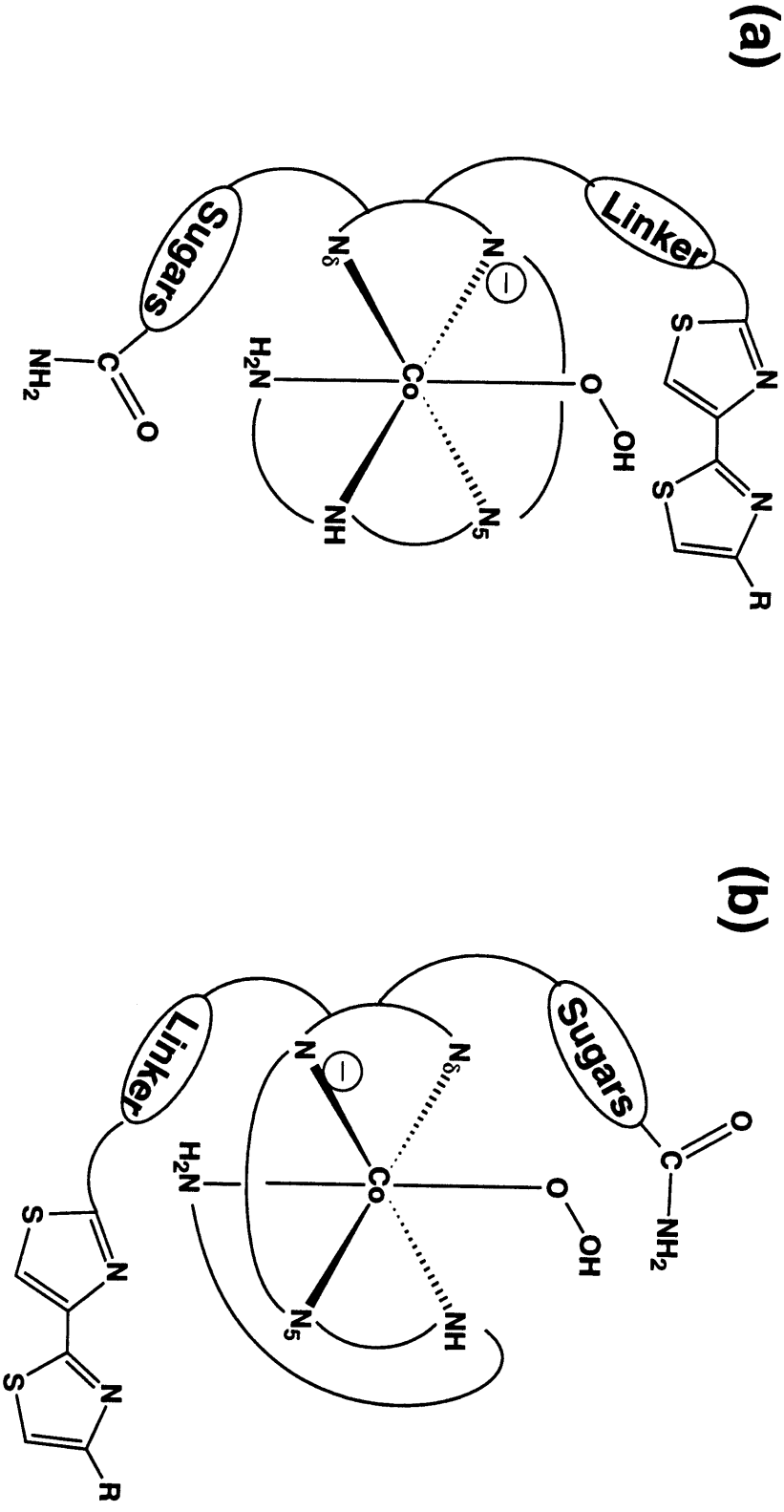
(a)
Sugars
Linker
N_δ
N
H_2N
Co
O
OH
NH
N_5
NH_2
C
O
S
N
S
N
R
(b)
Linker
Sugars
N
N_δ
H_2N
Co
O
OH
N_5
NH
O
C
NH_2
S
N
S
N
R

Second, the screw sense of the metallo-BLM obviously has a profound effect on its ability to bind to DNA. With HOO-CoBLM, given the extensive NOE constraints for its binding to several oligonucleotides,[11,16] only a single screw sense (Figure 4.4a) is compatible. As described in detail below, the HOO-Co-deglycoBLM binds to DNA in almost identical fashion to the parent. Based on these considerations, we feel confident that the HOO-Co-deglycoBLM and its parent have the same chiral ligand organization.

Primary Amine Axial Ligand.

The nature of the axial ligand has been one of contention for many of the metalloBLMs.[10,29,30] Our recent 2D NMR studies with HOO-CoBLM in conjunction with chemical and biochemical studies, have established in this case that the primary amine of β-aminoalanine and not the carbamoyl N or O of the mannose of the sugars is the second axial ligand.[10] Since our screw sense isomer (Figure 4.4a) requires both of these ligands to be on the same face, the distinction between these options is structurally, but we believe not chemically, a subtle one.

The major arguments concerning the primary amine ligation for a number of metalloBLMs have been associated with the examination of the coupling constants between the A-CαH and A-CβHs of the β-aminoalanine moiety.[10,29,30] It has been proposed that if the primary amine of β-aminoalanine is coordinated to cobalt as an axial ligand, as in the case of ZnBLM and HOO-CoBLM, then the rotamer population around Cα-Cβ bond of β-aminoalanine should be constrained to predominately a single rotamer (gauche(-) for both ZnBLM and HOO-CoBLM in Figure 4.5).[29,30] If on the other hand, the primary amine is not an axial ligand, as in the case of free apoBLM, the rotamer population is expected to be a mixture of

populations.[29,30] In the case of HOO-Co-deglycoBLM, the ability of the carbamoyl moiety to serve as an axial ligand of course has been eliminated. Thus, the only possibilities for the axial ligand are the favored primary amine, a H_2O molecule, or no ligand at all. In support of the primary amine, consider the following arguments. First, the J values between CαH and CβHs are 13.1 Hz and 3.2 Hz, indicative a predominately trans conformation of the Cα-Cβ bond of β-aminoalanine moiety (Figure 4.5). This is consistent with the ligation by the primary amine. Second, a sensitive probe of electronic environment is EPR spectroscopy and in fact extensive analysis of O_2-Co(II) BLM in comparison with the O_2-Co(II)-deglycoBLM suggest that their environments are strikingly similar.[33-35] Thus, we believe, that the axial ligand for HOO-Co-deglycoBLM is also the primary amine of β-aminoalanine. Third, crystallographic precedence for the primary amine as an axial ligand has been well documented in deglycosylated BLM analogs and model compounds, such as Cu-P3A, a biosynthetic precursor of BLM lacking both the sugar and the linker domains, and CoPMA, a BLM model compound (Figure 4.6b).[45,46]

Figure 4.5: Newman projections of possible conformation of the Cα-Cβ bonds of the β-aminoalanine (bottom) and β-hydroxyhistidine (top) moieties (the trans and gauche nomenclature refers to the definition by Akkerman et al.[30]).

β–hydroxyhistidine

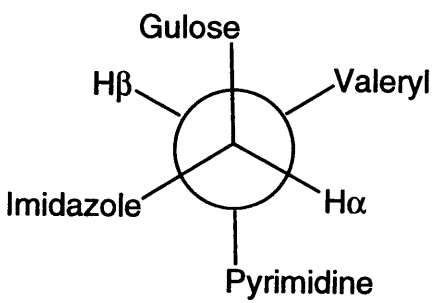

gauche(+)

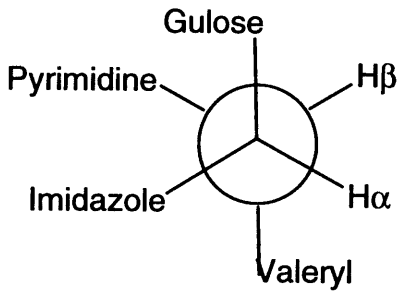

trans

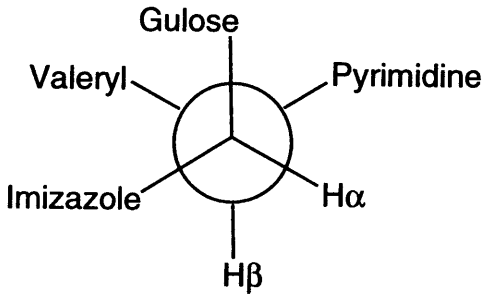

gauche(-)

β-aminoalanine

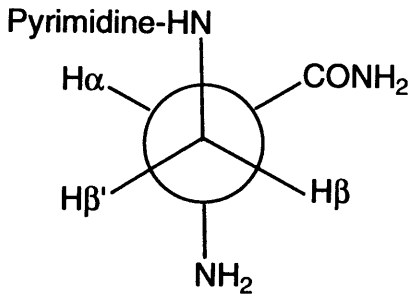

gauche(+)

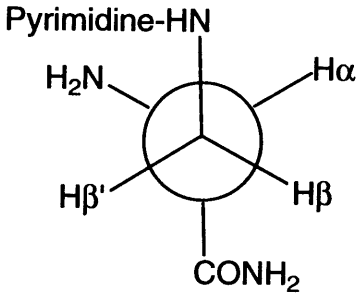

trans

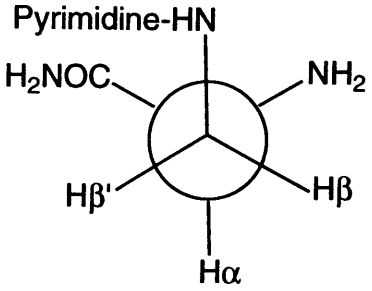

gauche(-)

Note, however, that the conformation of the Cα-Cβ bond of the β-aminoalanine in HOO-Co-deglycoBLM is trans (Figure 4.5) and different from that observed in its glycosylated parent, where a predominately gauche(-) conformation has been established (Figure 4.5). Although both conformations are feasible for the ligation by the primary amine, in both glycosylated compounds examined to date (HOO-Co-Phleomycin and HOO-CoBLM), the gauche(-) conformation predominates. On the other hand, Cu-P3A (by crystallographic analysis), CO-Fe-deglycoBLM (by NMR analysis of A-CαH-A-CβH of 13.0 and 3.7 Hz), a trans conformation is favored (Figure 4.5).[21,45] The prevalent difference in the conformation of the Cα-Cβ bond of the β-aminoalanine moiety between HOO-CoBLMs and HOO-Co-deglycoBLMs, if indicative of the corresponding FeBLMs, suggests that it is perhaps correlated with the reduction in the cleavage efficiency by the deglycoBLM, a subject of further discussion below.

Activated Fe-deglycoBLM.

The observation of conformational differences in the axial ligand could reflect the changes in the alignment of the primary amine of β-aminoalanine towards metal coordination and thus be manifested in the rates of formation and decomposition of the activated deglycoBLM (again the caveat is the assumption that Co is an excellent analog for the Fe). Recall that the formation of activated BLM requires, subsequent to Fe(II)BLM binary complex formation, binding of O_2, followed by the reduction to generate the HOO-Fe(III)BLM (activated BLM). This species has been shown by Burger et al. to be a long lived with a $t_{1/2}$ of 2 min. at 4 °C.[47,48] Ample biphysical studies of metallo-BLM analogs and model compound have demonstrated the importance of electronic balance between the coordinating ligand and Fe

in order to achieve the optimum low-spin activated Fe(III)BLM.[49-55] Loeb et al. have shown that the strong back-bonding from the iron to the pyrimidine ligand reduces the charge transfer between the iron and oxygen and is critical to preventing the ternary O_2-Fe(II)BLM complex from decomposing to O_2^- and Fe(III)BLM.[55] Another example includes a BLM A2 analog with the α-amino group of β-aminoalanine of BLM N-acetylated. It has been shown to form a stable binary complex with Fe(II), but fails to bind O_2 and thus exhibits no DNA cleavage.[54] These studies attest to the requirement for intricate partitioning of electron density between Fe and the coordinating ligands to achieve the maximum DNA cleavage.

The trans conformation of the Cα-Cβ bond of β-aminoalanine in HOO-Co-deglycoBLM perhaps reflects the poor alignment of the primary amine axial ligand towards the metal in metallo-deglycoBLM and thus impairs the ideal electronic distribution elaborated in BLM-mediated DNA cleavage. However, it is not known at present whether the impairment occurs before or after the formation of activated deglycoBLM or a combination of both. EPR measurement by Kenani et al. suggests that the stability of activated deglycoBLM is decreased to an intensity only 5% of that observed for activated BLM,[32] although evidence is not available regarding whether or not the oxygen binding by Fe(II)-deglycoBM, the 1e reduction to generate activated deglycoBLM, or its rapid decomposition once activated is responsible for the observed effect. A detailed understanding of the production of activated deglycoBLM awaits the determination of rate constants involved in the formation and decay of activated deglycoBLM via stopped-flow UV-Vis, RFQ-EPR and RFQ-Mössbauer measurements analogous to studies performed on activated BLM.[47,48,56]

A Possible Steric Effect by the Sugar Domain

The solution structure of HOO-CoBLM A2 and DNA cleavage studies with BLM analogs and model compounds suggest a possible structural basis for the sugars' contribution to the efficiency of DNA cleavage. A steric interaction between the gulose moiety and the β-aminoalanine moiety in BLM is perhaps responsible for confining the Cα-Cβ bond of the β-aminoalanine in the ideal gauche(-) conformation, imperative for the optimum DNA cleavage. Conversely, when this steric interaction is absent as in deglycoBLM, the Cα-Cβ bond of β-aminoalanine assumes the trans conformation and thus impairs the formation and/or the decomposition of activated Fe-deglycoBLM and reduces the DNA cleavage efficiency.

This proposal is consistent with several experimental observations. First, the NMR and molecular modeling studies have shown that the sugar domain, although not an axial ligand, is located in close proximity to the β-aminoalanine. The gulose moiety is within van der Waals distance of protons of the β-aminoalanine moiety and is conformationally less flexible than the terminal mannose moiety. Second, studies with demannosylBLM show that its DNA cleavage efficiency is almost identical to that of BLM, indicating that the terminal mannose including the 3'-carbamoyl group, is not important for DNA cleavage. In addition, an unusual BLM analog, α-D-mannopyranosyldeglycoBLM A2 prepared by inversion of the C5' stereocenter of gulose exhibits much diminished cleavage efficiency (8 fold) compared to BLM. This results underscores the importance of the α-L-gulose. Inversion at C5' of gulose has a profound effect on the conformation of the sugar, where the C2, C3, and C4 substitutents of α-D-mannopyranosyldeglycoBLM A2 are in opposite axial or equatorial positions comparing to α-L-gulose. This large conformational reorganization likely

eliminates the steric interaction important for maintaining the gauche(-) conformation in the Cα-Cβ bond of β-aminoalanine. Third, studies of PYML, a BLM model compound having a t-butylether group in place of the gulose moiety reveal that such a group can perhaps confer the same kind of steric interaction with the β-aminoalanine moiety (Figure 4.6a).[49-51] The Fe-(t-butylether)PYML model compound with a bulky t-butyl ether group attached to the β position of histidine has been shown to have 71% oxygen activating capacity of BLM, while the free hydroxyl group shows only 18 % activation in the same assay. Although the quantitation of oxygen activation is only accessed by EPR trapping of the hydroxyl radical formed (a minor event in actual BLM chemistry), it appears to correlate with the relative chemical reactivity among various PYML ligands. The authors, however, concluded that the enhancement in chemical reactivity by t-butylether is a consequence of steric or hydrophobic effects on oxygen activation. A more plausible explanation perhaps lies in the steric interaction between the bulky t-butyl group and the β-aminoalanine moiety to effect the gauche(-) conformation in the Cα-Cβ bond of β-aminoalanine and hence improve the net production of the activated species. Examination of the coupling constants between CαH and CβH of the histidine moiety in metallo-BLMs supports the hypothesis that the bulky t-butylether group can be positioned near the axial ligand. Among all metallo-BLMs and metallo-deglycoBLM studies thus far, similar J values ranging from 2.7 Hz to 3.4 Hz between H-CαH-H-CβH are observed (Table 4.2). This coupling constant range is consistent with a predominate trans conformation in the Hα-Hβ bond (Figure 4.5). A very different J value is observed in apo BLM of 5.8 Hz. This conformational rigidity in metallo-BLMs and metallo-deglycoBLMs is the result of the constraints from the deprotonated amide and imidazole both being the equatorial ligands (Figure

4.3). The absence of the sugar domain in both HOO-Co-deglycoBLM and CO-Fe-deglycoBLM does not affect the conformation of the H-Cα-H-Cβ bond (Table 4.2). Consequently, one might expect that any functional group of reasonable size attached to the β position of histidine would retain the same conformation at the H-Cα-H-Cβ bond, and remain structurally placed in the same vicinity as previously occupied by the sugar domain. A t-butylether group can position itself within the van der Waals distance of the β-aminoalanine moiety, and thus enhance the net production of the activated species by maintaining the gauche(-) conformation of Cα-Cβ bond of the β-aminoalanine moiety (Figure 4.5). The relatively small hydroxyl group is not bulky enough to exert the proposed steric interaction. However, it should be pointed out that the PYML ligands only mimic the metal binding domain of BLM. The formation of a racemic mixture of the metallo-PYMLs is more feasible without the presence of the linker region or the bithiazole tail as the steric enforcements to promote the formation of screw sense isomer observed in HOO-CoBLM. The potential existence of both screw sense isomers in Fe-PYMLs would obscure the effect of the t-butylether group in PYML.

The proposed steric interaction between the α-L-gulose and the β-aminoalanine moiety makes several predictions which can be tested experimentally. First, the measurements of the coupling constants of HOO-Co-demannosylBLM, HOO-Co-α-D-Mannopyranosyldeglyco BLM, Co-(t-butylether)PYML, and other metallo-deglycoBLM analogs should further determine if the correlation holds between steric bulk and alanine conformation. Second, molecular dynamic studies with metallo-demannosylBLM, metallo-mannopyranosyldeglycoBLM, metallo-(t-butylether)PYML or other analogs can be performed to test the conformational rigidity of the Cα-Cβ bond of β-aminoalanine among these

Figure 4.6: Structure of BLM model compounds.

(a)

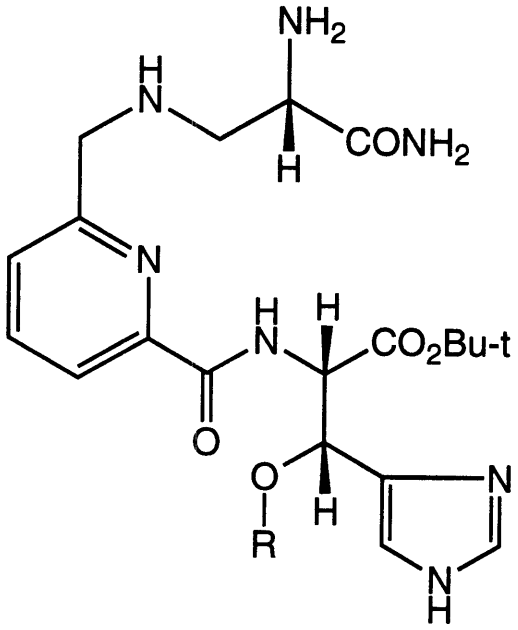

R=t-Bu or H

PYML-4

(b)

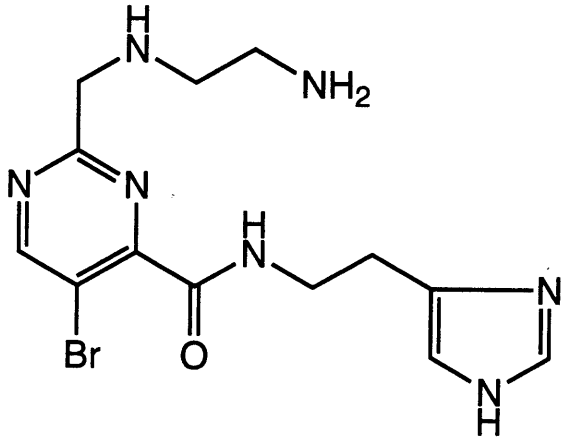

PMAH

analogs and predict the possibility of other functional groups that can have the similar effects. Third, the recent modular synthesis of BLM allows the isotopic labeling (C13 or N15) of either the β-aminoalanine moiety and/or the sugar domain of BLM. The ensuing NOE measurements between the sugar domain and the β-aminoalanine protons will be invaluable in providing structural evidence with respect to the proposed steric interaction and predicting new functional groups which may further improve DNA cleavage efficiency.

Binding Affinity of HOO-Co-deglycoBLM to oligonucleotide 1

Previous fluorescence quenching studies have shown that oligonucleotide **1** contains a single binding site for HOO-CoBLM with an apparent K_d of 0.17 ± 0.7 μM.[10,11] A similar measurement has been made with HOO-Co-deglycoBLM in an effort to examine the contribution of the sugar domain to DNA binding. Under identical conditions, an apparent K_d of 5.9 ± 0.7 μM was obtained. This lower DNA binding affinity of HOO-Co-deglycoBLM contrasts with the previous fluorescence quenching studies which showed that the apo forms of BLM and deglycoBLM exhibit the same DNA binding affinity.[57] The apparent inconsistency of the two studies can be resolved by considering the structural distinction between apo and metallo forms of BLM and deglycoBLM. The apo forms adopt an extended conformation[58] and upon metal complexation, undergo significant conformational reorganization to form octahedral metal complexes.[10,29,30,59] Consequently, it is not unexpected that the DNA binding by metallo-BLMs would be quite different from their respective apo forms and perhaps should be more relevant to DNA cleavage as well.

1D ^{1}H NMR Titration of HOO-Co-deglycoBLM with 1

The previous NMR titration of **1** with HOO-CoBLM exhibited the formation of a 1:1 complex in slow exchange on the NMR time scale, which allowed the detection of 60 intermolecular NOEs and the subsequent structural determination.[11] In an effort to delineate the role of the sugars in DNA binding and cleavage, the solution structure of HOO-Co-deglycoBLM bound to **1** has been determined.

The titration spectrum of HOO-Co-deglycoBLM with **1** monitored by 1D NMR is shown in Figure 4.7a-c and is similar to that previously reported with HOO-CoBLM complexed with DNA (Figure 4.7d). The disappearance of A3-H8 in free DNA upon addition of HOO-Co-deglycoBLM is accompanied by the generation A3-H8 and A13-H8 of new DNA/drug resonances (Figure 4.7b,c) indicating the formation of a 1:1 complex in slow exchange on the NMR time scale. The appearance of many minor features (asterisks in Figure 4.7c) is evident, in contrast to the titration with HOO-CoBLM (Figure 4.7d). The selective broadening of A3-H8 (Figure 4.7c) in the complex is also apparent. These subtle but discernible differences in DNA binding by the two congeners are apparent and will be the subject of further discussion.

The low complex concentration (~1 mM) of the complex due to limited availability of HOO-Co-deglycoBLM and the presence of minor species have complicated the proton assignments. Proton assignments for HOO-Co-deglycoBLM has followed the previously reported strategy for the assignment of HOO-CoBLM complexed with the same DNA (Table 4.3).[11] Highlighted below are the assignments for protons of particular interest and those in which difficulties were encountered.

One of the hallmarks of the intercalative mode of binding by the CoBLMs has been the upfield shift of the protons associated with the

Figure 4.7: Titration of d(CCAGGCCTGG) with HOO-Co-deglycoBLMat 20°C. Downfield region of the ^{1}H NMR (500 MHz): (a), (b), (c) decameric duplex DNA (1.0 mM) in 50 mM sodium phosphate (pH 6.8) with 0, 0.5, and 1 equivalent of Co-deglycoBLM A2 green added respectively; (d) decameric duplex DNA in 50 mM sodium phosphate (pH 6.8) with 1 equivalent of HOO-CoBLM added. (e) Free HOO-Co-deglycoBLM in 50 mM sodium phosphate (pH 6.8). Asterisks indicate the presence of minor complexes. Circles are peaks of impurities from sample handling.

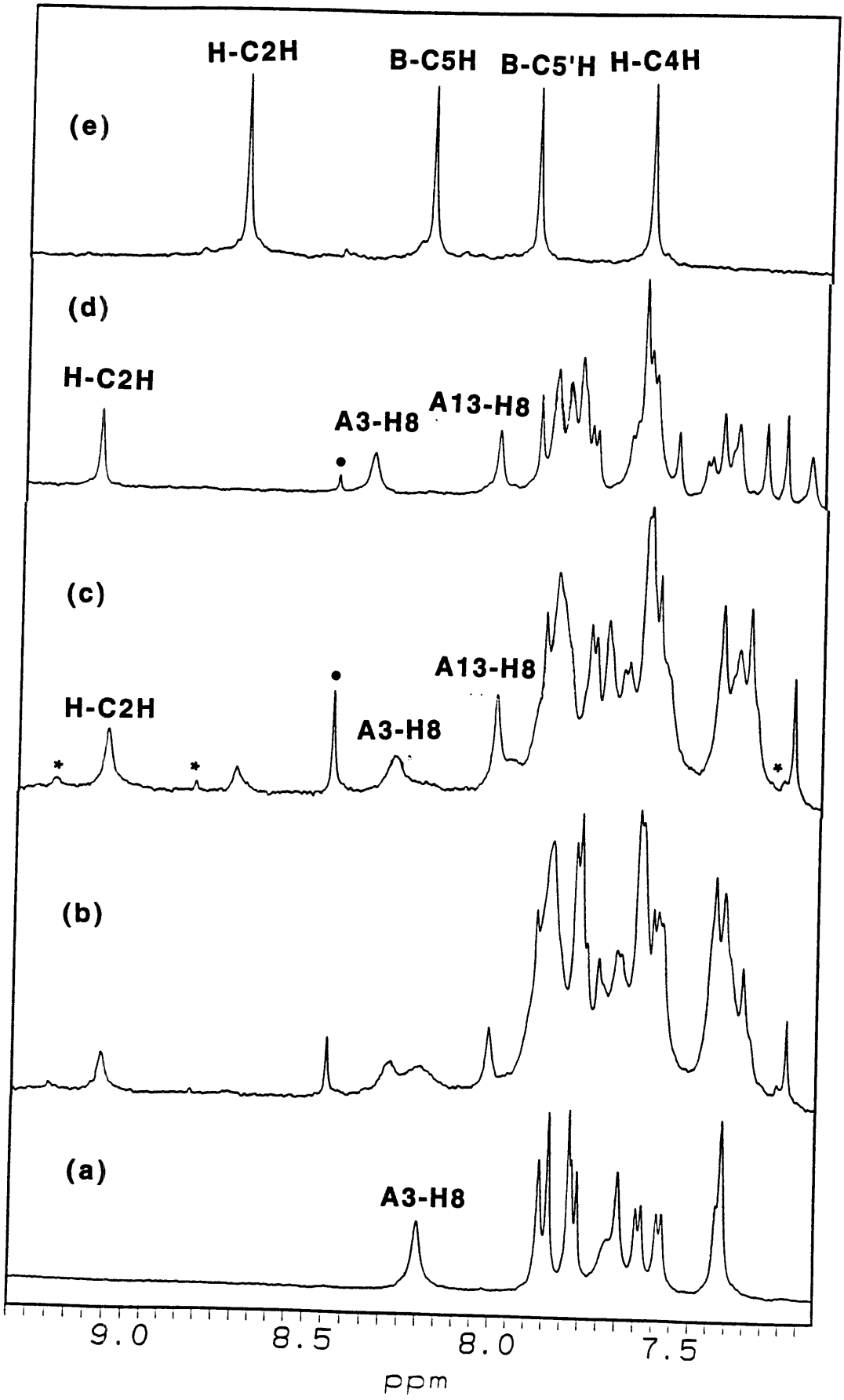
H-C2H
B-C5H
B-C5'H
H-C4H
(e)
(d)
H-C2H
A3-H8
A13-H8
(c)
H-C2H
A3-H8
A13-H8
(b)
(a)
A3-H8
9.0
8.5
8.0
7.5
ppm

bithiazole, B-C5H and B-C5'H, when bound to DNA.[11,12] The assignments of these two singlet protons, in the absence of any COSY connectivities, have utilized the relatively invariant thiazolium carbon chemical shifts of both free HOO-CoBLM and its complex with DNA obtained from HMQC experiments.[11,12] A similar strategy has been used in assigning the corresponding protons in HOO-Co-deglycoBLM bound to DNA. The HMQC spectrum of this complex is shown in Figure 4.8 and displays two C/H crosspeaks at the signature carbon chemical shifts of B-C5 (126.9 ppm) and B-C5' (117.4 ppm), assigned by comparison to 126.8 and 117.5 ppm respectively in HOO-CoBLM complex. In turn, the proton chemical shifts for B-C5H and B-C5'H in the complex with DNA are assigned to 7.32 ppm and 7.18 ppm respectively in the HMQC spectrum (Figure 4.8). Compared to the chemical shifts of B-C5H and B-C5'H in free HOO-Co-deglycoBLM (8.21 ppm and 7.93 ppm respectively), both bithiazole protons are upfield shifted, consistent with an intercalative mode of binding.

The NMR studies of the HOO-CoBLM complex have previously revealed that the sequence specificity of DNA cleavage by BLM is derived from the pyrimidine moiety.[11] More specifically, one of the 4-amino protons and N3 of the pyrimidine participate in hydrogen bonds with the N3 and one of the 2-amino protons of guanine, respectively, 5' to the cleavage site in d(GPy).[11] The NMR evidence for this hydrogen bonding network included the observation of a downfield shifted 4-amino proton of pyrimidine (10.36 ppm) and its NOE interactions with P-CH_3, G5-H1', G5-H4' and the imino protons of G5 and G4 (both are weak) in HOO-CoBLM bound to DNA.[11] In the HOO-Co-deglycoBLM complex, an exchangeable proton observed at 10.23 ppm also shows NOEs to P-CH_3, G5-H1' and G5-H4'. Thus, it is assigned to one of the P-NH_2 protons in HOO-Co-deglycoBLM bound to DNA. This

proton, however, does not show NOEs to the imino protons of G5 and G4, which is not surprising based on concentration limitations.

The fortuitous observation of the hydroperoxide proton in HOO-CoBLM bound to DNA previously provided the opportunity to examine the orientation of the metal-bound hydrogen peroxide ligand relative to the 4' hydrogen of C6, the site of cleavage.[11] This assignment (8.89 ppm) was supported by NOEs to the protons of the linker region of BLM and the deoxyribose protons of the cleavage site, as well as by molecular dynamics calculations.[11] By analogy An exchangeable proton at 9.02 ppm in HOO-Co-deglycoBLM complex has been assigned to the hydroperoxide proton of HOO-Co-deglycoBLM A2. This resonance shows many NOEs to the minor groove protons of the cleavage site C6 (Table 4.4) and protons of the linker region (Table 4.6) in a pattern similar to that observed in HOO-CoBLM. To ensure an unbiased assignment, the initial restrained molecular dynamics calculation described below was performed without the NOEs associated with the hydroperoxide proton. The distances between the hydroperoxide proton and the protons of the linker region and the C6 deoxyribose, derived from the resulting structural model were found to match well with the intramolecular and intermolecular NOEs observed by NMR.

Of the protons associated with the putative second axial ligand of the primary of the β-aminoalanine, the assignments of A-CαH and A-CβHs in Co-deglycoBLM bound to DNA has been difficult. The selective broadening of these protons was previously reported in case of HOO-CoBLM bound DNA.[11] This complication, in addition to the limited sample quantity, has prevented the unambiguous assignment of A-CαH and A-CβHs in this complex. Their tentative assignments are deduced from the following observations. The A-NH proton was first identified based on its NOE to H-

Figure 4.8: Expanded HMQC spectrum of the complex between HOO-Co-deglycoBLM and d(CCAGGCCTGG) (1 mM) in 50 mM sodium phosphate (pH 6.8) at 20°C.

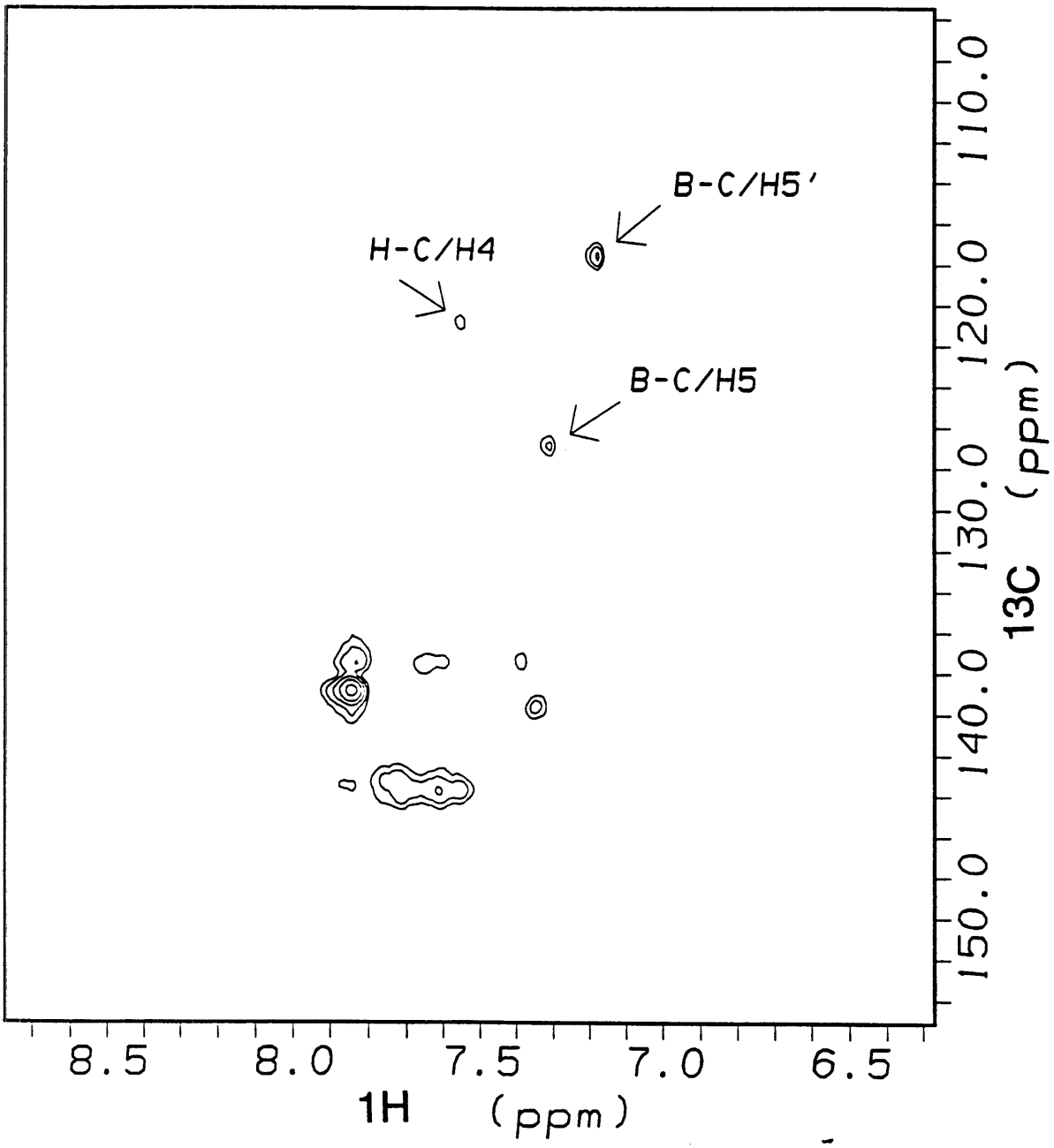
B-C/H5'
H-C/H4
B-C/H5
110.0
120.0
130.0
140.0
150.0
13C (ppm)
8.5
8.0
7.5
7.0
6.5
1H (ppm)

Table 4.3: Proton Chemical Shifts (ppm) of HOO-Co-deglycoBLM and HOO-CoBLM Complexed with DNA at 20 °C.

		HOO-Co-deglycoBLM pH 6.8	HOO-CoBLM pH 6.8
P	CαH	3.06	2.78
	CαH'	3.61	3.69
	CβH	5.25	5.16
	CH_3	2.59	2.61
	4-NH_2	6.86,10.23	7.14,10.36
H	CαH	4.86	5.01
	CβH	5.45	5.48
	C2H	9.06	9.10
	C4H	7.55	7.60
A	CαH	2.96	3.37
	CβH	3.08	2.46
	CβH'	3.50	3.24
	NH	5.71	5.69
V	αCH_3	0.67	0.65
	γCH_3	0.95	0.96
	CαH	1.23	1.21
	CβH	3.79	3.73
	CγH	3.47	3.51
	NH	9.07	8.78
	OH	6.71	6.79
T	CH_3	1.25	1.23
	CαH	4.53	4.53
	CβH	4.51	4.51
	NH	9.56	9.36
B	CαH	2.82	2.83
	CαH'	2.90	2.76
	CβH	2.95	2.93
	CβH'	3.69	3.76
	C5H	7.32	7.26
	C5'H	7.18	7.21
	NH	8.62	8.62
S	C$αH_2$	3.54, 3.67	3.56,3.46
	C$βH_2$	2.05,2.15	2.07,2.16
	CγH	3.34	3.43
	CγH'	3.44	3.43
	$(CH_3)_2$	2.97	2.97,3.00
	NH	7.73	7.81
CoOOH		9.02	8.89

C2H. This NOE is ubiquitous among metallo-BLMs as a result of the spatial arrangement of four equatorial ligands (Figure 4.3) and is readily identifiable in an uncrowded region of the NOESY spectrum (Table 4.6). The COSY spectrum in H_2O does not exhibit any crosspeaks associated with the A-NH, largely due to its broad linewidth and S/N constraints. Inspection of the TOCSY spectrum in H_2O, however, reveals a small crosspeak between A-NH and a resonance at 3.08 ppm. Corroboratively, the NOESY spectrum in H_2O also contains a NOE from A-NH to this resonance at 3.08 ppm. The resonance at 3.08 ppm is thus assigned to one of the A-CβHs. The COSY spectrum in D_2O shows a crosspeak between the resonance at 3.08 and 3.50 ppm, affording the assignment of the other A-CβH. Subsequent analysis of the NOESY spectrum in D_2O reveals NOEs from both A-CβHs to a resonance at 2.96 ppm, tentatively assigned to A-CαH. However, no COSY crosspeaks can be discerned between A-CβHs and A-CαH. The lack of COSY connectivity between A-CβHs and A-CαH may be due in large part to severe broadening of the A-CβH and A-CαH protons. However, it is also conceivably due to the small coupling constants between these protons as observed in the case of HOO-CoBLM bound to DNA. The reason for the severe broadening of the β-aminoalanine protons is not known at present. Also unclear is the size of the coupling constants between A-CβHs and A-CαH when bound to DNA. Because of the low S/N ratio associated with the A-CβH and A-CαH protons and much overlap in the region between 2-4 ppm due to minor peaks, many inter- and intramolecular NOEs associated with the β-aminoalanine protons are either absent or obscured in this complex.

Table 4.4: Intermolecular NOEs between HOO-Co-deglycoBLM and DNA at 20 °C.

5′ end	Strand 1	BLM residues	3′ end	Strand 2	BLM residues
G5	H4′	P-CH_3 /w	C16		
		P-NH_2(1) /w			
	H1′	P-CH_3 /w			
		P-NH_2(1) /w			
		P-NH_2(2) /m			
	NH				
C6	H5″	P-CH_3 / w	G15		
		V-γCH_3 /m			
	H5′	T-CαH/w			
		V-γCH_3 / w		NH	B-C5H′ /m
	H4′	CoOOH /w			B-CβH′ / w
		P-CH_3 /w			B-CβH / w
				H8	B-C5H / m
		V-γCH_3 /m			
	H2″	CoOOH /w			
	H2′	CoOOH /w			
	H1′	CoOOH / m			
		P-CH_3 / w			
		P-CβH /m			
	NH2h	B-C5H′ /m w			
C7	H5″	T-CαH /w	G14	H1′	B-C5H / s
	H5′	CoOOH /w		H2″	B-C5H / m
		T-CβH /w		H2′	B-C5H / m
		T-CαH /w			
	H4′			H4′	B-C5H / w
				NH	B-C5H′ / w
				H8	B-C5H / m
					S-CβH′ / w
	H1′	B-CαH′ / w			S-CβH / w
		B-CαH / w			S-CγH /w
					S-CγH' /w
T8			A13	H8	S-CH_3 /w
3′ end	Strand 1		5′ end	Strand 2	

[a] P-NH_2 (1) and P-NH_2 (2) are the hydrogens at 10.23 ppm and 6.86 ppm, respectively. [b] Used the H5' pseudoatom.

Table 4.5: Proton Chemical Shifts (ppm) of DNA in the DNA/HOO-Co-deglycoBLM Complex at 20 °C.

	H6/H8	H5/H2	Methyl	H1'	H2'	H2"	H3'	H4'	H5',5"
C1	7.73	5.94		5.94	1.98	2.46	4.65	4.12	3.74
C2	7.58	5.75		5.29	2.13	2.39	4.83	4.13	
A3	8.28	7.78		5.96	2.82	2.87	5.06	4.38	
G4	7.65			5.70	2.52	2.69	5.04	4.37	
G5	7.83			5.59	2.46	2.68	5.02	4.23	
C6	7.40	5.61		5.98	1.78	2.36	4.81	3.26	3.82, 3.95
C7	7.64	5.98		5.92	2.18	2.27	4.77	3.95	3.37, 3.73
T8	7.33		1.64	5.53	2.10	2.23	4.99	4.14	
G9	7.84			5.68	2.72	2.72	4.99	4.35	
G10	7.84			6.12	2.58	2.35	4.66	4.20	
C11	7.73	5.94		5.94	1.98	2.46	4.65	4.11	3.74
C12	7.58	5.71		5.14	2.12	2.29	4.81	4.07	
A13	8.00	7.89		5.99	2.54	2.71	5.01	4.34	
G14	7.39			5.21	2.42	2.72	5.03	4.31	
G15	7.60			5.74	2.52	2.77	4.79	4.32	
C16	7.29	5.24		5.68	2.17	2.35	4.77	4.15	
C17	7.53	5.58		5.96	1.97	2.36	4.73	3.72	3.95
T18	7.32		1.70	5.57	2.16	2.35	4.78	3.74	
G19	7.82			5.61	2.00	2.35	5.02	4.22	
G20	7.89			6.15	2.63	2.38	4.65	4.21	

	Imino	C amino
C1•G20		
C2•G19	12.90	8.45, 6.89
A3•T18	14.10	
G4•C17	13.07	8.73, 6.91
G5•C16	12.94	8.51, 6.34
C6•G15	12.59	7.95, 6.62
C7•G14	11.86	8.27, 7.21
T8•A13	14.26	
G9•C12	13.12	8.57, 6.98
C10•C11		

Table 4.6: Nontrivial Intramolecular NOEs within HOO-Co-deglycoBLM in DNA Complex at 20 °C.[a]

H-C2H---A-CβH′	w	V-αCH$_3$---H-CβH	w	V-OH---V-γCH$_3$	m
H-C2H---A-NH	m	V-γCH$_3$---H-CβH	w	V-OH---V-CβH	m
H-C2H---P-CβH	w	V-CγH---H-CβH	w	P-NH$_2$ (1)---P-CH$_3$	m
H-C2H---P-CαH	m	V-αCH$_3$---V-CγH	s	P-NH$_2$ (2)---P-CH$_3$	m
H-C2H---T-CH$_3$	s	V-γCH$_3$---V-CβH	s	CoOOH---T-NH	s
H-C2H---T-CβH	w	V-αCH$_3$---V-CβH	m	CoOOH---V-γCH$_3$	w
H-C2H---T-CαH	w	V-αCH$_3$---V-γCH$_3$	m	CoOOH---V-CγH	w
H-C2H---V-CαH	m	V-γCH$_3$---V-CαH	w	CoOOH---P-CβH	m
H-C2H---V-αCH$_3$	w	T-NH---V-CαH	m	CoOOH---V-OH	w
H-C2H---V-CβH	w	T-NH---V-NH	s	CoOOH---A-NH	w
H-C4H---V-γCH$_3$	w	V-NH---V-γCH$_3$	w	CoOOH---TCβ/αH	w
H-C4H---V-αCH$_3$	m	V-NH---V-αCH$_3$	w	T-NH---P-CβH	w
H-C4H---V-CγH	w	B-NH---T-CαH	m	T-NH---VαCH3	w
H-C4H---H-CβH	m	B-NH---T-CH$_3$	w	T-NH---VγCH3	w
P-CβH---B-CβH	w	S-CαH---S-CH$_3$	w	T-NH---V-CβH	m
V-CγH---H-CβH	w	S-CαH′---S-CH$_3$	w		

[a] w, m, s: weak, medium, strong NOE at 200 ms mixing time. P-NH$_2$ (1), 10.23 ppm; P-NH$_2$ (2), 6.86 ppm.

Proton Assignment of DNA in its Complex with HOO-Co-deglycoBLM

The 1D imino regions of DNA complexes with HOO-CoBLM and HOO-Co-deglycoBLM are compared in Figure 4.9. While free DNA is palindromic showing four imino protons at 20 °C, both complexes of HOO-Co-deglycoBLM and HOO-CoBLM with DNA exhibit all of the eight internal imino resonances (Figure 4.9). The 2-fold DNA symmetry is, as expected removed upon the formation of the drug/DNA complex. Immediately obvious is the similarity of the imino regions of the two drug/DNA complexes. Both show two downfield A•T imino protons and two upfield shifted G•C imino protons (Figure 4.9a,b). The two upfield shifted imino protons, previously assigned to the imino protons of G6•C15 and C7•G14 in HOO-CoBLM/DNA complex, are the result of intercalation between these two base pairs by the bithiazole rings.[11]

The sequential imino-imino walking in the NOESY spectrum of the DNA/Co-deglycoBLM complex is obscured by the low S/N ratio and the presence of minor peaks. In particular, some of which coincide with the predominate ones. Therefore, the assignments of the imino protons have been initially made based on their similarities to the previously assigned imino protons of the DNA/HOO-CoBLM complex and then verified in the NOESY spectrum to assure self-consistency. For example, the upfield shifted imino protons (Figure 4.9a) are first assigned to the imino protons of C6•G15 and C7•G14 respectively, based on their chemical shift comparisons with respective imino protons of DNA/HOO-CoBLM (Figure 4.9b). Both imino protons of C6•G15 and C7•G14 show NOEs to B-C5'H (Figure 4.10), consistent with the intercalation of the bithiazole rings between these two base pairs. Corroboratively, no NOE is observed between these two imino resonances as the separation between these base pairs is increased due to intercalation. The

Figure 4.9: 1D imino proton comparisons between DNA/HOO-Co-deglycoBLM (a) and DNA/HOO-CoBLM (b).

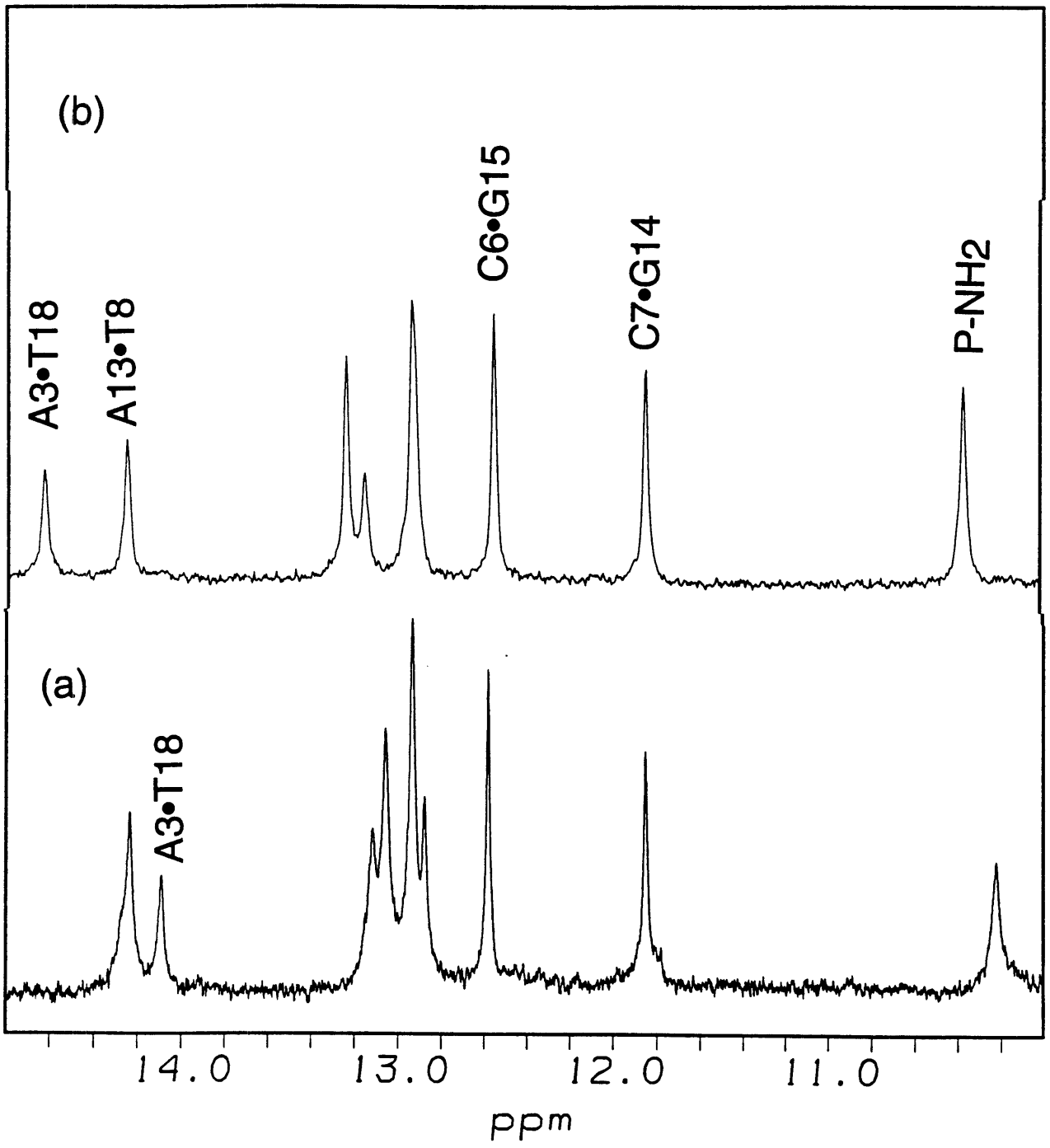
(b)
A3•T18
A13•T8
C6•G15
C7•G14
P-NH2
(a)
A3•T18
14.0
13.0
12.0
11.0
ppm

amino protons of cytosine and the H2 proton of adenine are subsequently assigned according to standard procedures (Figure 4.10).[60] The intensity of the A3•T18 imino proton is found to be abnormally low when compared to that of the A13•T8 base pair. The chemical shift of this proton (14.10 ppm in Figure 4.9a) is shifted downfield by 0.51 ppm relative to its value in DNA/HOO-CoBLM complex (14.62 ppm in Figure 4.9b). This peculiar abnormality appears to correlate with the aforementioned differential broadening of the A3-H8 proton observed in the 1D titration experiment and will be further discussed later.

Assignments of the nonexchangeable DNA protons (H1', 2'/2", 3', 4', and 5"/5') are achieved by analysing NOESY, TOCSY, DQF-COSY spectra using standard methods.[60] In general, the presence of minor peaks have again complicated the proton assignments of DNA complexed with HOO-Co-deglycoBLM. Patterns of base-to-H1' sequential walking of the two DNA strands are similar to that previously reported for the DNA/HOO-CoBLM complex. A region of particular uncertainty again revolves around the assignments of the A3•T18 deoxyribose protons, largely due to their large linewidths. All DNA sugars are consistent with C2'-endo like puckers except the cleavage site, C6, where a C3'-endo like sugar pucker is observed.

Restrained Molecular Dynamics Studies

Intramolecular NOEs within DNA and HOO-Co-deglycoBLM and intermolecular NOEs between DNA and HOO-Co-deglycoBLM have been classified based on visual inspection of the cross peak intensities in the 200 ms NOESY spectra collected in H_2O and D_2O. There are a total of 40 intermolecular NOEs (Table 4.4) and 46 intramolecular Co-deglycoBLM NOEs (Table 4.6).

Figure 4.10: Expanded NOESY spectrum (750 MHz) in H_2O of the complex between HOO-Co-deglycoBLM and d(CCAGGCCTGG) (1 mM) in 50 mM sodium phosphate (pH 6.8) at 20°C. Peak assignments are (A) G15-imino (12.59 ppm) to B-C5'H (7.18 ppm); (B) G14-imino (11.86 ppm) to B-C5'H (7.18 ppm) and G14-H1 (11.86 ppm) to one of the C7 amino protons (7.21 ppm); (C) One of the P-NH_2 (10.23 ppm) to the other P-NH_2 (6.86 ppm); (D) One of the P-NH2 (10.23 ppm) to G5-H1' (5.59 ppm).

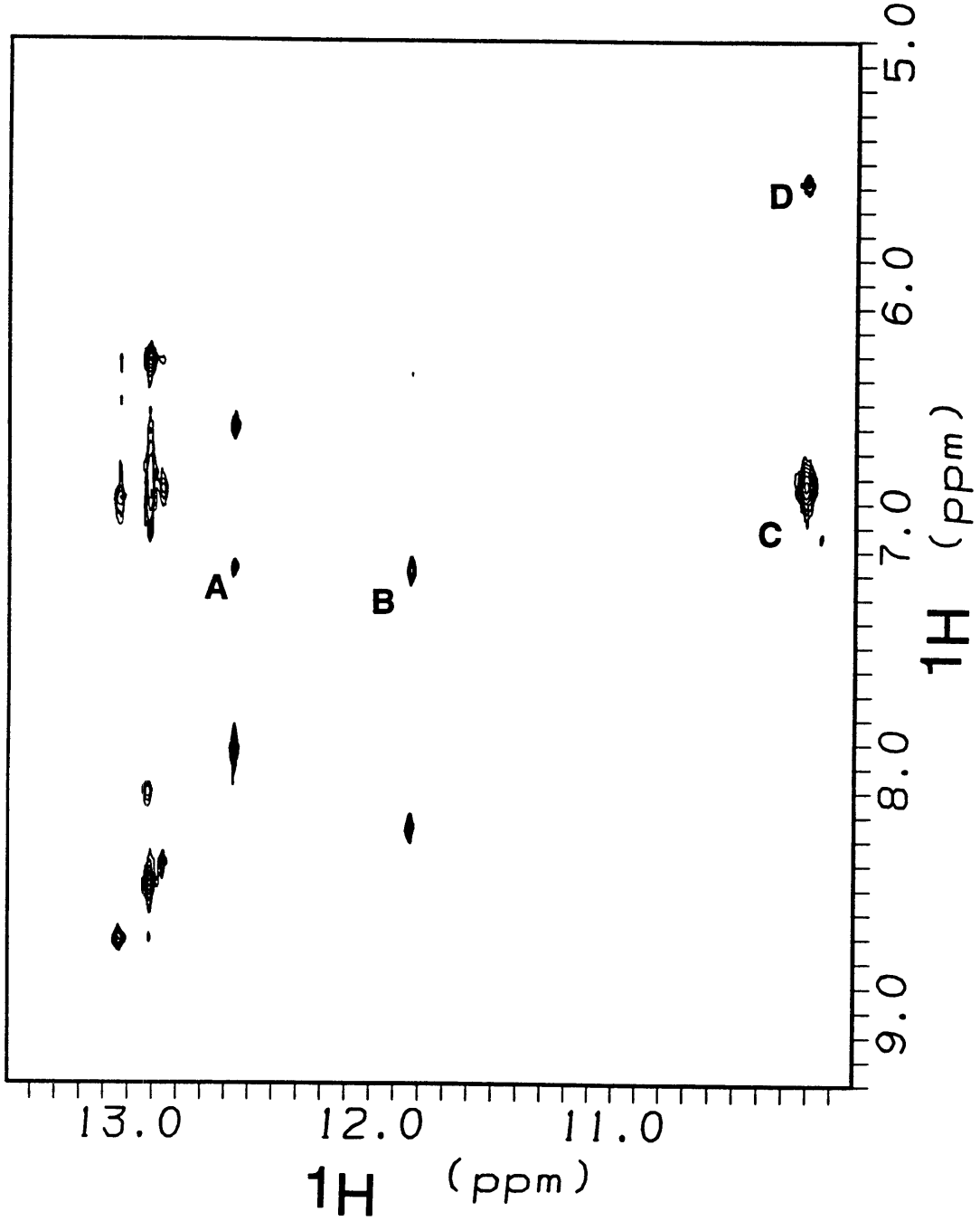
A
B
C
D
13.0
12.0
11.0
1H (ppm)
5.0
6.0
7.0
8.0
9.0
1H (ppm)

The initial starting structure was constructed by positioning the bithiazole moiety of HOO-Co-deglycoBLM between the C6•G15 and C7•G14 base pairs. The orientation was based on the NOE data showing specific interactions of B-H5 and B-H5' with residues of G14, G15, and C6 (Table 4.4). This initial structure was then submitted to minimizations and molecular dynamics simulated annealing calculations. The final distances are in very good agreement with distance constraints giving a rms deviations of 0.034 ± 0.002, and no constraint errors are over 0.2 Å. A final structure was obtained by averaging eleven separately determined structures, followed by minimization of the averaged coordinates. This structure is the basis for the following discussion.

Overall Structure of HOO-Co-deglycoBLM bound to 1:

The minimized structure of HOO-Co-deglycoBLM bound to oligonucleotide **1** is shown in Figure 4.11. This structure, not surprisingly, bears much resemblance to the structure determined for the cognate HOO-CoBLM bound to the same oligomer. The metal binding domain is situated in the minor groove near the cleavage site C6. The metal-bound hydroperoxide is sequestered in the vicinity of the H4' proton of C6, positioned to initiate cleavage chemistry. The sequence specific recognition is provided by two H-bonds between the pyrimidine moiety of HOO-Co-deglycoBLM and G5 within the minor groove. The bithiazole tail guided by the peptide linker region is inserted between base pairs C6•G15 and C7•G14 from the minor groove, with the sulfonium tail extending into the major groove. The structure obtained herein unambiguously confirms the earlier conclusion, based on the similarities in general sequence specificity of DNA cleavage, that the predominate mode of binding and molecular basis for

sequence specificity of deglycoBLM should be the same as BLM. However, subtle distinctions between the two complexes are evident and provide a structural basis for the small differences in binding and secondary cleavage specificity by the two congeners. These similarities and differences are elaborated below.

Mode of Binding and Sequence Specificity

The bithiazole rings in HOO-Co-deglycoBLM are inserted between base pairs C6•G15 and C7•G14, 3' to the cleavage site C6 (Figure 4.11). The trans orientation of the thiazolium rings to each other in this complex is almost identical to that in HOO-CoBLM bound to DNA. The terminal thiazolium ring is completely stacked between the bases of G14 and G15 and the penultimate thiazolium ring is partially stacked between the bases of C7 and C6. The intercalation of the thiazolium rings results in the unwinding of DNA by a total of 12° over the three steps, (G5•C16)~(C7•G14)~(T8•A13). The NOE between the sulfonium methyl protons and A13-H8 of DNA (Table 4.4) unambiguously locates the C-terminus of BLM in the major groove near A13 of DNA as observed in the case of HOO-CoBLM bound to DNA. The electrostaic interaction between this positively charged moiety and the DNA plays an important role in providing binding energy and anchoring the bithiazole rings.

The pyrimidine moiety of HOO-Co-deglycoBLM engages in two H-bonds with guanine in the minor groove. One of the hydrogen bonds is between one of the 4-amino protons of the pyrimidine in HOO-Co-deglycoBLM and the N3 of guanine at a distance of 1.9 Å and an angle of 155°. The other is between one of 2-amino protons of guanine and the N3 of the pyrimidine in HOO-Co-deglycoBLM at a distance of 1.9 Å and an angle of 155°.

Figure 4.11: The structure of HOO-Co-deglycoBLM (atoms colored by element, C=green , O=red, N=blue, S=yellow) bound to DNA (red, C6-H4'=white). The damaged strand is in the foreground, running 5'->3' from the upper right to lower left corner. The dotted lines indicate the H-bond interactions between the P moiety of HOO-Co-deglycoBLM, and the G5 of the DNA. Also indicated is the proximity of the distal oxygen of the hydroperoxide ligand to the C6-H4' (2.5 Å).

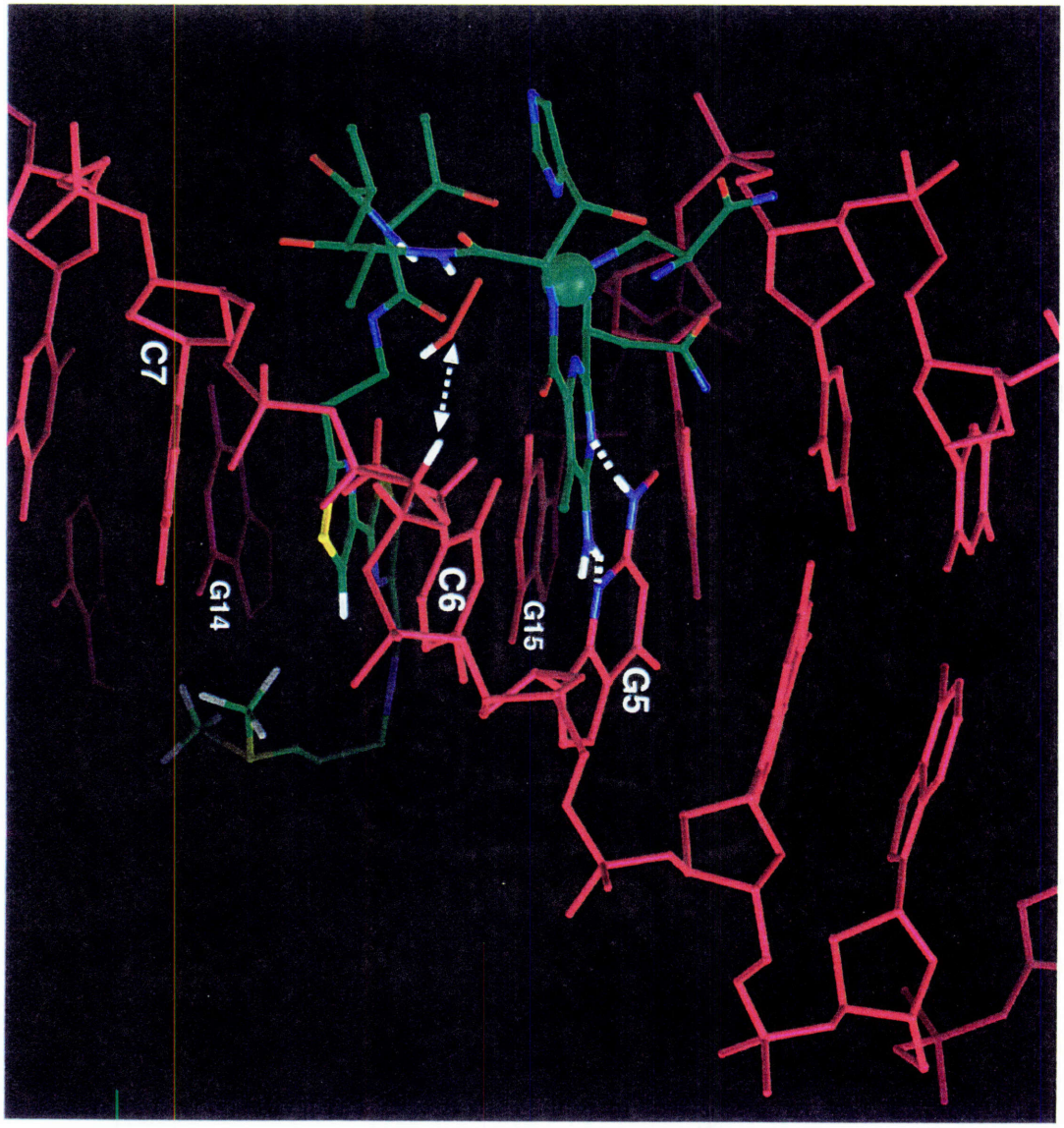
C7
G14
C6
G15
G5

This base-triple like recognition between the pyrimidine in the metal binding domain and the guanine 5' to the cleavage site is responsible for the observed sequence selectivity in G(Py) by deglycoBLM . The orientation of the metal binding domain, as well as the distances and angles of the two hydrogen bonds are similar to those observed in DNA/HOO-CoBLM complex.

The observation of the proton of the hydroperoxide in the complex between the HOO-CoBLM and DNA provided remarkable perspective on how the alignment of the metal-bound hydroperoxide towards the minor groove protons contributes to the site specific hydrogen atom abstraction at the 4' position.[11] Not surprisingly, the hydroperoxide proton in HOO-Co-deglycoBLM bound to DNA is also observed with similar chemical shifts and analogous sets of intermolecular and intramolecular NOEs (Table 4.4 and 4.6). The final structure reveals the proximity of the metal-bound hydrogen peroxide to the minor groove near the cleavage site with a distance of 2.5 Å between the distal oxygen and the H4' proton of C6. The orientation of the hydrogen peroxide towards the minor groove of C6 is almost superimposable to the arrrangement observed in HOO-CoBLM bound to DNA, suggesting a similar DNA cleavage mechanism by deglycoBLM.

The Subtle Differences Between the Two Complexes

The above model structure and a comparison with its glycosylated congener has provided, for the first time, structural evidence for the similarities in DNA binding and sequence specific DNA cleavage at d(GPy) sites by BLM and deglycoBLM. The similarities suggest that deglycoBLM analogs, available by synthetic methods,[20,39,61] will provide a good model to examine the ds cleavage process. In fact, recent studies[62] using the hairpin methodology described by Absalon et al.[37,38] have determined that ss:ds ratio

for Fe-deglycoBLM is half of Fe-BLM. This structure will thus provide the prototype for a number of deglycoBLM analogs that are now being analyzed in detail.[62]

We now begin to focus on the differences between the two complexes in an effort to understand how the lack of the sugar domain can lead to the subtle changes observed in sequence specificity at secondary cleavage sites.[22,36] Already revealed in the 1D titration spectra (Figure 4.7c) are the presence of minor species and the selective broadening of the A3•T18 protons in HOO-Co-deglycoBLM bound to DNA. Each of these two points and their implications will be discussed in turn.

Differences in Binding Affinity

The 35-fold reduction in binding affinity by the deglycosylated congener is hard to explain based on a comparison between the structures of HOO-Co-deglycoBLM and HOO-CoBLM bound to **1**. No specific interaction(s) are apparent between the sugars and the DNA. Thus, the reduction in binding affinity perhaps results from either the loss of non-specific van der Waals interactions between the sugar domain and DNA and/or the conformational differences between HOO-CoBLM and its deglycosylated congener, resulting in different H-bonding interactions. Both possibilities are elaborated below. In six of the eight final structures of HOO-CoBLM bound to DNA, the mannose moiety (e.g. M-C6H2) is within van der Waals distance of the DNA backbone and the deoxyribose protons of C17 and T18 (Figure 4.12). The modeling also consistently reveals the differences in the conformation in HOO-Co-deglycoBLM relative to HOO-CoBLM when bound to **1**. A hydrogen bond interaction appears to be present between a proton of the amide moiety of β-aminoalanine and O3' of C17 in the latter, which does not appear to be

present in the former. It should be noted, however, that the above putative hydrogen bond as well as the non-specific interactions between the sugar domain and DNA are thus far deduced only from the structures of eight restrained molecular dynamics calculations, and await additional confirmatory evidence.

The Minor Complexes

Under identical conditions, the binding of HOO-Co-deglycoBLM to oligonucleotide (CCAGGCCTGG) displays many small additional features (Figure 4.7c) that are absent in the complex between HOO-CoBLM and the same oligonucleotide. Attempts to unambiguously assign these protons have been unsuccessful because of their low abundance. However, the chemical shift comparisons and the analysis of NOESY spectra at lower contour levels have allowed these small resonances to be distinguished from spurious peaks. Some of these resonances in the downfield region appear to represent minor complexes formed between Co-deglycoBLM and DNA, based on the resemblance of their NOEs to the intramolecular NOEs shown in Table 4.6. For example, the small and most downfield shifted resonance at 9.21 ppm (Figure 4.9c) displays NOE crosspeaks to resonances at 7.58, 4.01, 5.35, 3.05, 2.89, and 1.29 ppm. Based on the chemical shift similarities, the NOE between resonances at 9.21 and 7.58 ppm resembles the intramolecular NOE between H-C2H (9.06 ppm) and H-C4H (7.55 ppm) shown in Table 4.6, and the NOE between resonances at 9.21 and 1.29 ppm to that between H-C2H (9.06 ppm) and T-CH_3 (1.25 ppm) shown in Table 4.6. Thus, the small resonances at 9.21, 7.58, 1.29 ppm can be tentatively assigned to another form of H-C2H, H-C4H and T-CH_3 protons respectively. The chemical shifts of this minor form of HOO-Co-deglycoBLM bound to DNA are not the same as either the free HOO-Codeglyco-BLM or the HOO-Co-deglycoBLM in its predominate complex with

DNA (Table 4.1 and 4.3). They perhaps represent a minor and distinct complex between HOO-Co-deglycoBLM and DNA.

Although the mode of binding in this minor complex is not discernible from the available information, a few possibilities can be ruled out. First, the molecular modeling studies show that it is highly unlikely to have two molecules of metallo-BLM in the minor groove of this decamer at the same time. Second, the purity of both HOO-Co-deglycoBLM and DNA have been analyzed by NMR prior to the titration, and thus it is also unlikely that this minor complex originates from contaminates. Finally, model studies using PMA ligand tethered with acridine revealed the presence of a racemic mixture of Co adduct of the model ligand (Figure 4.6b).[63] Thus, it should be considered that the HOO-Co-deglycoBLM of the opposite screw sense was present in small amounts. Based on the structure reported herein and the fact that the opposite screw sense would of necessity bind totally different to the DNA, it appears that only one isomer exists in our study. The difference between BLM and PMA may be the added chirality of the BLM not present in the PMA ligand (Figure 4.1 and 4.6b).

The most plausible model for this minor complex therefore is one in which the same HOO-Co-deglycoBLM binds to a different site on the DNA. Intergration of the two respective H-C2H protons at 9.21 and 9.06 ppm shows it is 1/20 of the predominate form. Because both complexes are in slow exchange on the NMR time scale, the ratio of the intergration of H-C2H protons reflects the ratio of equilibrium concentration of the two complexes and hence the differences in binding affinity. Finally, additional minor resonances appear in the titration spectrum (Figure 4.9c), and they may not all belong to the same minor complex. In conclusion, the HOO-Co-deglycoBLM can have additional secondary binding site in comparison to its parent. It is

Figure 4.12: An overlay of the final eight structures of HOO-CoBLM complexed with **1**, looking into the minor groove. The mannose moiety (yellow) is within the minor groove and is within van der Waals contact with the deoxyribose of either C17 or T18 in 6 of the eight structures.

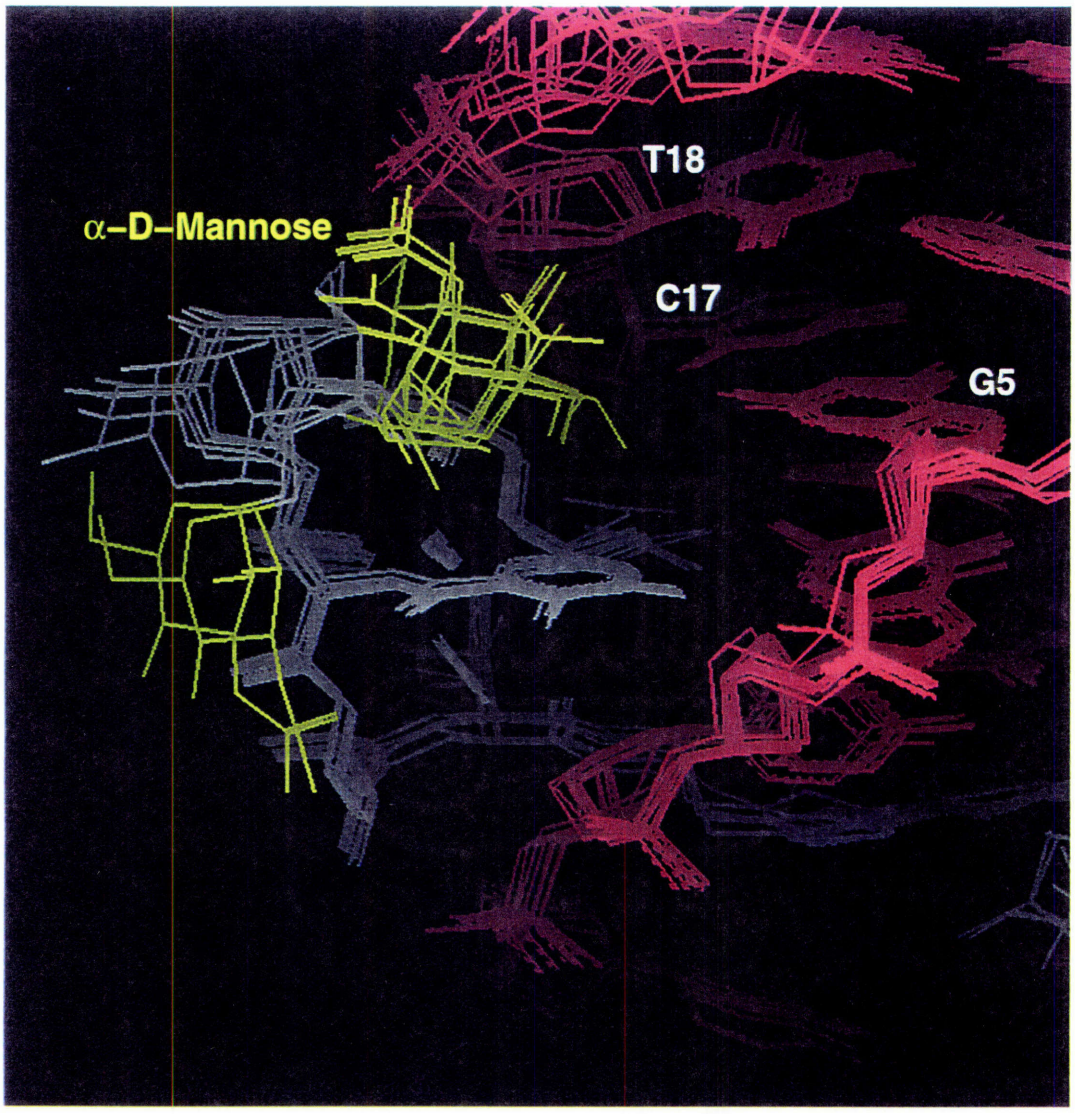
T18
α–D–Mannose
C17
G5

however not known at present whether this minor binding event will lead to a productive cleavage. Experiments are in progress to study the cleavage specificity of this oligonucleotide by metallo-deglycoBLMs. It is also not clear what structural changes in the absence of the sugar domain are responsible for creating new DNA binding sites, despite the conformity in global structure between the two congeners. The changes in local structure such as the movement of the amide groups of the pyrimidine and the β-aminoalanine moiety may alter the binding complementarity between metallo-deglycoBLM and DNA, which may change the binding preference for different DNA binding sites and/or create new ones.

The Selective Broadening of the A3•T18 base pair

The selective broadening of the base protons of A3•T18 base pair, apparent from A3-H8 (Figure 4.9c) in HOO-Co-deglycoBLM bound to DNA is observed. The linewidth of A3-H8 is 22 Hz at 20 °C[64] and is significantly broader than the linewidth of A13-H8 (11 Hz) (Figure 4.9c). The differential broadening of the A3•T18 base protons is also observed in the free DNA with A3-H8 having a linewidth of 13 Hz at 20 °C, greater than the average linewidth of other base protons (8 Hz). The broadening of this feature suggests the interchange between different local base structures. Interestingly, this flexibility is also apparent in the crystal structure of this oligonucleotide.[65] The X-ray structure reveals an unusual geometry between the base pairs of C2•G19 and A3•T18 ---no stacking between these two base pairs! This arrangement results from the sliding of the A3•T18 base pair and replaces the normal stacking in B-form DNA with another energetically more favorable conformation. Thus, the unstacking of A3•T18 base pair in free DNA in solution may facilitate the local movement of the bases with respect

to the normal Watson-Crick geometry as well and result in rapidly interconverting conformations leading to the broadening of A3-H8 proton in the NMR spectrum. The lack of stacking between base pairs C2•G19 and A3•T18 would also lengthen the internucleotide distance between A3 and C2, and between G19 and T18. In fact a 3 fold decrease in the intensity of crosspeak between A3-H8 and C2-H1' in comparison with the standard internucleotide base to H1' crosspeaks in B form DNA is observed.

When HOO-CoBLM is bound to this oligonucleotide, the motional broadening of the A•T base pairs differentiates between the now inequivalent A3•T18 and A13•T8 base pairs (Figure 4.8d). The conformational dynamics at the A3•T18 base pair remains, exemplified by the linewidth of A3-H8 at 14 Hz, broader than the average linewidth of other base protons (10 Hz) (Figure 4.8d). This result contrasts to the normal 10 Hz linewidth of the A13•T8 (Figure 4.8d). This differentiation of the motions experienced by two A•T base pairs is consistent with the orientation of HOO-CoBLM when complexed to DNA. The A13-H8 proton based on the NOE data is adjacent to the sulfonium methyl groups (Table 4.4) and its motions may be restricted by the presence of the bulky and positively charged sulfonium moiety. The A3•T18 base pair is quite remote from the binding by the metal binding region of BLM. The unstacking of A3•T18 and the resulting base dynamics seem to be unaffected.

In the complex between HOO-Co-deglycoBLM and DNA, the A3•T18 is two base pairs removed from the metal binding domain and the resulting dynamics of this base pair appears to be more dynamic in the deglyco complex (Figure 4.12). Support of this model is apparent by an examination of the imino protons associated with base pairs A3•T18 and A13•T8 (Figure 4.9a,b). The intensity of the imino proton of A3•T18 is considerably lower than that

of A13•T8 (Figure 4.9a). The flexibility in this region of the DNA/HOO-Co-deglycoBLM complex is also apparent from the broadening of the T18-H6 and T18-CH_3 protons. The enhanced local base dynamics of the A3•T18 appears to have also affected the chemical shifts of the relevant protons. For instance, the chemical shift of T18 (14.10 ppm) in Co-deglycoBLM bound to DNA is very different from that in the complex between HOO-CoBLM and DNA (14.62 ppm) (Figure 4.9). The A13•T8 base pair, on the other hand appears to be quite similar. Thus the sugars in the parent complex nuzzled adjacent to the G4 and G5 seem to restrict the dynamics of the A3•T18 base pair as well, perhaps by van der Waals interactions. This result supports the previous proposal that van der Waals interactions between sugar and DNA play a subtle, but important role in the binding affinity.

In summary, the absence of sugar domain in HOO-Co-deglycoBLM has affected the local DNA conformation apparent from the enhanced base conformational dynamics of the A3•T18 base pair. This DNA conformation change takes place several base pairs removed from the major binding site and the mechanism of this induced changes is unclear. Such changes in DNA conformation remote from the binding site of HOO-Co-deglycoBLM can be postulated to lead to the decreased binding and as a consequence lead to enhanced or diminished cleavage at the secondary sites.

References:

(1) Sikic, B. I.; Rozencweig, M.; Carter, S. K. Ed., *Bleomycin Chemotherapy*; Academic Press: Orlando, Florida, 1985.

(2) Umezawa, H.; Takita, T. in *Structure and Bonding*; Dunitz, J. D.; Hemmerich, P.; Jørgensen, C. K.; Reiner, D.; Goodenough, J. B.; Ibers, J. A.;

Neilands, J. B. Williams, R. J. P. Ed.; Springer-Verlag, New York, 1980; Vol. 40, pp 73-99.

(3) Hecht, S. M. *Summary of the bleomycin symposium;* Springer-Verlag: New York, 1979.

(4) Povirk, L. F.; Austin, M. J. F. *Mut. Res.* **1991**, *257*, 127-143.

(5) Povirk, L. F. in *Molecular Aspects of Anti-Cancer Drug Action;* Neidle Waring Ed.; 1983; pp 157-181.

(6) Hecht, S. M. *Bioconjugate Chem.* **1994**, *5*, 513-526.

(7) Kane, S. A.; Hecht, S. M. in *Progress in Nucleic Acid Research and Molecular Biology;* Cohn, W. E. Moldave, K. Ed.; Academic Press, San Diego, 1994; Vol. 49, pp 313-352.

(8) Stubbe, J.; Kozarich, J. W. *Chem. Rev.* **1987**, *87*, 1107-1136.

(9) Stubbe, J.; Kozarich, J. W.; Wu, W.; Vanderwall, D. E. *Acc. Chem. Res.* **1996**, *29*, 322-330.

(10) Wu, W.; Vanderwall, D. E.; Lui, S. M.; Tang, X.-J.; Turner, C. J.; Kozarich, J. W.; Stubbe, J. *J. Am. Chem. Soc.* **1996**, *118*, 1268-1280.

(11) Wu, W.; Vanderwall, D. E.; Turner, C. J.; Kozarich, J. W.; Stubbe, J. *J. Am. Chem. Soc.* **1996**, *118*, 1281-1294.

(12) Wu, W.; Vanderwall, D. E.; Stubbe, J.; Kozarich, J. W.; Turner, C. J. *J. Am. Chem. Soc.* **1994**, *116*, 10843-10844.

(13) Manderville, R. A.; Ellena, J. F.; Hecht, S. M. *J. Am. Chem. Soc.* **1995**, *117*, 7891-7903.

(14) Manderville, R. A.; Ellena, J. F.; Hecht, S. M. *J. Am. Chem. Soc.* **1994**, *116*, 10851-10852.

(15) Lui, S.-M.; Vanderwall, D. E.; Wu, W.; Tang, X.-J.; Turner, C. J.; Kozarich, J. W.; Stubbe, J. manuscript in preparation.

(16) Vanderwall, D. E.; Lui, S.-M.; Wu, W.; Tang, X.-J.; Turner, C. J.; Kozarich, J. W.; Stubbe, J. manuscript in preparation.

(17) Mao, Q.; Fulmer, P.; Li, W.; DeRose, E. F.; Petering, D. H. *J. Biol. Chem.* **1996**, *271*, 6185-6191.

(18) Muraoka, Y.; Suzuki, M.; Fujii, A.; Umezawa, Y.; Naganawa, H.; Takita, T.; Umezawa, H. *J. Antibiot.* **1981**, *34*,

(19) Boger, D. L.; Teramoto, S.; Honda, T.; Zhou, J. *J. Am. Chem. Soc.* **1995**, *117*, 7338-7343.

(20) Boger, D. L.; Teramoto, S.; Zhou, J. *J. Am. Chem. Soc.* **1995**, *117*, 7344-7356.

(21) Oppenheimer, N. J.; Chang, C.; Chang, L.-H.; Ehrenfeld, G.; Rodriguez, L. O.; Hecht, S. M. *J. Biol. Chem.* **1982**, *257*, 1606-1609.

(22) Shipley, J. B.; Hecht, S. M. *Chem. Res. Toxicol.* **1988**, *1*, 25-27.

(23) Sugiyama, H.; Kilkuskie, R. E.; Chang, L.-H.; Ma, L.-T.; Hecht, S. M.; van der Marel, G.; van Boom, J. H. *J. Am. Chem. Soc.* **1986**, *108*, 3852-3854.

(24) Sugiyama, H.; Ehrenfeld, G. M.; Shipley, J. B.; Kilkuskie, R. E.; Chang, L.-H.; Hecht, S. M. *J. of Natural Prod.* **1985**, *48*, 869-877.

(25) Nakayama, Y.; Kunishima, M.; Omoto, S.; Takita, T.; Umezawa, H. *J. Antibiot.* **1973**, *26*, 400-401.

(26) Hori, M. in *Bleomycin: chemical, biochemical, and biological aspects*; Hecht, S. M. Ed.; Springer-Verlag, New York, 1979; pp 195-206.

(27) Takahashi, K.; Ekimoto, H.; Aoyagi, S.; Koyu, A.; Kuramochi, H.; Yoshioka, O.; Matsuda, A.; Fujii, A. *J. Antibiot.* **1979**, *32*, 36-42.

(28) Oppenheimer, N. J.; Rodriguez, L. O.; Hecht, S. M. *Proc. Natl. Acad. Sci. USA* **1979**, *76*, 5616-5620.

(29) Akkerman, M. A. J.; Haasnoot, C. A. G.; Hilbers, C. W. *Eur. J. Biochem.* **1988**, *173*, 211-225.

(30) Akkerman, M. A. J.; Neijman, E. W. J. F.; Wijmenga, S. S.; Hilbers, C. W.; Bermel, W. *J. Am. Chem. Soc.* **1990**, *112*, 7462-7474.

(31) Sugiura, Y. *J. Am. Chem. Soc.* **1980**, *102*, 5208-5215.

(32) Kénani, A.; Bailly, C.; Helbecque, N.; Catteau, J.-P.; Houssin, R.; Bernier, J.-L.; Hénichart, J.-P. *Biochem. J.* **1988**, *253*, 497-504.

(33) Sugiura, Y.; Suzuki, T.; Muraoka, Y.; Umezawa, Y.; Takita, T.; Umezawa, H. *J. Antibiot.* **1981**, *34*, 1232-1236.

(34) Sugiura, Y.; Suzuki, T.; Otsuka, M.; Kobayashi, S.; Ohno, M.; Takita, T.; Umezawa, H. *J. Biol. Chem.* **1983**, *258*, 1328-1336.

(35) Umezawa, H.; Takita, T.; Sugiura, Y.; Otsuka, M.; Kobayashi, S.; Ohno, M. *Tetrahedron* **1984**, *40*, 501-509.

(36) Bailly, C.; Kénani, A.; Waring, M. J. *FEBS letters.* **1995**, *372*, 144-147.

(37) Absalon, M. J.; Wu, W.; Stubbe, J.; Kozarich, J. W. *Biochemistry* **1995**, *34*, 2076-2086.

(38) Absalon, M. J.; Stubbe, J.; Kozarich, J. W. *Biochemistry* **1995**, *34*, 2065-2075.

(39) Boger, D. L.; Colletti, S. L.; Teramoto, S.; Ramsey, T. M.; Zhou, J. *Bioorg. Med. Chem.* **1995**, *3*, 1281-1295.

(40) Bax, A.; Subramanian, S. *Journal of Magnetic Resonance* **1986**, *67*, 565-569.

(41) Bothner-By, A. A.; Stephens, R. L.; Warren, C. D.; Jeanloz, R. W. J. *J. Am. Chem. Soc.* **1985**, *106*, 811.

(42) Chang, C.-H.; Dallas, J. L.; Meares, C. F. *Biochem. Biophys. Res. Commn.* **1983**, *110*, 959-966.

(43) Sam, J. W.; Tang, X.-J.; Peisach, J. *J. Am. Chem. Soc.* **1994**, *116*, 5250-5256.

(44) Derome, A. E. *Modern NMR Techniques for Chemistry Research*; Pergamon Press: Oxford, 1987.

(45) Iitaka, Y.; Nakamura, H.; Nakatani, T.; Muraoka, Y.; Fujii, A.; Takita, T.; Umezawa, H. *J. Antibiot.* **1978**, *31*, 1070-1072.

(46) Tan, J. D.; Hudson, S. E.; Brown, S. J.; Olmstead, M. M.; Mascharak, P. K. *J. Am. Chem. Soc.* **1992**, *114*, 3841-3853.

(47) Burger, R. M.; Peisach, J.; Horwitz, S. B. *J. Biol. Chem.* **1981**, *256*, 11636-11644.

(48) Burger, R. M.; Kent, T. A.; Horwitz, S. B.; Münck, E.; Peisach, J. *J. Biol. Chem.* **1983**, *258*, 1559-1564.

(49) Kittaka, A.; Sugano, Y.; Otsuka, M.; Ohno, M. *Tetrahedron* **1988**, *44*, 2821-2833.

(50) Kittaka, A.; Sugano, Y.; Otsuka, M.; Ohno, M. *Tetrahedron* **1988**, *44*, 2811-2820.

(51) Kittaka, A.; Sugano, Y.; Otsuka, M.; Ohno, M.; Sugiura, Y.; Umezawa, H. *Tetrahedron Lett.* **1986**, *27*, 3631-3634.

(52) Otsuka, M.; Kittaka, A.; Ohno, M.; Suzuki, T.; Kuwahara, J.; Sugiura, Y. *Tetrahedron Lett.* **1986**, *27*, 3639-3642.

(53) Sugano, Y.; Kittaka, A.; Otsuka, M.; Ohno, M.; Sugiura, Y.; Umezawa, H. *Tetrahedron Lett.* **1986**, *27*, 3635-3638.

(54) Oppenheimer, N. J.; Rodriguez, L. O.; Hecht, S. M. *Biochemistry* **1980**, *19*, 4096-4103.

(55) Loeb, K. E.; Zaleski, J. M.; Westre, T. E.; Guajardo, R. J.; Mascharak, P. K.; Hedman, B.; Hodgson, K. O.; Solomon, E. I. *J. Am. Chem. Soc.* **1995**, *117*, 4545-4561.

(56) Burger, R. M.; Blanchard, J. S.; Horwitz, S. B.; Peisach, J. *J. Biol. Chem.* **1985**, *260*, 15406-15409.

(57) Boger, D. L.; Colletti, S. L.; Honda, T.; Menezes, R. F. *J. Am. Chem. Soc.* **1994**, *116*, 5607-5618.

(58) Haasnoot, C. A. G.; Pandit, U. K.; Kruk, C.; Hilbers, C. W. *J. Biomol. Struct. Dyn.* **1984**, *2*, 449-467.

(59) Xu, R. X.; Nettesheim, D.; Otvos, J. D.; Petering, D. H. *Biochemistry* **1994**, *33*, 907-916.

(60) Wüthrich, K. *NMR of Proteins and Nucleic Acids;* John Wiley & Sons, Inc: New York, 1986.

(61) Boger, D. L.; Honda, T.; Menezes, R. F.; Colletti, S. L. *J. Am. Chem. Soc.* **1994**, *116*, 5631-5646.

(62) Hoehn, S., unpublished results.

(63) Tan, J. D.; Farinas, E. T.; David, S.; Marscharak, P. M. *Inorg. Chem.* **1994**, *33*, 4295-4308.

(64) All linewidths are measured on 1D NMR spectra acquired at 500 MHz.

(65) Heinenmann, U.; Alings, C. *J. Mol. Biol.* **1989**, *210*, 369-381.